LEABHARLANN CHOLÁISTE NA TRÍONÓIDE, BAILE ÁTHA CLIATH | TRINITY COLLEGE LIBRARY DUBLIN
Ollscoil Átha Cliath | The University of Dublin

Terms and Conditions of Use of Digitised Theses from Trinity College Library Dublin

Copyright statement

All material supplied by Trinity College Library is protected by copyright (under the Copyright and Related Rights Act, 2000 as amended) and other relevant Intellectual Property Rights. By accessing and using a Digitised Thesis from Trinity College Library you acknowledge that all Intellectual Property Rights in any Works supplied are the sole and exclusive property of the copyright and/or other IPR holder. Specific copyright holders may not be explicitly identified. Use of materials from other sources within a thesis should not be construed as a claim over them.

A non-exclusive, non-transferable licence is hereby granted to those using or reproducing, in whole or in part, the material for valid purposes, providing the copyright owners are acknowledged using the normal conventions. Where specific permission to use material is required, this is identified and such permission must be sought from the copyright holder or agency cited.

Liability statement

By using a Digitised Thesis, I accept that Trinity College Dublin bears no legal responsibility for the accuracy, legality or comprehensiveness of materials contained within the thesis, and that Trinity College Dublin accepts no liability for indirect, consequential, or incidental, damages or losses arising from use of the thesis for whatever reason. Information located in a thesis may be subject to specific use constraints, details of which may not be explicitly described. It is the responsibility of potential and actual users to be aware of such constraints and to abide by them. By making use of material from a digitised thesis, you accept these copyright and disclaimer provisions. Where it is brought to the attention of Trinity College Library that there may be a breach of copyright or other restraint, it is the policy to withdraw or take down access to a thesis while the issue is being resolved.

Access Agreement

By using a Digitised Thesis from Trinity College Library you are bound by the following Terms & Conditions. Please read them carefully.

I have read and I understand the following statement: All material supplied via a Digitised Thesis from Trinity College Library is protected by copyright and other intellectual property rights, and duplication or sale of all or part of any of a thesis is not permitted, except that material may be duplicated by you for your research use or for educational purposes in electronic or print form providing the copyright owners are acknowledged using the normal conventions. You must obtain permission for any other use. Electronic or print copies may not be offered, whether for sale or otherwise to anyone. This copy has been supplied on the understanding that it is copyright material and that no quotation from the thesis may be published without proper acknowledgement.

Triple negative breast cancer-derived extracellular-vesicles as naturally-occurring biomarkers and therapeutic delivery systems

A thesis submitted to the University of Dublin, Trinity College towards a degree of Doctor of Philosophy

by

Keith O'Brien B.Sc (Hons)

Based on research carried out under the supervision of
Assoc. Prof. Lorraine O'Driscoll &
co-supervision of Prof. Marek Radomski

School of Pharmacy & Pharmaceutical Sciences,
Trinity Biomedical Sciences Institute,
Trinity College Dublin

December 2014

Declaration

I declare that this thesis has not been submitted as an exercise for a degree at this or any other university and it is entirely my own work. For research that has been carried out jointly or includes the published or unpublished work of others is duly acknowledged within the text wherever included. I agree that the Trinity College Library may lend or copy this thesis upon request.

Signed: Keith O' Brien

TRINITY COLLEGE
1 4 MAY 2015
LIBRARY DUBLIN

Thesis 10513

Summary

Background: In Ireland, breast cancer is the most commonly diagnosed cancer among women; and of the breast cancer subtypes, triple-negative breast cancers (TNBC) are the most aggressive. TNBCs account for 15%-20% of breast cancers, yet are responsible for a disproportionate number of breast cancer deaths. With no targeted treatments for TNBC, there is unmet clinical need for more effective targeted therapeutics. The relevance of extracellular vesicles (EVs) in cancer progression, diagnosis and therapeutics has been investigated, but not in TNBC. By transferring bioactive molecules, including proteins and nucleic acids, EVs have been shown to regulate hallmarks of cancer. Here, the potential of TNBC–derived EVs to mediate activities associated with metastasis is investigated; their nucleic acid contents analysed to determine their relevance as biomarkers; miRNA expression manipulated to assess therapeutic potential; and their clinical relevance as biomarkers evaluated using EVs from serum specimens of breast cancer patients and healthy volunteers.

Methods: EVs were isolated from the conditioned medium of the TNBC cells, Hs578T, and its more aggressive variant, Hs578Ts(i)$_8$. EVs were applied to breast cancer cells *in vitro* to assess their effects on proliferation, migration, invasion, *anoikis* and angiogenesis. MDA-MB-231 (another TNBC cell line) EVs were also investigated for their effects on invasion. *In vivo* distribution was assessed by fluorescently labelling EVs and injecting into mice. Global miRNA profiling of both cell and EV variants was performed by TaqMan low density array to discover tumour suppressors/biomarkers. DNA SNP sequencing was performed to assess their ability to carry mutated DNA that reflected the status of the cells of origin. Protein expression and tumour suppressive analysis of miR-370 and miR-134 was performed following transfection. EVs from miR-134 transfected cells were assessed for their ability to alter protein expression targeted by miR-134 and their influence on Hs578Ts(i)$_8$ aggression and drug sensitivity. EVs from the serum of breast cancer patients and healthy controls were assessed for their ability to alter cancer aggression. miR-134, miR-370, miR-376c, miR-889 and miR-655 levels

in EVs from breast cancer patients and healthy controls were assessed by qPCR for their potential as blood-based biomarkers

Results: TNBC-derived EVs have the ability to increase proliferation, migration, invasion and vasculogenesis of secondary cells *in vitro,* in a manner representing the phenotypes of their originating cells. TNBC-EVs are stable *in vivo*, where the more aggressive cell-derived EVs hone to areas associated with metastasis. miRNAs are largely conserved in EVs from both cell variants. EVs also contain DNA, which is present in both wild-type and mutated forms. Substantial down-regulation of miRNAs was observed in Hs578Ts(i)$_8$ cells and EVs compared to Hs578T cells and EVs. miR-370 and miR-134 both have tumour suppressive qualities in a TNBC cell line. miR-370 reduced the migration and invasion of Hs578Ts(i)$_8$ cells. miR-134 reduced STAT5B, Hsp90 and Bcl-2 expression, resulting in reduced aggression and increased cisplatin-induced apoptosis. EVs from miR-134 transfected cells reduced STAT5B and Hsp90 expression; reduced migration, invasion and increased anti-Hsp90 drug potency in Hs578Ts(i)$_8$ cells. EVs from the serum of TNBC and ER+ patients increase the metastatic potential of cells *in vitro,* with no significant differences between either subtype. We observed total RNA to be significantly increased in EVs derived from TNBC, ER+ and HER2+ breast cancer patients, compared to age-matched controls. miRNA analysis of TNBC cells and EVs was validated in sera of TNBC patients, and were also found in EVs form serum of ER+ and HER2+ breast cancer patients. Specifically, miR-134, miR-370 and miR-376c are reduced in breast cancer tumours. miR-134 and miR-370 from breast cancer sera-EVs are sensitive to discriminate stage 1 breast cancer from healthy individuals. miR-134, miR-370 and miR-376c from breast cancer sera-EVs significantly sensitive to detect stage 3 breast cancer

Conclusions: This thesis suggests that EVs play an active role in mediating the aggression of TNBC, and may signal for increased TNBC metastasis by influencing pre-metastatic niche formation. TNBC-derived EVs represent miniature maps of their originating tumour cells, and represent desirable entities for use as miRNA blood-based biomarkers.

Acknowledgments

Firstly, I would like to thank my supervisor Lorraine for her tireless work, support and guidance throughout my Ph.D. Not only has her guidance led to a thesis with such a wide range of practical procedures and results, but there is no doubt I have benefited, and will further benefit tremendously from the diverse academic involvements I have experienced under Lorraine's supervision. For this, I am very grateful. I am also grateful for the help from my co-supervisor, Marek, during my Ph.D.

I would also like to express wholehearted gratitude to every member of the O'Driscoll group, especially those who I have spent most of my time with in TCD; Claire, Susan and Sweta. Throughout my time in TCD, I have developed close bonds with you all, of which I am very fond. Claire, I could not have asked more from a colleague, but more importantly to me, I could not have asked more from a friend. You have always been there for me throughout the three and a half years, and no matter what the issue you always had a kind ear, practical advice and always made me laugh. You really made my experience in TCD an enjoyable one. Susan, looking back on the friendship we have developed over the three years, your endless support, kindness and positivity were, and are, truly priceless, of which I will never forget. Sweta, I am incredibly appreciative for everything you have done for me. I have learned so much from you, not only from the first few months of my Ph.D working side-by-side with you, but throughout our three years working together. No problem ever seemed too big, and your patience was always admirable. Thanks for helping me when I fainted in St. Vincent's Hospital too, that was embarrassing.

Of the relatively more recent members of the O'Driscoll group, I am also very grateful. Ye have brought fresh life to the group, brimming with knowledge and positivity. Sadhbh, thank you for such positivity in the office, it has been fun. Martina, thanks for all the help and being a constant source of logical advice in the lab, it is very much appreciated. Melissa, I have really enjoyed working with you, I will always remember our numerous Artic Monkeys conversations. And, the most recent addition, Vanesa; your arrival brought

with it, not only a bottomless pit of knowledge (somewhat like Google), but an infinite increase of singing and dancing. Thanks.

Of course there are many others who made my time in TCD enjoyable, such as Dr. Patrick Kelly (honorary pigeon member). Thanks for all the help and advice over the years, and always being around for a chat when needed. We had some good times. Meeting and befriending members of the School of Pharmacy labs are what stick out in my mind as being the most enjoyable. In this regard, I would like to thank the following: Stephany "ariverderci" Micallef, Shane, Andy, Adrian, Grainne, Brian/Money, Jason, Vilmar, Pauline, Eva, Julia, Svenja, Jun, Conor, Mary, Gary, Tadhgh, Pigeons, Timi, Vinny, Feri, Cathal, Johanna, Maria, Ines, Stefano, Billy, Sid and Tao.

I would also like to thank Agnes for being a rock in my life. Your love has unquestionably helped me get through my biggest challenge in life so far. I cannot express the magnitude of my pride and appreciation.

I would also like to thank Alan and Seán who always gave support and relief from the Ph.D life. I am forever grateful.

There is absolutely no doubt, that without the encouragement, support and guidance from my parents that I would not have got so far with my education. Your love and belief is more than a son could ever ask for. I would like to thank my brother Paul for everything you have done for me throughout the years. To my favourite sister (although, only sister), Ann-Marie .Thank you for everything. You have always been a source of help, from always being there to talk to about life in academia, making me laugh, and to our most recent endeavour of thesis-tennis. I am very grateful for everything.

Table of Contents

DECLARATION ..... **I**

SUMMARY ..... **II**

ACKNOWLEDGMENTS ..... **IV**

CHAPTER 1: INTRODUCTION **1**

1. ABSTRACT **2**

1.1. Cancer 4

1.2. Cancer development, invasion and metastasis 4

1.2.1. Primary tumour formation 4

1.2.2. Apoptosis 5

1.2.3. Angiogenesis 6

1.2.4. Metastasis 7

1.2.4.1. Invasion and migration 8

1.3. The biology of breast cancer 9

1.3.1. The biology of TNBC 10

1.3.2. TNBC is a heterogeneous subtype 10

1.3.3. TNBC treatment options 12

1.4. microRNAs 14

1.4.1. miRNA biogenesis 14

1.4.2. miRNAs in breast cancer 15

1.4.2.1. miRNA signatures in breast cancer 16

1.4.2.2. Mechanisms and implications of miRNA dysregulation in breast cancer 16

1.4.2.3. Implications of miRNA associated polymorphisms 17

1.4.2.4. Functional roles of miRNAs in breast cancer 18

1.5. The world of extracellular vesicles 21

1.5.1. Extracellular vesicles 21

1.5.1.1. Exosomes formation 23

1.5.1.2. MV Formation 25

1.5.1.3. EV mediated intercellular communication 27

1.5.2. EVs and cancer 28

1.5.2.1. EVs in breast cancer 28

1.5.2.2. EVs educate the pre-metastatic *in vivo* 29

1.5.3. miRNA in EVs 31

1.5.3.1. Incorporation of miRNA into EVs 32
1.5.3.2. EV-miRNAs as biomarkers 33
1.5.4. DNA in EVs 35
1.5.5. Therapeutic applications of EVs 36

1.6. Project aim: 39

CHAPTER 2 ..... **40**

2. ABSTRACT **41**

2.1. Introduction 43

2.2. Materials & Methods 45
2.2.1. Cell culture 45
2.2.2. Extracellular vesicle isolation from conditioned medium (CM) 46
2.2.2.1. EV quantification 48
2.2.3. Immunoblotting 48
2.2.3.1. Protein extraction 48
2.2.3.2. Protein quantification 49
2.2.4. Transmission electron microscopy (TEM) of EVs 50
2.2.5. Confocal microscopy 50
2.2.6. Proliferation rate measurement 51
2.2.6.1. Assessment of cell proliferation 51
2.2.6.2. Assessment of cell proliferation in response to EVs 51
2.2.7. Migration (wound healing assay) 52
2.2.7.1. Assessment of cell motility 52
2.2.7.1. Assessment of cell motility in response to EVs 52
2.2.8. Invasion assays 54
2.2.9. *Anoikis* assays 55
2.2.9.1. Analysis of cellular response to *anoikis* 56
2.2.9.2. Analysis of EVs on cellular response to *anoikis* 56
2.2.10. *In vitro* vasculogenesis and angiogenesis 56
2.2.11. *In vivo* distribution of EVs 57
2.2.12. Zymography 57
2.2.13. qPCR 58
2.2.14. Statistical Analysis 59

2.3. Results 60
2.3.1. EVs were successfully isolated from Hs578T and Hs578Ts(i)$_8$ cells and interact with secondary cells 60
2.3.2. Hs578Ts(i)$_8$ cells show increased proliferation and wound healing capabilty compared to its parent, less aggressive variant, Hs578T cells 62

2.3.3. Hs578Ts(i)$_8$ EVs increase the aggression of it's parental isogenic variant, Hs578T cells 63
2.3.4. Hs578Ts(i)$_8$-EVs increase the growth rate of recipient cells 65
2.3.5. Hs578Ts(i)$_8$-EVs increase the motility of recipient cells 66
2.3.6. Hs578Ts(i)$_8$–EVs increase invasive potential of recipient cells 68
2.3.7. EVs released from MDA-MB-231, another TNBC cell line, increase invasive potential of recipient cells 69
2.3.8. EVs confer *anoikis* sensitivity/resistance to secondary cells, representing innate characteristics of their cells of origin 70
2.3.9. Hs578Ts(i)$_8$-EVs compared to Hs578T-EVs stimulate greater vasculogenesis and angiogenesis 71
2.3.10. *In vivo* distribution of TNBC EVs 73
2.3.11. MMP-2 and MMP-9 are not transported in substantial quantities *via* Hs578T- or Hs578Ts(i)$_8$-EVs 77

2.4. Discussion 79

2.5. Conclusion 85

CHAPTER 3 ..... **86**

3. ABSTRACT **87**

3.1. Introduction 90

3.2. Materials and Methods 97
3.2.1. Cell culture 97
3.2.2. Extracellular vesicle isolation 97
3.2.3. Immunoblotting 97
3.2.4. Transmission electron microscopy 97
3.2.5. Isolation of total RNA from cells and EVs 97
3.2.6. Taqman low density array for global miRNA profiling of cells and EVs 99
3.2.6.1. Reverse transcription of miRNA 99
3.2.6.2. Pre-amplification 100
3.2.6.3. Performing TLDA real time assay 101
3.2.6.4. Analysing TLDA results 102
3.2.7. qPCR validation of miRNA expression 103
3.2.8. microRNA transfection of Hs578Ts(i)$_8$ cells 104
3.2.9. Immunoblotting transfected cells 105
3.2.10. Analysing growth rates of transfected cells 105
3.2.10.1. Acid Phosphatase method for assessing cell growth 106
3.2.11. Analysing migration and invasion rates of transfected cells 106
3.2.12. Analysing effect of miR-134 on apoptosis inducted by cisplatin treatment 107

3.2.12.1. 10X BB solution recipe 107
3.2.13. Assessing effects of miR-134 manipulation in association with anti-Hsp90 compounds 108
3.2.13.1. Determining the IC_{50} of Hs578Ts(i)$_8$ cells to 17-AAG and PU-H71 108
3.2.13.2. Assessing effects of miR-134 manipulation in association with anti-Hsp90 compounds 108
3.2.14. Isolation of EVs from transfected cells 109
3.2.15. qPCR of transfected cells and EVs 109
3.2.16. Treating cells with transfected EVs 110
3.2.16.1. Treating Hs578Ts(i)$_8$ cells for immunoblotting 110
3.2.16.2. Treating Hs578Ts(i)$_8$ cells for proliferation analysis 110
3.2.16.3. Treating Hs578Ts(i)$_8$ cells for migration analysis 110
3.2.16.4. Treating Hs578Ts(i)$_8$ cells for invasion analysis 111
3.2.16.5. Treating Hs578Ts(i)$_8$ cells for cisplatin-induced apoptosis analysis 111
3.2.16.6. Treating Hs578Ts(i)$_8$ cells for response to Hsp90 inhibitors 111
3.2.17. Statistical and bioinformatical analysis 112
3.2.18. Isolation of DNA from cells and EVs 112
3.2.19. Quantification of DNA by Qubit 113
3.2.20. Detection of single nucleotide polymorphisms (SNPs) by mass spectroscopy – Sequenom 113
3.2.20.1. PCR step 115
3.2.29.2. Shrimp alkaline phosphatase (SAP) reaction 116
3.2.20.3. Primer extension (iPLEX) reaction 117
3.2.20.4. Salt adduct removal step 118
3.2.20.5. Mass spectroscopy of samples 118
3.2.20.6. Validation 118

3.3. Results 119
3.3.1. EVs were successfully isolated from Hs578T and Hs578Ts(i)$_8$ cells 119
3.3.2. RNA was successfully isolated from Hs578T and Hs578Ts(i)$_8$ cells and their EVs 120
3.3.3. Endogenous control selection from TLDA analysis 121
3.3.4. TLDA analysis of miRNAs suggests that miRNA content is conserved in EVs . 123
3.3.5. miR-451, miR-122 and miR-142 are enriched in EVs compared to cells 125
3.3.6. TLDA analysis of miRNA presence indicates that miRNA levels are reduced in more aggressive TNBC cells and EVs compared to non-aggressive counterpart 127
3.3.7. miRNAs are expressed at significantly altered levels in Hs578Ts(i)$_8$ cells and EVs versus Hs578T cells and EVs respectively 129
3.3.8. Eighty-three miRNAs are commonly down-regulated in both Hs578Ts(i)$_8$ cells and EVs 132
3.3.9. The ten most substantially down-regulated miRNAs in Hs578Ts(i)$_8$ cells and their EVs originate from the14q32 locus 134

3.3.10. qPCR validated that miR-370, miR-134, miR-889 and miR-376c are all significantly down-regulated in Hs578Ts(i)$_8$ cells and EVs compared to Hs578T cells and EVs 136
3.3.11. Transient transfection of Hs578Ts(i)$_8$ cells with miR-370 successfully reduces invasion and migration; independent of Smoothened (SMO) 139
3.3.12. STAT5B and Hsp90 are increased in Hs578Ts(i)$_8$ cells 141
3.3.14. Transient transfection of Hs578Ts(i)$_8$ cells with miR-134 successfully reduces the levels of STAT5B, Hsp90 and Bcl-2 in Hs578Ts(i)$_8$ cells. 142
3.3.15. miR-134 transfection reduces the proliferation, invasion and migration of Hs578Ts(i)$_8$ cells 144
3.3.16. miR-134 augments cisplatin-induced apoptosis 145
3.3.17. Effect of miR-134 compared to currently effective anti-Hsp90 molecules 147
3.3.18. miR-134 positive EVs reduce the expression of STAT5B and Hsp90 150
3.3.19. miR-134 enriched EVs reduce the levels of migration and invasion of Hs578Ts(i)$_8$ cells. 152
3.3.20. miR-134-enriched EVs do not significantly alter cisplatin-induced apoptosis 153
3.3.21. miR-134-enriched EVs significantly increase the sensitivity of Hs578Ts(i)$_8$ cells to 17-AAG and PU-H71 154
3.3.22. dsDNA is present in Hs578T and Hs578Ts(i)$_8$ EVs 156
3.3.23. PHLPP2 is mutated in Hs578T and Hs578Ts(i)$_8$ cells and EVs 157
3.3.24. HRAS is mutated in Hs578T and Hs578Ts(i)$_8$ cells but not in their EVs 159
3.3.25. TP53 is mutated in Hs578Ts(i)$_8$ EVs only 161
3.3.26. Summary of SNP genotyping results 163

3.4. Discussion 164
3.4.1. miRNA in EVs and cells 164
3.4.2. DNA in EVs 174

3.5. Conclusion 177

CHAPTER 4 178

4. ABSTRACT 179

4.1. Introduction 182

4.2. Materials and Methods 186
4.2.1. Serum specimens 186
4.2.2. Isolation of EVs from serum specimens 191
4.2.3. Immunoblotting 191
4.2.4. Cell culture 192
4.2.5. Proliferation assay 192
4.2.6. Migration assay 192

4.2.7. Invasion Assay 193
4.2.8. Isolation of total RNA from serum derived EVs 193
4.2.9. Assessment of miRNA expression in breast cancer tumours 193
4.2.10. Real-time quantitative reverse-transcription PCR 194
4.2.11. Normalisation of miRNA levels in serum EVs 196
4.2.12. Statistical analyses 196

4.3. Results 197
4.3.1. EVs were isolated from control and patient sera 197
4.3.2. EVs from breast cancer sera increase cellular proliferation 198
4.3.3. EVs from breast cancer sera increase cellular motility 200
4.3.4. EVs from breast cancer sera increase the invasive capacity of HCC1954 and SKBR3 cells 202
4.3.5. EVs derived from breast cancer sera are enriched in total RNA 205
4.3.6. MammU6, miR-16, RNU44 and RNU48 are not effective endogenous controls for serum-EV miRNA analysis 207
4.3.7. miR-134 is significantly down-regulated in breast tumours, compared to normal tissue, and breast-cancer sera-EVs, compared to age-matched control sera-EVs. 209
4.3.8. miR-370 is significantly down-regulated in breast tumours, compared to normal tissue, and breast-cancer EVs, compared to age-matched control EVs. 213
4.3.9. miR-376c is significantly down-regulated in breast tumours, compared to normal tissue, and breast-cancer EVs, compared to age-matched control EVs. 217
4.3.10. Analysed together, miR-370 and miR-376c are vastly reduced in breast cancer serum EVs 221
4.3.11. Levels miR-134, miR-370 and miR-376c in serum EVs from stage 1, 2 and 3 breast cancers compared to age-matched healthy control sera-EVs 224
4.3.12. miR-889 and miR-655 are not significantly altered in TNBC derived sera-EVs 228

4.4. Discussion 230

4.5. Conclusion 235

CHAPTER 5 237

5. FINAL DISCUSSION AND CONCLUSIONS 237

5.1. Discussion 238

5.2. Conclusion 242

5.3. Future directions 243
5.3.1. Do Hs578Ts(i)$_8$ EVs increase cellular movement *in vivo*? 243

5.3.2. Can TNBC derived EVs influence the phenotypes of normal cells 244
5.3.3. More in-depth investigating using a larger panel of TNBC cell lines 244
5.3.4. Is miR-134 a potential tumour suppressor in other breast cancer subtypes? 244
5.3.5. Relevance of miR-370 and miR-376c as tumour suppressors 244
5.3.6. Assessing the relevance of miR-134 *in vivo* 245
5.3.7. Further investigation of the ability of EVs to carry miRNA therapeutics 245
5.3.8. Is total serum a reliable approach to circulating miRNA biomarker discovery? 246
5.3.9. Relevance of PHLPP2 mutation in TNBC-EVs 246
5.3.10. Relevance of TP53 mutation Hs578Ts(i)$_8$ TNBC-EVs 247
5.3.11. Relevance EV enclosed DNA mutations in breast cancer 247

6. REFERENCES 248

APPENDIX I 265

A: List of all genes and SNPs analysed in cells and EVs 266

B: Individual fold change values for miRNAs in Hs578Ts(i)$_8$ cells and their EVs, compared to Hs578T cells and their EVs 274

C: C_T values obtained as part of miR-134, miR-370 and miR-376c expression in sera EVs 283

APPENDIX II 286

PUBLICATIONS, PRESENTATIONS AND AWARDS 286

Research articles 287

Book chapter 287

Published abstracts 287

Awards 289

Local meetings, national and international conference presentations 289
Oral presentations 289
Poster presentations 291
Senior sophister student project supervision 291
September 2013-October 2013 291
September 2012-October 2012 291
September 2011-October 2011 291

Table of Figures

Figure 1.1: Frequency of cancer incidents in Ireland. 4
Figure 1.2: The process of primary tumour development, invasion and metastasis, emphasising commonly observed metastases in breast cancer. 7
Figure 1.3: Differences between normal breast tissue structures and abnormal structure in tumours during invasion 9
Figure 1.4: miRNA biogenesis and function 15
Figure 1.5: Cellular formation and release of EVs 23
Figure 1.6: Schematic of exosome production by the ubiquitinisation of surface proteins 25
Figure 1.7: Formation of MV by membrane budding. 26
Figure 1.8: Interaction of EVs with secondary cells. 27

Figure 2.1: A model for the selection of more invasive subclones using BD Matrigel™ invasion chambers. 45
Figure 2.2: Flow diagram illustrating the process of EV isolation from CM of cells 47
Figure 2.3: Wound healing assay set up to determine cellular motility/migration 53
Figure 2.4: Transwell chamber invasion assay set up. 54
Figure 2.5: *Anoikis* assay set up. 55
Figure 2.6: Successful EV isolation from Hs578T and Hs578Ts(i)$_8$ conditioned medium 61
Figure 2.7: Hs578Ts(i)$_8$ cell grow faster and have increased proliferation and migratory ability, as analysed by wound healing assay, compared to Hs578T cells. 62
Figure 2.8: EVs from the more aggressive, Hs578Ts(i)$_8$ variant, increases the aggressiveness of parental Hs578T cells, versus Hs578T EVs 64
Figure 2.9: Effect of 2μg of Hs578T and Hs578Ts(i)$_8$ derived EVs on the proliferation rates of SKBR3, MDA-MB-231 and HCC1954 cells 72 hrs post EV treatment. 66
Figure 2.10: Effect of Hs578T and Hs578Ts(i)$_8$ derived EVs on the motility of SKBR3, MDA-MB-231 and HCC954 Cells, as determined by wound healing assay. 67
Figure 2.11: Effect of Hs578Ts(i)$_8$-derived EVs on the invasive potential of Hs578T cells, as analysed by ECM coated 8μm pore size 24-well transwell chambers. 68
Figure 2.12: Effect of MDA-MB-231-derived EVs on the invasive potential of SKBR3 cells. 69
Figure 2.13: Characterisation of Hs578T and Hs578Ts(i)$_8$ *anoikis* resistance and the effect of Hs578T and Hs578Ts(i)$_8$ derived EVs on the *anoikis* resistance of SKBR3 cells, performed using poly-HEMA/EtOH coated 24-well plates 71
Figure 2.14: Hs578Ts(i)$_8$-EVs compared to Hs578T-EVs stimulate greater vasculogenesis/angiogenesis. 72
Figure 2.15: In vivo distribution of EVs 24 hrs post injection 74
Figure 2.16: In vivo distribution of EVs 48 hrs post injection 76
Figure 2.17: MMP-2 or MMP-9 in EVs is apparently not substantial contributor to secondary cell invasion. 78
Figure 2.18: Effects of EVs in TNBC metastasis. 81

Figure 3.1: Sequenom MassARRAY MALDI-TOF apparatus. 94
Figure 3.2: RNeasy spin column apparatus. 98
Figure 3.3: Loading TLDA card ports. 102
Figure 3.4: Schematic representation of the process of iPLEX-MALDI-TOF detection of SNPs 114
Figure 3.5: Isolation of EVs from CM of Hs578T and Hs578Ts(i)$_8$ cell.s 119
Figure 3.6: Total RNA was isolated from Hs578T and Hs578Ts(i)$_8$ cells and EVs 120
Figure 3.7: C_T values for endogenous controls RNU48, RNU44 and MammU6 in Hs578T and Hs578Ts(i)$_8$ cells. 122
Figure 3.8: Analysis of the miRNA relationship between Hs578T cells and EVs taking C_T values of <35 as present and ≥35 as absent. 123
Figure 3.9: Analysis of the miRNA relationship between Hs578Ts(i)$_8$ cells and EVs taking C_T values of <35 as present and ≥35 as absent. 124
Figure 3.10: miRNAs commonly present in Hs578T and Hs578Ts(i)$_8$ EVs but not detected in their cells of origin. 125
Figure 3.11: miRNA presence differences between Hs578T cells and EVs compared to Hs578Ts(i)$_8$ cells and EVs respectively. 128
Figure 3.12: miRNA expression differences of Hs578Ts(i)$_8$ cells and EVs versus Hs578T cells and EVs. 130
Figure 3.13: Graphical representation of the up- and down-regulated miRNAs in cells and EVs 131
Figure 3.14: Venn diagram analysis illustrating 83 commonly down-regulated miRNAs in both Hs578Ts(i)$_8$ cells and EVs. 132
Figure 3.15: Chromosomal origins of the commonly down-regulated miRNAs found in the Hs578Ts(i)$_8$ cells and EVs. 135
Figure 3.16: qPCR validation of miRNA expressions in Hs578Ts(i)$_8$ cells, compared to Hs578T cells. 137
Figure 3.17: qPCR validation of miRNA expressions in Hs578Ts(i)$_8$ EVs, compared to Hs578T EVs. 138
Figure 3.18: miR-370 slightly reduces the migration and invasion of Hs578Ts(i)$_8$ cells independent of targeting SMO protein levels. 140
Figure 3.19: STAT5B and Hsp90 are increased in Hs578Ts(i)$_8$ cells and EVs. Hs578Ts(i)$_8$ cells. 141
Figure 3.20: miR-134 mimic, compared to NC mimic reduces the expression of STAT5B, Hsp90 and Bcl-2 in Hs578Ts(i)$_8$ cells. 143
Figure 3.21: Effects of miR-134 on proliferation, migration and invasion. 144
Figure 3.22: Cells transfected with miR-134 increased cisplatin induced apoptosis. 146
Figure 3.23: Survival curves for Hs578Ts(i)$_8$ cells to determine their IC_{50} concentrations to 17-AAG and PU-H71 147
Figure 3.24: Effects of miR-134 on anti-Hsp90 treatments. 149
Figure 3.25: miR-134 positive EVs reduce the aggression of Hs578Ts(i)$_8$ cells. 151

Figure 3.26: Effects of miR-134 enriched EVs on migration and invasion. 152
Figure 3.27: miR-134-enriched EVs do not significantly alter cisplatin-induced apoptosis.. 154
Figure 3.28: Effect of miR-134 enriched EVs in combination with anti-Hsp90 compounds. 155
Figure 3.29: DNA is present in EVs. 156
Figure 3.30: Detection of mutated PHLPP2 in all Hs578T and Hs578Ts(i)$_8$ cells and EVs by mass spectrometry..... 158
Figure 3.31: Detection of mutated HRAS in Hs578T and Hs578Ts(i)$_8$ cells but not in their EVs by mass spectrometry..... 160
Figure 3.32: Detection of TP53 mutation in Hs578Ts(i)$_8$ EVs but not in cells by mass spectrometry..... 162

Figure 4.1: EVs were successfully isolated from control and TNBC serum..... 197
Figure 4.2: Breast cancer sera-EVs increase the proliferation of HCC1954 cells, compared to EVs from aged-matched healthy controls. 199
Figure 4.3: Breast cancer derived sera-EVs increase the migration of breast cancer cells. ... 201
Figure 4.4: Breast cancer derived serum EVs increase the invasion of breast cancer cells. .. 203
Figure 4.5: TNBC sera derived EVs increase the invasion of SKBR3 cells. 204
Figure 4.6: Breast cancer derived serum EVs are enriched in miRNA compared to control serum EVs. 206
Figure 4.7: Commonly used endogenous controls are not expressed equally in healthy derived EVs and breast cancer derived EVs 208
Figure 4.8: Compared to normal tissue, miR-134 is present at significantly reduced levels in breast cancer tumours (GSE26659 & GSE40525). 210
Figure 4.9: miR-134 is significantly down-regulated in breast cancer serum derived serum EVs compared to age-matched healthy control sera-EVs 212
Figure 4.10: miR-370 is present at significantly reduced levels in breast cancer tumours compared to normal tissue (GSE26659 & GSE40525). 214
Figure 4.11: miR-370 is significantly down-regulated in breast cancer sera-EVs compared to age-matched control sera-EVs 216
Figure 4.12: miR-376c is present at significantly reduced levels in breast cancer tumours compared to normal tissue (GSE26659 & GSE40525). 218
Figure 4.13: miR-376c is significantly down-regulated in breast cancer sera-EVs compared to age-matched control sera-EVs 220
Figure 4.14: Fold change of miRNA expression for stages 1, 2 and 3 of breast cancer compared to age-matched healthy control sera-EVs. 225
Figure 4.15: Expression of miR-889 and miR-655 in TNBC sera-derived EVs. 229
Figure 4.16: Summary of the major findings in this chapter..... 236

List of Tables

Table 1.1: Validated targets and functions of onco-suppressive miRNAs in TNBC 20
Table 1.2: Validated targets and functions of oncomiRs in TNBC 20

Table 2.1: Components used for reverse transcription 58
Table 2.2: Program used for cDNA synthesis 58
Table 2.3: Master mix ingredients used for qPCR analysis 59
Table 2.4: Program used for qPCR analysis 59

Table 3.1: Master mix components and volumes per reaction 99
Table 3.2: PCR program 100
Table 3.3: Master mix components and volumes per reaction for pre-amplification 100
Table 3.4: Pre-amplification PCR program 101
Table 3.5: Real time PCR components 101
Table 3.6: miRNA fold change of expression calculation using $\Delta\Delta C_T$ method 102
Table 3.7: Master mix preparation for cDNA synthesis 103
Table 3.8: Program used for cDNA synthesis 103
Table 3.9: Drug concentrations used to determine Hs578Ts(i)$_8$ IC_{50} values to anti-Hsp90 compounds 108
Table 3.10: PCR master mix ingredients 115
Table 3.11: PCR Program 115
Table 3.12: SAP Master Mix 116
Table 3.13: SAP Program 116
Table 3.14: Extension Reaction Master Mix 117
Table 3.15: Extension reaction program 117
Table 3.16: miRNAs detected in Hs578T EVs but undetectable in Hs578T cells 126
Table 3.17: miRNAs detected in Hs578Ts(i)$_8$ EVs but undetectable in Hs578Ts(i)$_8$ cells 127
Table 3.18: miRNAs commonly down-regulated in both Hs578Ts(i)$_8$ cells and their EVs compared to Hs578T cells and their EVs respectively 133
Table 3.19: Summary of DNA-SNP genotyping results 163
Table 3.20: Summary of the effects of miR-134 on Hs578Ts(i)$_8$ cells 173

Table 4.1: Serum specimens from ER+ patients used in this chapter (n=23) 187
Table 4.2: Serum specimens from TNBC patients used in this chapter (n=24) 189
Table 4.3: Serum specimens from HER2+ patients used in this chapter (n=4) 190
Table 4.4: Master mix components for reverse transcription 194
Table 4.5: Program used for reverse transcription 195
Table 4.6: Master mix components for reverse transcription 195
Table 4.7: Master mix components for reverse transcription 195
Table 4.8: miRNA fold change of expression calculation using ΔC_T method 196
Table 4.9: Sensitivity of EV-RNA concentrations to discriminate healthy individuals from those with breast cancer 206
Table 4.10: AUC values for miR-134 213
Table 4.11: AUC values for miR-370 217
Table 4.12: AUC values for miR-376c 221
Table 4.13: AUC values for miR-370 and miR-376c in TNBC derived sera-EVs 222
Table 4.14: miRNA levels in EVs from TNBC, ER+ and HER2+ patient sera compared to EVs from sera of age-matched controls 223
Table 4.15: AUC results for miR-134, miR-370 and miR-376c from stages 1-3 227
Table 4.16: AUC values for miR-889 and miR-655 in TNBC serum EVs 229

Table 5.1: Outline of proposed *in vivo* analysis 243

Abbreviations

ADP	Adenosine diphosphate
°C	Degrees Celsius
µg	Micro-gram
µl	Micro-litres
µm	Micro-metres
AGO2	Argonaute-2
AP	Adaptor protein
APAF-1	Apoptotic protease-activating factor 1
APC	Allophycocyanin
ARF6	Adenosine diphosphate-ribosylation factor 6
ATCC	American tissue culture collection
AUC	Area under curve
BACE-1	Beta-secretase 1
BALB/c	Bagg albino
BAX	Bcl-2 associated protein X
BB	Binding buffer
BBB	Blood brain barrier
BCIP/NBT	5-Bromo-4-chloro-3-indolyl phosphate - nitro blue tetrazolium chloride
Bcl-2	B cell lymphoma-2
Bcl-XL	B cell lymphoma extra large
BH3	Bcl-2 homology-3
BM	Basement membrane
BR	Broad range
BRCA1	Breast cancer 1, early onset
BRCA2	Breast cancer 2, early onset
BSA	Bovine serum albumin
$CaCl_2$	Calcium chloride
CCNJ	Cyclin J
CCP	Clathrin-coated pit
cDNA	Complementary deoxyribonucleic acid
CI	Confidence interval
CK2-α	Casein kinase 2, alpha 1
CM	Conditioned medium
CMA	Centre for microscopy and analysis
CNS	Central nervous system
COX2	Cyclooxygenase-2
CpG	Cysteine-phospho-guanine
CREB	cAMP response element-binding protein
CSO	Central statistics office
C_T	Cycle threshold

CTC	Circulating tumour cell
Da	Daltons
DAPI	4',6-diamidino-2-phenylindole
DC	Dendritic cell
dFBS	Depleted-Fetal bovine serum
DFS	Disease free survival
DGCR8	DiGeorge syndrome critical region gene 8
dH_2O	De-ionised water
DISC	Death-inducing signalling complex
DMEM	Dulbecco's modified eagles medium
DNA	Deoxyribonucleic acid
dNTP	deoxyribonucleotide trisphosphate
DRF3	Diaphanous-related formin-3
dsDNA	Double stranded deoxyribonucleic acid
dsRNA	Double stranded ribonucleic acid
ECM	Extracellular matrix
ECO	European cancer observatory
EGF	Epidermal growth factor
EGFR	Epidermal growth factor receptor
EMT	Epithelial-mesenchymal transition
ENPEP	Glutamyl aminopeptidase (aminopeptidase A)
EpCAM	Epithelial cell adhesion molecule
ER	Estrogen receptor
ER+	Estrogen receptor-positive
ERK	Extracellular signal-regulated kinase
ESCRT	Endosomal sorting complex required for transport
ESR1	ER α gene
EtOH	Ethanol
ETS1	Protein C-Ets-1
EU	European Union
EV	Extracellular vesicle
Ex vivo	Latin: Out of the living
FBS	Fetal bovine serum
FOXM1	Forkhead box protein M1
g	G-force
gDNA	genomic-Deoxyribonucleic acid
GDP	Gross domestic product
GEO	Gene expression omnibus
GFP	Green fluorescent protein
GISTs	Gastrointestinal stromal tumours
GW	Glycine/tryptophan

H_2O	DiHydrigen monoxide
HCl	Hydrochloric acid
HEPES	4-(2-hydroxyethyl)-1-piperazineethanesulfonic acid
HER2	Human epidermal growth factor receptor 2
HER2+	Human epidermal growth factor receptor 2-positive
HHT	Homoharringtonine
HMEC	Human mammary epithelial cells
HOXD10	Homeobox D10
HPLC	High-performance liquid chromatography
HRAS	Harvey rat sarcoma viral oncogene
Hrs	Hours
HSG	Human submandibular gland
Hsp	Heat shock protein
HUVEC	Human umbilical vein endothelial cells
i.e.	id est (Latin: That is)
IC_{50}	Half maximal inhibitory concentration
IDC-NOS	Invasive duct carcinoma - not otherwise specified
IHC	Immune-histochemistry
IL-4	Interleukin-4
IL-6	Interleukin-6
ILV	Intraluminal-vesicle
In vitro	Latin: Within glass
In vivo	Latin: Within the living
IVIS	*In vivo* imaging system
kDa	Kilo-Daltons
KRAS	Kirsten rat sarcoma viral oncogene homolog
kV	Kilo-volts
LAMP2	Lysosomal associated membrane protein 2
mABs	Mononclonal antibodies
MACS	Magnetic activated cell sorting
MACS	Modified magnetic activated cell sorting
MALDI-TOF	Matrix-assisted laser desorption/ioniztion - time of flight
MBC	Metastatic breast cancer
MCL-1	Myeloid cell leukeamia-1
MDSC	Myeloid-derived suppressor cells
MEGF9	Multiple epidermal growth factor-like-domains 9
MHC-I	Major histocompatibility complex-1
MHC-II	Major histocompatibility complex-2
Min(s)	Minute(s)
miRNA	Micro ribonucleic acid
ml	Millilitres

MMP	Metrixmetalloproteinase
MOMP	Mitochondrial outer membrane permeabilisation
mRNA	Messenger ribonucleic acid
MS	Mass spectrometry
MSDC	Myeloid-derived suppressor cells
mtDNA	Mitochondrial DNA
MV	Micro-vesicle
MVB	Multi-vesicular body
NaCl	Sodium chloride
NaN_3	Sodium azide
NC	Negative control
NCRI	National cancer registry Ireland
NK	Natural killer
nm	nano-metres
nM	nano-Mole
NMSC	Non-melanoma skin cancer
NOXA	Phorbol-12-myristate-13-acetate-induced protein 1
NS	Non-significant
NSCLC	Non-small cell lung cancer
NT	Non-transfected
ORF	Open reading frame
OS	Overall survival
PACT	Protein kinase R-activating protein
PAGE	Polyacrylamide gel electrophoresis
PARP	Poly-A-ribose-polymerase
PAZ	Piwi/Argonaute/Zwille
PBS	Phosphate buffered saline
PCR	Polymerase chain reactin
pCR	Pathological complete response
PDGF	Platelet-derived growth factor
PELP1	Proline-glutamic acid- and leucine-rich protein 1
PFS	Progression free survival
PHLPP2	PH domain and leucine rich repeat protein phosphatases-2
PI	Propidium iodide
PI3K	Phosphatidylinositol 3-kinase
PIP_2	Phosphatidylinositol 4,5-bisphosphate
PKC	Protein kinase C
PLD	Phospholipase D
Pmel17	Premelanosome protein-17
POL II	RNA polymerase II
POL III	RNA polymerase III

Poly-HEMA	Polyhydroxyethylmethacrylate
PR	Progesterone receptor
PR+	Progesterone receptor-positive
Pre-miRNA	Precursor micro-ribonucleic acid
Pri-miRNA	Primary micro-ribonucleic acid
PS	Phosphatidylserine
PTEN	Phosphatase and tensin homolog
PUMA	p53 upregulated modulator of apoptosis
p-value	Probability value
PVDF	Polyvinylidene fluoride
qPCR	Quantitative polymerase chain reaction
ranGTP	ran-guanosine-5'-triphosphate
RANKL	Receptor activator of nuclear factor kappa-B ligand
RhoC	Ras homolog gene family, member C
RISC	Ribonucleic acid-induced silencing complex
RNA	Ribonucleic acid
ROC	Receiver operating characteristic
RPMI	Roswell park memorial medium
RQ	Relative quantification
RT	Reverse transcription
RVG	Rabies-virus glycoprotein
SAP	Shrimp alkaline phosphatase
SCID	Severe combined immunodeficiency
SDS	Sodium dodecyl sulphate
SDS–PAGE	Sodium dodecyl sulphate-polyacrylamide gel electrophoresis
Sec(s)	Second(s)
SEM	Standard error of mean
siRNA	Small interfering ribonucleic acid
SJH	St. James Hospital
SMAC	Second mitochondria-derived activator of caspases
SMO	Smoothened
SNARE	Soluble N-ethylmaleimide-sensitive factor attachment protein receptor)
SNP	Single nucleotide polymorphism
SOX4	Sry-related HMG box 4
SSB	Single strand break
ssDNA	Single stranded deoxyribonucleic acid
ssRNA	Single stranded ribonucleic acid
STAT	Signal transducer and activator of transcription
STAT5B	Signal transducer and activator of transcription 5B
TARBP2	Trans-activating response RNA binding protein-2
TEM	Transmission electron microscopy

TKI	Tyrosine kinase inhibitor
TLDA	TaqMan low density array
TLR	Toll like receptor
TNBC	Triple negative breast cancer
TNF-α	Tumour necrosis factor - alpha
TP53	Tumour protein 53
TRBP	Trans activating response ribonucleic acid binding protein
Tris	Tris(hydroxymethyl)aminomethane
Tris-HCl	Tris(hydroxymethyl)aminomethane-hydrochloric Acid
TWIST1	Twist-related protein 1
Ub	Ubiquitin
UCD	University College Dublin
UTR	Untranslated region
V	Volts
VEGF	Vascular endothelial growth factor
Vol.	Volume
Vps	Vacuolar protein sorting
w/v	Weight per volume
XIAP	X-linked inhibitor of apoptosis
YLL	Years of lost life
ZEB1	Zinc finger E-box binding homeobox 1
ZEB2	Zinc finger E-box binding homeobox 2
$\Delta\Delta C_T$	Delta-delta Cycle-threshold

Chapter 1: Introduction

The influences of extracellular-vesicles and microRNAs in breast cancer progression and metastasis

1. Abstract

Cancer is the second leading cause of death in the world, after diseases affecting the circulatory system. Excluding non-melanoma skin cancer, breast cancer is the most commonly diagnosed cancer among women in Ireland, accounting for one third of all invasive female cancer diagnosed. Metastatic breast cancer (MBC) is responsible for the second most common cause of cancer deaths in women, after lung cancer. Of the breast cancer subtypes, triple-negative breast cancers (TNBC) are the most aggressive.

TNBC is classified by lack of ER, PR and HER2 expression. TNBCs are responsible for 15-20% of breast cancer diagnoses, yet are responsible for a disproportionate number of MBCs and fatalities. With no targeted treatments available for TNBC, this subtype has been left behind from advances in targeted breast cancer therapy. There remains an urgent unmet clinical need to discover targeted therapies to effectively treat TNBC. Investigating molecular mechanisms involved in TNBC progression and metastasis is hoped to lead researches into discovering effective target sites for therapeutic intervention. Once such mechanism involved in cancer progression is microRNA (miRNA) dysregulation.

Recently, the field of miRNA research has exploded, with the consistent observations that miRNA dysregulation in cancer is responsible for a plethora of metastatic characteristics. Additionally, they pose as attractive molecules for use as therapeutics. However, mechanisms for miRNA encapsulation for use as therapeutics have been unstable *in vivo* due to detection by the immune system. The use of naturally occurring membrane vesicles (extracellular vesicles) is showing much promise for use as miRNA delivery systems due to their apparent targeting capabilities and immunological inertness.

Extracellular vesicles (EVs) are actively shed from most cells *in vitro* and their presence has been observed in almost all biological fluids analysed, suggesting broad bioactivity *in vivo.* As their bioactive contents tend to greatly correlate with their cells of origin, they have been shown to be responsible for increasing cancer aggression. Intercepting their oncogenic signals is posing as an attractive mechanism for blood-based biomarkers.

This chapter explores the mechanisms involved in cancer progression and metastasis, with heavy emphasis placed on breast cancer and TNBC metastasis. Specifically, this chapter details the processes involved in cancer establishment and metastasis, while moving on to the involvement of miRNAs in cancer progression, therapeutics and diagnostics. The field of EVs is then explored, providing detailed backgrounds into mechanisms involved in their formation, to their involvement in cancer progression, miRNAs and subsequently how they may be manipulated for use as diagnostics and therapeutics.

1.1 Cancer

Cancer is a group of related diseases characterised by aberrant growth and spread of malfunctioning cells which can be fatal if uncontrolled. Tumours subsequently arise from the aberrant cellular growth to develop tissues of abnormal form and function. Although the exact cellular processes and cause(s) of cancer formation remain elusive, it is known that both external factors, such as tobacco, infectious organisms and radiation, as well as internal factors such as genetic dispositions, immune conditions and metabolic mutation, can greatly predispose individuals to cancer [1].

The National Cancer Registry of Ireland (NCRI) reported 18,500 new invasive cancer cases in Ireland between 2008 and 2010, with 8,316 deaths in 2010. Non-melanoma skin cancer (NMSC) is responsible for most cancer cases (7,986/yr), with prostate (3,014/yr), breast (2,767/yr), colorectal (2,387/yr) and lung (2,010/yr) cancers commonly diagnosed also. Figure 1.1 represents the most commonly diagnosed cancers in Ireland [2].

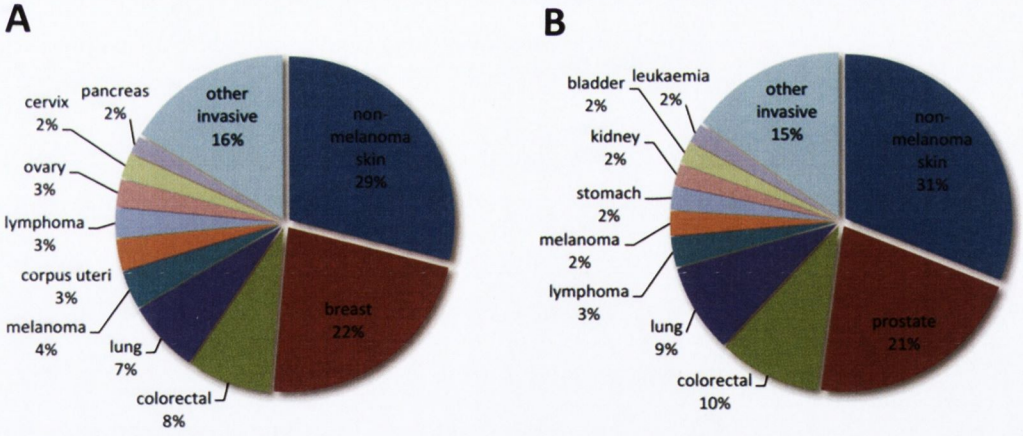

Figure 1.1: Frequency of cancer incidents in Ireland.

A: Incidence in females **B:** Incidence in males [2].

1.2. Cancer development, invasion and metastasis

1.2.1. Primary tumour formation

Tumour development and progression is a multi-step process where cancer cells multiply at the site of the first occasion of abnormal uncontrolled cell division. This process, leading to primary tumour mass development, may remain undetected for many years, reaching a size of 10^{10} or 10^{11} cells before becoming noticeable to the patient or physician. Although troublesome,

primary tumours are responsible for only 10% of cancer-related deaths [1] as they can often be effectively treated with surgery and radiation therapy [3]. The remaining 90% of deaths result from metastatic tumours, *i.e.* cancerous growths developing due to circulating tumour cells (CTC) establishing in distant regions [1]. Treatment strategies for metastases are largely ineffective [3].

1.2.2. Apoptosis

Throughout the transition of primary tumour formation to metastatic disease, tumour cells accumulate genetic alterations allowing for increased and inappropriate cell survival and growth. This increased cellular growth is challenged by apoptosis; an ordered process of programmed cell death designed to eliminate malfunctioning and/or damaged cells. It is therefore imperative for the survival of a cancer cells to circumvent apoptosis [4].

Cancer cells are under constant stress and subjected to unprecedented levels of apoptotic signals, yet manage to evade apoptosis by disabling apoptotic pathways [5]. Disruption of the pro- *versus* anti-apoptotic balance in cells can result from the over-expression of anti-apoptotic proteins, such as Bcl-2, or by the down-regulation of pro-apoptotic proteins. In order to overcome cellular stress, cancer cells frequently overexpress members of the Bcl-2 anti-apoptotic family For example, overexpression of Bcl-2 has been shown to protect LNCaP (prostate cancer) cells from apoptosis [6]. Similarly, increased metastatic potential of MCF7 cells (breast cancer) *in vivo* was observed when transfected with Bcl-2 [7]. Bcl-2 and Bcl-XL have also been shown to confer resistance to apoptosis by inhibiting the action of chemotherapeutics. Interestingly, targeting Bcl-2 expression using anti-sense Bcl-2 phosphorothioate oligodeoxynucleotides in BT-474, ZR-75-1 and MDA-MB-231 breast cancer cell lines increased their chemosensitivity to doxorubicin, mitomycin C, paclitaxel and docetaxel [8]. In contrast, Bcl-2 overexpression in MCF7 cells significantly suppressed butyrate-induced stimulation of apoptosis [9]. Such findings solidify the importance of apoptosis, not only in cancer progression, but also in cancer treatment. Interaction of micro RNAs (miRNAs) with apoptotic proteins has also been observed. miR-15 and miR-16 expression has been observed to be inversely correlated with Bcl-2 expression and both

miRNAs have been shown to inhibit the translation of Bcl-2 messenger-RNA (mRNA) in chronic lymphocytic leukaemia to induce apoptosis [10]. Similarly, miR-195, miR-24-2 and miR-365-2 have been shown to inhibit Bcl-2 expression to induce apoptosis in MCF7 breast cancer cells [11].

Malfunctioning p53 also has major implication for impaired apoptosis regulation in cancer cells. Mutation/inactivation of the tumour protein 53 (TP53), a tumour suppressor, occurs is ~50% of cancers [12]. Mutation of the p53 gene has severe knock-on implications for apoptotic pathways due to interference with a number of apoptosis associated proteins, such as: BAX, p53 upregulated modulator of apoptosis (PUMA), phorbol-12-myristate-13-acetate-induced protein 1 (NOXA) and APAF-1 [4].

1.2.3. Angiogenesis

In order to survive and obtain oxygen and vital nutrients for tumour progression, proliferation and later metastasis, the tumour must create its own vascular system, by a process known as angiogenesis. To achieve this, the tumour taps into the body's own pre-existing vascular network. This process occurs when the tumour reaches a few millimetres in diameter, thus inducing the "angiogenic switch", when a vascular system is required for tumour progression. In order to create its very own blood supply network, cancer cells exploit their environment by releasing cytokines and growth factors, such as vascular endothelial growth factor (VEGF), which, in turn, stimulates the proliferation and sprouting of endothelial cells. However, the resulting vascular system is ill-defined and leaky, which causes irregular blood flow [13]. This "leaky" nature of the tumour's vascular system allows for the recruitment of activated platelets, which release angiogenic and permeability factors, thus amplifying the local response by releasing platelet-derived growth factor (PDGF). Perivascular cells are also activated by activated endothelial cells, which allow for a more stable vascular system [14]. Additionally, tumour-associated fibroblasts deposit extracellular-matrix (ECM) proteins and secrete stimulatory factors [15-17]. Inflammatory cells also respond to the tumour presence, by releasing factors that can influence angiogenesis, both positively and negatively [18, 19].

1.2.4. Metastasis

Metastasis represents the beginning of the fatal progression of cancer, where death occurs due to failure of organs at metastatic sites, para-neoplastic syndromes and problems arising from aggressive and systematic anti-cancer therapies [3]. Treatment strategies for metastasis, including chemotherapy, hormonal therapy and radiation typically have limited benefits in metastatic disease and merely offer minimal survival extension [20].

The danger of metastasis can be described using breast cancer metastasis as an example. Primary breast cancer tumours are relatively simple to control and, alone, pose minimal threat, as the female body remains functional without mammary glands, meaning tumour progression can be largely contained by surgery. Once metastasis occurs, more vital body functions are compromised. Upon metastasis to the bones, micro- and macrometastases can cause bone corrosion and skeletal collapse. Metastases to the brain impacts on nervous system, just as lung metastases pose more life threatening situations [1]. A model of primary tumour development to metastatic tumour is outlined in Figure 1.2.

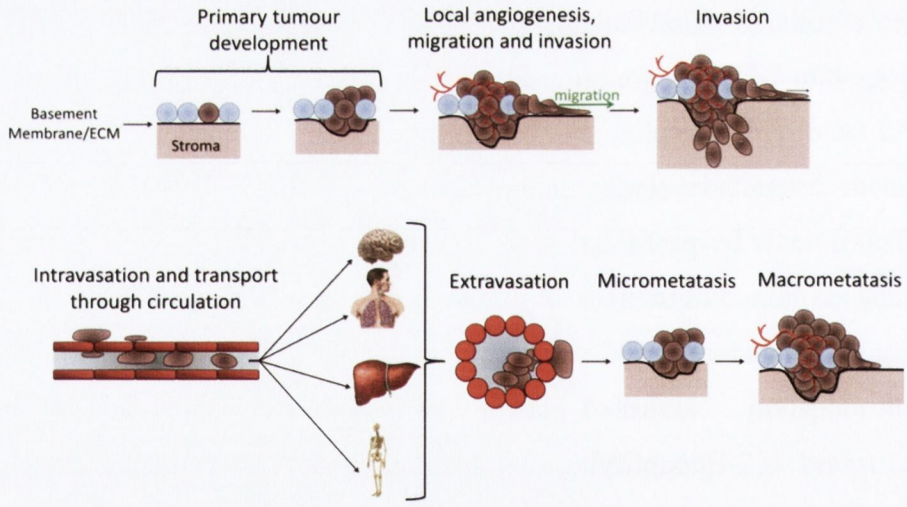

Figure 1.2: The process of primary tumour development, invasion and metastasis, emphasising commonly observed metastases in breast cancer.

Once primary tumours have formed, cells may invade and migrate into the stromal tissues, through the basement membrane/extracellular-matrix (ECM). Entry into the circulatory system (intravasation) allows for CTCs to reach distant sites. While in circulation, CTCs must evade the immune system and resist anchorage independent apoptosis (*anoikis*). CTCs then arrest in the vessels and extravasate into tissues to establish themselves as metastatic tumours, representing micrometastases. Micrometastases grow to subsequently colonise the region as vascularised macrometastases.

1.2.4.1. Invasion and migration

Epithelial cells, such as cells affected in breast cancer (carcinomas), grow in thin sheets, sitting on intricate, deep layers of mesenchymal tissue known as "stroma". Between the cells and stoma there lies an extracellular-matrix (ECM). This is depicted in Figure 1.2 as the basement membrane (BM) which acts as a physical barrier for cancerous cells from the rest of the body. It is on the epithelial side of the BM where primary tumours develop and are considered benign if they have not invaded through the ECM and BM. However, malignancy occurs when this mass of primary tumour cells gain the ability to break through the ECM and BM, invading the local stroma, posing a danger to the rest of the body [1].

Invasion symbolises the onset of the metastatic process and is hallmarked by the alterations in tumour cells adherence to the ECM, proteolytic degradation and remodelling of the surrounding stromal tissue and increased cellular motility/migration, which allows for cells to navigate through the remodelled stromal tissue. The action of proteases, such as matrix-metlloproteinases (MMPs), allow for the increased ability of cells to invade through stromal tissue. This occurs, not only by destruction of the ECM, but it also frees up chemokines and growth factors, activates latent proteins on cell surfaces, and it has been implicated to act as a protective measure in tumorigenesis [21, 22]. In addition, cell growth, survival and inflammation are influenced in a paracrine manner through the action of MMPs. This is because MMPs can induce the release of growth factors, including epidermal growth factor (EGF), tumour necrosis factor-α (TNF-α), VEGF and receptor activator of nuclear factor kappa-B ligand (RANKL) [23].

Tumour cell migration involves the establishment of cell-ECM adhesions in the direction of cell movement, loss of adhesion at the rear end, where attachments are re-established towards the leading end of the cell. This allows for the cell to move/pull in a forward motion through the ECM [20]. Motility has shown to be induced by almost all growth factors *in vitro*. Cellular interaction with the environment through paracrine loops also allow for increased motility and invasion [24]. A diagram, representative of the superficial appearance of milk ducts open to onset of metastasis (invasion) is depicted in Figure 1.3.

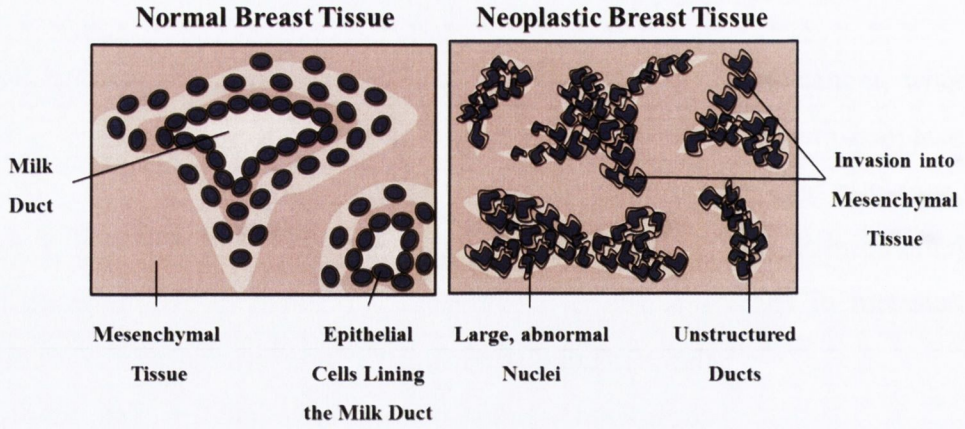

Figure 1.3: Differences between normal breast tissue structures and abnormal structure in tumours during invasion.

In normal breast tissue, the milk duct is lined by epithelial cells (nuclei stained purple), and are surrounded by mesenchymal tissue (or, stroma) consisting of fibroblasts, adipocytes and a collagen matrix. In neoplastic breast tissue, cancer cells which arise from the epithelial cells surrounding the milk ducts have abnormally large, ill-defined nuclei and do not hold a well-structured milk duct. These cells also invade the surrounding mesenchymal tissue [1].

1.3. The biology of breast cancer

Breast cancer is a heterogeneous group of carcinomas initiating in the epithelial cells of the mammary glands, which are morphologically and clinically diverse [25]. Perou *et al.* in 2000 [26] identified four breast cancer sub-classifications:

(i) Normal-like - although this category could be based on contamination of breast cancer cells with cells from healthy tissue.

(ii) Luminal - estrogen receptor positive (ER+) and progesterone receptor positive (PR+).

(iii) Human epidermal growth factor receptor 2+ (HER2+) - overexpression of the HER2 oncogene.

(iv) Basal-like - generally lack ER, PR and HER2 receptors, and are mostly classified as triple-negative breast cancer (TNBC) [26]. However, TNBC and basal-like are not synonymous, as only 70% of TNBCs are basal-like based on gene expression profiling of 142 TNBC patients [27].

These breast cancer subtype findings have been validated using both RNA-based techniques [28-32] and immune-histochemistry (IHC) [33]. Each subtype pertains to independent sets of risk factors, treatment regimens and treatment responses [25]. More recently, another subtype, termed "claudin low" has been added to this list [30]. However, in the clinical setting, breast

cancers are typically defined by their expression, or lack of expression, of the hormone receptor proteins ER, PR, and the oncogene HER2/neu, which may allow for personalised treatments. Targeted treatments generally consist of targeted antibodies or small molecules. The use of tamoxifen and aromatase inhibitors are established endocrine therapeutic approaches for ER+ breast cancers [34-36]. Success has been found by targeting the HER2+ oncogene in HER2 overexpressing breast cancers by trastuzumab (Herceptin) (humanised antibody) and lapatinib (small molecule inhibitor). Due to their lack of expression of ER, PR and neither over-expression nor amplification of HER2, TNBCs remain without a targeted treatments.

1.3.1. The biology of TNBC

TNBC is a highly aggressive, heterogeneous breast cancer subtype which is responsible for 15-20% of breast cancer cases [37]. It has been reported that TNBC is associated with rapidly advancing disease, higher incidents in younger women (< 40 yrs), women of African-American and Hispanic descent and individuals living in lower socioeconomic regions. Occurrences of TNBC is associated with a shorter time to relapse and death, with TNBC diagnoses commonly occurring at a later stage after visceral metastasis [38]. Local relapse commonly occurs between year one and three post-diagnosis [39]. TNBCs also present more commonly as interval cancers. Large primary tumours are seen at this stage, but low incidents of lymph node positivity are observed in relation to the size of the tumour [40]. Adding to the severity of TNBC, metastases tend to be more aggressive than observed in other subtypes, tending to colonise the lungs, brain [41] and less frequently to the bones [42]. Metastases to the central nervous system (CNS) are regularly observed, which may be due to either overall poor disease control, or an innate susceptibility of TNBCs to metastasise to the CNS [27]. As TNBC tend to show sensitivity to standard chemotherapeutic treatments when diagnosed and treated at an early stage, it is imperative that reliable diagnostic markers are discovered for the early diagnosis of TNBC [43].

1.3.2. TNBC is a heterogeneous subtype

Basal-like breast cancers are often and inaccurately mistaken for TNBCs due to distinctive overlap between the two subtypes, yet they are not the same [44],

although TNBCs are predominantly basal-like (~70%) [27]. Attempts are being made to further sub-classify this already sub-classification of breast cancer. TNBC gene expression profiles from 21 breast cancer data-sets, amounting to 587 TNBC tissue specimens, were analysed in 2011 [45], from which six TNBC subtypes were identified based on their intrinsic gene profiles:

(i) Basal 1
(ii) Basal 2
(iii) Mesenchymal
(iv) Mesenchymal stem cell-like
(v) Immunomodulatory
(vi) Androgen pathway enriched.

Basal 1 and basal 2 sub-groups had comparatively greater expression of genes associated with cell cycle and DNA damage response. Mesenchymal and mesenchymal stem cell-like sub-groups had amplified expression of epithelial-mesenchymal transition (EMT) genes. The immunomodulatory sub-group was observed to be enriched for gene ontologies in immune cell processes, whereas androgen pathway enriched, as the name would suggest, have higher levels of genes involved in androgen receptor signalling [45].

Similarly, histopathological analysis and gene expression profiles of 97 TNBC specimens determined that TNBCs are classified as basal-like based on their gene expression profile, but hierarchical clustering identified five distinctly different TNBC subtypes [46]. TNBC subtypes can also be classified based on histological analysis. Histologically, invasive ductal carcinoma, not otherwise specified (IDC-NOS) accounts for the majority of TNBCs. Relatively rare histologies also fall under the TNBC bracket, including adenoid cystic carcinoma, apocrine carcinoma and medullary and metaplastic carcinomas [44].

The claudin-low subtype, which is defined by its lack of expression of claudin genes and characterised by its stem cell-like nature; increased ability to invade into stromal tissue; and the ability to infiltrate immune cells, appear to be triple-negative also [47, 48]. Adding to the complexity of TNBCs, copy number variations are commonly observed in TNBC, compared to other breast cancer subtypes [49]. High frequency copy numbers of phosphatase and tensin

homolog (PTEN), VEGF and epidermal growth factor receptor (EGFR) have been identified in TNBC [50].

Considerable connections have been made between TNBCs and breast cancer 1 (BRCA1) early onset - a gene coding for tumour suppressive proteins - mutations, DNA repair, transcription and cell cycle regulators [51], which have been observed in 50% of TNBCs [52, 53]. As dysfunctional BRCA1 interferes with the repair of double-strand DNA breaks, this allows for the opportunity to treat TNBCs with chemotherapies and poly-A-ribose-polymerase (PARP) inhibitors [54], as discussed further in Section 1.3.3.

1.3.3. TNBC treatment options

TNBC tend to show relative sensitivity and greater pathological complete response (pCR) to neoadjuvant anthracycline-based chemotherapeutic treatments than ER+ breast cancers [53]. This can result in a better prognosis for a subset of TNBC patients compared to those with other breast cancer subtypes [42]. One such neoadjuvant chemotherapeutic routinely used for TNBC is cisplatin. Cisplatin is a DNA cross-linking agent, shown to be effective in treatment of TNBCs. A study of 25 patients, treated with four cycles of cisplatin at 75 mg/m^2 every 21 days, yielded a pCR rate of 72% [55].

Although chemotherapy can show some levels of success, residual disease commonly remains in TNBC patients post-neoadjuvant treatment. Greater frequencies of relapse are observed which is likely to be due to the lack of targeted treatment available [56] and, for patients who do not achieve pCR, relapse rates are high contributing to a worse survival rate compared to luminal breast cancers [27]. There appears to be a group of TNBCs who respond well, and another group who show no benefit; suggesting that developing optimised chemotherapeutic strategies for TNBC patients would be of substantial importance. However, identification of patients who are intrinsically responsive/resistant has not yet been possible [53].

Potential targeted therapy approaches to treating TNBCs are PARP inhibitors. PARPs have been observed to be upregulated in many cancers, including TNBC [57]. PARP inhibits DNA repair in tumour cells and acts to bind the exposed ends of damaged DNA to recruit enzymes for repair of single strand

breaks (SSBs). Inhibition of PARP leads to the accumulation of SSBs which signal to cancel cell replication and leads to DNA double strand break [58]. Iniparib and olaparib are two of the most clinically evaluated PARP inhibitors in TNBC and have shown to increase progression free survival (PFS) and overall survival (OS) of TNBC [59].

TNBCs are likely to express EGFR, which acts to stimulate cell replication [58]. Monoclonal antibodies (mAbs), e.g. cetuximab, have been shown to target the extracellular domain of EGFR to hinder ligand-receptor association and prevent EGFR internalisation into the cell. Such mAbs may also act to initiate an immune response to the EGFR expressing cell. Tyrosine kinase inhibitors (TKIs), e.g. gefitinib, have also been developed which target the intracellular domain of EGFR to disable it [60]. Studies are showing that, alone, EGFR inhibitors have low efficacy in TNBC patients but have the potential to improve the efficacy of other agents, such as taxanes [61] and carboplatin [62].

Targeting heat-shock protein (Hsp90) expression is showing promise in TNBC treatment. Hsp90 is an attractive target for breast cancer treatment, as it is required for stabilisation of several proteins involved in breast cancer progression, including ER, HER2, PR [63] and Bcl-2 [64]. In a study on three TNBC cell lines, 1μM PU-H71 (an anti-Hsp90 compound) induced significant cytotoxicity of MDA-MB-468, MDA-MB-231, and HCC-1806 after 72 hrs, which is 5 to 10 times higher than its half maximal inhibitory concentration (IC_{50}) of growth inhibition. PU-H71 also induced substantial apoptosis in these cells. *In vivo* analysis showed 80-90% MDA-MB-468 cell death when tumour bearing mice were treated with 2.5μM PU-H71 for 48 hrs. In addition, high intratumoral PARP cleavage was observed. When treated with 75 mg/kg in the MDA-MB-231 model, PU-H71 induced 100% complete response [65]. These results suggest that targeting Hsp90 expression could have potential in the treatment of TNBC.

1.4 microRNAs

miRNAs, first discovered in 1993 [66], are small (22–25 nucleotide), non-coding RNAs that typically function to halt mRNA translation by binding the 3' un-translated region of target mRNAs [67, 68]. Consequently, miRNAs can act as regulators of cell processes such as apoptosis, differentiation and proliferation [69]. miRNAs account for 1-5% of the human genome and can regulate at least 30% of protein coding genes [70-72]. As tumours all have distinct miRNA profiles [73-75], there lies much hope in correlating these signatures with cancer diagnosis, prognosis, treatment response prediction as well as allowing for the potential discovery of tumour suppressing miRNAs.

1.4.1 miRNA biogenesis

miRNA biogenesis begins in the nucleus, where transcription is commonly mediated by RNA polymerase II (POL II) [72, 76] or, less frequently, by RNA polymerase III (POL III) [77]. Transcription produces long, primary-miRNA (pri-miRNA), which is then processed by the "microprocessor complex" in the nucleus. The microprocessor complex is comprised of the ribonuclease III-type endonuclease (Drosha), along with the double-stranded RNA-binding protein DiGeorge syndrome critical region gene 8 (DGCR8). DGCR8 recognises the pri-miRNA at the ssRNA-dsRNA junction to ensure Drosha-mediated cleavage, producing a precursor miRNA (pre-miRNA) of ~60-70 nucleotides in length [72]. The pre-miRNA must be chaperoned out of the nucleus for processing. To do this, pre-miRNA complexes with exportin-5 and ran-guanosine-5'-triphosphate (ranGTP) [72]. This subsequently comes in contact with dicer, protein kinase R-activating protein (PACT) and the human immunodeficiency virus trans-activating response RNA-binding protein (TRBP) [78]. Initiation of binding is induced by dicer recognition (by its Piwi/Argonaute/Zwille (PAZ) domain) of the 2 nucleotide 3'overhang of the pre-miRNA and cleavage is mediated by dicer's catalytic site. This produces a double stranded miRNA duplex [79]. This miRNA-miRNA duplex is then transported to the Ago (recruited by TRBP) protein within RNA-induced silencing complex (RISC). Cleavage of the pre-miRNA by dicer results in mature miRNA of ~22 nucleotides in length, one strand of which will become the functional mature miRNA. [80]. When two mature miRNAs originate from

the same pre-miRNA, they are termed -3p (from the 3' arm) or 5p (from the 5' arm) [81]. Diagrammatic representation of miRNA biogenesis and subsequent function is detailed in Figure 1.4 below.

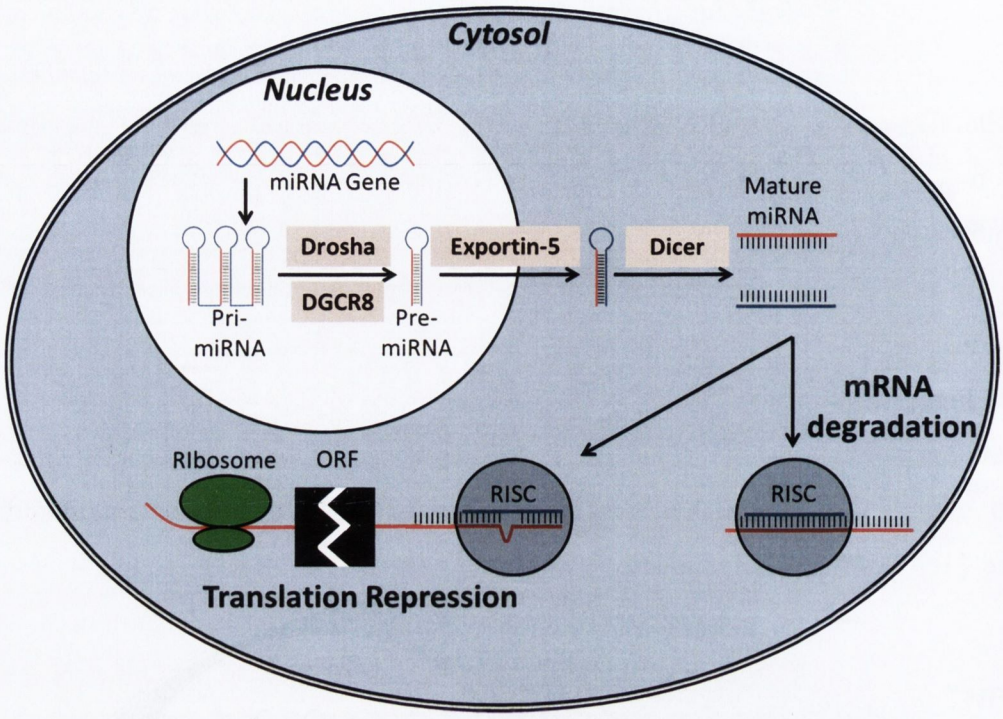

Figure 1.4: miRNA biogenesis and function.

miRNA biogenesis is initiated in the nucleus where pri-miRNA in transcribed. Pri-miRNA is then cleaved by Drosha and DCCR8, to form pre-miRNA. Pre-miRNA is transported from the nucleus by Exportin-5, where Dicer initiates double-stand cleavage to yield mature miRNA. Mature miRNA can mediate mRNA degradation or halt mRNA translation by targeting sites in the open reading frame (ORF).

1.4.2 miRNAs in breast cancer

miRNAs hold much interest with regards to cancer progression, as they may act as either tumour suppressors (oncosuppressor miRNAs), or as oncogenes (oncomiRs), depending on the functions of their target mRNA(s) [82]. Additionally, miRNA polymorphisms affecting miRNA interactions have been identified; both in the miRNAs and in their mRNA target regions (see Section 1.4.2.3). These have been associated with increased risk of breast cancer incidence. Adding to the complexity of miRNAs in cancer, altered miRNA expression has been attributed to differential expression and epigenetic regulation of miRNA processing enzymes [83].

1.4.2.1 miRNA signatures in breast cancer

Attempts have been made to classify breast cancer subtypes based on their miRNA signatures. Since the first analyses of miRNAs were performed in 2005 on breast cancer specimens compared to healthy tissues [84], numerous studies have emerged attempting to determine clinical outcomes based on miRNA signatures. These studies found that basal and luminal breast cancers show differentially expressed miRNAs [85, 86] and that ER, PR and HER2 subtypes could be classified based on miRNA profiles [56]. Hierarchical clustering analysis of miRNA profiles from lymph node negative breast cancers showed that four main subgroups can be identified (ER PR and HER2), with TNBC being the most distinctive miRNA signature [87, 88]. It has been implicated that there is a global downregulation of miRNAs in TNBC [89].

1.4.2.2 Mechanisms and implications of miRNA dysregulation in breast cancer

The significance of miRNA dysregulation in cancer progression may be explained by the observation that 50% of all miRNAs discovered so far are derived from fragile regions in the genome; areas associated with tumourigenesis. Additionally, comparative genomic hybridisation analysis in breast cancer determined that 73% of miRNA genes originate from regions commonly affected by copy number variations [90].

miRNAs are frequently observed to be down-regulated in cancer, allowing for the increased translation of oncoproteins. Commonly, silencing of miRNAs occurs through hypermethylation of miRNA-associated cytosine-phosphate-guanine (CpG) islands, and this is also the case in breast cancer. The miR-125b promoter region has been observed to be hypermethylated in invasive breast cancers, allowing for increased Protein C-Ets-1 (ETS1) expression, a miR-125b target gene [91]. miR-335 promotor hypermethylation was observed in MDA-MB-231 and CN34 breast cancer cells, as well as in primary tumours. This has been associated with increased invasion and metastatic colonisation of MDA-MB-231-LM2 cells (aggressive variant of MDA-MB-231 cells) [92].

Hypermethylation is not the only method of miRNA dysregulation, as problems may arise from the process of miRNA biogenesis. Down-regulation of the enzymes involved in miRNA biogenesis has been reported in cancers,

including breast cancer. Dicer has been observed to be down-regulated in breast cancer, and has been reported as a biomarker for primary breast cancer diagnosis [93] and for metastasis [94]. Additionally, a frameshift mutation has been identified in trans-activating response RNA binding protein-2 (TARBP2), which resulted in the reduced efficiency of miRNA processing in colorectal cancer [95]. Frameshift mutations have also been observed in exportin-5 (a protein involved in chaperoning pre-miRNA from the nucleus to the cytoplasm), which prevents its association with pre-miRNA [96]. Interestingly, miRNAs can also influence miRNA biogenesis. For example, miR-103 and miR-107 have been shown to target Dicer to inhibit miRNA processing, which correlated to poor prognosis in breast cancer [97].

1.4.2.3 Implications of miRNA associated polymorphisms

Bioinformatics analysis predicts that there are >20,000 single nucleotide polymorphisms (SNPs) associated with miRNA promoters in humans, meaning that miRNA expressions can be greatly altered due to variants in transcription factor binding sites [98]. The first reported, and most described, SNP affecting miRNAs in breast cancer was reported in 2009, when Hu *et al.* described an SNP affecting miR-196a2 which increased breast cancer susceptibility [99]. Similar findings regarding miR-146a (rs2292832) has been identified and correspond to increased susceptibility to early onset breast cancer [100]. A miR-27a (rs895819) associated SNP has been identified which, apparently, acts to protect against familial breast cancer incidence in people under 50 years of age [101].

Polymorphisms in the target region of miRNA binding have the potential to greatly affect the functionality of the miRNA. Such polymorphisms may result in the incomplete or non-binding of miRNAs to its mRNA target region, preventing mRNA degradation or inefficiently halting mRNA translation and so allowing for the increased expression of oncogenes/tumour suppressing proteins [83]. Such polymorphisms have been shown to be associated with breast cancer, with polymorphisms in the target regions being associated with reduced cancer risk. miRNA associated SNPs may also serve as prognostic indicators [102].

Polymorphisms may also alter the nucleotide sequence of the miRNA binding sites in mRNA. Such a polymorphism has been described in the mRNA of the ER α gene (ESR1) (rs2747648) which prevents the association of miR-453 and seems to reduce the risk of breast cancer [103]. Similarly, a polymorphism has been identified in Kirsten rat sarcoma viral oncogene homolog (KRAS) (rs61764370) in TNBC, which prevents the effective binding of let-7 [104].

1.4.2.4 Functional roles of miRNAs in breast cancer

One of the most interesting roles of miRNAs in cancer is their ability to mediate cancer metastasis [82]. miR-21 was one of the first oncomiRs recognised in breast cancer, where it was observed to be overexpressed, subsequently mediating cell survival and proliferation, as well as amplifying invasion, extravasation and metastasis [105]. miR-21 has been linked to advanced clinical stage, lymph node metastasis and overall poor prognosis [106, 107]. Similarly, miR-10b is one of the most studied miRNAs due to its ability to increase breast cancer invasiveness in the human mammary epithelial cells (HMECs) and SUM14 cell lines, and inhibition of miR-10b reduced MDA-MB-231 invasion. miR-10b expression is regulated by the oncoprotein Twist-related protein 1 (TWIST1), a protein involved in the invasion of cells into stromal tissue. Forced overexpression of miR-10b in SUM149 cells, a non-metastatic breast cancer cell line, resulted in increased tumour size and stromal invasion *in vivo*. The effect of miR-10b can be attributed to its action in targeting the translation of homeobox D10 (HOXD10). This results in the overexpression of the ras homolog gene family member C (RhoC), a pre-metastatic protein suppressed by HOXD10 [108]. Additionally, systemic treatment of mice bearing tumours of 4T1 cells with miR-10b antagomiRs reduced breast cancer metastasis [109]. Furthermore, miR-373 and miR-520c have been shown to increase the aggression of MCF-7 breast cancer cells by suppressing CD44, an adhesion molecule that suppresses tumour metastasis. [110].

Regarding the tumour suppressive nature of miRNAs in breast cancer, miR-335 targets Sry-related HMG box 4 (SOX4) to reduce metastatic potential. [111]. miR-335 has also been shown to reduce the metastatic potential of the neuroblastoma cell lines SK-N-AS, CHP-212 and Kelly [112], as well as

gastric cancer cells (SGC-7901) *in vivo* [113]. Other miRNAs, such as miR-125a, miR-125b [114] and miR-205 [115] regulate important oncogenes in breast cancer, such as HER2 and HER3. miR-205 has been reported to be down-regulated in breast cancers, and its loss is associated with lack of vascular invasion by supressing VEGF-A to interfere with angiogenesis [116]. In addition, miR-205 also negatively regulates invasion of cells into the stromal tissue by targeting zinc finger E-box binding homeobox 1 (ZEB1) and zinc finger E-box binding homeobox 2 (ZEB2) (transcription factors) [117]. The reported functional relevance of miRNAs in TNBC are summarised in Table 1.1 for onco-suppressive miRNAs and Table 1.2 for oncomiRs.

Table 1.1: Validated targets and functions of onco-suppressive miRNAs in TNBC			
miRNA	**Validated Target**	**Biological implications**	**Reference**
miR-200a/b	ZEB1/ZEB2, Suz 12, EphA2	Stimulate the differentiation of mammary epithelial cells	[118]
miR-200c	ZEV1/ZEB2	Inhibit epithelial-mesenchymal transition in MDA-MB-231 cells	[119]
	Meosin; Fibronectin	Inhibit migration in BT579 cells	[120]
	TrkB	Reverse *anoikis* resistance	[120]
miR-205	E2F1; LamC1	Reduce proliferation, tumour growth and cell cycle in MDA-MB-231 and BT579 cells	[121]
miR-203	BIRC5	Reduce proliferation in MDA-MB-231 and MDA-MB-468 cells	[122]
	LASP1	Inhibit migration in MDA-MB-231 and MDA-MB-468 cells	[122]
miR-31	WAVE3; RhoA; Radexin	Reduce metastatic potential *in vivo* using MDA-MB-231 cells	[123, 124]
	PRKCE	Induce apoptosis and increase chemo- and radio-sensitivity in MDA-MB-231 cells	[125]
miR-34a	AXL	Inhibit migration of MDA-MB-231 cells	[126]

Adapted from Table 1, D'Ippolito et al. [56]

Table 1.2: Validated targets and functions of oncomiRs in TNBC			
miRNA	**Validated Target**	**Biological implications**	**Reference**
miR-181a/b	Bim	Inhibit apoptosis in MDA-MB-231 cells	[127]
	ATM	Inhibit DNA double strand repair in MDA-MB-231 cells	[128]
miR-146 and miR-146b-5p	BRCA1	Control BRCA1 mediated proliferation and homologous recombination in MDA-MB-231, MDA-MB-157 and MDA-MB-468 cells	[128]
miR-182	PFN1	Inhibit proliferation, invasion and induce apoptosis in MDA-MB-231 cells	[129]

Adapted from Table 1, D'Ippolito et al. [56]

Understandably, the therapeutic value of miRNAs is being extensively investigated. However, utilising miRNAs therapeutically has encountered problems. Naked miRNA has a short half-life in serum and subsequently accumulates in the kidneys and liver [130, 131]. Additionally, as miRNAs are negatively charged, they have difficulty crossing hydrophobic cell membranes [131]. Vectors, *e.g.* viral vectors, have been developed to encapsulate and deliver miRNAs, but, so far, are not very well tolerated *in vivo* [132]. To overcome such obstacles, research in miRNA therapeutics has advanced with the discovery of extracellular vesicles (EVs) (nano sized membrane vesicles). EVs may act as efficient, alternative methods by which miRNAs can be used as therapeutics [133], and will be discussed in Section 1.5.

1.5 The world of extracellular vesicles

1.5.1 Extracellular vesicles

Extracellular vesicles (EVs) were discovered in two independent studies in 1983 and 1984 when multivesicular bodies (MVBs) from reticulocytes fused with the cell membrane to release nano-sized membrane vesicles [134, 135]. However, their biological significance remained unnoticed until 1996 when they were observed to stimulate the adaptive immune response [136]. Since then, it has been broadly reported that cells actively release EVs into extracellular milieu to mediate intercellular communication by interacting with and transferring their contents from cell-to-cell. These membrane vesicles may originate from two cellular mechanisms; either by cell membrane budding or *via* the endosomal system. This has created two sub-categories of EVs, *i.e.* micro-vesicles (MVs) and exosomes, respectively [137]. Literature typically, but somewhat crudely, differentiate exosomes and MVs based on their size; exosomes being 40-100nm and MVs generally considered as 100-1,000nm in diameter. However, MVs of 100nm can also bud from the cell membrane, and once vesicles have been released their origin cannot accurately be determined, allowing for misinterpretation of the type of vesicle being investigated [138]. For this reason, many researchers working in this area favour the more all-encompassing term, extracellular vesicles (EVs). This thesis is concerned with investigating the relevance of exosomes and MVs collectively in TNBC, so the

term EVs has been selected for use here as the exact cellular mechanism of origin of the vesicles is not priority of interest.

Since their initial description, EVs have been shown to be a product of many more cell types, including T-cells [139], B-cells [136], dendritic cells (DC) [140], platelets [141], mast cells [142], intestinal epithelial cells [143] neuronal cells [144], and Schwann cells [145], as well as single celled eukaryotes [146], and the protozoan parasites. They have been detected in a range of biological fluids, such as breast milk [147], saliva [148], tumour ascites [149], amniotic fluid [150], urine [150] and semen [151], suggesting that their presence has the potential to exert effects on disease progression, and have potential use as disease biomarkers. Detection of EVs in such diverse cells and body fluids has lead researchers to discover that these structures have pathological and physiological relevance [152-156]. More recently, the potential for EVs to be used as vaccines and drug delivery systems [133, 157, 158] is being investigated as well as holding hope for use as vehicles for gene therapy [159].

Through the process of exosomes and MV formation, EVs have been shown to encapsulate a range of cellular components such as miRNAs, transmembrane receptors, cytosolic proteins [154], viruses/prions [160] and DNA [161]. This allows for the horizontal transfer of bioactive molecules to distant sites. This phenomenon particularly interested cancer researchers, who subsequently implicated that exosomes play functional roles in cancer progression [162-165]. As EVs encapsulate a diverse range of bioactive molecules, they may also have important implications for use as minimally-invasive biomarkers, by intercepting their signals in biofluids [166]. Although such studies support a functional role for EVs, their global function, implications in disease progression and potential as therapeutic delivery vehicles have not yet been fully elucidated or utilised.

The processes of both mechanism of EVs release are illustrated in Figure 1.5.

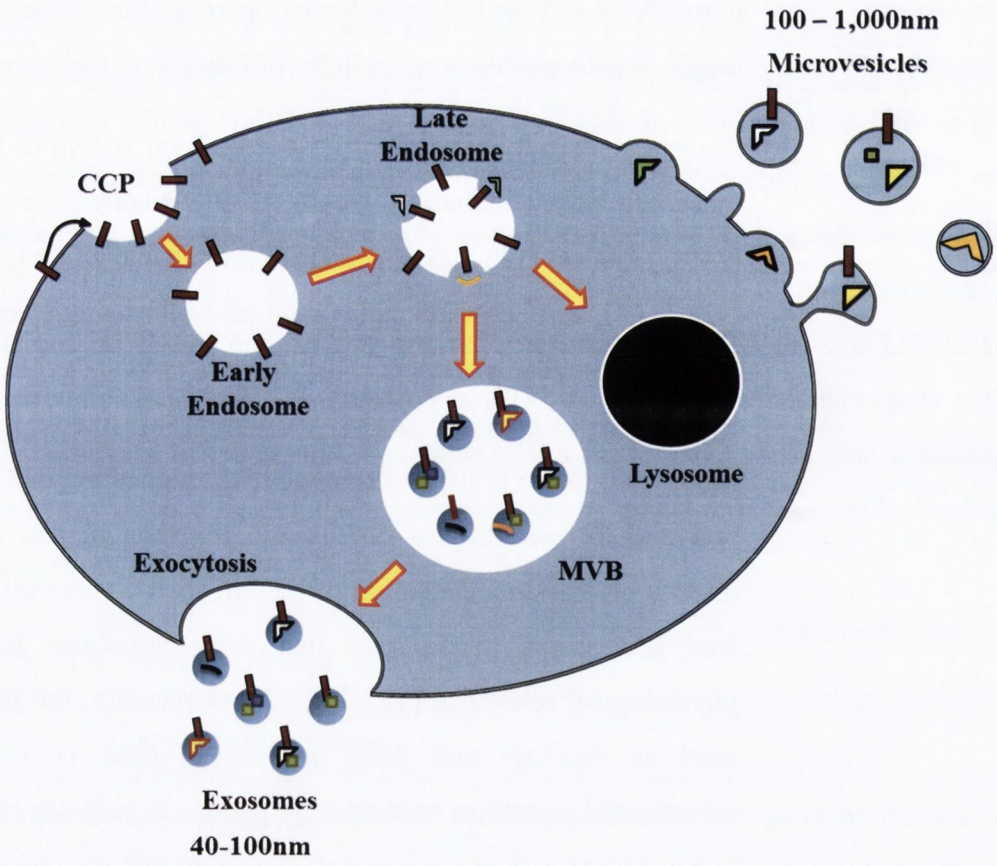

Figure 1.5: Cellular formation and release of EVs.

Exosome formation begins at the cell membrane with the pinching in of the membrane at a clathrin-coated pit (CCP), creating an endosomal-like structure. This process results in the development of intraluminal-vesicles (ILVs) by the inward budding of the limiting membrane of the endosome, which captures bioactive molecules. This matures to form multi-vesicular bodies (MVBs) (endosomes containing many ILVs). The MVB may have two fates (i) transport to a lysosome for degradation or (ii) transport to the cell membrane, to which it fuses and expels the ILVs into the extracellular milieu. Once released, these ILVs are then termed exosomes. MVs on the other hand, are formed by direct budding from the cell membrane, capturing cytosolic fragments within their membranes also.

1.5.1.1 Exosomes formation

Exosome formation begins by monoubiquitinisation of cell-surface receptors inducting internalisation to the cytosol [167, 168]. This process acts as a sorting signal for proteins to be incorporated into MVBs [169]. Similarly, oligoubiquitination has been implicated in the protein sorting process, as well as in increasing the efficiency of MVB sorting [170]. Protein ubiquitination leads to the involvement of the endosomal sorting complex required for transport (ESCRT), which is a major regulator of MVB sorting. It is by the recognition of monoubiquitinated by ESCRT 1, ESCRT 2 and ESCRT 3 that

proteins are carried to, and processed for, inclusion within the MVBs [171]. In order for this process to be in perfect synchronisation, adaptor proteins (AP) recognise the ubiquitinated protein(s), as well as activating the ESCRT, to include the tagged protein for inclusion in ILVs, subsequently to be released as part of an exosome. The ESCRT-ubiquitinated protein complex disassociates by the action of adenosine triphosphate vacuolar protein sorting 4 (Vps-4) [172]. Ubiquitination of proteins, such as Vps-27, is subsequently recognised by the ESCRT, enabling further ESCRTs and TSG101 to initiate Alix. As a result, this system aids packaging of the cargo into the ILVs [173, 174] (see Figure 1.6). Not all proteins, however, are targeted for the inclusion within MVBs by ubiquitination. The transferrin receptor, which is unable to be ubiquitinated, is included independent of ubiquitination. Such proteins are included into the membrane of ILVs based on their intrinsic physical properties and ability to be included into lipid raft structures [175]. Data also suggests that the ESCRT is still involved in transferrin receptor inclusion, despite its inability to be ubiquitinated [176]. Yet, inclusion of the protein premelanosome protein-17 (PmeI17) is both ubiquitin-and ESCRT-independent [177].

In order for MVBs to move to and fuse with the cell membrane, members of GTPases and Rab family members are employed. In addition, alternate observations have been reported in different cell types for the involvement of other molecules. In the K562 erythroleukemia cell line, RAB11 is required for Ca2+ dependent exosome secretion [178]. RAB27A and RAB27B have been shown to act together to release MHC-II exosomes by HeLa-CIITA cells [179] and RAB35 allows for the secretion of LP-enriched exosomes in oligodendroglial cells [180]. Alternatively, WNT bound exosomes have been shown to be secreted through the action of YKT6, a soluble *N*-ethylmaleimide-sensitive factor attachment protein receptor (SNARE) [181].

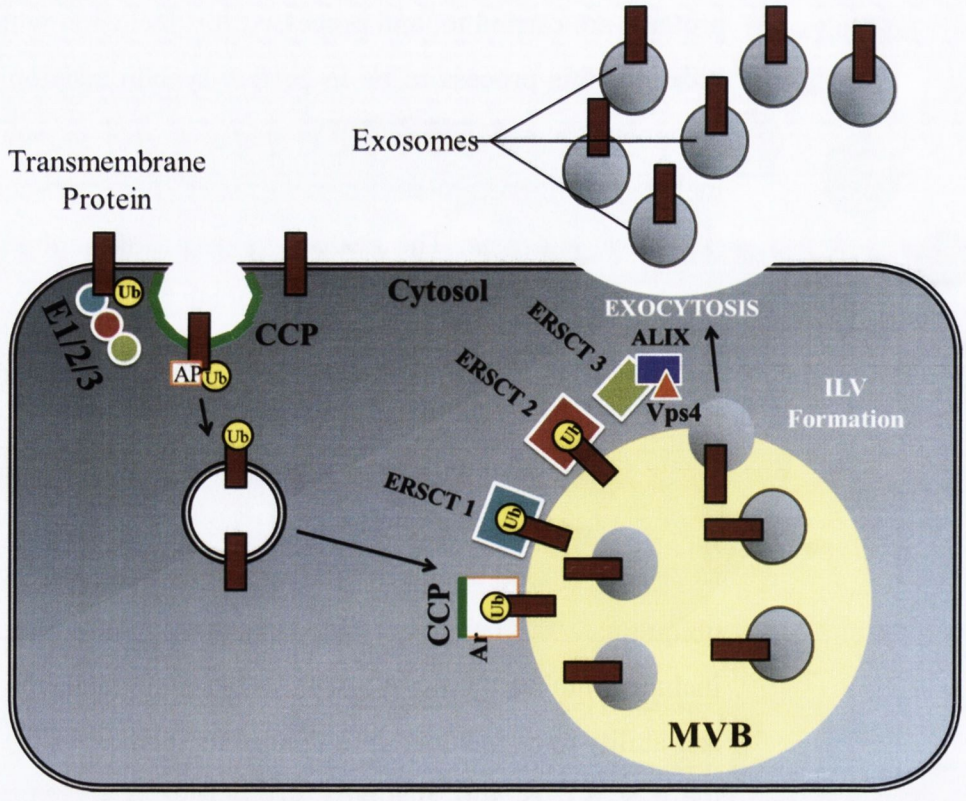

Figure 1.6: Schematic of exosome production by the ubiquitinisation of surface proteins. Legend: Ub, Ubiquitin; E1, Ubiquitin-activating enzyme; E2, Ubiquitin-conjugating enzyme; E3, Ubiquitin-protein ligase; AP, Adaptor protein; CCP, Clathrin-coated pit; ESCRT, Endosomal sorting complex required for transport; Vps4, Vacuolar protein sorting 4; ALIX, ALG-2 interacting protein X (aka PDC6I); ILV, Intraluminal vesicles. A diagram representing a typical exosome, with typical contents, is portrayed in Fig 1.7 below.
CD63).

1.5.1.2 MV Formation

Membrane composition of MVs is substantially different from the cell of origin, which may allow for their specialised functions. For example, phosphatidylserine is translocated to the outer membrane at sites of MV budding [182]. Cholesterol is an absolute requirement for MV formation and release [183, 184]. By translocating to the outer membrane, phosphatidylserine promotes MV release by inducing alterations in cell membrane morphology to promote membrane curvature and detachment [185]. The incorporation of cellular proteins within the MV appears to be selective and mediated by adenosine diphosphate (ADP)-ribosylation factor 6 (ARF6) protein [186]. Subsequent shedding of the MVs appears to be controlled by the action of actin-myosin based contraction, in which ARF6 appears to also have an influential role. Here, ARF6 promotes MV release by activating phospholipase

D (PLD) to induce extracellular signal-regulated kinase (ERK), subsequently initiating local myosin light chain kinase to phosphorylate the myosin light chain [186]. Additionally, ARF6 mediated phosphatidylinositol 4,5-bisphosphate (PIP_2) is needed for the relocation of phosphatidylserine [185]. Reduced expression of diaphanous-related formin-3 (DRF3), a protein partially responsible for actin-based cellular processes, has been observed as part of MV release, which suggests a role of actin cytoskeleton-based fission [187]. DRF3 also acts in conjugation with small Rho family-GTPases. Through these interactions, they can mediate actin nucleation. Communication between ARF6 and Rho family members is also necessary for MV release [185]. Through MV formation, bioactive molecules are encapsulated, and represented in Figure 1.7.

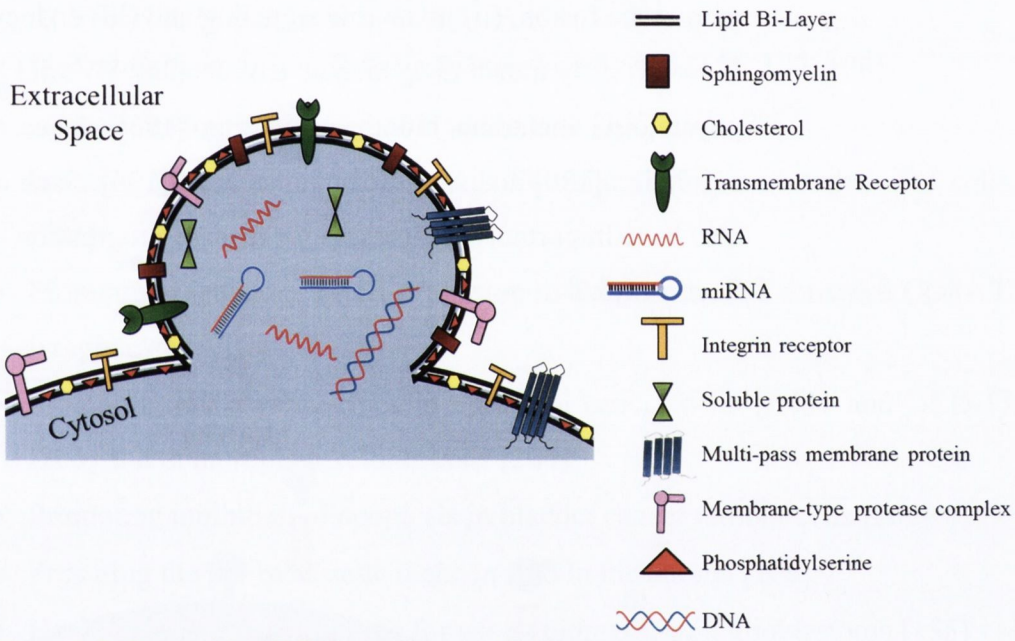

Figure 1.7: Formation of MV by membrane budding.

MVs are formed by the outward budding and fission of the cell membrane [188]. Phosphatidylserine is translocated from the inner lipid membrane leaflet to the outer in MVs, specifically where shedding takes place, which may act as a mechanism of immune system evasion, promoting tumour cell survival [189]. MVs have the ability to internalise bioactive molecules, including nucleic acids, and soluble proteins such as proteases and cytokines (although not all proteins are encapsulated). Additionally, transmembrane proteins, growth factors and MHC molecules have all been observed as part of MVs. Unlike apoptotic bodies, MVs do not enclose cellular organelles or nuclear factors [190].

1.5.1.3 EV mediated intercellular communication

For EVs to successfully communicate with secondary cells, they must have the ability to interact with them and transfer their contents. Targeting of EVs to cells may be a specific process. Evidence for this was observed when B-cell derived-EVs bound to follicular dendritic cells in lymphoid follicles [191] and intestinal epithelial cell line-derived EVs preferentially interacted with dendritic cells (DCs) [192]. To enable this selective targeting, EVs have been shown to contain specific cell surface proteins, such as cell adhesion molecules and integrins. These proteins apparently allow binding to and uptake by specific cell types [137].

Three major mechanisms of EV interaction with secondary cells include (i) membrane fusion, (ii) juxtacrine signaling and (iii) endocytosis, as illustrated in Figure 1.8. By transferring bioactive molecules, EVs aid in maintaining healthy physiology, including blood coagulation [183], tissue repair [193], immune regulation [136] and stem cell maintenance [194]. Such communication events also have important implications for disease progression as will be discussed in Section 1.5.2

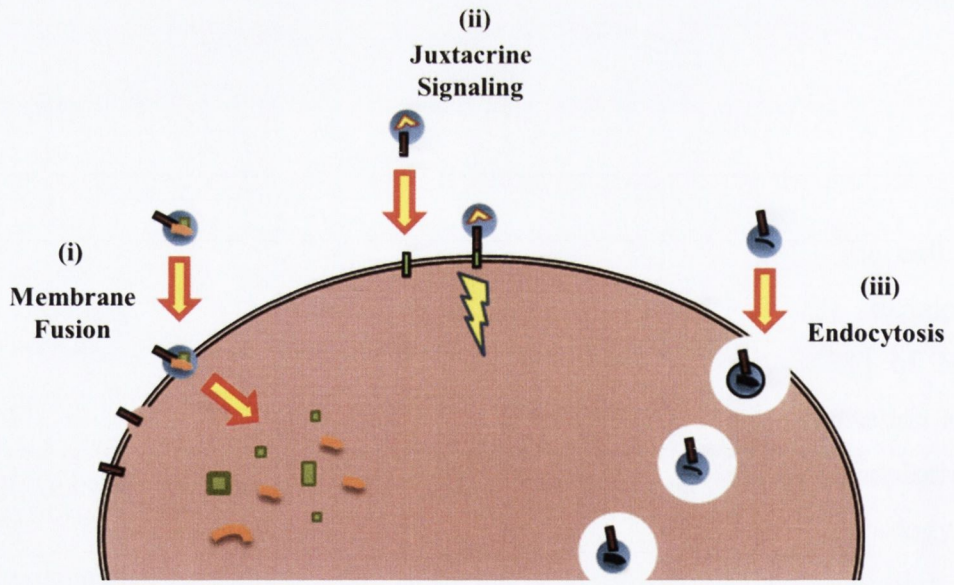

Figure 1.8: Interaction of EVs with secondary cells.

Once expelled from the cells of origin, EVs may then interact with secondary/target cells, by three proposed mechanisms: **(i)** membrane fusion, allowing proteins, lipids and nucleic acids to be directly off loaded into the cytosol of the secondary/target cell; **(ii)** juxtacrine signaling, thus initiating signal transduction cascades; and **(iii)** endocytosis where the exosomes are engulfed into the secondary/target cell.

1.5.2 EVs and cancer

The roles of EVs in cancer development, progression and as diagnostics are potentially far-reaching and increasingly intricate. EVs are proving to play a pivotal role in cancer development and are providing a fresh insight into the mechanisms by which tumours have the ability to mould their microenvironment to favour tumour progression.

EVs are proposed to be of importance in cancer for reasons including the following:

- Mediating anti-tumour effects by tumour antigen presentation to CD8+ T-cells [195]
- Increasing the growth rate of implanted TS/A tumour cells in murine models by reducing natural killer (NK) cell activity [196]
- Increasing tumour proliferation *in vitro* and *in vivo* [155, 197, 198]
- Increasing angiogenesis *in vitro* and *in vivo* [155, 197-199]
- Inducing matrix protease release in fibroblasts [200] and endothelial cells [201]
- Promoting regulatory T-cell expansion in tumour reactive activated CD8+ T lymphocytes [202]
- Promoting EMT phenotypes in epithelial cancer cells (A431 and DLD-1) [203] and in multiple myeloma cells [204]
- Promoting inhibition of apoptosis in bladder cancer tumour cells [205]
- Preparing the pre-metastatic niche *in vivo* in melanoma [206]
- Having potential significance for use as biomarkers in glioblastoma [155]
- Protecting HeLa cells from radiation therapy by inhibiting apoptosis [207].
- Hindering cytotoxic T-cell induced death by transferring Tumour necrosis factor-alpha (TNF-α) [208].
- Contributing to cisplatin resistance by exporting cisplatin from ovarian cancer cells [209, 210].

1.5.2.1 EVs in breast cancer

In 2006, Liu *et al.* [196] observed that pre-treatment of mice with EVs derived from the murine mammary tumour cells TS/A and 4T.1 appeared to accelerate the growth of implanted TS/A tumours in BALB/C and nude mice by inhibiting the action of NK cells [196]. *In vivo*, green fluorescent protein

(GFP)-tagged MDA-MB-231 EVs were demonstrated to interact with, and become incorporated into tumour cells [211]. It has been established that miR-223 can be shuttled *via* tumour-associated macrophages to promote invasion in SKBR3 and MDA-MB-231 breast cancer cells [212]. Through EV-mediated transfer of amphiregulin (an EGFR ligand), the invasive capability of two breast cancer cell variants, LM2-4175 (lung metastasis variant of MDA-MB-231 cells) and LMO-1833 (bone metastasis variant of MDA-MB-231 cells) was increased [213]. EVs derived from the TNBC cell line, MDA-MB-231, have been shown to transform an immortalised fibroblast cell line, NIH3T3, by provoking a tumorigenic phenotype and inducing tumour formation in mice as a result of EV mediated transfer of transglutaminase and fibronectin [214]. Furthermore, EVs appear to contribute to trastuzumab resistance in HER2+ breast cancer, and shuttle full-length HER2 both in active and inactive forms. The EV-bound HER2 interacted with trastuzumab, both in cell culture derived EVs and serum derived EVs, which appeared to protect cancer cells from the anti-proliferative effects of this drug [215]. We have recently shown that EVs derived from TNBC cell line variants can increase the aggression of secondary cells in a manner representative of the innate phenotypes of the originating cells [198].

1.5.2.2 EVs educate the pre-metastatic *in vivo*

The pre-metastatic niche has emerged as an important feature of cancer metastasis. The pre-metastatic niche was first described in 2005 by Kaplan *et al.* [216]. They observed that tumour-derived VEGF and placental growth factor promote recruitment of $VEGFR1^+$ hematopoietic progenitor cells, which formed clusters in secondary organs. This process allowed for the formation of a pre-metastatic niche, favourable for disseminating $CXCR4^+$ tumour cells to form secondary tumours. Since then, there has been mounting evidence suggesting that the primary tumour plays an important role in influencing the pre-metastatic niche. This process appears to be orchestrated by secretion of cytokines and growth factors from primary tumour cells, which results in the recruitment of bone marrow cells to metastatic regions. Cellular interactions in the pre-metastatic niche have commonly been assumed to take place by cell-to-cell contact or by the release of soluble tumour-derived factors. However,

recent understandings of how tumour derived EVs act *in vivo* is shedding light on their influence on the pre-metastatic niche [217].

One of the breakthrough studies performed to investigate the role of EVs in pre-metastatic niche formation was performed by Hood *et al.* [206]. By injecting fluorescently labelled B16-F10 (mouse cell line) EVs, and comparing their behaviour against empty liposome constructs, they observed trafficking of melanoma EVs to sentinel lymph nodes. Not only this, but they observed that the melanoma-EVs evidently recruit DiO-labelled B16-F10 melanoma cells to the lymph nodes by enhancing migration of melanoma cells to melanoma EV rich sites. They proposed that EVs influence the pre-metastatic niche by up-regulating multiple metastatic pathways. Similarly, B16-F10 melanoma derived EVs were found to increase the metastatic potential of primary tumours by educating/reprogramming bone marrow progenitors by up-regulating the receptor tyrosine kinase MET. Vascular "leakiness" was also induced by EVs to promote tumour growth, as well as promoting a vasculogenic phenotype, inducing mobilisation and pro-metastatic behaviour of bone-marrow derived cells. In addition to these findings, pre-treating bone marrow with EVs derived from an aggressive cell line can increase the metastatic potential and colonisation of tumours [218]. It has also been suggested that B16-F10 melanoma derived EVs enhanced the metastatic potential in BALB/C mice in a phosphatidylserine (PS) dependent manner, possibly by down-regulating the host's anti-inflammatory and/or anti-tumoural immune response [182].

In highly metastatic rat pancreatic adenocarcinoma (BSp73ASML), CD44v, working together with EVs, is required for the establishment of a soluble matrix which promotes leukocytes, stroma and endothelial cell activation in the pre-metastatic organ. [219]. Similarly, $CD105^{+}$ renal cancer stem cell derived EVs can stimulate angiogenesis in the lung pre-metastatic by increasing VEGFR1 expression [219]. EV mediated transfer of miRNA (as detailed further in Section 1.5.3) has also been implicated in influencing the establishment of the pre-metastatic niche. Rana *et al.* [220] demonstrated that EVs derived from rat pancreatic adenocarcinoma BSp73ASML cells educate specific tissues *in vivo* by transferring oncomiRs to induce a pro-metastatic phenotype.

Building a broader picture of the interactions and trafficking of EVs *in vivo* is important so that the disease-mediating mechanisms of EVs and, indeed, their therapeutic implications are understood. Fluorescently labelled EVs from EL-4 (mouse lymphoma cell line) were found to hone towards, and predominantly accumulate in the liver, lungs, kidney and spleen within an hour after intraperitoneal injection [157]. In a study dedicated to investigate the "pharmacokinetic" distribution of EV *in vivo*, fluorescent EVs were collected from B16-BLB murine melanoma cells and injected intravenously into BALB/C mice for visualisation. After initial injections, EVs tended to hone towards the liver, which might suggest that EVs get shuttled through the circulatory system to the liver, where they get trapped or cleared from circulation [221]. In addition, as EVs are negatively charged entities, this also suggested that the liver acts to remove them from circulation, just as observed using liposomes *in vivo* [222]. Post liver processing, it was found that EVs are then shuttled to the lungs [221].

1.5.3 miRNA in EVs

The first report demonstrating the transfer of nucleic acids by EVs was reported in 2007, when Valadi *et al.* [154] described the presence of small RNAs and mRNAs in EVs. Further investigation demonstrated that the EV-RNAs could be transported from mouse mast cells to secondary human mast cells where they were functional [154]. Montecalvo *et al.* [223] demonstrated that EVs from DCs express different miRNAs, depending on the maturation of the DC. The EV-miRNA was then shown to be functionally transferred *via* EVs to sequester target mRNA translation in receiving cells [223]. Through the encapsulation of miRNAs within EVs, the membrane effectively acts as protection, as demonstrated by the discovery of functional miRNAs in EVs derived from faeces [224].

The functional effects of miRNAs in EVs derived from cancer cells have begun to emerge. Through the transfer of miRNAs by EVs, translational repression of mRNAs has been observed, which, in turn has shown to induce cell migration, invasion, metastasis, inflammation, immune responses, angiogenesis and pre-metastatic niche development [225]. Specifically, EVs derived from the K562 leukaemia cells increased the rate of human umbilical vein endothelial cell

(HUVECs) tubule formation and migration by transferring miR-92a. The transference of miR-92a resulted in reduced expression of integrin α5, a miR-92a target [226]. Endothelial cell growth and vessel formation has been shown to be induced by EV-miRNA from $CD105^+$ renal cancer stem cells. This resulted in enhanced lung metastasis when implanted *in vivo.* These miRNAs included miR-29a, miR-650 and miR-151 [227]. Another study detected the presence of 15 miRNAs differentially regulated in melanoma EVs compared to normal melanocyte EVs, which are known to be associated with melanoma invasion and metastasis [228]. EV-miRNAs may also act as ligands by binding to toll like receptors (TLRs) on target cells. Fabbri *et al.* [229] observed that miR-21 and miR-29a, secreted in EVs from mouse LLC lung cancer cell lines, interacted with, and bound to murine TLR7 and human TLR8. This initiated TLR mediated pro-metastatic inflammatory response [229]. Taken together, the above example studies provide strong evidence for a highly influential role of EV mediated transfer of miRNA in cancer progression.

1.5.3.1 Incorporation of miRNA into EVs

The mechanism of miRNA trafficking onto EVs is unclear. Mechanisms are being investigated, such as the observation that EV-RNA share specific sequence motifs which could act as cis-acting elements for incorporation into EVs [230]. It has been observed that MVBs are located in regions of miRNA-loaded RISC accumulation [231] and are associated with glycine/tryptophan (GW)-bodies (cytoplasmic foci, where post translational regulation of mRNA occurs). GW-bodies are enriched in GW182 and argonaute-2 (AGO2) proteins Observations that EVs contain high levels of miRNA processing proteins, AGO2 and GW182, suggest that these proteins may play roles in processing miRNAs into EVs [231]. The ESCRT system has been implicated also, as ESCRT-II has been found to be an RNA-binding complex. In addition, silencing of some of the ESCRT components led to an over-accumulation of GW182 and compromised miRNA-mediated gene silencing. This suggests that GW182 and miRNA-loaded AGO2 are processed by the ESCRT system [232]. The GW182 protein may be important for miRNA stability in EVs. [233]. More recently, a study has demonstrated that miRNAs are released in EVs by a ceramide-dependent secretory mechanism [234].

There also appears to be a mechanism of selective incorporation of miRNAs into EVs, at the expense of the miRNA presence in the cell. Profiling hepatocellular cancer cells and their EVs found that 11 miRNAs were solely identified in the EVs, but not in the cells [235]. Similar observations have been reported elsewhere. miRNAs from the let-7 family of miRNAs appear to be selectively incorporated into EVs in metastatic gastric cancer [236]. It has also been observed that the majority of transcribed miR-451 and miR-1246 are released in EVs from the breast cancer cell lines MDA-MB-231, MCF7, BT20 and SKBR3 cells compared to their levels in their cells of origin. Interestingly, this study observed that miR-451 is retained in MCF10A cells, a non-tumourigenic cell line, as well as in a non-related normal fibroblast call line, IMR90, but reduced is the more aggressive cell lines [237]. Similarly, miR-451 was observed to be enriched in hepatocellular EVs, but not detected in their cells of origin [235]. miR-451 has received seemingly contradictory reports in breast cancer studies. miR-451 abundance had been previously reported in breast cancer tissue sections, and, although miR-451 accumulates interstitially, its presence is low in cancerous mammary epithelia [86]. It has been suggested upon observation of miR-451 enrichment in EVs that the release of miR-451 in EVs may explain how miR-451 accumulates interstitially in breast cancer tumours and, as it appears to be selectively incorporated into malignant breast cancer cells, miR-451 may have important diagnostic implications [237].

1.5.3.2 EV-miRNAs as biomarkers

Ideally, a biomarker should be sensitive enough to determine cancer presence at an early stage in disease progression, allow for the monitoring of disease progression and have value as predictive biomarkers for cancer progression and response to therapy.

Diagnostic methods currently used for breast cancer are quite invasive, with the "triple assessment" involving examination, scan and biopsy. These processes include uncomfortable experiences for patients, including mammographies, which can give varied interpretation and inconsistent rates of false positive results [238]. As these procedures are quite time consuming it means that patients who have breast cancer experience a lack of prioritisation they deserve due to excess strain placed on the health care system [239]. Regarding breast

cancer, more effective biomarkers are urgently needed, as for example, not all patients who test positive for HER2 expression are sensitive to anti-HER2 treatments, such as trastuzumab [240]. For the above reasons, there is a great urgency for the discovery of a blood-based minimally invasive biomarker for cancer [239].

As EVs have been shown to contain a subset of functional miRNAs [154], are evidently released in greater concentrations from some tumour cells than healthy cells [241], and the majority of detectable miRNAs from serum and saliva are present in EVs [148], they have the potential to provide an enriched miRNA signature of the parent tumour, therefore having the potential to act as cancer biomarkers. As EVs can be obtained from "minimally-invasive" sites, such as serum, pleural effusions and tumour ascites of cancer patients [242, 243], drawbacks of profiling tumour masses could be circumvented.

Detection of nucleic acid biomarkers in EVs is very much in its infancy; however, significant discoveries have been made to justify the optimism surrounding EV-miRNA. Taylor and Taylor [244] described the presence of the eight diagnostic miRNA (miR-21, miR-141, miR-200a, miR-200b, miR-200c, miR-203, miR-205 and miR-214) in tumour derived EVs (n=50) that have been previously considered as markers of ovarian cancer. Not only are these miRNAs present in the tumour-derived exosomes, but they also show a strong correlation with the tumours miRNA profile. The levels of the diagnostic miRNAs differ significantly between benign and cancer [244]. Additionally, analysis of the miRNA profiles of the glioblastoma-serum-derived exosomes (n=3) showed high concentrations of miR-21 [155], a miRNA known to be overexpressed in glioblastoma tumours [245] which could potentially provide a diagnostic biomarker for an early glioblastoma. Similar studies have been performed in a number of cancers, contributing to the identification of the potential of EV-miRNAs in lung cancer [246], oesophageal squamous cell carcinoma [247], colon cancer [248] and leukaemia [226] as blood-based biomarkers.

1.5.4 DNA in EVs

Recently, observations regarding the presence of both mitochondrial and genomic DNA (gDNA), and their function in EVs have been reported [161, 249]. As for RNA in EVs, DNA is shown to be packaged within EVs and can apparently be successfully transferred from one cell to another [161]. The relevance of this is that the transferred DNA can effect and regulate the coding of gDNA, which has implications on the expression of mRNA and protein in recipient cells [161]. Waldenstrom *et al.* [249] demonstrated that chromosomal DNA sequences can be transferred within EVs and shuttled to the cytosol and the nuclei of recipient fibroblast cells [249]. The presence of mitochondrial DNA (mtDNA) in EVs was reported by Guescini *et al.* [250] when they described the presence of mtDNA in glioblastoma and astrocyte cells which can be transferred between cells [251]. A very recent study demonstrated that >10kb fragments of dsDNA are present in the serum of cancer patients and, more significantly, that KRAS and p53 mutations can be identified in these EVs. Additionally, serum EVs from these cancer patients was found to contain gDNA representative of all chromosomes. This paves the way for further analysis which may identify a role of serum EVs as gDNA-based disease biomarkers [252].

Single stranded DNA (ssDNA) was observed in EVs from glioblastoma cells, as well as from glioblastoma tumours *in vivo*, representing gDNA and complimentary-DNA (cDNA). Interestingly, while analysing the DNA presence in EVs derived from c-Myc (oncogene) overexpressing medulloblastoma cells and tumours, it was observed that this overexpression is represented in their derived EVs. Similar to previous observations that tumour-derived EVs contain greater levels of RNA than non-tumour derived EVs, greater levels of DNA was also observed in tumour derived EVs compared to controls [253]. Such observations as elevated c-Myc DNA in EVs from c-Myc over-expressing cells demonstrates the potential for use of EV-DNA as a clinical blood-based biomarker [253].

Additionally, the observation that DNA can be shuttled from cell-to-cell to communicate DNA functionality [161], may lead researchers to manipulating EVs to chaperone DNA of therapeutic value to diseased cells. Although these

finding are conclusively demonstrating the presence of DNA in EVs, the process by which DNA is incorporated into the EVs has yet to be determined.

1.5.5 Therapeutic applications of EVs

Although EVs are typically associated with adverse roles in human disease, they have also been shown to have substantial therapeutic value. EVs derived from stem cells have been shown to reduce apoptosis and increase cell proliferation [193, 254]. For example, a single treatment of rats with MSC-derived EVs immediately after ischaemia-reperfusion injury bestowed a protective effect from acute kidney injury by inhibiting apoptosis and stimulating proliferation of tubular epithelial cells [193]. Similar findings were observed where EVs from endothelial progenitor cells protect the kidney from ischaemia-reperfusion injury through miRNA reprogramming of resident renal cells [255] and by amplifying neoangiogenesis of pancreatic islets [256]. By stimulating apoptosis, EVs from human adult liver stem cells can reduce tumour growth *in vivo* [257]. Embryonic stem cell derived EVs have been shown to promote tissue regeneration by reprogramming hematopoietic progenitors through mRNA and protein transfer [194] and through mRNA transfer they can accelerate hepatic regeneration [254].

Cancer research, and indeed biomedical research as a whole, has identified a wide range of potential targets for disease treatment, but has hit stumbling blocks with respect to targeting such sites. These shortcomings are due to a number of factors, including their challenging cellular location (intracellular); high expression in a broad spectrum of cell types; and poorly soluble drugs which are liable to degradation [258]. The use of miRNAs therapeutically has shown lack of efficacy in treating disease due to short half-life and difficulty crossing cell membranes [130, 131]. EVs have emerged with great promise due to their ideal attributes for drug delivery vehicles [258]. Specifically, they are present in diverse range of biological fluids, which suggests that they are broadly tolerated in the body. Their ability to transfer bioactive molecules from cell to cell, such as major histocompatibility complex-1 (MHC-I) and major histocompatibility complex-2 (MHC-II) [259], mRNAs, miRNAs [154], gDNA [161] and mtDNA [251] also suggests that they may be manipulated into carrying such bioactive molecules representing therapeutics for targeting to

desired areas and cell types. One of the most desirable characteristics observed in EVs is their ability to target specific cell types and hone towards certain tissues *in vivo*, such as melanoma derived EVs honing towards the lymph nodes during metastasis [206]. The discovery of their ability to cross the blood brain barrier (BBB) has been one of the major findings in this area of research [133]; and their immunologically inertness when derived from certain cells (*e.g.* DCs and mesenchymal stem cells) [260] mean EVs are attractive entities for use as therapeutic delivery systems.

The first study to successfully demonstrate that exogenous nucleic acids, miRNAs in particular, can be transferred by EVs was reported in 2010. This study established that when THP-1 monocytes were transfected with miR-150 using lipofectamine 2000, their expelled EVs were subsequently enriched in miR-150 and showed functional bioactivity in recipient cells when transferred through EVs [261]. In one of the pioneering studies to investigate the relevance of EVs in siRNA delivery, Alvarez-Erviti *et al.* [133] demonstrated that siRNAs can be efficiently targeted to the mouse brain, crossing the BBB and inhibiting target mRNA translation. Similarly, EVs electroporated with siRNA can effectively deliver the siRNA to monocytes and lymphocytes resulting in target gene knockdown [262]. Of particular relevance of breast cancer, Ohno *et al.* [263] have observed that EVs can selectively deliver let-7a to EGFR-expressing xenograft breast cancer tissue in $RAG2^{-/-}$ mice. Such studies continue to emerge supporting the promise EVs hold as exogenous siRNA delivery vehicles in cancer [264].

The potential of EV therapy is starting to be realised, with the advent of EVs in clinical trials, demonstrating that EVs are well tolerated in humans. Escudier *et al.* [265] analysed the potential, feasibility and safety of using autologous exosomes in a phase I trial. This trial set out to investigate the effects of MAGE3 pulsed exosomes as an immunisation approach on 15 patients on stage III/IV melanoma, whilst investigating the response of T-cells and clinical outcomes. Tumour regression was noted in skin and lymph node lesions only, with no grade II toxicity observed with the maximal tolerated dose not being reached [265]. This study demonstrated, in principle, that exosomes-based

immunotherapy is feasible in terms of large scale exosome production for patient treatments.

Similarly, the feasibility of exosome vaccinations was demonstrated by Morse *et al.* [266] who reported that DC derived exosomes were tolerated in humans with advanced non-small cell lung cancer (NSCLC) [266]. In 2008, Dai *et al.* [267] conducted a study on 40 patients with advance colorectal cancer. Although treatment with ascites-derived exosomes alone did not bestow beneficial tumour-specific anti-tumour cytotoxic T-lymphocyte response, treatment with ascites-derived exosomes in combination with treatments of granulocyte–macrophage colony-stimulating factor did [267].

In addition to these studies, a clinical study is commencing in Ireland. This study aims to investigate the relevance of exosomes and freely circulating extracellular RNAs and proteins for use as predictive biomarkers for HER2 therapies in breast cancer (Protocol number: ICORG 10-15)

1.6 Project aim:

The overall aim of this Ph.D was to establish whether EVs have relevance in TNBC progression, diagnosis and therapeutics. To examine whether EVs may increase the metastatic potential of tumour cells, this study initially aimed to investigate if EVs derived from the TNBC cell line variants, Hs578T and it's more aggressive subclone, Hs578Ts(i)$_8$, could mediate increased breast cancer aggression.

Once this was established, the aim of the project turned to investigate the nucleic acid contents of the EVs to elucidate their mechanism(s) of action. To examine this, the miRNA and DNA contents of TNBC cell variants and their derived EVs were analysed. A number of goals were set out as part of the profiling analyses:

- Determine if the miRNA and DNA contents of EVs are representative of their originating cells.
- Identify key miRNAs lost in both aggressive TNBC Hs578Ts(i)$_8$ cells and EVs compared to Hs578T cells and EVs, which may represent tumour suppressors.
- Establish whether EVs derived from tumour cells have potential for use as circulating DNA and miRNA biomarkers.

From global miRNA profiling, we identified miR-134 to be down-regulated in aggressive cells and their derived EVs. This study then explored the tumour suppressive potential of miR-134 by performing functional assays and protein expression analyses. Furthermore, this study aimed to determine if EVs could be used as miRNA therapeutic delivery vesicles.

Finally, this Ph.D aspired to establish whether EVs have clinical relevance in TNBC. To do this, EVs from patients-sera were investigated to see if they could induce increased cellular aggression, compared to sera-EVs from healthy individuals. To investigate whether EVs have biomarker potential, key miRNAs identified from global miRNA profiling were analysed in EVs derived from the sera of patients diagnosed with TNBC, ER+ breast cancer and HER2+ breast cancer, compared to EVs from the sera of healthy individuals.

Chapter 2

Triple-negative breast cancer derived EVs mediate metastasis-associated phenotypic alterations in breast cancer

Parts of this chapter have been published in the European Journal of Cancer, 2013, with additional data also presented.

Paper title: Exosomes from triple-negative breast cancer cells can transfer phenotypic traits representing their cells of origin to secondary cells.

O'Brien K, Rani S, Corcoran C, Wallace R, Hughes L, Friel AM, McDonnell S, Crown J, Radomski MW, O'Driscoll L.

European Journal of Cancer, 2013.

2. Abstract

Background: Triple-negative breast cancer (TNBC) accounts for 15-20% of breast cancers and is responsible for a disproportionate number of deaths, with the incidence of metastasis being the primary cause of fatality. Investigating the mechanisms of communication that enable and support metastasis may allow for the discovery of therapeutic targets, as well as potential biomarkers for clinical utility. One such communication mechanism is mediated by exosomes and microvesicles, collectively termed extracellular vesicles (EVs). EVs have recently been implicated in mediating the aggression of secondary cells, educating the pre-metastatic niche and facilitating cancer progression through metastasis. We therefore investigated the relevance of these EVs in TNBC aggression. Specifically, we compared phenotypic altering effects of EVs derived from the claudin-low, less aggressive and non-tumourigenic TNBC cell line Hs578T and its more invasive, tumourigenic Hs578Ts(i)$_8$ isogenic variant, as well as EVs from TNBC from another TNBC cell line, MDA-MB-231. Additionally, as a pilot study we aimed to investigate the behaviour of these EVs *in vivo*.

Methods: EVs were isolated from conditioned medium (CM) of Hs578T, Hs578Ts(i)$_8$ and MDA-MB-231 cells by differential filtration and ultracentrifugation. Successful isolation was confirmed by transmission electron microscopy and immunoblotting. EV-cell interactions were confirmed and visualised by confocal microscopy. Subsequent analysis of secondary/recipient cells in response to EVs included proliferation; motility/migration, invasion, *anoikis* resistance and endothelial tubule formation assays, by applying EVs to secondary breast cancer cells *in vitro*. For *in vivo* analysis, EVs were fluorescently labelled and injected into the tail vein of BALB/C nude mice. Organs were analysed *ex vivo* using the *In Vivo* Imaging System (IVIS) to determine EV concentration after 24 and 48 hrs. The relevance of EV-mediated MMP signalling was also investigated.

Results: Hs578Ts(i)$_8$-EVs *versus* Hs578T-EVs significantly increased the proliferation, migration and invasion capacity of all four recipient cell lines evaluated *i.e.* Hs578T, SKBR3, MDA-MB-231 and HCC1954, in a manner representing the innate phenotypes of their parental cells. Hs578Ts(i)$_8$-EVs increased sensitivity of SKBR3, MDA-MB-231 and HCC1954 to *anoikis* when compared to the effects of Hs578T-EVs reflecting the fact that Hs578Ts(i)$_8$ cells are themselves innately more sensitive to *anoikis*. In relation to vasculogenesis and subsequent angiogenesis, Hs578Ts(i)$_8$-EVs *versus* Hs578T-EVs stimulated significantly more endothelial tubule formation *in vitro*. EVs were also observed to be stable *in vivo* and have the ability to cross the blood brain barrier (BBB). Additionally, the aggressive derived EVs tend to hone towards organs commonly observed in metastasis, especially in the lungs and liver. MMP-2 activity was not observed in either Hs578T or Hs578Ts(i)$_8$ derived EVs.

Conclusion: This study supports the hypothesis that TNBC-derived EVs may be involved in cancer cell-to-cell communication, conferring aggressive, metastasis-associated phenotypic traits to secondary cells that reflect those of their cells of origin. Results suggest that TNBC-EVs may act to educate the TNBC pre-metastatic niche *in vivo.*

2.1. Introduction

EVs are expelled from eukaryotic cells and have attracted much interest in recent years since the realisation that these are not merely debris, but rather miniature maps of their cell of origin, with both physiological and pathological relevance [268], as explained in detail in Chapter 1, Section 1.5. Accumulating evidence indicates that exosomes (~30-120nm) and microvesicles (up to 1000nm), collectively termed EVs, play important roles in cell-to-cell communication [153-155]. In cancer, these entities have been implicated in carcinogenesis and tumour growth; moulding the tumour microenvironment; promoting angiogenesis; and modulating immune response [156, 162-165], as detailed in Section 1.5.2

Triple-negative breast cancer (TNBC), although constituting a minority of breast cancers (15-20%), causes a disproportionate number of metastatic cases and breast cancer deaths. TNBC, which has ~70% overlap with the basal subtypes [26, 269], is classified by its lack of expression of estrogen receptors (ER), progesterone receptors (PR) and neither over-expression nor amplification of human epidermal growth factor receptor 2 (HER2) gene. Although sensitive to chemotherapy, the lack of expression of the above receptors substantially limits treatment options available for TNBC. Consequently, TNBCs receive inferior treatment regimens as they are innately insensitive to widely used targeted approaches such as endocrine therapies and trastuzumab, which have proven effective at reducing breast cancer mortality. Additionally, compared to other breast tumours, TNBC occurs most frequently in younger patients (<50 years), and those tumours tend to be at a higher-grade at presentation, with more aggressive behaviour. Patients with TNBC typically relapse with distant metastases rather than with local, more manageable recurrence and have an increased likelihood of developing visceral metastases, including central nervous involvement. TNBC is associated with a shortened disease-free interval post-surgery and post-adjuvant treatment, and ultimately, a shortened overall survival [270-273]. Furthermore, TNBC is a heterogeneous group, within which the claudin-low subtype is associated with worst prognosis [274]. A more detailed description of TNBC was discussed in Section 1.3.1.

Compared to the overall prevalence of breast cancer, a limited number of reports have indicated EVs to be of relevance in breast cancer [215, 275, 276]. The focus in this area of research has typically been on HER2-overexpressing cells and their EVs.

Here, in what we believe to be the first study specifically considering EVs in the context of TNBC, we have included analysis of EVs from the claudin-low TNBC cell line Hs578T [277] and its isogenic subclone, Hs578Ts(i)$_8$ [278], as well as analysing the effects of EVs from another TNBC cell line, MDA-MB-231 on invasion. Hs578Ts(i)$_8$, compared to Hs578T parent cells, has the same genetic background but significantly increased capacity to proliferate, migrate, invade through extracellular matrix and produce tumours in mice. This cell line pair is, therefore, very useful for investigating the capabilities of EVs to transfer phenotypic traits representative of their cell of origin to secondary recipient cells.

2.2. Materials & Methods

2.2.1. Cell culture

Hs578T (TNBC; carcinoma; derived from human mammary gland tumour) and its isogenic subclone, Hs578Ts(i)$_8$, were gifts from Dr. Linda Hughes and Dr. Susan McDonnell (University College Dublin) and grown in Dulbecco's Modified Eagles Medium (DMEM) (Sigma-Aldrich; Cat. #: D5671) containing 10% fetal bovine serum (FBS) (PAA; Cat. #: A15-151), 2mM L-Glutamine (Sigma-Aldrich; Cat. #: G7513), and 10μg/ml of insulin (Sigma-Aldrich; CAT#: I0516). Hs578Ts(i)$_8$ cells are a more aggressive cell variant, isolated from the parental Hs578T population by Hughes *et al.* [278] by a series of eight successive passages through matrigel coated cell culture inserts with 8μm pores. This process resulted in the isolation of Hs578Ts(i)$_8$ cells which are 3 fold more invasive, 2.5 fold more migratory, produced 25 times more colonies in soft agar and could produce tumours in nude mice, thus establishing a cell line model for a later stage of TNBC metastasis. The process of isolating the Hs578Ts(i)$_8$ cells is outlined in Figure 2.1 below.

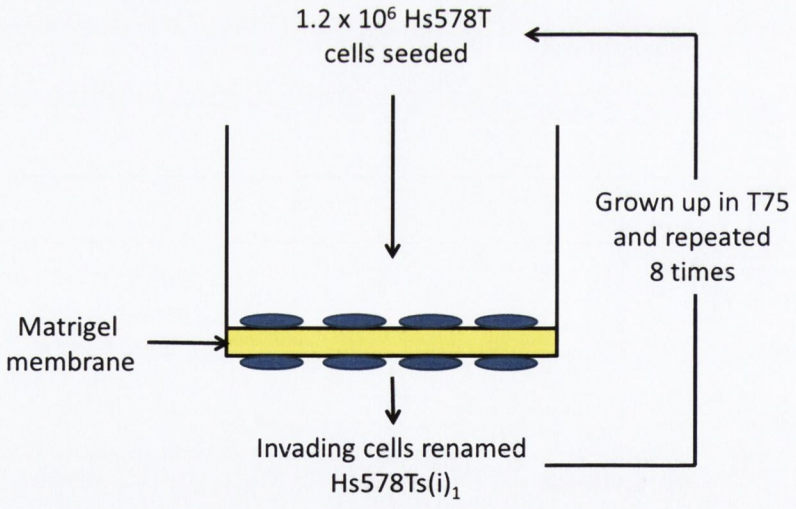

Figure 2.1: A model for the selection of more invasive subclones using BD Matrigel™ invasion chambers.

This is the process used by Hughes *et al.* [278] in UCD to develop the Hs578Ts(i)$_8$ cell variant from Hs578T cells. Briefly, 1.2x10^6 parental cells are seeded into the chamber; cultured for 5 hrs; invading cells collected from the bottom of the membrane by trypsinisation and subsequently cultured. Eight successive rounds of this process allowed for the selection of more invasive cells form the parental cells. Diagram adapted from Hughes *et al.* [278]

SKBR3 (HER2/c-erb-2 gene product overexpressing; adenocarcinoma; mammary gland/breast; derived from human metastatic site: pleural effusion), MDA-MB-231 (TNBC; adenocarcinoma; mammary gland/breast; derived from human metastatic site: pleural effusion) and HCC1954 (Her2/neu overexpressing; TNM stage IIA, grade 3, ductal carcinoma; derived from human mammary gland; breast/duct) were obtained from the American Tissue Culture Collection (ATCC). These cells were grown in Roswell Park Memorial Institute medium (RPMI)-1640 (Sigma-Aldrich; Cat. #: R0883) containing 10% FBS and 2mM L-Glutamine. All cells were grown at 37°C; 5% CO_2. Routine mycoplasma testing was performed by quantitative polymerase chain reaction (qPCR) (Promokine; Cat. #: PK-CA91-3025B) every three months determining no mycoplasma infection. Additionally, Hs578T and Hs578Ts(i)$_8$ cells were also analysed off-site on two separate occasions by Mycoplasma Experience Ltd, UK, confirming that mycoplasma-free cell cultures were maintained for the entirety of this project.

2.2.2. Extracellular vesicle isolation from conditioned medium (CM)

Hs578T and Hs578Ts(i)$_8$ were seeded ($1x10^5$ cells/flask) in 9xT75 flasks, in complete medium and allowed to attach overnight. Medium was then replaced with DMEM containing 10% EV-depleted-FBS (dFBS) (PAA; Cat. #: A15-151), 2mM L-Glutamine (Sigma-Aldrich; Cat. #: G7513), 1% penicillin/streptomycin (Invitrogen, Cat. #: 15070-063), 10µg/ml insulin (Sigma-Aldrich; Cat. #: I0516). FBS was depleted of EVs by subjecting the FBS to an ultracentrifugation spin of 110,000g for 16 hrs, at 4°C, as previously described in our book chapter [279]. Penicillin/streptomycin was used only for flasks set up for EV isolations using dFBS to reduce the possibility of bacterial contaminations occurring as a result of the increased handling of FBS throughout the depleting procedure and was not used for routine cell culture.

Cells were subsequently cultured for 5 days in dFBS-medium to grow to 80%-90% confluency. CM was then removed and EVs were isolated from CM as we have detailed in our published book chapter [279]. CM was centrifuged at 2,000g for 10 mins at 4°C to remove cells and larger cell debris. The

supernatant was then filtered using 0.45µm pore syringe filters (PAL; Cat. #: 4564) to further eliminate cell debris and larger membrane vesicles from the sample. Of note, 0.45µm pore syringe filters were used as 0.22µm pore syringe filters gave low EV yields, not allowing for analysis to be performed. The resulting CM was then transferred to sterile 28ml polyallomer ultracentrifuge tubes (Beckman-coulter; Cat. #: 358651) and ultracentrifuged at 110,000g for 75 mins at 4°C on a SW28 swinging bucket rotor. EV pellets were washed in sterile phosphate buffered saline (PBS) (Sigma-Aldrich; Cat. #: D8662) and ultracentrifugation was repeated at 110,000g for 75 mins at 4°C in 28ml polyallomer ultracentrifuge tubes using a SW28 swinging bucket rotor. The resulting EV pellets were resuspended in 200µl of sterile PBS and EV quantities were determined using the Bio-Rad protein assay (Bio-Rad; Cat. #: 500-0006). EVs were stored at -80°C for later use and analysis. EV quantities used for assays are detailed in the methods Section for individual assays. EV isolation is illustrated in Figure 2.2 below.

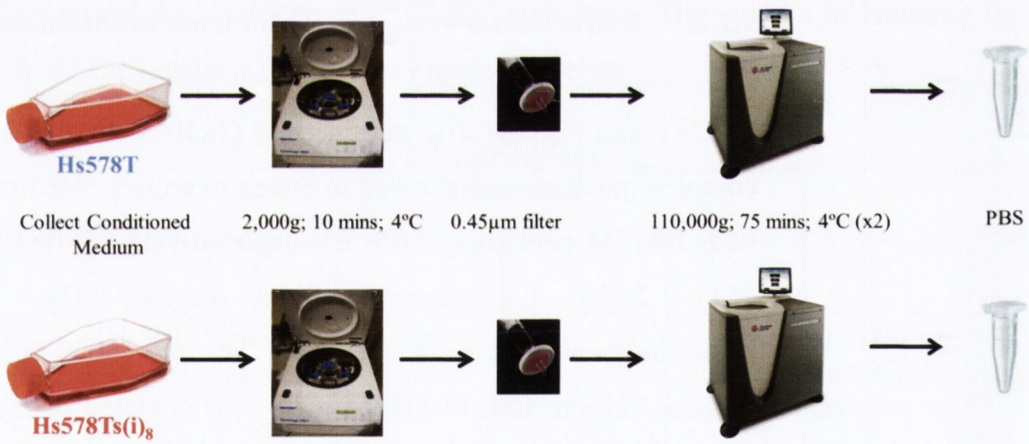

Figure 2.2: Flow diagram illustrating the process of EV isolation from CM of cells

2.2.2.1. EV quantification

EV quantities were determined using the Bio-Rad protein assay (Bio-Rad; Cat. #: 500-0006). An EV sample (10µl) was placed in a 96-well plate for analysis. Protein standards of bovine serum albumin (BSA) (Sigma-Aldrich; Cat. #: A9413) were prepared at the following concentrations to produce a standard curve: 0µg/ml, 25µg/ml, 50µg/ml, 100µg/ml, 200µg/ml, 400µg/ml and 800µg/ml. Bio-Rad Dye reagent was diluted 1:5 with water and 200µl of this solution was added to each well containing the protein or standards. The plate was incubated at room temperature in the dark for 5 mins and read at 595nm a FlouStar Optima microplate reader (BMG Labtech).

2.2.3. Immunoblotting

2.2.3.1. Protein extraction

Cell pellets were collected from cell culture flasks. Medium was aspirated from the flask and replaced with 3ml of sterile PBS and cells were scraped using a sterile cell scraper. The resulting cell suspension was then centrifuged at 13,000g for 5 mins to form a pellet, and subsequently washed twice in 1ml of PBS by centrifugation to yield a clean cell pellet. Total cellular proteins were extracted from cell pellets using 100µl of cell extraction buffer (Invitrogen, Cat. #: FNN0011) with protease inhibitor (Roche; Cat. #: 05892970001) and phosphatase inhibitors as appropriate (Roche; Cat. #: 04906837001). EV samples were collected as detailed in Section 2.2.2, and resuspended in 20µl of cell extraction buffer (Invitrogen, Cat. #: FNN0011) with protease inhibitor (Roche; Cat. #: 05892970001) and phosphatase inhibitors as appropriate (Roche; Cat. #: 04906837001) to extract total EV proteins, instead of resuspending in PBS. Lysate suspensions were then incubated 3 times on ice for 10 mins, vortexing for 15 secs between each 10 min incubation. Lysates were then centrifuged using a bench-top centrifuge at 13,000g for 15 mins at 4°C. Any residual pellet was discarded, as the supernatant represents the protein lysate fraction.

2.2.3.2. Protein quantification

Protein was quantified using Bio-Rad protein assay Dye Reagent (Bio-Rad, Cat. #:5000006) to determine the amount of protein obtained from the extraction procedure. A protein lysate sample (1µl) was diluted in 9µl of dH_2O to yield a 1:10 dilution. This 10µl sample was placed in a 96-well plate for analysis. Protein standards of BSA were prepared (0µg/ml, 25µg/ml, 50µg/ml, 100µg/ml, 200µg/ml, 400µg/ml and 800µg/ml). Bio-Rad Dye reagent was diluted 1:5 with water and 200µl of this solution was added to each well containing the protein or standards. The plate was incubated at room temperature in the dark for 5mins before being read at 595nm a FluoStar Optima microplate reader (BMG Labtech).

Proteins were made up to the desired concentrations at which point an appropriate volume of 4X loading buffer was added to the sample, then placed at 95°C for 5 mins and left on ice until loading the gel wells.

Immunoblotting was performed under reducing conditions using β-mercaptoethanol. Proteins (20-30µg; exact quantities are indicated where appropriate in the results section) were resolved on 12.5% Sodium dodecyl sulphate (SDS) gels and transferred to Polyvinylidene fluoride (PVDF) membranes (Bio-Rad laboratories, Cat. #: 162-0177) by semi-dry transfer. Blots were washed 3 times (5 mins each) with wash buffer (PBS + 0.1% Tween (Sigma-Aldrich, Cat. #: P2287)); then blocked in 5% (w/v) non-fat milk in PBS+ 0.1% Tween (Bio-Rad laboratories; Cat. #: 170-6404), washed 3 times and incubated overnight at 4°C, gently rocking with primary antibodies to: PDC6I/Alix (Rabbit; 1:1000; Abcam; Cat. #: ab76608), TSG101 (Mouse; 1:1000; Abcam; Cat. #:ab83) or CD63 (Mouse; 1:500; Abcam; Cat. #: ab8219). Blots were subsequently washed 3 times for 5 mins in washing buffer. Membranes were then incubated with the appropriate horseradish peroxidase-conjugated secondary antibodies *i.e.* anti-mouse (Cell Signalling, Cat. #: 7074; 1:1000 dilution) or anti-rabbit (Cell Signalling, Cat. #: 7076; 1:1000 dilution) for 1 hr at room temperature. Protein bands were visualized by chemiluminescence (ThermoFisher: Cat. #: 34080). Detection was performed

with a Chemidoc exposure system (Bio-Rad Laboratories). Densitometry was performed using ImageJ software.

2.2.4. Transmission electron microscopy (TEM) of EVs

A ~10µl aliquot of EVs was placed onto parafilm (Sigma-Aldrich, Cat. #: P7793). A 300 mesh copper grid (Agar Scientific) was placed on top of the drop for 45 mins. The grid was subsequently washed thrice in 0.05M phosphate buffer (freshly prepared using DiHydrogen potassium phosphate (Merck, Cat. #: 1.04873.0250) and dipotassium hydrogen phosphate (Merck, Cat. #:1.05104.1000)) for 5 mins, fixed in 3% glutaraldehyde (Agar Scientific, Cat. #: 101504) for 10 mins, washed 3 times for 5 mins in dH_2O and contrasted in 2% uranyl acetate (BDH, Cat. #: 30550). Grids were examined at 100kV using a JEOL JEM-2100 transmission electron microscope. All TEM analyses were performed in the Centre for Microscopy and Analysis (CMA), Trinity College Dublin, with the help of Neal Leddy, Chief Technical Officer.

2.2.5. Confocal microscopy

EVs were labelled with CellTracker™-CM-DiI label (Molecular Probes, Invitrogen; Cat. #: C-7000) during the first ultracentrifugation step in the EV isolation procedure, although in the presence of 1.0 µM DiI (Invitrogen; Cat#: C-7000) during the first ultracentrifugation step (Section 2.2.2), as described in a previous publication [206]. CM was centrifuged at 2,000g for 10 mins at 4°C to remove cells and larger cell debris. EV pellets were washed in sterile PBS and ultracentrifugation repeated at 110,000g for 75 mins at 4°C in 28ml polyallomer ultracentrifuge tubes and on a SW28 swinging bucket rotor. The resulting EV pellets were resuspended in 200µl of sterile PBS and EV quantities were determined using the Bio-Rad protein assay (Bio-Rad; Cat. #: 500-0006). $2x10^4$ SKBR3 cells were seeded in 8 chambers of a confocal chamber slide and treated with 2µg of Hs578T or Hs578Ts(i)$_8$ DiI-labelled, and allowed to culture for 24 hrs. After 24 hrs, medium was removed, and cells were fixed as follows:

- Washed x2 with 300µl PBS for 5 mins each
- Fixed with 300µl methanol (-20°C) for 10 mins
- Washed x2 with 300µl PBS for 5 mins each
- Treated with 300µl 0.1% Triton-X (Sigma-Aldrich; Ct. no #: X100) (in PBS) for 8 mins
- Washed x2 with 300µl PBS for 5 mins each
- Blocked with 1% BSA (Sigma-Aldrich; Cat. #: A9413) for 30 min at 37°C
- Washed x2 with 300µl PBS for 5 mins each
- Treated with Floursave (Merck; Cat. #: 345789) (to preserve the fluorescent signal)
- Mounted with a cover slip and stored in the dark, at 4°C until analysed by confocal microscopy

Interaction of labelled EVs with cells was assessed by Olympus FV1000 confocal microscope.

2.2.6. Proliferation rate measurement

2.2.6.1. Assessment of cell proliferation

To assess the growth rates of Hs578T and Hs578Ts(i)$_8$ cells, 5x10^3 cells/well were seeded in 24-well plates and allowed to culture for 72 hrs. After 72 hrs, cells were trypsinised, centrifuged and counted with a Neubauer haemocytometer.

2.2.6.2. Assessment of cell proliferation in response to EVs

To assess if EVs have any effects on, and transfer proliferation characteristics representative of the differing Hs578T cell line variants, Hs578T, SKBR3, MDA-MB-231 and HCC1954 cells were seeded at 2x10^3 cells/well in 96-well plates, using 10% dFBS medium and 2µg/well of either Hs578T-EVs or Hs578Ts(i)$_8$-EVs, in equal volumes. After 72 hrs, cells were trypsinised, centrifuged and counted with a Neubauer haemocytometer as above.

2.2.7. Migration (wound healing assay)

2.2.7.1. Assessment of cell motility

To assess the motility rates of Hs578T and Hs578Ts(i)$_8$ cells, $3x10^5$ cells/well were seeded in 24-well plates and grown to confluency, then scratched with a 200µl pipette tip, washed twice with DMEM, and medium replaced with fresh complete medium with 1% FBS, as illustrated in Figure 2.3 below. The wounded areas were monitored and photographed by phase contrast microscopy and measured using Olympus Cell^A Image Acquisition Software.

2.2.7.1. Assessment of cell motility in response to EVs

Hs578T, SKBR3, MDA-MB-231 and HCC1954 cells ($3x10^5$ cells/well) were seeded in 24-well plates and grown to confluency, then scratched with a 200µl pipette tip, washed twice with media, and 10µg/well of Hs578T-EVs or Hs578Ts(i)$_8$-EVs, in equal volumes, were added with fresh complete medium with 1% dFBS, as illustrated in Figure 2.3 below. The wounded areas were monitored and photographed by phase contrast microscopy and measured using Olympus Cell^A Image Acquisition Software.

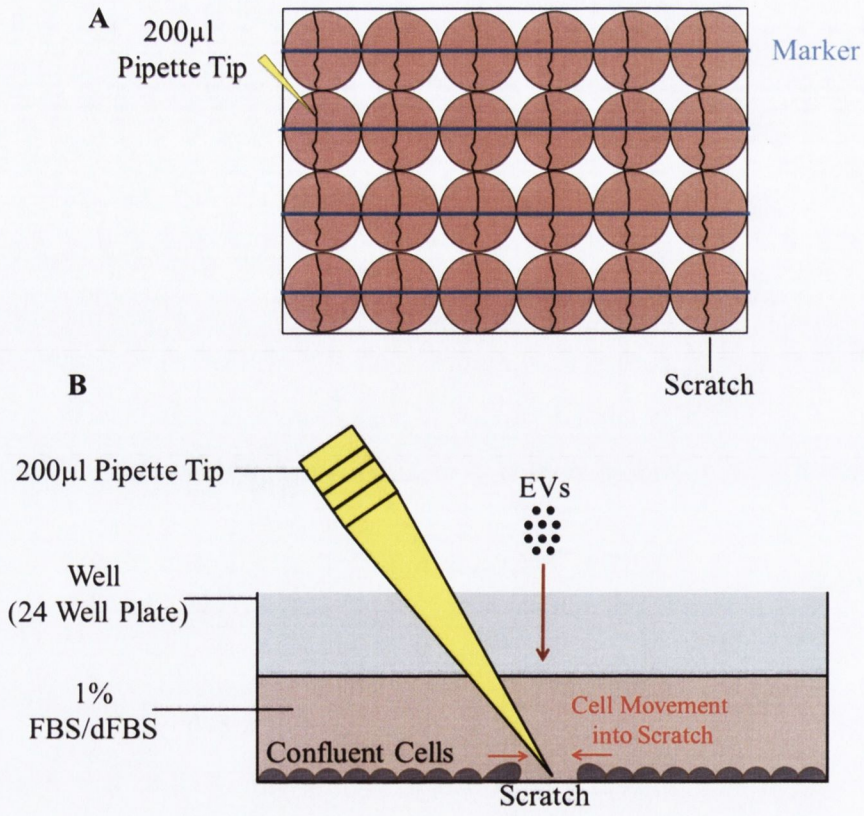

Figure 2.3: Wound healing assay set up to determine cellular motility/migration.

A: Arial view of the set-up of wound healing assay on a 24-well plate. This illustrates the scratching of the cells with a 200µl pipette tip and marking the underside with a permanent marker, ensuring the same scratch area can be located after time-points for accurate measurements. **B:** Cross section view of wound healing assay illustrating confluent cells being scratched by a 200µl pipette tip in a 24-well plate. It also illustrates how cells move into the area scratched by the tip, corresponding to motility rate EV addition is also demonstrated.

2.2.8. Invasion assays

Invasion assays were performed using 8µm pore size 24-well transwell chambers (Unitech, Cat. #: 353097). Prior to seeding, transwell chambers were coated with 100µl of 1:10 ECM (Sigma-Aldrich, Cat. #: E1270) diluted in DMEM, and left at 4°C overnight. 2 hrs prior to seeding the assay, ECM coated inserts were placed at 37°C, subsequently washed 3 times with base medium in preparation of seeding cells. Medium containing 10% dFBS (500µl) was added to each well. Hs578T ($5x10^4$), SKBR3 ($5x10^4$), MDA-MB-231 ($5x10^4$) or HCC1954 ($2.5x10^4$) cells, in 500µl complete 10% dFBS medium, were added to each insert. 5 hrs later, when cells had attached, medium within the inserts was replaced with medium containing 1% dFBS and 15µg of Hs578T, Hs578Ts(i)$_8$ or MDA-MD-231 EVs in equal volumes. After 72 hrs, medium was removed, inside of the insert wiped twice with PBS-soaked Q-tip, and stained with 1% crystal violet (Sigma-Aldrich, Cat. #: C6158). Crystal violet staining was solubilized in 10% acetic acid and absorbance was measured at 595nm on a FlouStar Optima microplate reader (BMG Labtech). The set-up of the transwell inserts is illustrated in Figure 2.4 below.

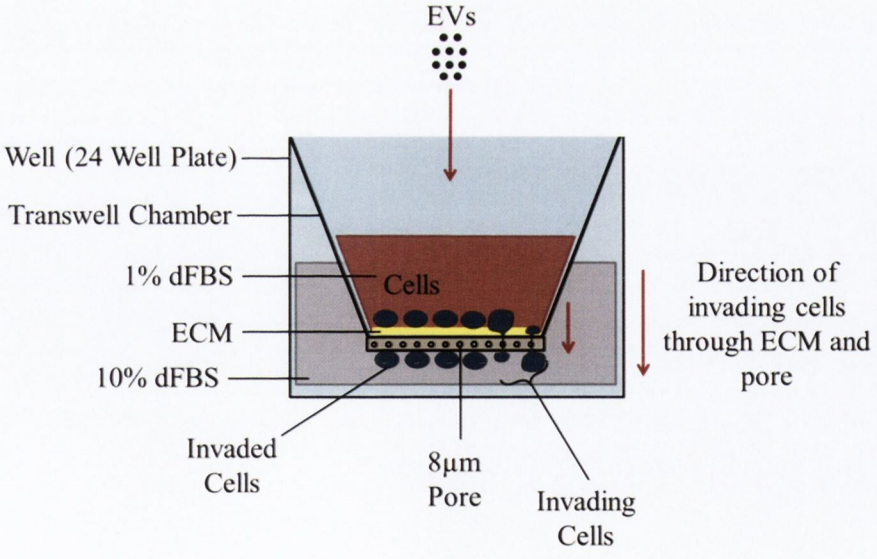

Figure 2.4: Transwell chamber invasion assay set up.

8µm pore sized transwell inserts are pre-coated with ECM in a 24 well plate, to which cells are seeded on top in 500µl of 10% FBS. 500µl of 10% FBS is placed in the well beneath the insert. Once cells attached, medium in the insert is replaced with 500µl of 1% FBS, to with 15µl of EVs are added. Cells are allowed to culture/invade for 72 hrs, after which invaded cells are stained with crystal violet.

2.2.9. *Anoikis* assays

Anoikis is a form of programmed cell death (apoptosis), which is induced when anchourage dependant cells detach from the surrounding ECM [280]. To replicate this event *in vitro*, 24-well plates were coated with 200µl/well of 12mg/ml poly-hydroxyethyl methacrylic acid (poly-HEMA) (Sigma-Aldrich, Cat. #: P3932) in 95% ethanol, and allowed to dry overnight in a laminar flow cabinet. A second coating was performed and allowed to dry overnight again. This was performed to prevent the attachment of the cells to the well. To act as a control, allowing the cells to attach to the base of the well, control wells were treated twice, overnight with 95% ethanol and allowed to dry, just as with the poly-HEMA coated wells. Prior to seeding cells, wells were washed with sterile PBS (Sigma-Aldrich Cat. #: D8537). This set up is illustrated in Figure 2.5 below.

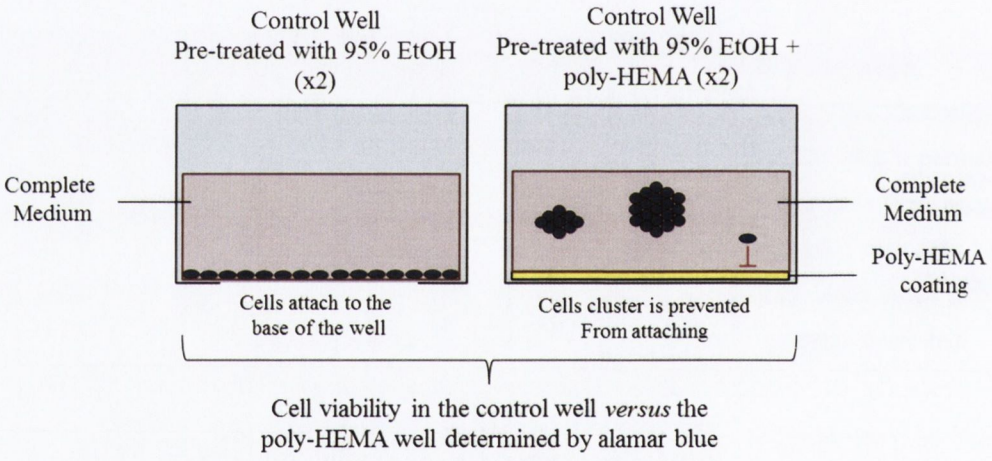

Figure 2.5: *Anoikis* assay set up.

Anoikis analysis determines cell viability when adherent cells are prevented from attaching to the well base.

2.2.9.1. Analysis of cellular response to *anoikis*

Hs578T and Hs578Ts(i)$_8$ cells ($5x10^4$ cells/well) were plated onto poly-HEMA-coated 24-well plates –or 95% ethanol-coated control plates- and cultured for 24 hrs. Alamar blue dye (100µl; Invitrogen Cat. #: DAL1100) was added/well and absorbance read at 570nm on a FlouStar Optima microplate reader (BMG Labtech). Percentage cell death of cells grown on poly-HEMA was calculated against cells grown without poly-HEMA coating.

2.2.9.2. Analysis of EVs on cellular response to *anoikis*

To assess if EVs transfer *anoikis* characteristics to recipient cells representative of their cells of origin, SKBR3, MDA-MB-231 and HCC1954 cells ($5x10^4$ cells/well) were seeded onto poly-HEMA plates with 10µg of Hs578T-EVs or Hs578Ts(i)$_8$-EVs, and were cultured for 72 hrs. Percentage cell death was calculated as described above in Section 2.2.9.1.

2.2.10. *In vitro* vasculogenesis and angiogenesis

The effects of EVs on vasculogenesis and angiogenesis was analysed using the V2a Kit (TCS-Cellworks; Cat. #: ZHA-4000) according to manufacturer's instructions. Briefly, human endothelial cells were cultured over a period of 14 days in a 24-well plate, where the cells were subjected to Hs578T-EVs or Hs578Ts(i)$_8$-EVs (10µg) treatment; added freshly every 48 hrs. 14 days post seeding, cells were fixed with 70% EtOH. Tubules were stained for CD31 (PECAM-1) using an anti-CD31 antibody (1:400) (TCS-Cellworks). CD31 tubule visualisation was achieved with the addition of the insoluble substrate 5-Bromo-4-chloro-3-indolyl phosphate - nitro blue tetrazolium chloride (BCIP/NBT), resulting in tubules forming a dark purple colour. Tubules were photographed, and quantitative measurement of tubule development (*i.e.* the combined total lengths of the network of tubules formed) was determined using ImageJ software "skeletonise" function. Tubules were stained and photographed using ImageJ software to measure tubule formation.

2.2.11. *In vivo* distribution of EVs

To investigate the behaviour of TNBC EVs *in vivo*, EVs were labelled as described in Section 2.2.5. 50µg of labelled EVs, in 100µl of DMEM, were injected into the tail vein of BALB/C nude mice in triplicate. Animals were sacrificed after 24 and 48 hrs when organs removed for *ex vivo* fluorescence analysis by *in vivo* imaging system (IVIS) to determine relative concentrations of EVs. In vivo distribution analysis of fluorescently labelled EVs was performed by Dr. Monika Jarzabek under the supervision of Dr Annette Byrne at an in vivo core facility, RSCI, Dublin, where ethical approval was granted.

2.2.12. Zymography

Zymography to detect matrixmetalloprotease (MMP) activity was performed as previously described [281]. Total cellular proteins were extracted from cells and EVs using cell extraction buffer, as described in Section 2.2.3.1. Proteins (10µg) were electrophoresed on a Sodium dodecyl sulphate-polyacrylamide gel electrophoresis (SDS–PAGE) containing 0.2% gelatin (Sigma-Aldrich; Cat. #: G8150). Gels were run on ice at 150V for 2 hrs and were subsequently washed with 2.5% Triton (Sigma-Aldrich; Cat. #: X100), twice for 20 mins each, rocking and at room temperature. Three 20 min washes were then performed using zymography buffer (0.15M NaCl (Sigma-Aldrich; Cat. #: S9888), 5mM $CaCl_2$ (Sigma-Aldrich; Cat. #: C5080), 0.05% NaN_3 (Sigma-Aldrich; Cat. #: S2002), and 50mM Tris-HCl (Sigma-Aldrich; Cat. #: T6791) buffer, pH 7.5), with fresh zymography buffer replaced after the final washing step. Gels were placed at 37°C in zymography buffer for 48 hrs and stained over-night with 0.025% commassie brilliant blue G250 (Sigma-Aldrich; Cat. #: B1131) in 25% methanol (Sigma-Aldrich; Cat. #: 322415), 10% acetic acid (Sigma-Aldrich; Cat. #: 272226), in H_2O. The gels were subsequently destained over-night with 8% acetic acid and 4% methanol in H_2O, rocking at room temperature. Gels were photographed using a Gel Doc™ XR+ System (Bio-Rad laboratories), and bands measured by densitometry using imageJ software.

2.2.13. qPCR

Total RNA was isolated from cell lines and EVs using the RNeasy Mini Kit (Qiagen; Cat. #: 74104). cDNA was prepared from 48ng of cell- or EVs-derived total RNA, respectively, using a High capacity cDNA reverse transcription Kit (Life Technologies; Cat. #: 4368814), using the components listed in Table 2.1 below. 10µl of RNA samples was added to the below master mix for the reaction.

Table 2.1: Components used for reverse transcription

Component	Volume per Reaction (µl)
10X Reverse transcription buffer	2.0
25X dNTPs	0.8
10X Random primers	2.0
Multiscribe reverse transcriptase, 50 U/µl	1.0
RNase inhibitor	1.0
Nuclease free H_2O	3.2
Total volume per reaction	10

The following program was used to perform the reverse transcription, setting the reaction volume to 20µl:

Table 2.2: Program used for cDNA synthesis

	Step 1	Step 2	Step 3	Step 4
Temperature	25°C	37°C	85°C	4°C
Time	10 mins	120 mins	5 mins	∞
Set reaction volume to 20µl				

qPCR analysis was performed using Taqman gene expression assays for mmp-2 (Hs01548724_m1, ABI, UK) and mmp-9 (Hs00957555_m1, ABI, UK), using the master mix outlines in Table 2.5 below. cDNA for both genes were amplified and threshold cycle (C_T) established, using a Mastercycler® ep Realplex (Eppendorf) using the setting outlines in Table 2.3 below.

The reaction was set up using the following master mix:

Table 2.3: Master mix ingredients used for qPCR analysis	
Component	**Volume per reaction (µl)**
20X taqman gene expression assay (primer)	1.0
2X taqman gene expression master mix	10.0
cDNA (from RT-PCR)	4.0
RNase-free water	5.0
Total volume	**20.0**

The following program was used to perform the qPCR, setting the reaction volume to 20µl:

Table 2.4: Program used for qPCR analysis			
	Step 1 (1X)	**Step 2 (40X)**	
Temperature	95°C	95°C	60°C
Time	10 mins.	12 secs.	60 secs

2.2.14 Statistical Analysis

Statistical analysis was performed using Excel. p-values were generated using Student's t-tests. $p<0.05$ was considered to be statistically significant. Results are displayed as n=3±SEM. GraphPad was used for graph generation.

2.3. Results

2.3.1. EVs were successfully isolated from Hs578T and Hs578Ts(i)$_8$ cells and interact with secondary cells

After performing the isolation procedure, the first step in this analysis was to establish if EVs had been successfully isolated using the protocol detailed in Section 2.2.2. To assess this, immunoblot analysis was performed to determine the presence of three proteins accepted as markers of EVs. These include

- PDC6I/Alix (96kDa cytoplasmic protein) which functions in the sorting of cargo into the MVB for processing into the ILV.
- TSG101 (44kDa tumour susceptibility gene 101) functions in the biogenesis of MVB formation, by binding to ubiquitinated cargo proteins, and is necessary for sorting endocytic ubiquitinated cargos into MVBs.
- CD63 (53kDa tetraspanin) is involved in late endosome formation [137].

TEM analysis was also elected to be performed to identify if the vesicles isolated were typically within the expected size-range (30-120nm) for EVs. Comparative total protein content was assessed on EVs expelled from Hs578T and Hs578Ts(i)$_8$ cells to establish if the quantities released were similar or significantly different. Immunoblot analysis for the presence of PDC6I/Alix, TSG101 and CD63 (Figure 2.6A) and TEM analysis (Figure 2.6C(i) and Figure 2.6C(ii)) confirmed successful isolation of Hs578T-EVs and Hs578Ts(i)$_8$ EVs. As expected, the proteins assessed were present in the EVs donor cell lines (Figure 2.6A). EVs quantities expelled from Hs578T and Hs578Ts(i)$_8$ cells were similar, showing no significant differences ($p=0.582$) (Figure 2.6B). TEM analysis indicated the isolates to be mainly nanosized EVs (~100nm in diameter) with the characteristic round or "saucer shape", for both EVs derived from Hs578T (Figure 2.6C(i)) and Hs578Ts(i)$_8$ (Figure 2.6C(ii)).

To establish whether our isolated EVs have the ability to interact/communicate with, or be taken up into secondary cells, Hs578Ts(i)$_8$-derived EVs were fluorescently labelled using the CM-DiI dye and applied to SKBR3 cells. Confocal microscopic observation determined that both Hs578T (Figure

2.6D(i)) and Hs578Ts(i)$_8$-derived EVs (Figure 2.6D(ii)) interact with, and are taken up by SKBR3 cells.

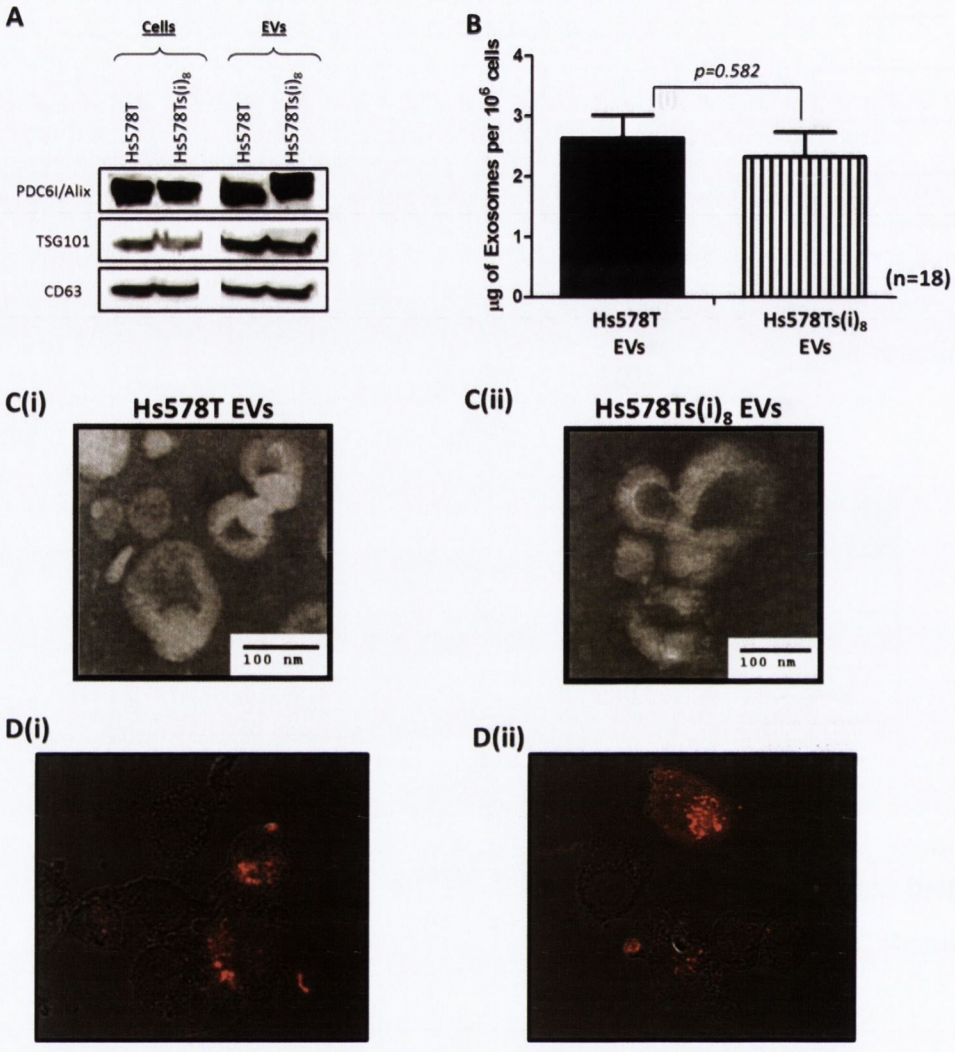

Figure 2.6: Successful EV isolation from Hs578T and Hs578Ts(i)$_8$ conditioned medium. Successful isolation of EVs from medium conditioned by Hs578T and Hs578Ts(i)$_8$ cells was confirmed by **A:** immunoblot analysis of exosomal/EV markers, PDC6I/Alix, TSG101 and CD63. **B:** EV protein analysis indicated similar quantities of exosomes to be expelled from Hs578T and Hs578Ts(i)$_8$ cells, analysed by Bio-Rad protein assay (n=18). **C:** TEM showed nano-sized vesicles of 30–120 nm diameter, for both **C(i):** Hs578T and **C(ii):** Hs578Ts(i)$_8$ samples (scale bar = 100 nm). **D(i):** CM-DiI (red) labelled Hs578T-derived EVs and **D(ii):** Hs578Ts(i)$_8$-derived EVs interact with SKBR3 cells.

TEM was performed with the help of Neal Leddy, Chief Technical Officer, CMA TCD.

2.3.2. Hs578Ts(i)$_8$ cells show increased proliferation and wound healing capabilty compared to its parent, less aggressive variant, Hs578T cells.

As Hughes *et al.* [278] previously determined that Hs578Ts(i)$_8$ cells are three times more invasive and two and a half times more migratory than Hs578T cells, we elected to analyse their aggressive characteristics in more detail, to further elucidate their aggression. To add to Hughes *et al.* findings, here Hs578Ts(i)$_8$ cells were found to proliferate more rapidly (4.6 fold; p=0.006; Figure 2.7A) than Hs578T cells and also had increased wound healing capability (2.4 fold, P=0.0003) after 24 hrs (Figure 2.7B).

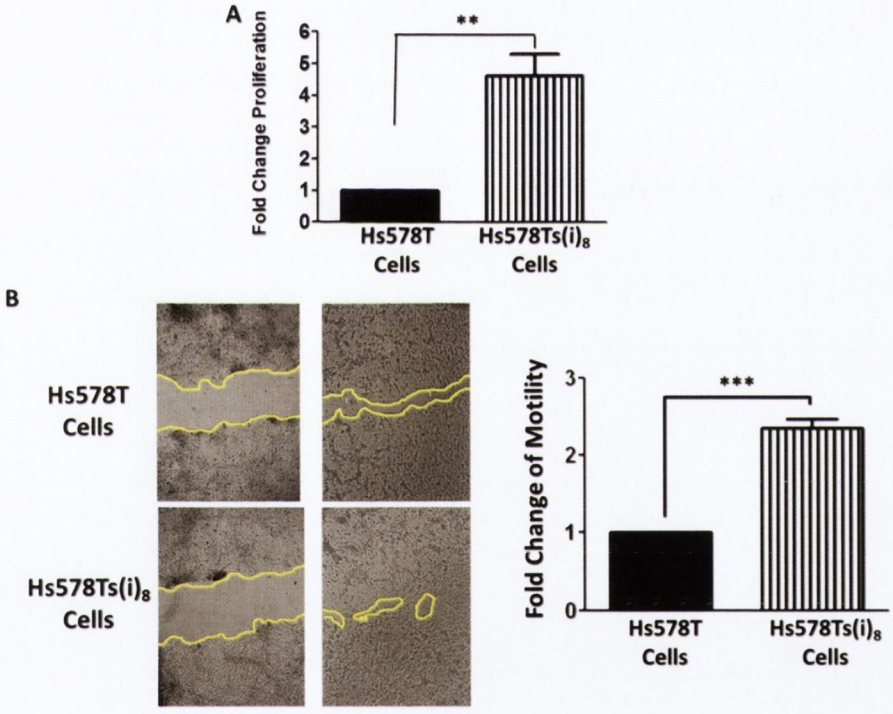

Figure 2.7: Hs578Ts(i)$_8$ cell grow faster and have increased proliferation and migratory ability, as analysed by wound healing assay, compared to Hs578T cells.

Here, the growth rates and wound healing abilities of Hs578T cells was compared to Hs578Ts(i)$_8$ cells. Analysis, determined that Hs578Ts(i)$_8$ cells **A:** proliferate at a greater rate, as determined by cell counting, and **B:** have increased wound healing capacity/motility than its isogenic variant, Hs578T cells. Results are displayed as n=3±SEM, where *=$p<0.05$, **=$p<0.01$, ***=$p<0.001$ (Student's t-test)

2.3.3. Hs578Ts(i)$_8$ EVs increase the aggression of it's parental isogenic variant, Hs578T cells

Once it had been established that EVs from TNBC cells can interact with, and be taken up into the cytoplasmic region of secondary cells, we next examined whether such interactions can mediate phenotypic alterations in cells. Initial analyses compared the effects of EVs derived from the TNBC cell line variants on a number of metastatic-associated phenotypes of cancer, by applying them to the parental Hs578T cells. In keeping with the observations that Hs578Ts(i)$_8$ cells grow faster (Figure 2.7A), have increased wound healing activity (Figure 2.7B) and are more invasive [278], here EVs expelled from Hs578Ts(i)$_8$ *versus* Hs578T cells significantly increased the proliferation of Hs578T cells by 1.4 fold; p=0.00005 (Figure 2.8A). Additionally, these EVs also increased that rates of Hs578T motility by 1.3 fold; p=0.0002 (Figure 2.8B), and invasion by 1.1 fold; p=0.003 (Figure 2.8C(ii)), all results mirroring findings of the innate phenotypes of the isogenic variant cells, as observed in Figure 2.7 and by Hughes *et. al* [278]. Comparing the effects of Hs578Ts(i)$_8$ EVs to a "No EV" control, using an equal volume of PBS as the volume of Hs578Ts(i)$_8$ EVs used, it was demonstrated that Hs578Ts(i)$_8$ EVs increase the rate of Hs578T invasion by 1.3 fold; p=0.02) (Figure 2.8C(ii)).

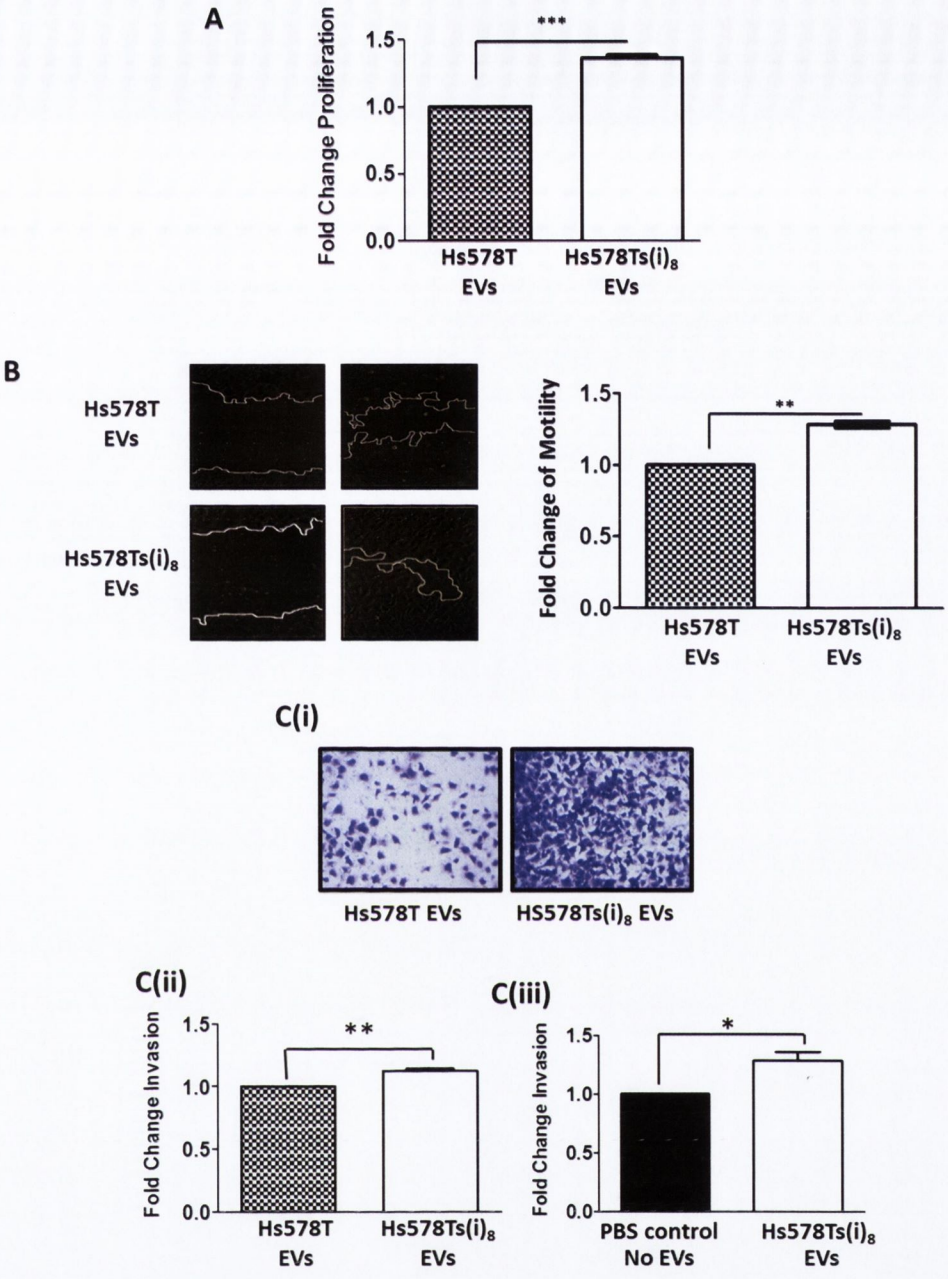

Figure 2.8: EVs from the more aggressive, Hs578Ts(i)$_8$ variant, increases the aggressiveness of parental Hs578T cells, versus Hs578T EVs.

This figure demonstrates that, when the effects of EVs from Hs578T and Hs578Ts(i)$_8$ are compared, the more aggressive-derived EVs significantly increase the rates of **A:** proliferation (2μg EVs), **B:** migration (10μg EVs), as shown by wound healing assay, and **C(i):** invasion (15μg EVs). **C(ii):** Similarly, Hs578Ts(i)$_8$-derived EVs increase the rate of Hs578T cell invasion compared to the Hs578T EVs and **C(iii)** compared to the same volume of PBS as a "no EV" control. Results are displayed as n=3±SEM, where *=$p<0.05$, **=$p<0.01$, ***=$p<0.001$ (Student's t-test)

2.3.4. Hs578Ts(i)$_8$-EVs increase the growth rate of recipient cells

To further investigate if EVs expelled from these TNBC cell line variants could transfer phenotypic characteristic representative of their cell line of origin to secondary "recipient" cells, we assessed the ability of the EVs to communicate a number of characteristics that differ between Hs578T and Hs578Ts(i)$_8$ cells on three more breast cancer cell lines. This further analysis was performed to ensure that any results obtained using the Hs578T cells (Figure 2.8) were not likely to be recipient cell line-specific but more broadly relevant. For this reason, the effects of Hs578T *versus* Hs578Ts(i)$_8$ EVs on three different secondary cell lines were evaluated. Firstly, their comparative effect on growth rate was analysed. In keeping with the observation that EVs from Hs578Ts(i)$_8$ cells increase the rate of proliferation of Hs578T cells, compared to the effects of Hs578T EVs, 2μg of EVs expelled from Hs578Ts(i)$_8$ *versus* Hs578T cells significantly increased the proliferation of all three recipient cell lines. Specifically, the growth rate of SKBR3 cells (HER2 over-expressing cell line) was 1.52-fold ($p=0.016$; Figure 2.9A) greater in the presence of 2μg of Hs578Ts(i)$_8$-EVs compared to 2μg of Hs578T-EVs. For MDA-MB-231 cells (TNBC cell line), the increase was 1.94-fold ($p=0.018$; Figure 2.9B); and for HCC1954 (HER2-overexpressing cell line), the increase was 1.58-fold ($p=0.048$; Figure 2.9C).

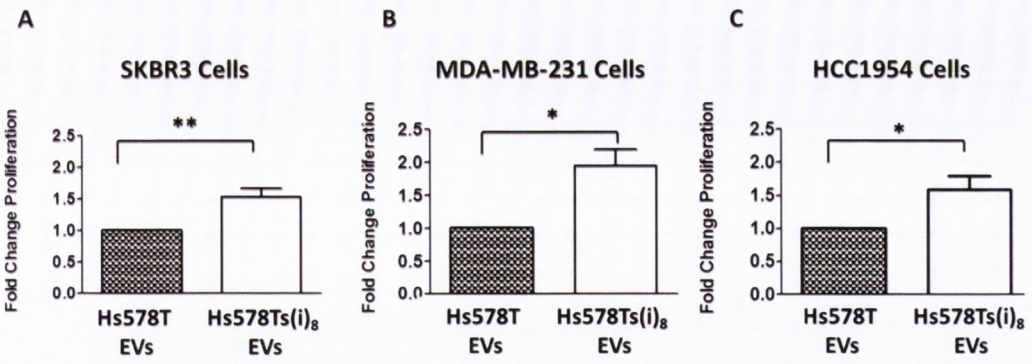

Figure 2.9: Effect of 2μg of Hs578T and Hs578Ts(i)$_8$ derived EVs on the proliferation rates of SKBR3, MDA-MB-231 and HCC1954 cells 72 hrs post EV treatment.

Proliferation assays were performed by seeding 2x10^3 of either SKBR3, MDA-MB-231 or HCC1954 cells in the presence of 2μg of either EVs in a 96-well plate and subsequently performing a haemocytometer cell count 72 hrs post treatment. **A:** Effect of Hs578Ts(i)$_8$ EVs versus Hs578T EVs on SKBR3 proliferation; **B:** Effect of Hs578Ts(i)$_8$ EVs versus Hs578T EVs on MDA-MB-231 proliferation; **C:** Effect of Hs578Ts(i)$_8$ EVs versus Hs578T EVs on HCC1954 proliferation. Results are displayed as n=3±SEM, where *=$p<0.05$, **=$p<0.01$, ***=$p<0.001$ (Student's t-test).

2.3.5. Hs578Ts(i)$_8$-EVs increase the motility of recipient cells

Prior to the studies reported here, using migration inserts (8μm pore size suitable for use with 24-well tissue culture plates), applying a fixed number of Hs578T or Hs578Ts(i)$_8$ cells into respective inserts and assessing movement through the pores with time –defined as migration– Hughes *et al.* [278] had established that the Hs578Ts(i)$_8$ variant cells is 2.5 fold more migratory than Hs578T cells. To add to this observation, Figure 2.7B demonstrated that Hs578Ts(i)$_8$ cells are 2.4 fold more motile, as determined by wound healing assay. In keeping with this trend, here we found 10μg of Hs578Ts(i)$_8$-EVs *versus* 10μg of Hs578T-EVs significantly increased the motility of each of the 3 recipient cell lines evaluated *i.e.* SKBR3 (2.64 fold, p=0.033; Figure 2.10A); MDA-MB-231 (3.92 fold, p=0.010; Figure 2.10B); and HCC1954 (1.27 fold, p=0.001; Figure 2.10C) cells.

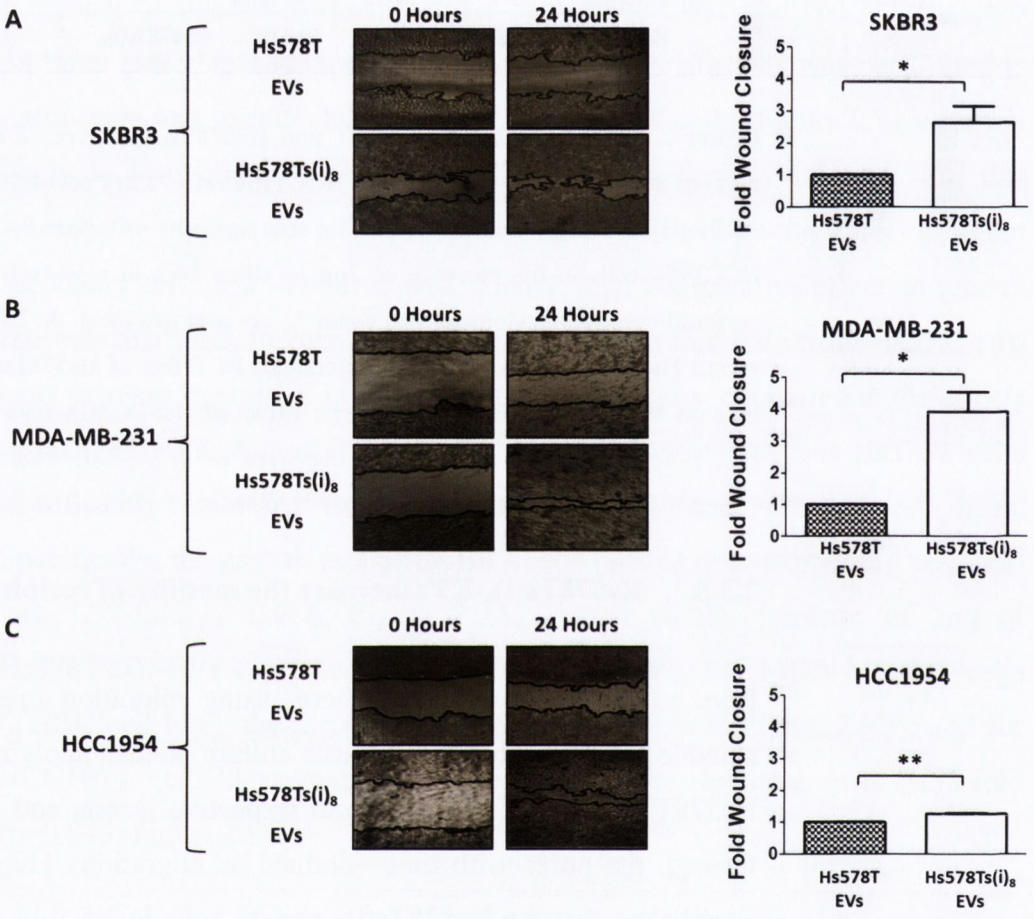

Figure 2.10: Effect of Hs578T and Hs578Ts(i)$_8$ derived EVs on the motility of SKBR3, MDA-MB-231 and HCC954 Cells, as determined by wound healing assay.

Wound healing assays were performed to assess secondary cell motility in response to Hs578T and Hs578Ts(i)$_8$ EVs. This figure illustrated the effect of 10µg of **A:** SKBR3, **B:** MDA-MB-231 and **C:** HCC1954 cells, compared to the effects of 10µg of Hs578T EVs on migration. Results are displayed as n=3±SEM, where *=$p<0.05$, **=$p<0.01$, ***=$p<0.001$ (Student's t-test).

2.3.6. Hs578Ts(i)$_8$–EVs increase invasive potential of recipient cells

Hs578Ts(i)$_8$ had previously been established as approximately three fold more invasive than Hs578T cells [278]. Here, Hs578Ts(i)$_8$-derived EVs applied to Hs578T were found to increase the invasion of three more breast cancer cell lines. Specifically, 15µg of Hs578Ts(i)$_8$-EVs *versus* 15µg of Hs578T-EVs were found to significantly increase invasion of SKBR3 (1.42-fold, p=0.016 (Figure 2.11A), MDA-MB-231 (1.52 fold, p=0.0004 (Figure 2.11B) and HCC1954 (1.19 fold, p=0.021 (Figure 2.11C).

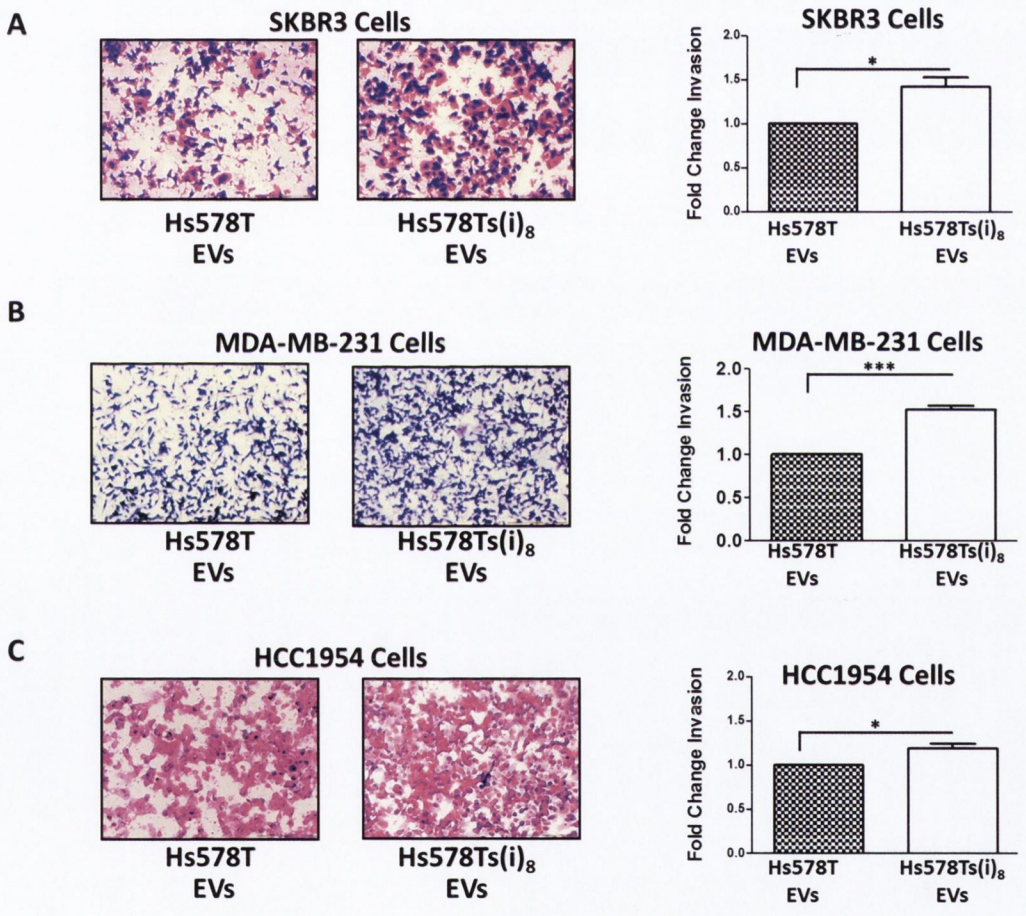

Figure 2.11: Effect of Hs578Ts(i)$_8$-derived EVs on the invasive potential of Hs578T cells, as analysed by ECM coated 8µm pore size 24-well transwell chambers.

Cells were seeded in the presence of 15µg EVs in 1% dFBS complete DMEM medium and allowed to invade for 72 hrs. This figure illustrates the effect of 15µg of Hs578Ts(i)$_8$ EVs on increasing the invasive capability of **A:** SKBR3 , **B:** MDA-MB-231 and **C:** HCC1954 cells, compared to the effects of 15µg of Hs578T EVs. Results are displayed as n=3±SEM, where *=p<0.05, **=p<0.01, ***=p<0.001 (Student's t-test).

2.3.7. EVs released from MDA-MB-231, another TNBC cell line, increase invasive potential of recipient cells

In order to determine if these affects are specific to EVs derived from the Hs578T and Hs578Ts(i)$_8$ variants or are potentially more broadly relevant, EVs from another TNBC cell line, MDA-MB-231, were functionally assessed. Following confirmation of successful EV isolation by immunoblot detection of PDC6I/Alix, TSG101 and CD63 (Figure 2.12A), 15µg of MDA-MB-231-derived EVs were found to significantly increase (by 1.24 fold, p=0.001) SKBR3 invasion (Figure 2.12B), similar to the effects reported above.

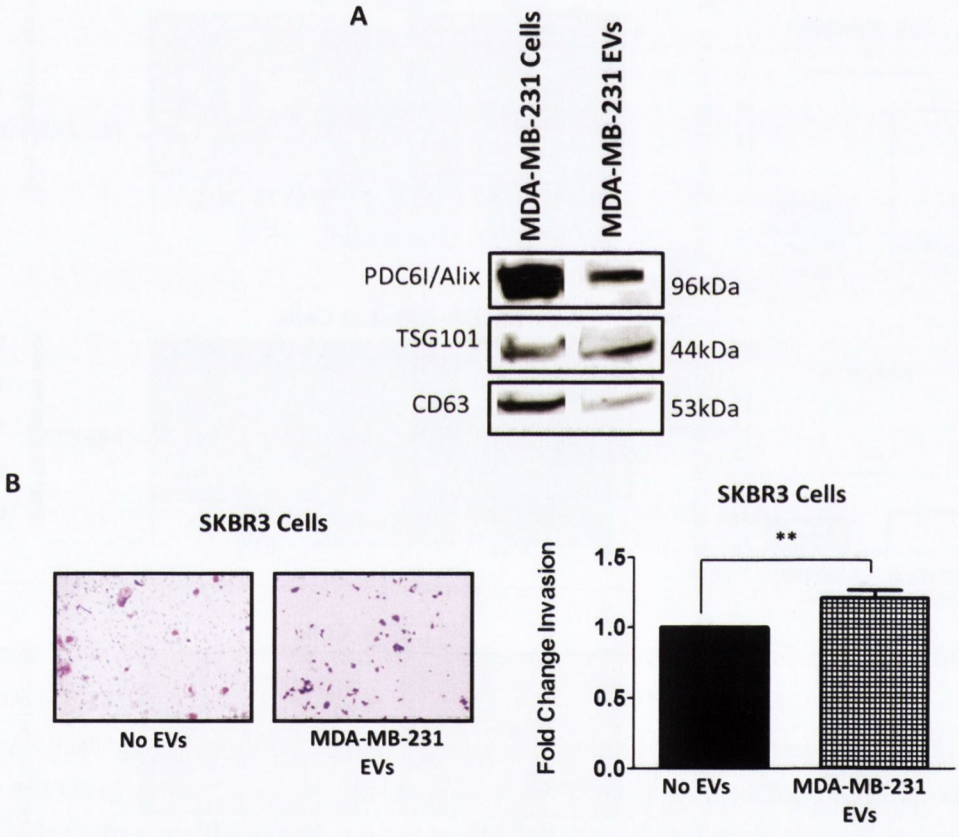

Figure 2.12: Effect of MDA-MB-231-derived EVs on the invasive potential of SKBR3 cells.

As above, invasion assays were performed on ECM coated 8µm pore size 24-well transwell chambers. Cells were treated with 15µg of EVs in 1% dFBS complete DMEM medium and allowed to invade for 72 hrs. This figure illustrates **A:** successful isolation of EVs from MDA-MB-231 cells as determined by immunoblot detection of PDC6I/Alix, TSG101 and CD63. **B:** the effect of 15µg of MDA-MB-231 EVs on SKBR3 invasive capability, compared to untreated cells (no EVs). Results are displayed as n=3±SEM, where *=$p<0.05$, **=$p<0.01$, ***=$p<0.001$ (Student's t-test).

2.3.8. EVs confer *anoikis* sensitivity/resistance to secondary cells, representing innate characteristics of their cells of origin

Most breast cancers are of epithelial cells, which typically grow whilst attached to a basement membrane, rather than existing in suspension. For such cells to survive in suspension, as required for circulating tumour cells to be transported in the blood stream or lymphatic's and progress to forming tumour metastasis, these cells must resist a form of programmed cell death termed *anoikis. Anoikis* is defined as programmed cell death induced when anchorage dependent cells detach from the basement membrane [282-284]. Here, using standard methods [285, 286] as described in Section 2.2.9, we attempted to mimic this situation *in vitro* by coating tissue culture plates with poly-HEMA and thus inhibiting the ability of the cells to attach to the tissue culture plastic. We subsequently assessed the ability of the cells to survive *i.e.* to resist *anoikis.* Possibly counter-intuitively, Hs578Ts(i)$_8$ cells were found to be 14% ($p=0.009$) more sensitive to *anoikis* than Hs578T cells. Representative images are shown (Figure 2.13A(i)) and graphical image depicting the percentage difference (Figure 2.13A(ii)).

Subsequently determining if this characteristic could be carried to secondary cells *via* EVs, we observed that the same trend was communicated *i.e.* 10μg of Hs578Ts(i)$_8$-EVs, compared to 10μg of Hs578T-EVs, conferred greater *anoikis* sensitivity to SKBR3 (13%, $p=0.008$; Figure 2.13B(i)), MDA-MB-231 (9%, $p=0.017$; Figure 2.13B(ii)), and HCC1954 (13%, $p=0.0001$; Figure 2.13B(iii)).

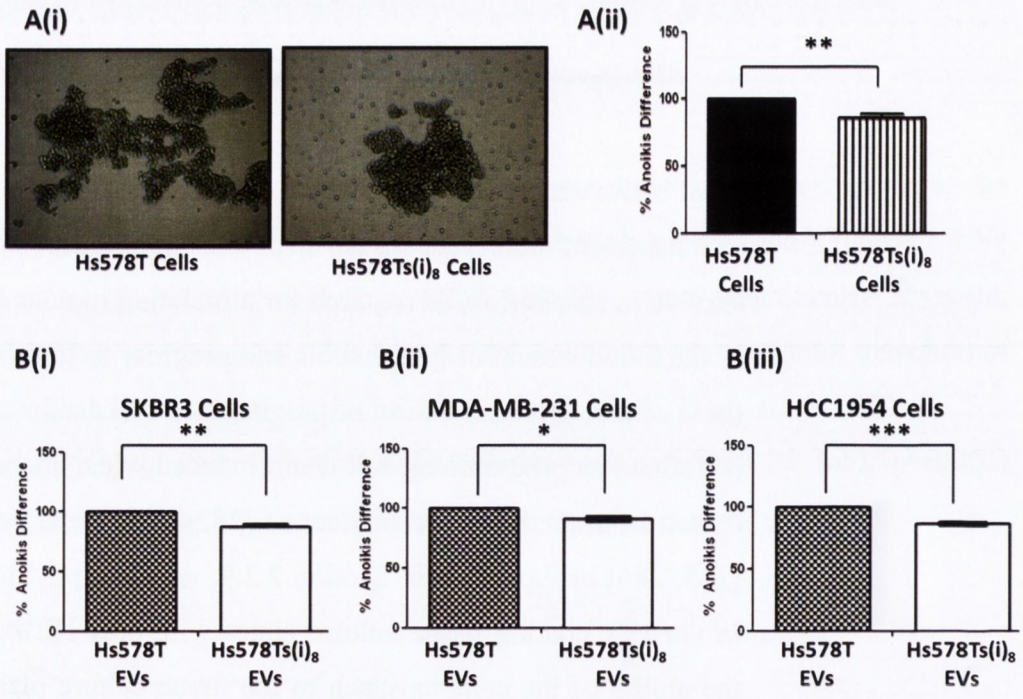

Figure 2.13: Characterisation of Hs578T and Hs578Ts(i)$_8$ *anoikis* resistance and the effect of Hs578T and Hs578Ts(i)$_8$ derived EVs on the *anoikis* resistance of SKBR3 cells, performed using poly-HEMA/EtOH coated 24-well plates.

A: Initial investigation into the innate response to *anoikis* in Hs578T versus Hs578Ts(i)$_8$ cells, determined that Hs578Ts(i)$_8$ cells are more sensitive to *anoikis* than the parental, Hs578T cells. **B:** This figure illustrates the effect of 10μg of Hs578Ts(i)$_8$ EVs versus 10μg of Hs578T EV increasing the *anoikis* sensitivity of **B(i)** SKBR3, **B(ii)** MDA-MB-231 and **B(iii)** HCC1954 cells. Results are displayed as n=3±SEM, where *=$p<0.05$, **=$p<0.01$, ***=$p<0.001$ (Student's t-test).

2.3.9. Hs578Ts(i)$_8$-EVs compared to Hs578T-EVs stimulate greater vasculogenesis and angiogenesis

Two distinct mechanisms, vasculogenesis and angiogenesis, implement the formation of vascular networks. Vasculogenesis is the process of new blood vessel formation from endothelial cells. Angiogenesis is the subsequent process by which these vessels take shape from these existing blood vessels by "sprouting" of endothelial cells thus expanding the vascular tree [287, 288]. For tumour mass survival and continuous growth, tumours must develop a blood vessel network to help carry oxygenated blood and nutrients to the cancer cells within the tumour mass. So here we were interested in establishing

if the EV populations under analysis could in anyway influence this phenomenon.

To investigate this, here we used endothelial cells (supplied as V2a Kit; TCS-Cellworks), as described in Section 2.2.10, which we exposed to either 10µg of Hs578Ts(i)$_8$-derived EVs or 10µg of Hs578T-derived EVs. We assessed the ability of the endothelial cells to form vessels and subsequently expand the network of vessels from these now pre-existing vessels over a period of 2 weeks. These studies indicated that Hs578Ts(i)$_8$-derived EVs could induce greater (2.87 fold, p=0.0004) angiogenesis after their addition to endothelial cells compared to the affects resulting from exposure to Hs578T-EVs, as indicated visually (Figure 2.14A) and quantitatively (Figure 2.14B).

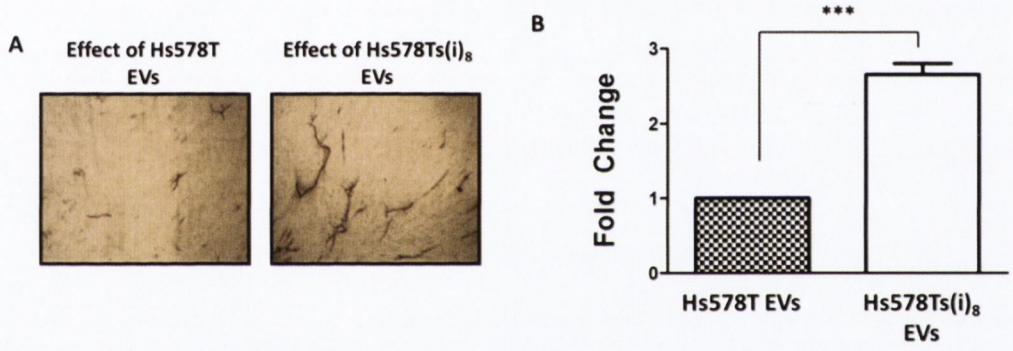

Figure 2.14: Hs578Ts(i)$_8$-EVs compared to Hs578T-EVs stimulate greater vasculogenesis/angiogenesis.

In vitro vasculogenesis/angiogenesis assays, performed in triplicate, indicated that Hs578Ts(i)$_8$-EVs stimulated significantly more endothelial tubule formation compared to the response of these cells to Hs578T-EVs. This is shown as **A:** images of the tubule formation 14 days after EVs exposure (n=3), and **B:** graphically, representing the quantitative effects illustrating a 2.87-fold increase of tubule formation (n=3) (p=0.0004). Results are displayed as n=3±SEM, where *=p<0.05, **=p<0.01, ***=p<0.001 (Student's t-test).

2.3.10. *In vivo* distribution of TNBC EVs

To investigate the relevance of Hs578T an Hs578Ts(i)$_8$ in pre-metastatic niche preparation and their behaviour *in vivo*, 50µg of DiI-labelled EVs were intravenously injected *via* the tail vein into BALB/C nude mice. 24 hrs and 48 hrs post injection organs analysed *ex vivo* by IVIS to quantify the fluorescent signal corresponding to the levels of EVs present in each organ. For this, a number of organs were analysed: liver, spleen, kidneys, heart, lymph nodes, bone, lungs and brain. *Ex vivo* fluorescence analysis (representative images Figure 2.15A) determined that after 24 hrs there was an insignificant ($p=0.58$) difference in overall EV presence between Hs578T and Hs578Ts(i)$_8$ EVs, suggesting that overall EV presence did not differ (Figure 2.15B). Fluorescence analysis determined that the majority of EVs from both Hs578T and Hs578Ts(i)$_8$ cells were trafficked to the liver, representing a 1.6 fold increase from Hs578T EVs and 1.9 fold increase for Hs578Ts(i)$_8$ EVs compared to the no-EV control (Figure 2.15C). Mice treatments and ex vivo analyses were performed in an in vivo core facility by Dr. Monika Jarzabek in RCSI, Dublin, under the supervision of Dr. Annette Byrne.

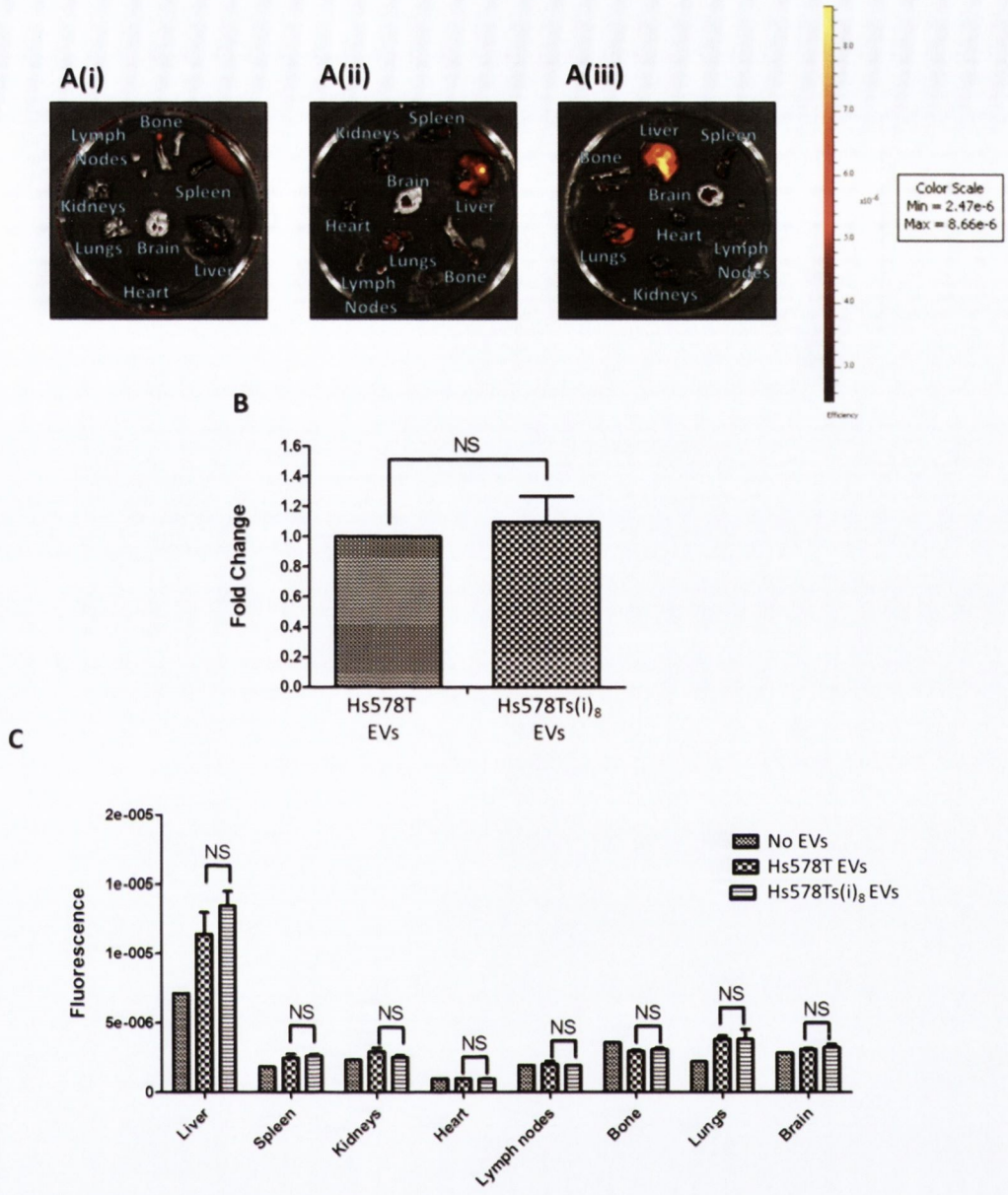

Figure 2.15: In vivo distribution of EVs 24 hrs post injection.

A: Representative bioluminescence images from harvested organs 24 hrs post EV injection from **A(i)** No EVs **(ii)** Hs578T EVs and **(iii)** Hs578Ts(i)$_8$ EVs. **B:** Overall fold change of presence on Hs578T versus Hs578Ts(i)$_8$ EVs *in vivo* after 24 hrs. **C:** Fluorescence readings for the presence of EVs in the liver, spleen, kidneys, heart, lymph nodes, bone, lungs and brain after 24 hrs. Results are displayed as n=3 mice ±SEM, where NS=non-significant (Student's t-test).

Mice treatments and ex vivo analyses were performed at an in vivo core facility by Dr. Monika Jazarbek under the supervision of Dr. Annette Byrne in RCSI, Dublin.

Similarly, *ex vivo* fluorescence analyses were performed on organs 48 hrs post injection (representative images Figure 2.16A). To note, results displayed for 48 hrs post injection represent two mice, as one animal succumbed soon after intravenous injection of Hs578Ts(i)$_8$ EVs. This analysis determined that after 48 hrs there was a mean trend of 1.4 fold increase of Hs578Ts(i)$_8$ EVs overall presence compared to the presence of Hs578T EVs (Figure 2.16B). Fluorescence analysis determined that after 48 hrs (mouse 1: Figure 2.16C and mouse 2: Figure 2.16D), there was a trend for the EVs from both Hs578T and Hs578Ts(i)$_8$ EVs to be trafficked to the liver, representing a 1.6 fold increase from Hs578T EVs and 2.3 fold increase for Hs578Ts(i)$_8$ EVs compared to the no-EV control. Notably, substantially greater levels of Hs578Ts(i)$_8$ EVs were found to be present in the lungs (1.6 fold) and lymph nodes (1.6 fold) compared to Hs578T EVs, suggesting that more aggressive derived EVs hone towards these areas pre-metastasis. Results also show that EVs from both cell lines can cross the BBB into the brain.

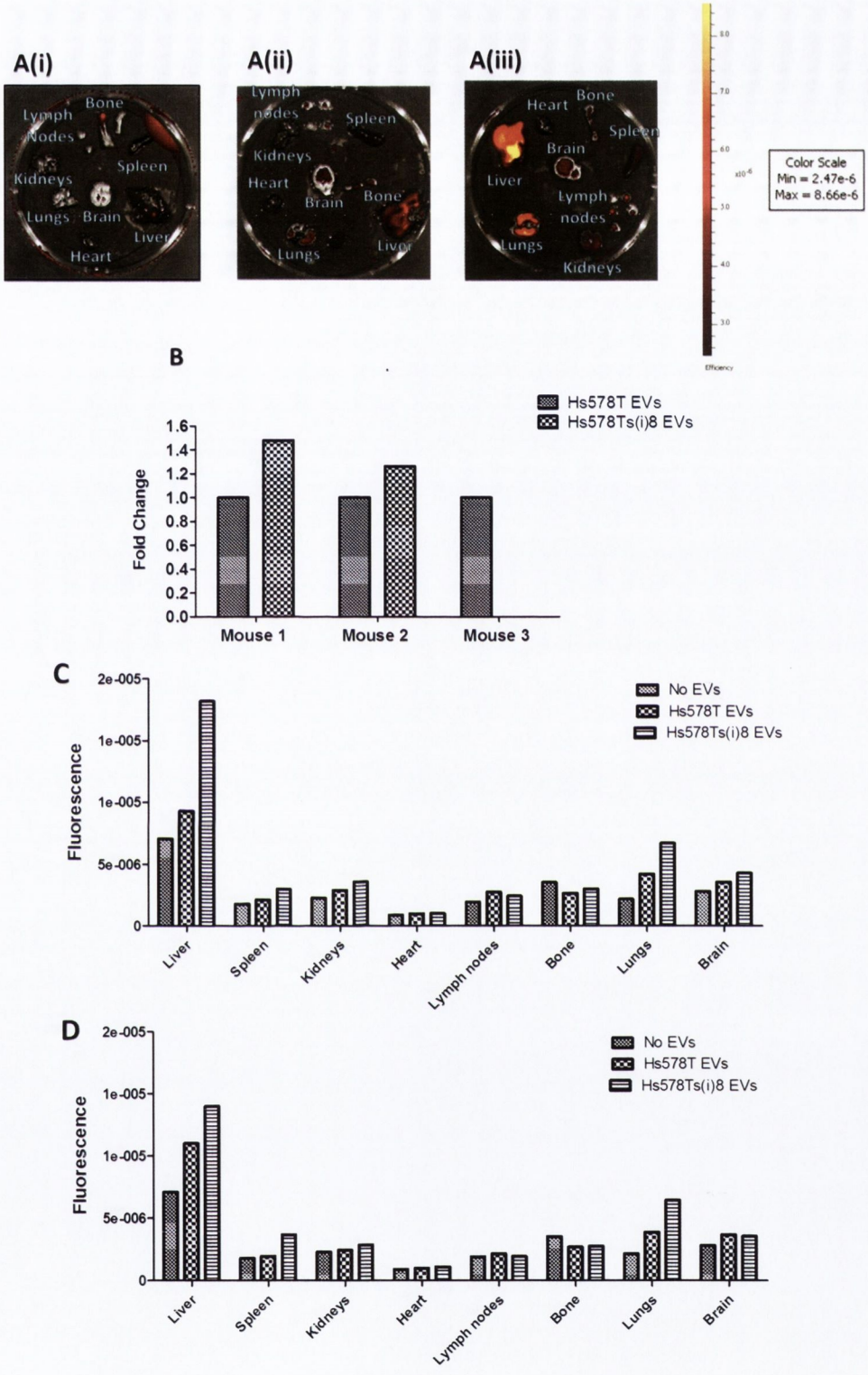

Figure 2.16: In vivo distribution of EVs 48 hrs post injection.

A: Representative bioluminescence images from harvested organs 48 hrs post EV injection from **A(i)** No EVs **(ii)** Hs578T EVs and **(iii)** Hs578Ts(i)$_8$ EVs. **B:** Overall fold change of presence on Hs578T versus Hs578Ts(i)$_8$ EVs *in vivo* after 48 hrs . **C:** Fluorescence readings in mouse 1 for the presence of EVs in the liver, spleen, kidneys, heart, lymph nodes, bone, lungs and brain after 48 hrs. **D:** Fluorescence readings in mouse 2 for the presence of EVs in the liver, spleen, kidneys, heart, lymph nodes, bone, lungs and brain after 48 hrs Results are

displayed represent 3 mice for Hs578T EVs and 2 mice for Hs578Ts(i)$_8$ EVs (one animal succumbed soon after intravenous injection of Hs578Ts(i)$_8$ EVs).

Mice treatments and ex vivo analyses were performed at an in vivo core facility by Dr. Monika Jazarbek under the supervision of Dr. Annette Byrne in RCSI, Dublin.

2.3.11. MMP-2 and MMP-9 are not transported in substantial quantities *via* Hs578T- or Hs578Ts(i)$_8$-EVs

Matrixmetalloproteinases (MMPs) are zinc-dependent endopeptidases capable of degrading extracellular matrix. MMP-2 and MMP-9 secretion is elevated in several types of human cancers and their elevated expression has been associated with poor prognosis [289]. The typical methods for MMP-2 and MMP-9 activity analysis is *via* zymography *i.e.* an electrophoretic technique, based on SDS-PAGE, that includes a substrate co-polymerized with the polyacrylamide gel, to enable detection of enzyme activity. qPCR is also a possibility for assessing corresponding mRNA levels and using Affymetrix microarrays, Hs578Ts(i)$_8$ cells have been shown to contain substantially higher levels of mmp-2 mRNA compared to that expressed by Hs578T cells [278].

Here zymography analysis of Hs578T and Hs578Ts(i)$_8$ cell samples showed significantly greater MMP-2 activity in Hs578Ts(i)$_8$ cells compared to Hs578T cells (2.37 fold; p=0.0005) (Figure 2.17A (i)). MMP-9 enzyme activity was undetected in both cell lines. The same analysis for MMP-2 using both cell and their respective EVs samples, confirmed MMP-2 activity in cells; but not in the corresponding EVs (Figure 2.17A(ii)). To determine if the corresponding mRNA was present, qPCR analysis of aliquots of the same samples detected mmp-2 mRNA in Hs578T cells after approximately 34 cycles, while mmp-2 mRNA was detected in Hs578Ts(i)$_8$ cell samples significantly (p=0.004) earlier (at approximately 30 cycle threshold, C_T (Figure 2.17B). However, assessing the corresponding EVs, mmp-2 mRNA was undetected in both Hs578T-EVs and Hs578Ts(i)$_8$-EVs within 40 cycles. Similarly, mmp-9 mRNA was detected in both cell variants, with significantly (p=0.004) higher levels in Hs578Ts(i)$_8$ compared to Hs578 cells; *albeit* levels of mmp-9 mRNA were overall lower than levels of mmp-2 mRNA (Figure 2.17C). As for mmp-2, mmp-9 mRNA was undetected in corresponding EVs within 40 cycles of qPCR.

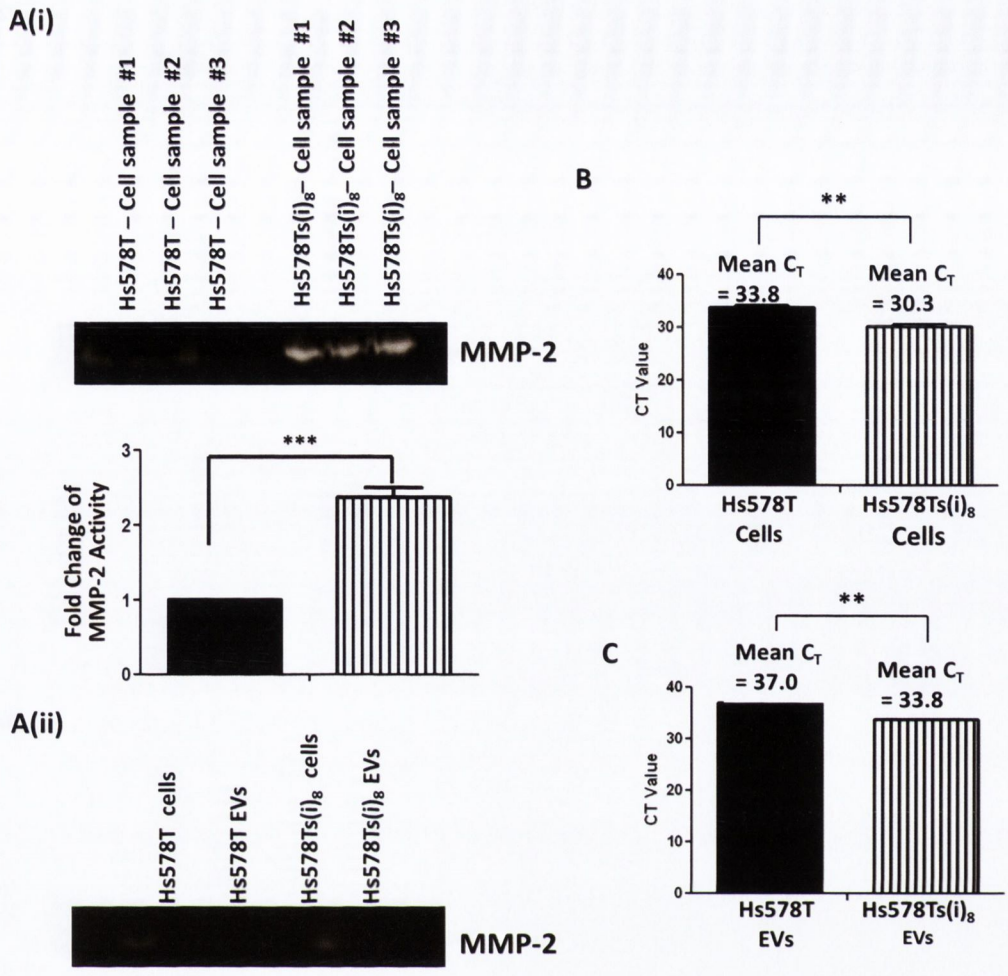

Figure 2.17: MMP-2 or MMP-9 in EVs is apparently not substantial contributor to secondary cell invasion.

A(i): Zymography analysis of Hs578T and Hs578Ts(i)$_8$ cell samples, showed substantially higher MMP-2 activity in Hs578Ts(i)$_8$ compared to Hs578T (zymogram – *top*; densitometry-derived data – *bottom*) (n=3). **A(ii):** The same analysis for MMP-2 using both cell and EV samples confirmed MMP-2 activity in cells, but not in the corresponding EVs (n=3). qPCR analysis of aliquots of the same samples detected **B**: mmp-2 mRNA in Hs578T cells after approximately 34 cycles, while mmp-2 mRNA was detected in Hs578Ts(i)$_8$ cell samples significantly (p=0.004) earlier. mmp-2 mRNA was undetected in corresponding EVs within 40 cycles (n=3). **C:** Similarly, mmp-9 mRNA was detected in both cell variants, with significantly (p=0.004) higher levels in Hs578Ts(i)$_8$ compared to Hs578T cells. mmp-9 mRNA was undetected in corresponding EVs within 40 cycles of qPCR. Results are displayed as n=3±SEM, where *=p<0.05, **=p<0.01, ***=p<0.001 (Student's t-test).

2.4. Discussion

This chapter sought to discover a potential role of EVs in the progression of TNBC cancer by examining the hallmarks of metastasis *i.e.* to increase proliferation, increase motility, increase invasion of cells through ECM, as well as increasing vasculogenesis-angiogenesis and assessing their influence on *anoikis* [198]. Prior to our publication on this work, limited numbers of studies were performed and indicated that breast cancer cell-derived exosomes and/or microvesicles to have functional relevance. Lau and Wong [276] assessed the effects of MDA-MB-231 (TNBC cell line) "exosome-like microvesicles" on human submandibular gland (HSG) cells, using lysed exosome-like microvesicles as controls. Intact exosome-like particles, compared to controls, increased the total amount of RNA in HSG cells and resulted in increased levels of 88 proteins in subsequent HSG-derived exosome-like particles. Of particular relevance to HER2+ breast cancers, exosomes from HER2-overexpressing breast cell lines, BT474 and SKBR3 (compared to those from melanoma cells, as control), sequestered the therapeutic antibody trastuzumab and thus substantially reduced its binding to tumour cells, with an overall effect of reducing *in vitro* antibody-dependent cellular cytotoxicity [215]. In the same study, Ciravolo *et al.* [215] demonstrated that in the serum from patients with invasive breast cancer (n=12), approximately one-third of the serum HER2 was found to be exosome-associated. Advancing on this, exosomes from HER2+ (SKBR3, BT474), but not HER2-negative (MDA-MB-231), cells decreased trastuzumab's anti-proliferative effects on SKBR3 cells, while the effect of lapatinib (targeting EGFR and HER2) was unaffected.

In cancer, it is typically the metastases that result in death. As MBC is not currently curable, the primary goal of current therapies is to restore the patients quality of life [290]. Metastasis is a multi-step event involving invasion at the primary site, intravasation of tumour cells through ECM to either blood or lymphatic vessels to circulate. These cells must be able to subsequently extravasate at the distant organ and establish secondary tumours or metastases. Recent studies indicate that EVs may be involved in preparing the pre-metastatic niche and subsequently attracting cancer cells to that site, further

highlighting the importance of elucidating their potential role in cancer and cancer metastasis [206, 218]. In TNBC specifically, visceral metastases to the lung, liver, bone and brain are commonly observed [290]. As TNBC is a particularly problematic and frequently presenting with aggressive behaviour and relapsing with distant metastases rather than with local sites, we decided to investigate if EVs play a role in their metastasis in order to elucidate a broader picture of TNBC metastasis, and the role of EVs in these events. It is for this reason that a number of phenotypes were investigated, pertaining to stages in TNBC metastasis. These phenotypes were performed using *in vitro* assays. *In vivo* analysis was performed to investigate whether EVs hone toward specific areas associated with TNBC metastasis which would suggest that they aid in pre-metastatic niche formation. The relevance of these assays to TNBC metastasis are highlighted in Figure 2.18 below, indicating where TNBC EVs were analysed as part of this study.

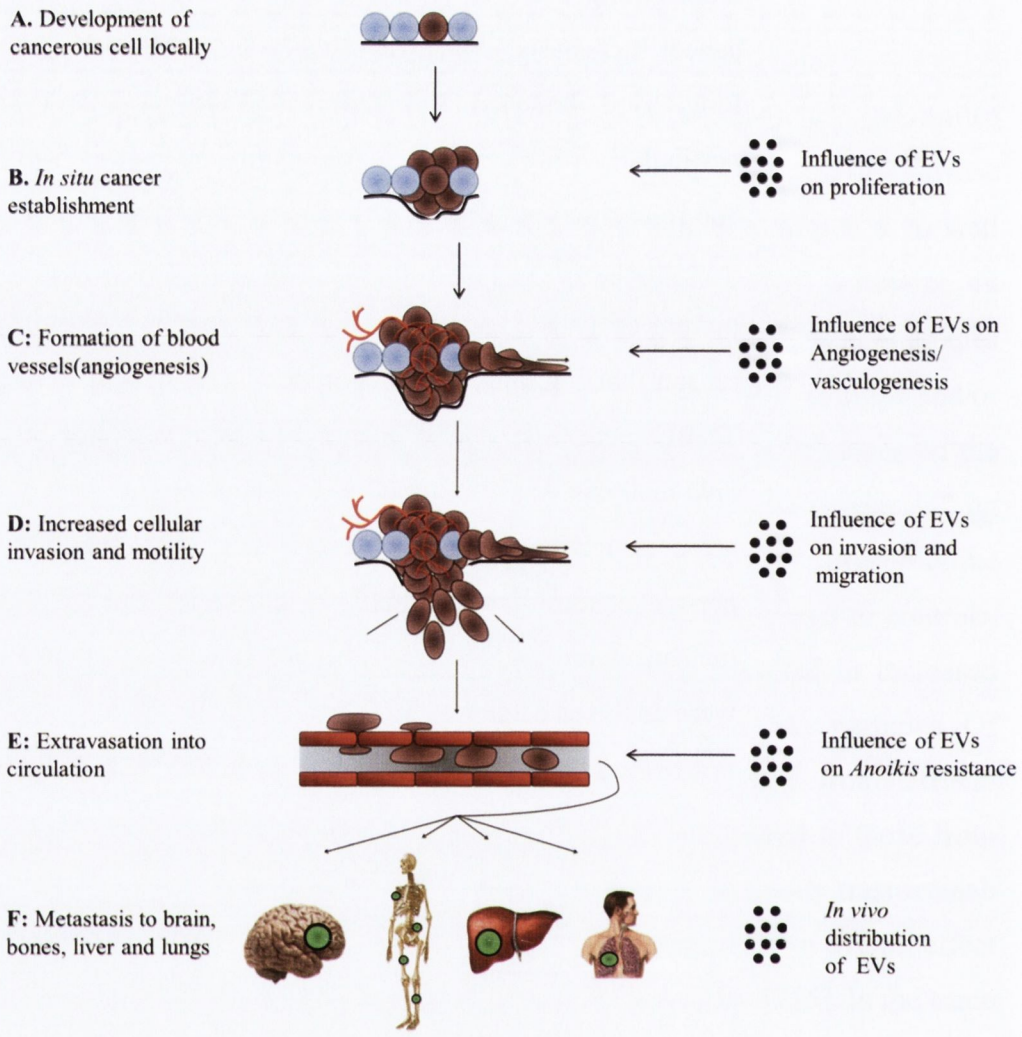

Figure 2.18: Effects of EVs in TNBC metastasis.

This diagram represents the potential influence of EVs in this process as analysed and determined in this chapter.

Of note, a concern with studies aimed at elucidating the functional relevance of EVs is identifying a suitable control vesicle. Depending on the scientific question being asked exosomes/EVs from cells lacking a specific receptor may be relevant. For other studies, saline/PBS or culture medium are used, but raise the concern of being unable to control for potential physical or mechanical effects, in addition to the biological effects of these nano-sized entities. Recent studies have involved generating nano-sized liposomes specifically for this purpose [206]. Here, for the main parts of this analysis, we had the opportunity to compare EVs isolated -in parallel and under precisely the same conditions- from matching isogenic populations, to assess if phenotypic characteristics

established as differing significantly between the cell populations would be passed on to secondary "recipient" cells.

TEM and immunoblotting confirmed successful isolation of EVs of nano-size, shape and markers indicative of EVs, especially representative of exosomes, as they showed characteristic "saucer-like" shape and detection of exosomal protein markers in our isolated sample. As typical for reported studies of exosomes, we cannot definitively claim a complete absence of microvesicles that are not exosomes; however this was not the intended focus for these analyses. The aim of this study was to investigate if epigenetic information can be relayed and transfer phenotypic changes to recipient cells secreted *via* nano-sized vesicles, rather than being critically concerned about the specific dimensions of the packages in which they are contained. Thus for the remainder of this discussion we will therefore refer to these vesicles as EVs. To ensure that any observations made by analysing the effects of these EVs were not specific to one recipient cell line, all subsequent analyses of these EVs included three secondary recipient cell lines, SKBR3, MDA-MB-231 and HCC1954, with proliferation, migration and invasion also analysed on the parental Hs578T cell line.

Prior to this study, Hs578Ts(i)$_8$ was identified and characterised by Hughes *et. al* [278]. Hs578Ts(i)$_8$ is significantly more proliferative, motile and invasive than Hs578T cells. Here our initial analyses was focussed on determining if EV phenotypic effects on secondary cells would reflect the cellular origin of the Hs578T- and Hs578Ts(i)$_8$-derived EVs, respectively, to increase metastatic phenotypes. Confocal microscopy analysis of labelled EV populations indicated their successful interaction/uptake by secondary cells. We have observed that applying these EVs to SKBR3, HCC1954, MDA-MB-231 and Hs578T cells, their proliferation, migration and invasion are all significantly increased in a manner representing their cells of origin, suggesting that TNBC derived EVs play an influential role in the increasing the aggression and metastatic potential of primary tumours. Additionally, Hs578Ts(i)$_8$ EVs increased the vasculogenesis of human endothelial cells suggesting they may

aid in the neovascularisation and angiogenesis process, facilitating tumour establishment.

Conversely, Hs578Ts(i)$_8$ were found to be more sensitive to *anoikis* than the parental Hs578T cells. This is somewhat unexpected, due to their otherwise more "aggressive" nature. Interestingly, a similar observation had been previously reporting when assessing *anoikis* resistance in LNCaP isogenic variant cells [291]. Briefly, two isogenic variants were isolated from LNCaP cells *i.e.* LNCaP-LN-4, a highly-metastatic variant and LNCaP-PRO-5, a non-metastatic variant. When analysing the *anoikis* resistance of the variants against each other, they observed that the highly-metastatic LNCaP-LN-4 were at least as sensitive to *anoikis* as the non-metastatic LNCaP-PRO-5 cells. While we are not in a position to speculate as to why this might be, this apparent lack of connection between invasion and *anoikis* may be of interest to further investigate in subsequent studies.

In order to investigate a potential mechanism of action used by the Hs578Ts(i)$_8$ EVs to exert increased aggression, the potential relevance of MMP transfer *via* EVs was considered. MMPs are involved in degrading ECM, necessary for invasion into the mesenchymal tissue [21, 23, 292]. So here we elected to study these enzymes in Hs578T and Hs578Ts(i)$_8$ variants and their corresponding EVs. To establish their relevance in the cells initially, MMP-2, but not MMP-9, enzyme activity was detected in Hs578T and Hs578Ts(i)$_8$ cell samples, with significantly greater MMP-2 activity in Hs578Ts(i)$_8$ cells, as would be expected. Neither MMP-2 nor MMP-9 activity was detected in their corresponding EVs. Furthermore, subsequent qPCR analyses indicated mmp-2 and mmp-9 mRNA present within Hs578T and Hs578Ts(i)$_8$ cells, but neither transcript was detected in the corresponding EVs –using the same quantity of starting total RNA and up to 40 cycles of real-time PCR. This result demonstrates that EVs derived from these cell lines are exerting their effects through a mechanism independent of direct MMP transfer.

Following on from these *in vitro* investigations, we elected to investigate the behaviour and potential relevance of EVs in promoting pre-metastatic niche formation. To perform this, EVs were isolated and fluorescently labelled from Hs578T and Hs578Ts(i)$_8$ cells and separately injected into the tail vein of BALB/C nude mice. This analysis determined that EVs are stable *in vivo* and that after 24 hrs no substantial difference in behaviour was observed between either Hs578T or Hs578Ts(i)$_8$ EVs. However, after 48 hrs differences became apparent between the two sets of EV populations. Taking all organs together, a trend of a 1.4 fold increase of overall Hs578Ts(i)$_8$ EV presence was observed compared to Hs578T EV presence, suggesting that more aggressive-derived EVs are more stable *in vivo* and may exert their effects for a more sustained period of time. Not only this, but substantial increases of Hs578Ts(i)$_8$-EV concentrations were observed in the lungs, spleen and liver of the mice compared to Hs578T EVs; with a less substantial increase observed in the brain of the mice. This suggests that the more aggressive derived EVs hone towards areas commonly implicated in TNBC metastasis, potentially educating the pre-metastatic niche favourable for disseminating tumour cells to establish. Our findings compliment previous findings which demonstrate the majority of EVs accumulate in the liver, lungs, kidney and spleen [157]. However, accumulation in the liver has been suggested to be a mechanism of EV clearance from the body. Of those EVs which survive hepatic confrontation, are subsequently trafficked to the lungs. [221].

The findings as part of the *in vivo* study suggest that EVs derived from the more aggressive cell line variant (Hs578Ts(i)$_8$) accumulate in greater concentrations in commonly observed metastatic regions suggests a more functional implication in TNBC metastasis, rather than fundamental trafficking. It may also suggest that EVs derived from Hs578Ts(i)$_8$ cells have greater ability to circumvent liver degradation, allowing them to exert their effects on pre-metastatic sites for a more sustained period of time. Such an observation correlates with previous discoveries that EVs have the potential to educate the pre-metastatic niche *in vivo* to facilitate metastasis to the lymph nodes [206]. Although *in vivo* findings reported here show promise, it must be noted that as only two mice from the Hs578Ts(i)$_8$-EV group survived for *ex vivo* analysis for the 48 hr time-point. Therefore, further investigation must be

performed using larger numbers of mice to confirm the importance of these observations.

2.5 Conclusion

These results support our hypothesis that, in TNBC, cellular communication *via* EVs may – at least in part – confer aggressive behavior to secondary cells by increasing the metastatic potential of a primary tumour and may prepare the pre-metastatic niche *in vivo*. Moving on from these discoveries, future studies will focus on identifying the specific molecules involved. To do this, the miRNA and DNA contents of both Hs578T and Hs578Ts(i)$_8$ EVs will be compared to potentially identify mediators of the phenotypic alterations (Chapter 3). In addition, future studies also aim to determine whether these observations are clinically relevant by obtaining EVs from the sera breast cancer patients to analyse their effect on secondary cell aggression, compared to EVs from the sera of healthy donor individuals (Chapter 4).

Chapter 3

Nucleic Acid (miRNA and DNA) analysis of TNBC cells and EVs with functional assessment of dysregulated miRNAs

3. Abstract

Background: miRNAs, small non-coding RNAs, have gathered much interest as they have the ability to regulate metastatic phenotypes, are showing potential in the treatment of breast cancer and can represent biomarkers for cancer. To identify potential miRNA biomarkers, or indeed, tumour suppressors, miRNA profiling methods have been employed. Although much promise has surrounded miRNA therapeutics, systems developed for miRNA delivery *in vivo* have been unsuccessful. It is therefore urgent to develop a method of miRNA delivery if the potential of miRNA therapies are to be realised and fully exploited. EVs are holding promise for use as miRNA delivery systems as they are well tolerated *in vivo*, capable of bypassing the immune response and can cross the blood-brain barrier (BBB). In recent years, DNA has been identified in EVs, and hold promise as extracellular DNA biomarkers for cancer.

Methods: EVs were isolated from the conditioned medium (CM) of Hs578T and Hs578Ts(i)$_8$ cells in triplicate, along with harvesting their cell pellets. Total RNA was isolated from cells and EVs and subjected to TaqMan Low Density array (TLDA) analysis for global profiling of 378 miRNAs. Fold changes of miRNA expression were compared between Hs578T and Hs578Ts(i)$_8$ cells and EVs using the delta-delta-cycle-threshold ($\Delta\Delta C_T$) method. Validation of miRNA expression was performed by qPCR. Functional analysis was performed by transiently transfecting of miR-370 and miR-134 into Hs578Ts(i)$_8$ cells to investigate their impact on proliferation, migration and invasion. Online miRNA target prediction software (TargetScan Human Release 6.2) was used to identify proteins potentially regulated by miR-134 and miR-370. Immunoblotting was performed to investigate the proteins affected by miR-134 and miR-370. Additionally, the potential of miR-134 to increase cisplatin induced-apoptosis and anti-Hsp90 drug potency was investigated. To identify mutated DNA sequences, DNA-SNP genotyping was performed on Hs578T and Hs578Ts(i)$_8$ cells and their EVs. using Sequenom MALDI-TOF technology.

Results: miRNA profiling determined that miRNA presence is largely conserved in EVs, compared to their cells of origin. miRNA levels are reduced in more aggressive cells and EVs, where there was a tendency for miRNA presence to be down-regulated. In total, four miRNAs were found to be significantly up-regulated and ninety-three down-regulated in Hs578Ts(i)$_8$ cells *versus* Hs578T cells. Although no miRNAs were found to be up-regulated in Hs578Ts(i)$_8$ EVs *versus* Hs578T EVs, 173 miRNAs were significantly down-regulated. Eighty-three of these miRNAs were commonly down-regulated in cells and EVs. The top ten of these down-regulated miRNAs are encoded by the chromosomal locus, 14q32.2. miR-134 was found to suppress STAT5B translation to reduce Hsp90 and Bcl-2, resulting in reduced cellular aggression and increased cisplatin-induced apoptosis. miR-134 transfection with lipofectamine does not appear to increase Hs578Ts(i)$_8$ sensitivity in combination with anti-Hsp90 compounds. Interestingly, treating aggressive TNBC (Hs578Ts(i)$_8$) cells with EVs manipulated to be enriched with miR-134 reduced STAT5B and Hsp90 expression to reduce cellular aggression and increase sensitivity to two anti-Hsp90 compounds, independent of effects on proliferation. However, miR-134 enriched EVs did not alter cisplatin-induced apoptosis. Functional analysis performed using miR-370 mimic, determined that this miRNA can also reduce Hs578Ts(i)$_8$ migration and invasion. dsDNA is present in Hs578T and Hs578Ts(i)$_8$ EVs. DNA-SNP genotyping showed PHLPP2 is mutated in cells and EVs, Harvey rat sarcoma viral oncogene (HRAS) mutated in all cells only, and TP53 is mutated in Hs578Ts(i)$_8$ derived EVs only.

Conclusions: This study has determined that EVs from TNBC cells represent the miRNA profile of their cells of origin, by 79.2% similarity in Hs578T and 74.8% in Hs578Ts(i)$_8$ EVs. There is a tendency for miRNAs to be lost in more aggressive cells and EVs. We conclude that miR-134 loss plays a functional role in increasing the aggression of TNBC and that miR-134 may represent a potential onco-suppressor for TNBC treatment. Interestingly, encapsulating miR-134 in EVs may provide a promising therapeutic strategy by repressing STAT5B and Hsp90 levels, thereby reducing cancerous aggression and increased anti-Hsp90 sensitivity. Our results suggest that miR-134 may be of

therapeutic value in TNBC, and encapsulating miR-134 in EVs could provide an efficient mechanism for miRNA based therapeutics. Furthermore, preliminary analysis shows that miR-370 could also prove to be an important molecule for TNBC treatment. We also provide evidence that EVs contain dsDNA and could show potential for use as extracellular-DNA biomarkers.

3.1. Introduction

To follow on from the previous chapter and published paper [152], the miRNA and DNA contents of the cells and EVs derived from them were investigated. This was performed in an attempt to discover the mechanism of action of the EVs, potentially discover a biomarker for TNBC progression or to identify miRNAs that may represent therapeutic entities as tumour suppressors.

miRNAs have been introduced in detail in Section 1.4. miRNAs act to suppress mRNA translation by attaching to their 3' UTR [293] and have emerged as potent regulators of diverse cellular and biological processes, including apoptosis, proliferation and differentiation [294], which has lead researchers to investigate their relevance in cancer [74], including breast cancer, as detailed in Section 1.4.2 [295]. miRNAs are commonly down-regulated in cancers and so have therapeutic potential as tumour suppressing agents. Recently, miR-148a has been identified to act as a tumour suppressor in epithelial-mesenchymal transition and metastasis of hepatoma cells by analysing its effects *in vivo* [296]. Additionally, a number of miRNAs have been identified to function as tumour suppressors in breast cancer, including miR-31, miR-205, miR-335, miR-124, miR-340 miR-196 [297], miR-200 and miR-141 [298]. Some miRNAs have been shown to induce apoptosis and chemosensitivity [299]. In depth investigation of the miRNA profile of TNBC may lead to discovering potential tumour suppressors which may prove to have therapeutic value.

It has been established that EVs contain miRNA [154] and that miRNAs can be transferred from cell-to-cell by EVs, subsequently mediating epigenetic alterations in distant cellular locations [300]. Recently, it has also been shown that EVs can be manipulated to transfer miRNAs representing therapeutics to secondary cells and that they may act in combination with vascular endothelial growth factor inhibitors by interfering with tumour angiogenesis in the treatment of leukaemia [226]. A detailed description of the use of EVs as miRNA therapeutic vesicles can be seen in Section 1.5.5.

TNBC represents an unmet clinical need for targeted therapeutics, which has been described in Section 1.3.3. One treatment option currently showing promise in TNBC treatment is the chemotherapeutic cisplatin. Cisplatin is a platinum-containing anti-cancer drug, which react *in vivo* to bind to, and cross-link DNA to trigger apoptosis. In a study of 25 patients, treated with four cycles of cisplatin at 75 mg/m^2 every 21 days, showed a pCR rate of 72% [55]. There is also optimism regarding the use of anti-Hsp90 compounds for TNBC treatment. Hsp90 is a chaperone protein that assists in the efficient folding and stabilisation of other proteins, including proteins associated with tumour growth, including Bcl-2 [64]. One such anti-Hsp90 compound showing promise in TNBC treatment is PU-H71. In a study in MDA-MB-468, MDA-MB-231, and HCC-1806 TNBC cell lines, PU-H71 induced significant cytotoxicity, as well as substantially inducing apoptosis in these cells. This drug has also shown effectiveness *in vivo*. Treatment of MDA-MB-468 tumour bearing with 2.5μM PU-H71 for 48 hrs showed 80-90% tumour death [65]. For this reason, targeting Hsp90 in TNBC is holding promise.

One of the proteins we became interested in as part of this chapter is Signal transducer and activator of transcription 5B (STAT5B). As a STAT protein, STAT5B has the ability to regulate gene expression, including regulating Hsp-90 transcription as shown in SKBR3 cells [301]. STAT5B have been shown to be overexpressed in breast cancers, and are involved in a cellular differentiation, proliferation and cell survival, and apoptosis [302] so has emerged as an attractive target for therapeutic intervention [303].

Somatic mutations are present in the genome of all cancer cells [304]. They may arise due to number of factors, including proofreading errors during DNA replication, exposure to exogenous or endogenous mutagens, enzymatic modifications of DNA or malfunctioning DNA repair mechanisms [305]. Occurrences of certain cancers are attributed to exposures to mutagens. This is most obviously highlighted in lung cancers, where exposure to tobacco smoke acts to mutate the DNA. In contrast, incidents of colorectal cancers appear to be more highly associated with defective DNA mismatch repair processes [306]. Somatic mutations include nucleotide substitutions, insertions and

deletions, copy number alterations, rearrangements as well as epigenetic influences which act to alter DNA sequences. Such aberrations can be broken down into two broad spectra based on their direct functional influence, or lack of, in cancer progression. Those mutations which confer an advantageous functional effect on cancer growth and oncogenesis are termed driver mutations, whereas passenger mutations classify all other cancer mutations. Although passenger mutations do not confer any "Mendelian" advantage, they may be useful in determining the aetiology and pathogenesis of cancer [304].

Of course breast cancers are no different. Evidence suggests that breast cancer is the cumulative consequence of an abundance of environmental insults and generic alterations [307]. Epidemiological studies have suggested an association between increased breast cancer risk and a number factors, such as high birth weight [308], obesity [309], estrogen stimulation [310] and family history of breast cancer, suggesting an inherited predisposition to breast cancer [311]. Although acquired somatic mutations are responsible for 90% of breast tumours, the HER2 amplifying mutation is the only one currently used to define a breast cancer subtype, as not others have been conclusively identified [312]. Initial, smaller early stage breast cancer genome sequencing studies all identified mutations in potentially cancer-causing genes, and appeared to be unique events in each patient case [313-318]. Using Sequenom technology, one of the largest breast cancer studies was performed on 267 stage I-III breast cancer tumours to investigate mutations of 28 potentially targetable genes. Of the most mutated genes were PIK3CA, PHLPP2 and KRAS, with FBXW7 mutations being the most common mutation in TNBC [319]. In another large scale study, 183,916 acquired somatic mutations were identified across 21 breast cancer specimens which also identified an important role of PIK3CA, as well as TP53 [320].

Sequencing technologies have made remarkable advances recently, overcoming traditional limitations of scale which have held back the field [321]. Advances in mutational screening were constrained by PCR-based methods which relied on sequencing the coding exons of protein-coding genes to pinpoint nucleotide substitutions and insertions/deletions [304]. However, advances now allow for thousands of somatic mutations to be identified from

one cancer specimen [305]. This has allowed for the identification of over 520 cancer genes (http://cancer.sanger.ac.uk/cancergenome/projects/census/) and somatic mutations from clinical specimens allowing researchers access to greater levels of information about the mutational nature and their implications in cancer [322].

Single nucleotide polymorphism (SNP) genotyping using the Sequenom MassArray iPLEX platform represents one of the favourable methods for SNP genotyping as it yields accurate results from a customisable platform and allows for a throughput of >100,000 genotypes/day/system. The foundation of the assay is based on a primer extension. PCR is used for the initial amplification of the specific locus of interest. This is followed by a locus-specific extension reaction where an oligonucleotide primer anneals upstream from the SNP region of interest, with mass modified dideoxynucleotide terminators present in the reaction. The primer extension is made according to the sequence of the variant site. Matrix-assisted laser desorption/ionization - time of flight (MALDI-TOF) mass spectrometry is used to determine the distinct mass of the extended primer to identify the SNP allele. Specifically, each spot on the chip is shot under vacuum with MALDI-TOF. The laser beam functions as a desorption and ionisation source in MALDI mass spectrometry. The matrix allows for the absorption of the energy emitted by the laser light, which causes some of the illuminated substrate to vaporise. Some of the analyte subsequently get carried into the vacuum due to the rapidly expanding matrix plume to aid in the sample ionisation process. As the matrix molecules absorb most of the laser energy, this minimises sample damage and ion fragmentation. The vaporised/ionised samples are then transferred electrostatically into a time-of-flight mass spectrometer (TOF-MS). Here, samples are separated from matrix ions. Once separated, samples are individually analysed based on mass-to-charge (m/z) ratios. Detection of an ion at the end is based on the time-of-flight. This is proportional to the square root of its m/z [323]. Diagrammatic representation of the Sequenom MassARRAY MALDI-TOF apparatus is shown in Figure 3.1 below.

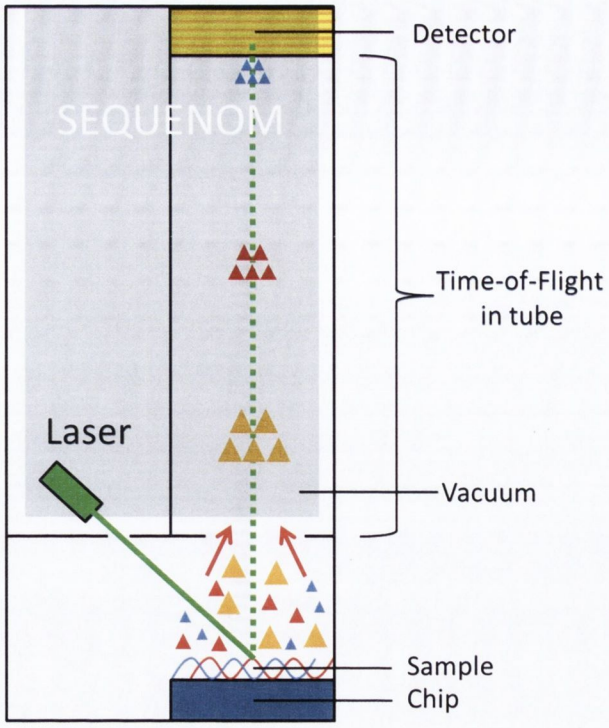

Figure 3.1: Sequenom MassARRAY MALDI-TOF apparatus.

Samples are irradiated by a laser resulting in desorption and ionisation vaporised/ionised molecules then enter the time-of-flight tube with a detector at the end. Separation of molecules in the time-of-flight tube is proportional to the mass of the ionised molecules *i.e.* smallest first.

Research over the last decade has reported the presence and implications of DNA in EVs. EVs have been shown facilitate the functional transfer of DNA from cell-to-cell [161, 249]. For example, chromosomal DNA from cardiomyocytes can be transferred by EVs to the cytosol and nuclei of recipient cells [249]. Similarly, mtDNA has been observed in EVs derived from glioblastoma and astrocytes, which can be transferred to receiving cells [251].

Such reports are surprising, as it was initially thought that EVs do not contain DNA [154]. However, not only has functional DNA been observed in EVs, but mutations have been reported to be detectable in these entities. In a small scale study on pancreatic cell lines (n=2 cell lines) and sera specimens (n=2 sera specimens), mutated forms of KRAS and TP53 were identified. Interestingly, mutated forms of KRAS and TP53 were identified in the EV fraction of the sera, but not in the EV-depleted sera specimens. This suggests that EVs are enriched in extracellular DNA mutations, when compared to sera as a whole. Such a report suggests that serum-derived EVs may be used to identify DNA

mutations for cancer prediction, diagnosis, treatment and therapeutic resistance [252].

Recently, the Lyden group in Cornell Medical College have reported similar findings, albeit in more detail. They reported that the majority of DNA in EVs is double stranded, and is present in EVs derived from all cell lines analysed, representing melanoma (seven cell lines), breast (five cell lines), lung (two cell lines), prostate (one cell line) and pancreatic cancers (two cell lines). However, extremely low yields of DNA were present in fibroblast-derived EVs (two cell lines). Using B16-F10 (melanoma) EVs as a model system, high throughput whole-genome sequencing showed that whole genome coverage was present in the EVs, but lacked the presence of mtDNA [324], although mtDNA was observed in previous studies of C2C12 myoblasts [250]. More interesting, driver mutational analysis determined that BRAF was mutated in EVs derived from all mutated BRAF carrying melanoma cells. Similarly, EGFR was mutated in NSCLC EVs derived from EGFR mutated cells. Using a pre-clinical animal model of melanoma, they determined that BRAF mutations can be detected in circulating EVs, strongly suggesting that EVs may hold potential as an effective method for biomarkers for cancer diagnosis and monitoring [324].

Advancing on these studies, here we examined the miRNA contents of the EVs to potentially identify mediators of the EV-induced signals and questioned whether the EVs could be manipulated into transporting miRNAs of choice to secondary cells, for use as therapeutic delivery vesicles. In addition, we isolated DNA from Hs578T and Hs578Ts(i)$_8$ cells and their EVs. To investigate whether cellular DNA is conserved in EVs, SNP genotyping was performed in RCSI, Beaumont Hospital by Dr. Sinead Toomey using the Sequenom MassArray iPLEX platform. This study also aimed to establish whether EVs have potential use as extracellular DNA biomarkers for TNBC diagnosis.

From this study we have identified loss of miR-134 in cells and EVs to be associated with increased cellular aggressiveness and our functional studies support its potential use as a therapeutic agent in TNBC, through its targeting of STAT5B [325] and subsequently reducing Hsp90 [301] and Bcl-2 [326]

levels. We have also confirmed the presence of dsDNA in EVs, which can capture mutated DNA sequences. This observation suggests that EVs have potential use minimally-invasive biomarkers for breast cancer diagnosis.

3.2. Materials and Methods

3.2.1. Cell culture

Hs578T and Hs578Ts(i)$_8$ cells were cultured as descried in Chapter 2, Section 2.2.1.

3.2.2. Extracellular vesicle isolation

EVs were isolated from the CM of Hs578T and Hs578Ts(i)$_8$ cells as described in Chapter 2, Section 2.2.2.

3.2.3. Immunoblotting

All cell and EV samples were collected and prepared for immunoblotting as described in Chapter 2, Section 2.2.3. Briefly, cell pellets and EVs were lysed using cell extraction buffer, with protease and phosphatase inhibitors, and prepared to desired concentrations in 4X loading buffer. 30µg of protein lysates were resolved on 12% SDS gels (Lonza; Cat. #: BMA59515) and transferred onto PVDF membranes (Bio-Rad; Cat. #: 162-0177). Blots were blocked in 5% (w/v) BSA in PBS containing 0.1 % Tween-20 and incubated overnight at 4^o C with primary antibodies to PDC6I/Alix (1:1000; Abcam), TSG101 (1:1000; Abcam), CD63 (1:500; Abcam), STAT5B (1:500; Cell Signalling), Hsp90 (1:1000; StressMarq) or β-Actin (1:1000, Sigma-Aldrich). Secondary antibodies were incubated for 1 hr at room temperature.

3.2.4. Transmission electron microscopy

TEM analysis was performed as described in Chapter 2, Section 2.2.4.

3.2.5. Isolation of total RNA from cells and EVs

RNA was isolated from cells and EVs in biological triplicate, with cells harvested from the flasks where the EVs were isolated from. Total RNA was isolated from cells and EVs using the miRNeasy mini kit (Qiagen; Cat. #: 217004), adapting the manufacturer's protocol to a protocol optimised by

Exiqon. Cell pellets were harvested by trypsinisation and washed twice with 1ml PBS by centrifugation at 13,000g for 5 mins, removing all excess PBS after the final centrifugation step. EVs were isolated as described in Section 2.2.2. Cells and EVs were suspended in 200µl of PBS and lysed using 750µl of QIAzol lysis reagent, and vortexed for 1 min and incubated at room temperature for 5 mins. 200µl of chloroform (Sigma-Aldrich, Cat. #: C2432) was then added to each sample and shaken vigorously for 15 secs, placed on the bench at room temperature for 2 mins, and then centrifuged at 12,000g at 4°C for 15 mins. An upper aqueous phase developed, which was taken from the Eppendorf to a new tube, where 1.5 times its volume of 100% molecular grade ethanol (Sigma-Aldrich, Cat. #: E7418) was added and mixed by pipetting. A 700µl aliquot was taken and added to an RNeasy spin column (see Figure 3.2) and centrifuged at 13,000g at 22°C for 30 seconds. This step was repeated for the remaining of the aqueous phase – ethanol mixture. 700µl of RWT buffer was added to the spin column and centrifuged at 13,000g for 1 min. 500µl of RPE buffer was added and centrifuged at 13,000g for 1 min; and repeated two more times. The spin column was then placed in a new collection tube and centrifuged for 2 mins at 13,000g. The columns were left open for 1 min and transferred to a labelled, RNase-free Eppendorf tube. Nuclease-free water (Ambion, Cat. #: AM9916) (50µl for cells; 20µl for EVs) was gently added to the filter in the spin column, incubated for 1 min at room temperature and spun for 1 min at 13,000g at room temperature to elute the total RNA. RNA quantities were determined using a Nanodrop ND-1000 spectrophotometer.

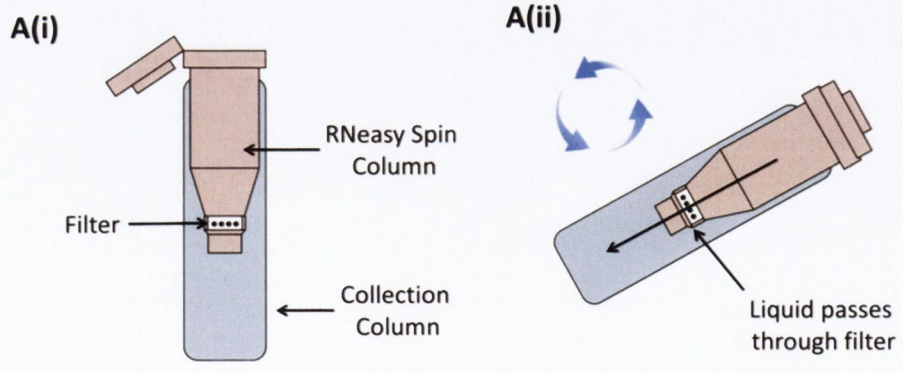

Figure 3.2: RNeasy spin column apparatus:

A(i): RNeasy spin column apparatus. **B(ii):** Upon centrifugation, any liquid passes throught the filter.

3.2.6. Taqman low density array for global miRNA profiling of cells and EVs

Taqman low density arrays (TLDA) (Life Technologies) were used for miRNA profiling. Human microArray A cards Set v.2.0 (Life Technologies; Cat. #:4398965) were used and consist of 378 functionally defined miRNAs plus endogenous controls (4x MammU6, 1x RNU48 and 1x RNU44). TLDA analysis was performed with the help of Dr. Claire Corcoran.

3.2.6.1. Reverse transcription of miRNA

Reverse transcription (RT) was performed using the TaqMan MicroRNA Reverse Transcription kit (Applied Biosystems; Cat. #: 4366595) following manufacturers instructions. Total RNA was reverse transcribed using TaqMan miRNA Reverse Transcription Kit (Applied Biosystems; Cat. #: 4366596) in combination with the MegaPlex primers pool set A (Applied Biosystems; Cat. #:4399966). The RT master mix was prepared as detailed in Table 3.1 below.

Table 3.1: Master mix components and volumes per reaction

Component	Company	Cat. #	Volume per reaction
MegaPlex RT primers (10X) human pool A	Applied Biosystems	4399966	0.80µl
dNTPs with dTTP (100mM)	Applied Biosystems	4366596	0.20µl
MultiScribe reverse transcriptase (50U/µl)	Applied Biosystems	4366596	1.50µl
10X reverse transcriptase buffer	Applied Biosystems	4366596	0.80µl
$MgCl_2$	Applied Biosystems	4400928	0.90µl
RNase inhibitor (20U/µl)	Applied Biosystems	4366596	0.10µl
Nuclease free water	Ambion	AM9916	0.20µl

4.5µl of the RT master mix was added to the apropriate wells of a 96 well PCR plate, and 3µl of RNA was then loaded into the appropriate wells, and left on ice for 5 mins. PCR was performed using the ViiA™ 7 Real-Time PCR System (Applied Systems) as outlined in Table 3.2 below.

Table 3.2: PCR program					
	1X Cycle	**40X Cycles**	**Hold**	**Hold**	**Hold**
Temperature	16°C	42°C	50°C	85°C	4°C
Time	2 mins	1 min	1 sec	5 mins	∞

3.2.6.2. Pre-amplification

2.5µl of cDNA was pre-amplified following manufacturer's instructions, with master mixes made according to Table 3.3 below, and inverted six times to mix and briefly centrifuged.

Table 3.3: Master mix components and volumes per reaction for pre-amplification			
Component	**Company**	**Cat. #**	**Volume per reaction**
TaqMan pre-amp master mix (2X)	Applied Biosystems	4391128	12.5µl
MegaPlex pre-amp primers (10X) Human pool A	Applied Biosystems	4399223	2.5µl
Nuclease free water	Ambion	AM9916	7.5µl
Total			22.5µl

22.5µl of master mix was put into each well as appropriate, to which 2.5µl of cDNA product was added as approprite. 96 well plates were sealed with MicroAmp clear adhesive film (Applied Biosystems, Cat. # 4306311), and briefly centrifuged to bring all components to the bottom of the well. Plates were then incubated on ice for 5 mins, and PCR performed according to the program outlined in Table 3.4 below, using the ViiA™ 7 Real-Time PCR System (Applied Systems).

Table 3.4: Pre-amplification PCR program		
Stage	**Temperature**	**Time**
Hold	95°C	10 min
Hold	55°C	2 min
Hold	72°C	2 min
Cycle (12 Cycles)	95°C	15 sec
	60°C	4 min
Hold	99.9°C	10 min
Hold	4°C	∞

Once the PCR program was over, plates were briefly centrifuged and 75µl of RNase free 0.1 X TE pH 8.0 (Ambion, Cat. #AM9858) was added to each product.

3.2.6.3. Performing TLDA real time assay

The real time assay mix was made as outlined in Table 3.5 below for each sample.

Table 3.5: Real time PCR components			
Component	**Company**	**Cat. #**	**Volume per reaction**
TaqMan universal PCR master mix no AmpErase® UNG (2X)	Applied Biosystems	4440048	450µl
Diluted pre-amp product	N/A	N/A	9µl
Nuclease free water	Ambion	AM9916	441µl

The mixture was inverted six times to mix and briefly centrifuged, and 100µl aliquots added to each port of the TLDA plate, as shown in Figure 3.3 below. TLDA plates were then centrifuged at 330g for 1 min and loaded into the ViiA™ 7 Real Time PCR System (Applied Biosystems) and ran using the TLDA default thermal cycling conditions.

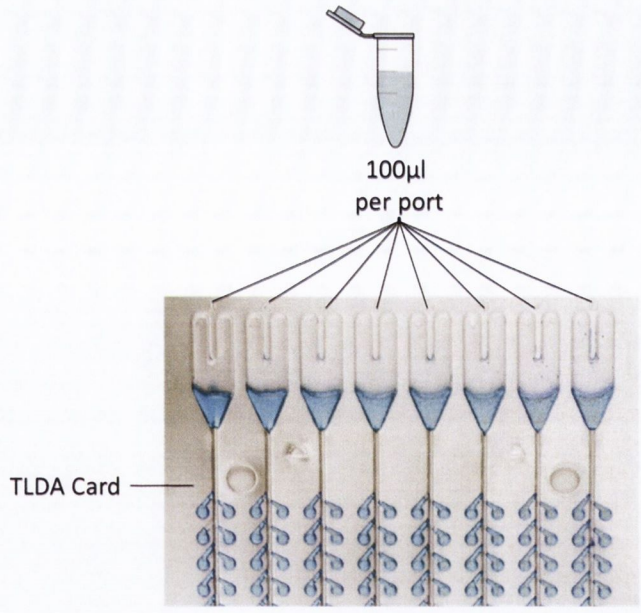

Figure 3.3: Loading TLDA card ports.

100µl of the real time PCR component mixture pipetted into each port and centrifuged.

3.2.6.4. Analysing TLDA results

Cycle threshold values were determined using SDS software. Relative quantities of miRNAs were calculated using the $\Delta\Delta C_T$ method after normalisation to RNU48 as the endogenous control. An outline of how the $\Delta\Delta C_T$ method is calculated is shown in Table 3.6 below.

Table 3.6: miRNA fold change of expression calculation using $\Delta\Delta C_T$ method

Calculation	Definition
C_T	Cycle threshold where miRNA is detected
ΔC_T	C_T of parent cells/EVs *(minus)* C_T of RNU48
$\Delta\Delta C_T$	C_T of variant cells/EVs *(minus)* ΔC_T of parent cells/EVs
$2^{(-\Delta\Delta CT)}$	Fold Change

3.2.7. qPCR validation of miRNA expression

In order to validate key findings from the miRNA profiling, qPCR was performed for specific miRNAs of interest. All TaqMan miRNA assays (miR-134: Assay ID: 001186; miR-370: Assay ID: 002275; miR-655: Assay ID: 001612; miR-376c: Assay ID: 002122; and miR-889: Assay ID: 002202) were purchased from Applied Biosystems. cDNA synthesis was performed using TaqMan miRNA reverse transcription assays kit (Applied Biosystems; Cat. #: 4366596) according to manufacturer's instructions. Reverse transcriptions were performed using 10ng of total RNA. Master mixes for each primer were made according to Table 3.7 below:

Table 3.7: Master mix preparation for cDNA synthesis	
Component	**Volume per reaction**
100mM dNTPs	0.15µl
Multiscribe reverse transcriptase	1.00µl
10X Reverse transcription buffer	1.50µl
RNase inhibitor	0.19µl
Nuclease free water	4.16µl
5X RT primer	3.00µl
Total	10.00µl
5µl of 2ng/µl (10ng) of RNA was added to the reaction as appropriate	

RT was performed under the following conditions:

Table 3.8: Program used for cDNA synthesis		
Step	**Time**	**Temperature**
Hold	30 mins	16°C
Hold	30 mins	42°C
Hold	5 mins	85°C
Hold	∞	4°C

qPCR was performed using TaqMan microRNA assay kit (Applied Biosystems; 4427975), using 1.33µl of cDNA product from reverse transcription. qPCR was performed using a Mastercycler® ep Realplex (Eppendorf). As for TLDA data analysis, relative quantities of miRNA were calculated using the $\Delta\Delta C_T$ method after normalising using RNU48 as the endogenous control and a 2-fold increase or decrease, and p-values <0.05 as significant, were used for determining if a miRNA was comparatively up- or down-regulated.

3.2.8. microRNA transfection of Hs578Ts(i)$_8$ cells

Hs578Ts(i)$_8$ cells were transfected with 30nM of miR-134 (Applied Biosystems; Cat #: 4464066; ID: MC10341), miR-370 (Applied Biosystems; Cat #: 4464066; ID: MC12868) or negative control (NC) (Applied Biosystems; Cat #: 4464058; ID: Negative control (NC) #1) mimics. To achieve this, Hs578Ts(i)$_8$ cells were seeded at a density of $1.5x10^5$ cells/well in 2mls of complete Hs578Ts(i)$_8$ growth medium in a 6 well plate and allowed to attach overnight. The following day, medium was replaced with fresh 2mls of complete medium. 5µl of lipofectamine 2000 (Invitrogen, Cat. #: 11668-027) per well was diluted in 250µl of Opti-MEM medium (Invitrogen, Cat. #:11058-021), mixed by inverting the tube and incubated for 5 mins. Simultaneously, 30nM of miRNA mimic was diluted in 250µl of Opti-MEM and mixed by inverting the tube and also allowed to incubate for 5 mins. After 5 mins, the lipofectamine/Opti-MEM mixture was mixed with the miRNA/Opti-MEM mixture and incubated for 20 mins at room temperature. The 500µl mixture was subsequently added drop by drop to the cells as appropriate and allowed to transfect for 4 hrs at 37°C/5% CO_2. Medium was then removed and cells were gently washed twice with medium to remove any excess lipofectamine 2000. Medium was then replaced with fresh 2mls of medium to negate any toxic effects of lipofectamine 2000. For proliferation (Section 3.2.10), migration (Section 3.2.11) and invasion (Section 3.2.11) assays, transfected cells were trypsinised, counted and seeded at appropriate concentrations 48 hrs post transfection. To analyse apoptosis (Section 3.2.12), 24 hrs post transfection cells were treated with 15µM cisplatin for 24 hrs and apoptosis analysed by

flow cytometry. For immunoblotting, cells were cultured for 72 hrs when cell pellets were harvested and lysed for analysis.

3.2.9. Immunoblotting transfected cells

Hs578Ts(i)$_8$ cells were transfected as described in Section 3.2.8. Cell pellets were collected 72 hrs post transfection and prepared for immunoblotting as described in Section 2.2.3. Total cellular proteins (30μg) were resolved on 12% PAGEr Gold precast gels for protein electrophoresis (Lonza, Cat. #: 59515) and transferred by semi-dry transfer to PVDF membranes (Bio-Rad; Cat. #: 162-0177) at 20V for 1 hr. Blots were incubated in blocking buffer (5% BSA (Sigma-Aldrich, Cat. #A9413) in PBS/0.1% Tween (Sigma-Aldrich, Cat. #: P2287)) at room temperature while rocking for 1 hr. Primary antibodies for SMO (1:500; Santa-Cruz), β-Actin (Sigma-Aldrich), STAT5B (1:500; Cell Signalling) and Hsp90 (1:1000; StressMarq) were prepared in 3% BSA in PBS/0.1% tween. Membranes were incubated in primary antibodies overnight, gently rocking, at 4°C. Membranes were then incubated with appropriate horseradish peroxidase-conjugated secondary antibodies *i.e.* anti-mouse (Cell Signalling, Cat. #: 7074; 1:1000 dilution) or anti-rabbit (Cell Signalling, Cat. #: 7076; 1:1000 dilution) for 1 hr at room temperature and proteins were visualised by chemiluminescence (ThemoFisher: Cat. #: 34080). Detection was performed with a Chemidoc exposure system (Bio-Rad Laboratories). Densitometry of the protein bands was performed using ImageJ software and normalised to β-actin

3.2.10. Analysing growth rates of transfected cells

Proliferation analysis was initiated 48 hrs post transfection of cells and allowed to culture for 48 hrs before analysing growth rates. To perform this, transfected Hs578Ts(i)$_8$ cells (with miR-134, miR-370 or NC mimic cells) were trypsinised, counted and seeded at a density of $2x10^3$ cells per well in a 96 well plate in triplicate and allowed to grow for 48 hrs, when cell growth was measured using the acid phosphatase method, as described in Section 3.2.10.1.

3.2.10.1. Acid Phosphatase method for assessing cell growth

Sodium acetate buffer was prepared using the following ingredients:

- 500ml of dH_2O
- 4.1g sodium acetate (Sigma-Aldrich, Cat. #: S2889)
- 500µl Triton X-100 (Sigma-Aldrich, Cat. #: T8787)
- pH to 5.5 using HCl (Sigma-Aldrich, Cat. #: H1758)
- Sored at 4°C

Phosphatase substrate buffer was made freshly prior to adding to the cells. 0.027g of 10mM p-nitrophenol phosphate (VWR, Cat. #: 27963.101) was added per 10ml of sodium acetate buffer. Medium was removed from wells and cells washed twice with 100µl of PBS. 100µl of phosphatase substrate buffer was then added to each well of the 96-well plate, using a multichannel pipette. Plates were then wrapped in foil and placed in the incubator at 37°C/5% CO_2 for 1.5 hrs. Subsequently, 50µl of 1M NaOH was added to stop the reaction, yielding a yellow colour. Absorbance was then read at 405nm using a FlouStar Optima microplate reader (BMG Labtech).

3.2.11. Analysing migration and invasion rates of transfected cells

Migration and invasion analysis was initiated 48 hrs post transfection of cells and allowed to culture for 48 hrs before analysing migration. To perform migration analysis, transfected Hs578Ts(i)$_8$ cells (with miR-134, miR-370 or NC mimic cells) were trypsinised, counted and seeded at a density of $2.5x10^4$ cells on an 8µm pore sized 24-well transwell chamber (Unitech; Cat. #: 353097) in 500µl of 1% FBS DMEM medium. For invasion analysis, transfected Hs578Ts(i)$_8$ cells (with miR-134, miR-370 or NC mimic cells) were trypsinised, counted and seeded at a density of $2.5x10^4$ cells on an ECM (Sigma-Aldrich, Cat. #: E1270) coated 8µm pore sized 24-well transwell chamber (Unitech; Cat. #: 353097) in 500µl of 1% FBS DMEM medium. Below the chamber, in the well, 500µl of 10% FBS was present in DMEM medium. After 48 hrs, medium was removed and the inside of the chamber wiped twice with a PBS-soaked Q-tip. Cells which had passed through the

pores were stained with 1% crystal violet (Sigma-Alrrich; Cat. #: C6158) and allowed to dry for photographing. Crystal violet staining was solubilised in 10% acetic acid and the absorbance was read at 595nm on a FluorStar Optima microplate reader (BMG Labtech).

3.2.12. Analysing effect of miR-134 on apoptosis inducted by cisplatin treatment

To analyse the effects of miR-134 on apoptosis induction, cells were transfected as described in Section 3.2.8. 24 hrs later, transfected cells were treated with 15μM cisplatin for 24 hrs to induce apoptosis in the cells. 24 hrs post-cisplatin treatment, conditioned medium was collected and cells were trypsinised and pelleted. Conditioned medium was used to neutralise trypsin and to collect any apoptotic cells which may be present in the conditioned medium. Cell pellets were resuspended in 2ml 1X binding buffer (BB), centrifuged at 200g and supernatant discarded and resuspended in 30μl of BB solution. 20μl of cell suspension was placed into an Eppendorf, to which 5μl of Annexin-V-allophycocyanin (APC) (BD Biosciences; Cat #: 550474) was added with 5μl of propidium iodide (PI) staining solution (BD Biosciences; Cat#:556463). 70μl of 1X BB was also added and incubated at room temperature in the dark for 15 mins. 400μl of 1X BB solution was subsequently added and mixed by pipetting. Levels of apoptosis was analysed on $2x10^4$ cells using a BD Accuri™ C6 flow cytometer. All flow-cytometry analyses were performed with the help of Dr. Vanesa Martinez.

3.2.12.1. 10X BB solution recipe

0.1 M HEPES
1.4 M NaCl
25 mM $CaCl_2$
Adjust to pH 7.4
Stored at 4°C

3.2.13. Assessing effects of miR-134 manipulation in association with anti-Hsp90 compounds

3.2.13.1 Determining the IC_{50} of $Hs578Ts(i)_8$ cells to 17-AAG and PU-H71

To determine the IC_{50} concentrations of $Hs578Ts(i)_8$ cells to anti-Hsp90 compounds, 17-AAG and PU-H71, toxicity assays were performed using a range of drug concentrations, outlined in Table 3.9. $Hs578Ts(i)_8$ cells were seeded at a density of $2x10^3$ cells per well in 96 well plates and allowed to attach overnight. The following day cells were treated with the following drug concentrations for 48 hrs:

Table 3.9: Drug concentrations used to determine $Hs578Ts(i)_8$ IC_{50} values to anti-Hsp90 compounds

17-AAG	0nM, 20nM, 40nM, 60nM, 80nM, 100nM, 120nM, 140nM, 160nM, 180nM, 200nM and 220nM.
PU-H71	0nM, 10nM, 20nM, 30nM, 40nM, 50nM, 60nM, 70nM, 80nM,

Cell viability was assessed by the acid phosphatase method as described in 3.2.10.1

3.2.13.2 Assessing effects of miR-134 manipulation in association with anti-Hsp90 compounds

To investigate if miR-134 transfection can amplify the sensitivity of $Hs578Ts(i)_8$ cells to anti-Hsp90 compounds (17-AAG and PU-H71), $Hs578Ts(i)_8$ cells were transfected with miR-134 or NC mimics and allowed to grow for 48 hrs. Transfected cells were then trypsinised, counted and seeded at a density of $2x10^3$ cells/well in a 96 well plate and allowed to attach overnight. The following day, transfected cells were treated with 17-AAG (70nM) or PU-H71 (60nM) drugs. Cell viability was assessed 48 hrs later using the acid phosphatase method as described in Section 3.2.10.1. This analysis was performed with the help of Dr. Martina Gogarty.

3.2.14. Isolation of EVs from transfected cells

Cells were transfected as described in Section 3.2.8. EVs were isolated from CM taken from transfected cells 48 hrs post transfection. Due to small volumes of CM involved ExoQuick-TC™ exosome precipitation solution (Systems Biosciences; Cat. #: EXOTCxxA-1) was elected to be used for this analysis, and performed as per manufacturer's instructions. Under sterile conditions, 10ml of CM was collected from transfected cells and centrifuged at 3,000g for 15 mins to remove cells and debris. Supernatant was kept, and transferred to a sterile tube, to which 2ml of ExoQuick-TC solution was added. Samples were refrigerated for 12 hrs. Samples were subsequently centrifuged at 1,500g for 10 mins at 4°C to yield a pellet of EVs. All supernatant was carefully aspirated and samples were centrifuged at 1,500g for 5 mins to enable the removal of any residual ExoQuick-TC solution. EV pellets were then suspended in 100µl of sterile PBS and quantified using the Bio-Rad protein assay as described in Chapter 2, Section 2.2.3.2.

3.2.15. qPCR of transfected cells and EVs

To determine whether cells and EVs successfully took up the miRNA mimics, qPCR was performed on the transfected cells and their derived EVs. Cells and EVs were collected 48 hrs post transfection and total RNA was isolated from cells and EVs as described in Section 3.2.5. To show that the miRNAs are enclosed within the EVs, 10ml of CM was collected and treated with 5µg/ml RNase A (Sigma-Aldrich; Cat. #: R4875-100MG) for 30 mins at 37°C, according to a method outlined in a previous report [226]. qPCR was performed as described in Section 3.2.7, as for validation of miRNA expression in cells and EVs.

3.2.16. Treating cells with transfected EVs

To investigate whether EVs derived from transfected cells can relay the tranfected miRNA information to non-tranfected (NT) cells, Hs578Ts(i)$_8$ cells were treated with EVs enriched in miR-134 or NC mimic miRNAs. Depending on the analysis performed, cells were treated with different concentrations of EVs.

3.2.16.1. Treating Hs578Ts(i)$_8$ cells for immunoblotting

Hs578Ts(i)$_8$ cells were seeded in 6 well plates at a density of $2x10^4$ cells per well in the presence of 40µg of EVs from miR-134 mimic trasfected cells or NC mimic ransfected cells and cultured for 48 hrs. Cells were collected and prepared for immunoblotting as described in Section 2.2.3 and performed according to Section 3.2.9.

3.2.16.2. Treating Hs578Ts(i)$_8$ cells for proliferation analysis

Hs578Ts(i)$_8$ cells were seeded at a density of $2x10^3$ cells in a 96 well plate in the presence of 2µg of miR-134-mimic derived EVs or NC-mimic derived EVs. Cells were cultured for 48 hrs and growth rate assessed using the acid phosphatase method as described in Section 3.2.10.1.

3.2.16.3. Treating Hs578Ts(i)$_8$ cells for migration analysis

Hs578Ts(i)$_8$ cells were seeded at a density of $2.5x10^4$ cells on an uncoated 8µm pore sized 24-well transwell chamber and allowed to attach for 5 hrs in complete, 10% FBS in DMEM, medium Medium was replaced with 1% FBS in complete DMEM and 10µg of miR-134 or NC mimic derived-EVs were added. Cells were cultured for 48 hrs and results analysed as described in Section 3.2.11.

3.2.16.4. Treating Hs578Ts(i)$_8$ cells for invasion analysis

Hs578Ts(i)$_8$ cells were seeded at a density of $2.5x10^4$ cells on an ECM coated 8μm pore sized 24-well transwell chamber and allowed to attach for 5 hrs in complete, 10% FBS in DMEM, medium Medium was replaced with 1% FBS in complete DMEM and 10μg of miR-134 or NC mimic derived-EVs were added. Cells were cultured for 48 hrs and results analysed as described in Section 3.2.11.

3.2.16.5. Treating Hs578Ts(i)$_8$ cells for cisplatin-induced apoptosis analysis

Hs578Ts(i)$_8$ cells were seeded at a density of $1.5x10^5$ cells in a 6 well plate in the presence of 5μg of EVs and cultured for 24 hrs. After 24 hrs, medium was removed and cells were treated with 15μM of cisplatin and retreated with 5μg of either miR-134 enriched EVs or NC-mimic enriched EVs. 24 hrs later, cells were analysed for apoptosis following the method outlined in Section 3.2.12 using the BD Accuri™ C6 flow cytometer. All flow-cytometry analyses were performed with the help of Dr. Vanesa Martinez.

3.2.16.6. Treating Hs578Ts(i)$_8$ cells for response to Hsp90 inhibitors

To investigate the potency of Hsp90 inhibitors on Hs578Ts(i)$_8$ cells following exposure to miR-134-enriched EVs derived from miR-134-overexpressing Hs578Ts(i)$_8$ cells, the following was performed: Hs578Ts(i)$_8$ cells were seeded at a density of $2x10^3$ cells per well of a 96-well plate and allowed to attach overnight. The following day, 2μg of EVs derived from miR-134 or NC mimic-transfected cells were added to each well in combination with 17-AAG (70 nM) or PU-H71 (60 nM) drugs, as determined to be the IC_{50} values of Hs578Ts(i)$_8$ cells to these compounds (Section 3.2.13). Cell viability was assessed, 48 hrs later, using the acid phosphatase method as described in Section 3.2.10.1.

3.2.17 Statistical and bioinformatical analysis

Online miRNA target prediction software (TargetScan Human Release 6.2) was used to identify proteins potentially regulated by miR-134 and miR-370. Statistical analysis was performed in Microsoft Excel. P-values were generated using Student's T-tests, with $p<0.05$ considered as statistically significant. GraphPad Prism 5.0 was used for graph generation (Graph Pad Software Inc, La Jolla, USA). Linear regression analysis and the calculation of R^2 were performed on GraphPad Prism 5.0 and p-values were calculated based on deviation from zero. GraphPad Prism 6.0 was used for volcano plot generation.

3.2.18 Isolation of DNA from cells and EVs

DNA was isolated from cells and EVs using the QIAamp DNA mini kit (Qiagen; Cat. #: 51304), following manufacturers guidelines for isolation of DNA from cultured cells. Cell pellets were harvested from the same flasks as used for EV isolation. Cells were collected by trypsinisation and washed twice with 1ml PBS by centrifugation at 13,000g for 5 mins, removing all excess PBS after the final centrifugation step. EVs were isolated as described in Section 2.2.2. Cells and EVs were suspended in 400µl of PBS to which 40µl of Proteinase K was added and 400µl of buffer AL, vortexed for 15 secs and incubated at 56°C for 10 mins. Samples were then briefly centrifuged and 400µl of 100% molecular grade ethanol (Sigma-Aldrich, Cat. #: E7418) added and briefly centrifuged. 700µl of this was transferred to a QIAamp Mini Spin Column and centrifuged at 6,000g for 1 min and filtrate discarded. The remaining sample was then added to the QIAamp Mini Spin Column and centrifuged at 6,000g for 1 min and filtrate discarded. 500µl of buffer AW1 was added to the QIAamp Mini Spin Column and centrifuged at 6,000g for 1 min and filtrate discarded. 500µl of buffer AW2 was added to the QIAamp Mini Spin Column and centrifuged at 13,000g for 3 mins and filtrate discarded. The collection tube was discarded and the spin column then added to a fresh collection tube and centrifuged at 13,000g for 1 min. Spin columns were then placed in a labelled, nuclease-free Eppendorf. 200µl of buffer AE was gently

added to the filter in the spin column, incubted for 1 min at room temperature. Spin columns were then spun at 6,000g for 1 min to eulte the DNA.

3.2.19 Quantification of DNA by Qubit

dsDNA quantifications were determined using the Qubit dsDNA Broad Range (BR) assay kiy (Invitrogen; Cat. #: Q32850) and the Qubit fluorometer 1.0 (Invitrogen). The assay is and designed to quantitate 2–1,000ng of dsDNA. The Qubit working solution was prepared by diluting 15µl of Qubit dsDNA BR reagent in 199µl of Qubit dsDNA BR buffer per sample and briefly vortexed. DNA standards were prepared by adding 10µl of each standard to 190µl of Qubit working solution (Standard #1: 0ng/ul DNA; Standard #2: 100ng/ul DNA). 1µl of DNA samples were then added to 199µl of working solution, vortexed and incubated at RT for 2 mins. The Qubit fluorometer was then calibrated using the DNA standards and calibration saved. Samples were then placed in the fluorometer to evaluate the concentration of dsDNA.

3.2.20 Detection of single nucleotide polymorphisms (SNPs) by mass spectroscopy – Sequenom

To investigate whether SNPs are present in either cell variants or their derivative EVs, their DNA (10ng) was subjected to a mass spectroscospy-based SNP genotyping analysis to evaluate 284 relatively frequent, mutations observed in 49 breast cancer-related genes. [Full list of mutations assessed can be found in Appendix IA, Table A1 of this thesis]. All primers were designed using Sequenom, Inc. A schematic representation of the process of the protocol used is illustrated in Figure 3.4 below. Detection of single nucleotide polymorphisms (SNPs) by mass spectroscopy – Sequenom was performed at the Sequenom Core Facility, RCSI, Beaumont Hospital by Dr. Sinead Toomey.

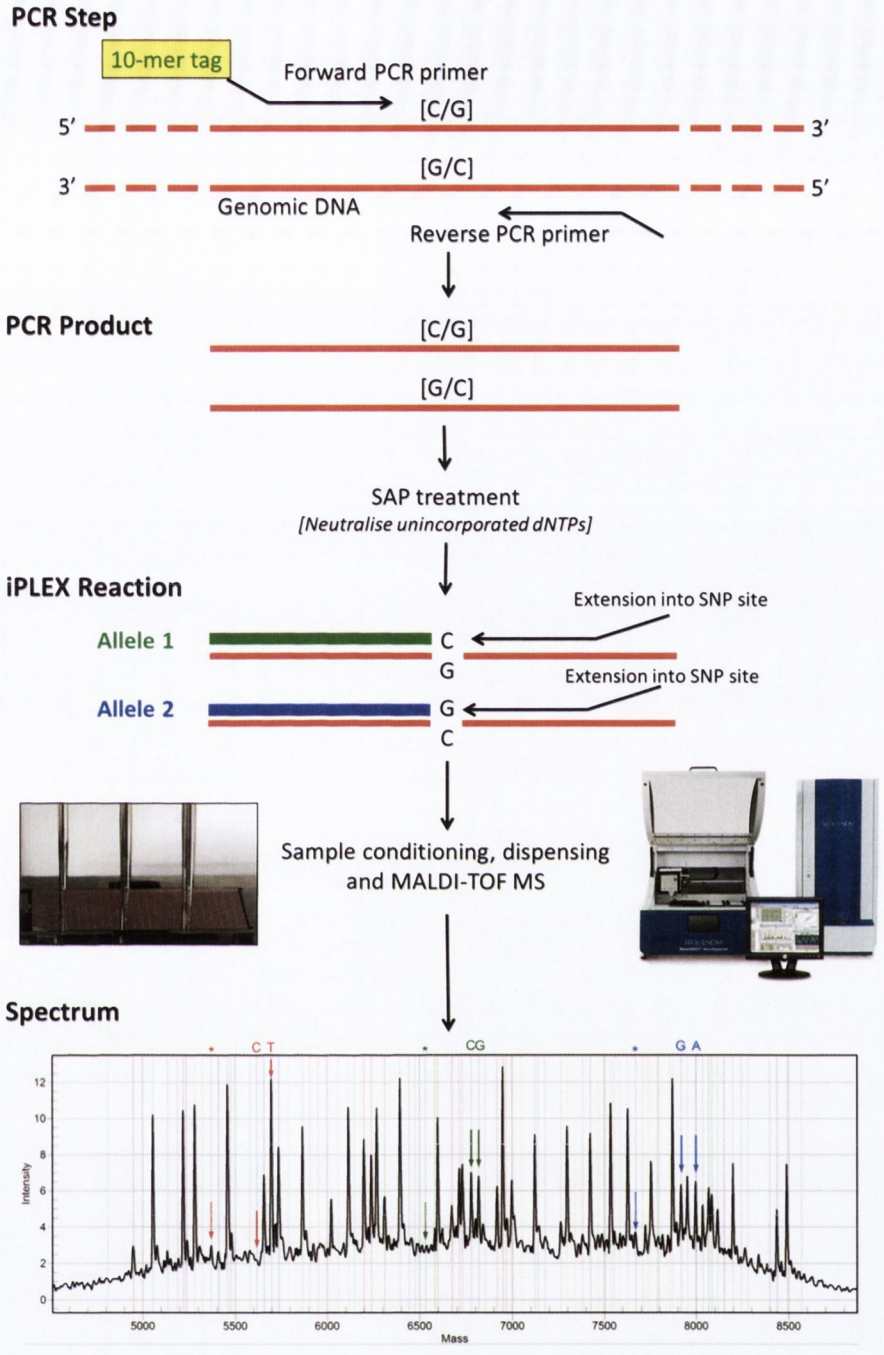

Figure 3.4: Schematic representation of the process of iPLEX-MALDI-TOF detection of SNPs.

Adapted from Gabriel et al. [323]

3.2.20.1 PCR step

All reagents were allowed to thaw at room temperature and then kept on ice, and master mixes were prepared using the ingredients outlined in Table 3.10 below.

Table 3.10: PCR master mix ingredients	
Component	**Vol. per RXN (µl)**
10X PCR Buffer	0.5
$MgCL_2$	0.4
dNTP's	0.1
Taq Polymerase	0.2
PCR Primer Mix (0.5µM)	1.0
Nuclease free water	0.8
Total	**3.0**

3µl of master mix was added to each well of a 96 well plate as appropriate, to which 2µl of 5ng/µl DNA was added as to each well appropriate. PCR plates were sealed with adhesive film, briefly centrifuged, vortexed and briefly centrifuged again before loading into the thermal-cycler for amplification. PCR was run according to the program outlined in Table 3.11 below.

Table 3.11: PCR Program			
Stage	**Temperature**	**Time**	**Stage description**
Hold	94°C	5 mins	Initial denaturation
45 Cycles	94°C	20 secs	Denaturation
	56°C	30 secs	Annealing
	72°C	1 min	Extension
Hold	72°C	3 mins	Final extension
Hold	4°C	∞	Hold

3.2.29.2 Shrimp alkaline phosphatase (SAP) reaction

To remove any unincorporated primers and dNTPs, an ExoSAP reaction was performed. All components, except SAP enzyme, were allowed to thaw at room temperature and then kept on ice. SAP enzyme was taken from -20°C storage immediately prior to use. SAP master mix was prepared using the ingredients outlined in Table 3.12 below.

Table 3.12: SAP Master Mix

Component	Vol. per RXN (µl)
Nuclease free water	1.53
SAP Enzyme	0.30
SAP Buffer	0.17
Total	2.00

2µl of SAP master mix was added to each well of a 96 well plate as appropriate and plates covered with adhesive film. Plates were then briefly centrifuged, vortexed and briefly centrifuged again before loading into the thermal-cycler. The reaction was run according to the program outlined in Table 3.13 below.

Table 3.13: SAP Program

Temperature	Time
37°C	40 mins
85°C	10 mins
4°C	∞

3.2.20.3 Primer extension (iPLEX) reaction

All components, except extension enzyme, were allowed to thaw at room temperature and then kept on ice. Extension enzyme was taken from -20°C storage immediately prior to use. Extension master mix was prepared using the ingredients outlined in Table 3.14 below.

Table 3.14: Extension Reaction Master Mix	
Component	**Vol. per RXN (µ)**
Nuclease free water	0.4926
10X iPLEX Pro Buffer Plus	0.2222
iPLEX extension mix	0.2
Probe mix in 3 bins	1.0444
iPLEX enzyme	0.041
Total	**2.00**

2µl of extension reaction master mix was added to each well of a 96 well plate as appropriate and plates covered with adhesive PCR film. Plates were then briefly centrifuged, vortexed and briefly centrifuged again before loading into the thermal-cycler. The reaction was run according to the program outlined in Table 3.15 below.

Table 3.15: Extension reaction program				
Stage	**Stage (2)**	**Temperature**	**Time**	**Stage description**
Hold	N/A	94°C	30 secs	Initial denaturation
40 Cycles	N/A	94°C	5 secs	Denaturation
	5 Cycles*	52°C	5 secs	Annealing
	N/A	80°C	5 secs	Extension
Hold	N/A	72°C	3 mins	Final extension
Hold	N/A	4°C	∞	Hold

** 5 cycles sit within the 40 cycles*

3.2.20.4 Salt adduct removal step

Clean Resin (Sequenom) was spread on a clean, dry simple plate using a scraper plate so that the resin settled evenly into all wells and the plates were allowed to dry at room temperature for ten mins. While the resin dried, 41µl of high-performance liquid chromatography (HPLC)-grade water was added to each well of the iPLEX Pro extension reaction product. Dried clean resin was added to each well. This was performed by gently inverting the sample plate on top of the dimple plate, aligning the wells over the resin samples. Keeping the sample and dimple plates pressed together, both plates were inverted allowing the resin to fall into the sample wells. The plates were sealed and rotated for 30 mins at room temperature. The plate was subsequently centrifuged at 3,200 g for 5 mins to pellet the resin.

3.2.20.5 Mass spectroscopy of samples

10nl of the desalted primer extension reactions were spotted onto Sequenom spectrochip II-G96 matrix chips using the Sequenom MassARRAY nanodispenser. Chips were ran on a Sequenom MassArray matrix-assisted laser desorption/ionization (MALDI)-TOF MassArray system and the MassArray Analyser 4 software was used to give a visual interpretation of the mass spectra data, which was inspected visually to ensure accurate recordings. Reactions where >15% of the resultant mass ran in the mutant sites were scored as positive.

3.2.20.6 Validation

Validation of the mutated SNPs were performed a described in Section 3.2.20, using freshly isolated samples for re-analysis. Only this SNPs identified to be mutated from the SNP genotyping were re-ran for validation.

3.3. Results

3.3.1. EVs were successfully isolated from Hs578T and Hs578Ts(i)$_8$ cells

In order to confirm EV isolation from the CM of Hs578T and Hs578Ts(i)$_8$ cells, immunoblot and TEM analysis was performed on the samples. Immunoblot analysis successfully detected the presence of PDC6I/Alix, TSG101 and CD63 (Figure 3.5A). TEM analysis detected the presence of EVs sized from 30-100nm in both Hs578T and Hs578Ts(i)$_8$ samples (Figure 3.5B).

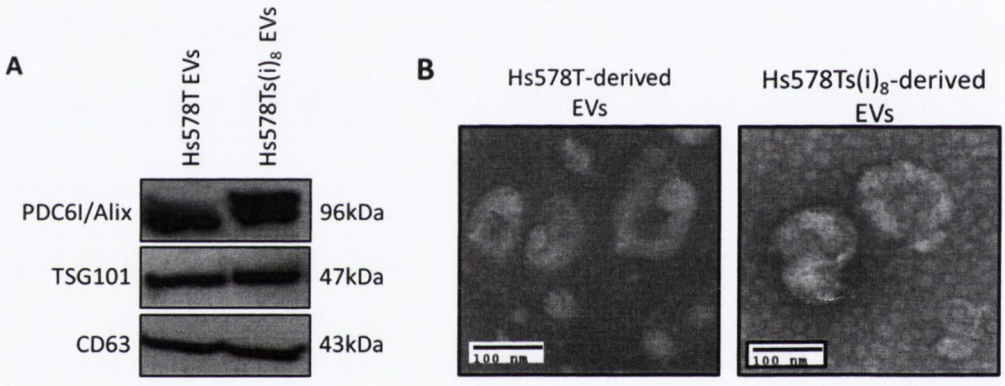

Figure 3.5: Isolation of EVs from CM of Hs578T and Hs578Ts(i)$_8$ cell.s

A: Immunoblot analysis successfully detected the presence of three EV protein markers, PDC6I/Alix, TSG101 and CD63. **B:** TEM analysis showed nano-sized vesicles of 30-100nm in diameter (scale bar = 100nm).

TEM was performed with the help of Neal Leddy, Chief Technical Officer, CMA TCD.

3.3.2. RNA was successfully isolated from Hs578T and Hs578Ts(i)$_8$ cells and their EVs

Total RNA was successfully isolated in triplicate from Hs578T and Hs578Ts(i)$_8$ cells and EVs derived from them using the Qiagen miRNeasy mini kit. Quantifications show no significant differences between the levels of RNA obtained from 1x10^6 Hs578T and Hs578Ts(i)$_8$ cells (Figure 3.6A). Total RNA was also successfully isolated in triplicate from EVs released from Hs578T and Hs578Ts(i)$_8$. Quantification showed a significant increase of total RNA presence per 1µg of EVs in Hs578Ts(i)$_8$ EVs compared to Hs578T. Total RNA presence increased from 4.9ng per µg in Hs578T EVs to 15.5ng per µg of Hs578Ts(i)$_8$ EVs (p=0.007) (Figure 3.6B). To determine RNA purity the 260/280 ratio was measured. This showed that pure RNA was isolated from Hs578T cells (260/280: 1.99), Hs578Ts(i)$_8$ cells (260/280: 2.02), Hs578T EVs (260/280: 1.89) and Hs578Ts(i)$_8$ EVs (260/280: 1.90) (Figure 3.6C)

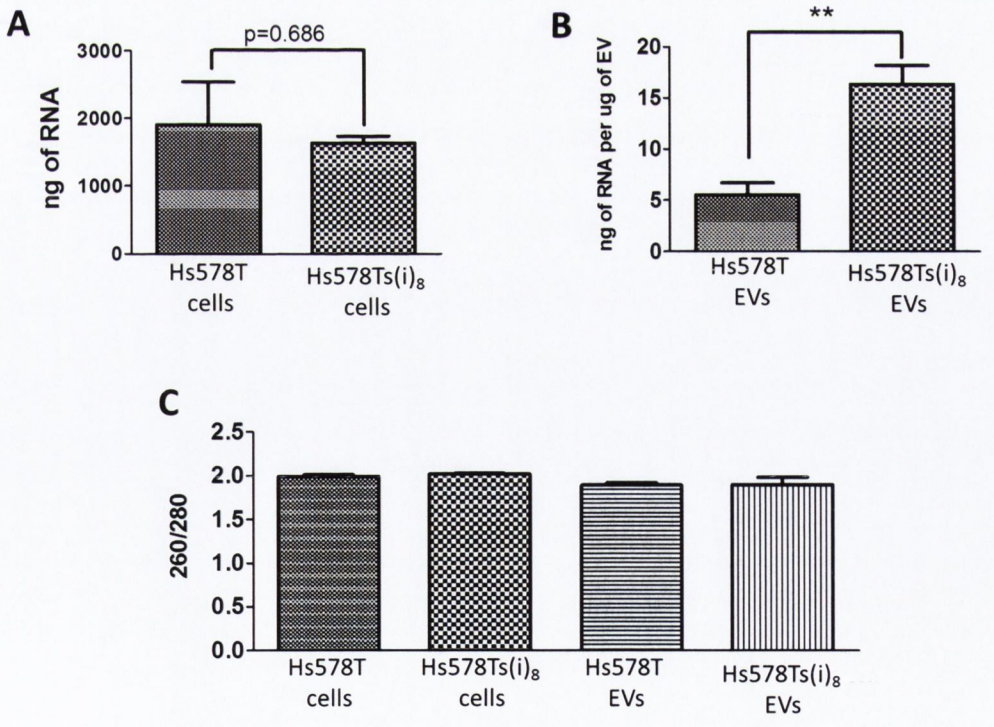

Figure 3.6: Total RNA was isolated from Hs578T and Hs578Ts(i)$_8$ cells and EVs

A: Total RNA quantifications obtained from 1x10^6 Hs578T and Hs578Ts(i)$_8$ cells. **B:** Total RNA quantifications obtained from 1µg of Hs578T and Hs578Ts(i)$_8$ EVs. **C:** Graphical representation of the mean 260/280 values obtained for all cell and EV samples. Results are displayed as n=3±SEM, where **=p<0.01 (Student's t-test).

3.3.3. Endogenous control selection from TLDA analysis

In order to accurately calculate the relative fold changes of miRNA expression levels using the $\Delta\Delta C_T$ method, they can be normalised to endogenous controls [327]. TLDA cards include three commonly used endogenous controls, RNU48, RNU44 and MammU6 in order to detemine the most efficient miRNA for the users analysis. Expression levels determined that there is no significant difference between the expression levels of any of the three endogenous control miRNAs between Hs578T cells and Hs578Ts(i)$_8$ cells. Similarly, no significant difference was observed between Hs578T EVs and Hs578Ts(i)$_8$ EVs (Figure 3.7).

Results determined a mean C_T value of 19.2 and 19.5 for RNU48 in Hs578T cells and Hs578Ts(i)$_8$ cells respectively ($p=0.317$) (Figure 3.7A(i)). Similarly, no significant difference of RNU48 expression was observed between Hs578T and Hs578Ts(i)$_8$ EVs ($p=0.394$) (Figure 3.7A(ii)). No significant differences of C_T values were observed for RNU44 between the cell samples ($p=0.096$) (Figure 3.7B(i)); or EV samples ($p=0.140$) (Figure 3.7B(ii)). Analysis of MammU6 also showed no significant differences between cell samples ($p=0.794$) (Figure 3.7C(i)) or EV samples ($p=0.342$) (Figure 3.7C(ii)).

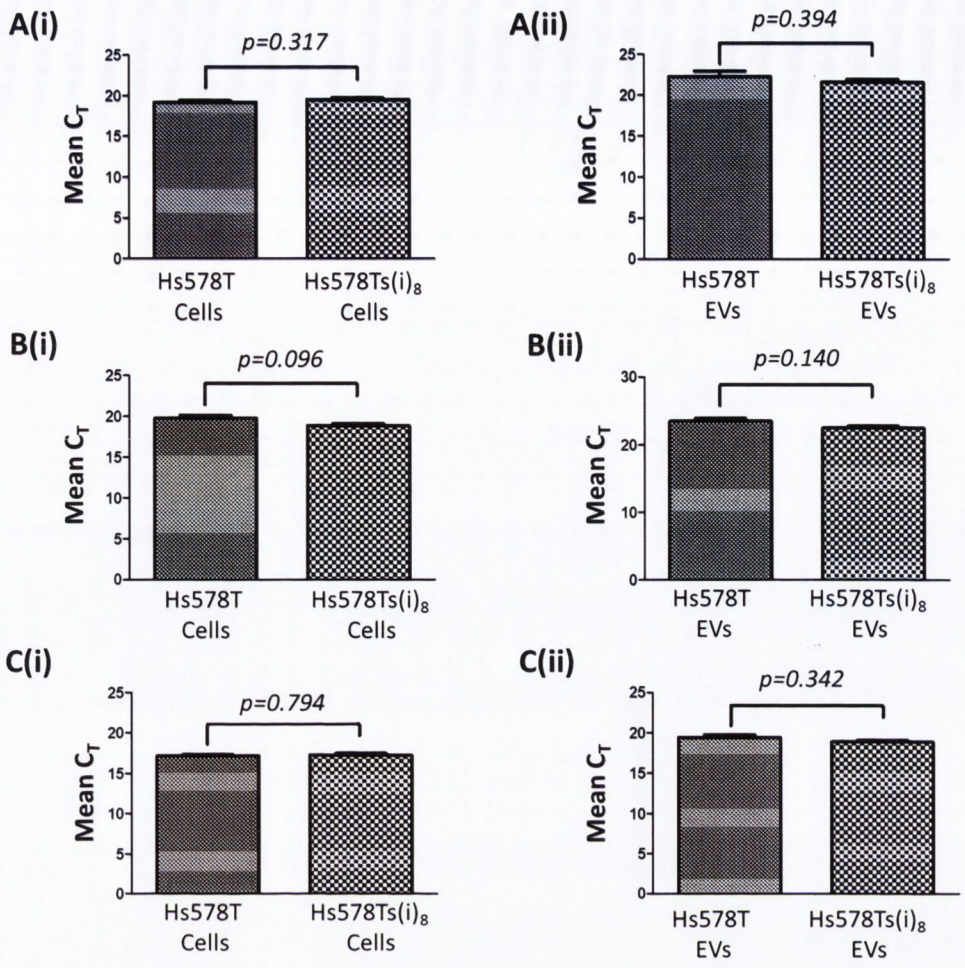

Figure 3.7: C_T values for endogenous controls RNU48, RNU44 and MammU6 in Hs578T and Hs578Ts(i)$_8$ cells.

A(i): C_T values for RNU48 in Hs578T and Hs578Ts(i)$_8$ cells and **A(ii)** Hs578T and Hs578Ts(i)$_8$ EVs. **B(i):** C_T values for RNU44 in Hs578T and Hs578Ts(i)$_8$ cells and **B(ii)** Hs578T and Hs578Ts(i)$_8$ EVs. **C(i):** C_T values for MammU6 in Hs578T and Hs578Ts(i)$_8$ cells and **C(ii)** Hs578T and Hs578Ts(i)$_8$ EVs. Results are displayed as n=3±SEM (Student's t-test).

3.3.4. TLDA analysis of miRNAs suggests that miRNA content is conserved in EVs

In order to establish of the similarities/differences of the overall miRNA presence in EVs compared to their cells of origin, miRNA presence was compared between cells and EVs (n=3), taking C_T values of < 35 to be present in the sample, and $C_T \geq 35$ as absent from the sample. Of the 308 miRNAs detected in Hs578T cells and/or their EVs, 244 of these miRNAs were found to be present in both cells and EVs. This corresponds to 79.2% similarity (Figure 3.8A). Figure 3.8B graphically illustrates these findings, demonstrating a total of 308 miRNAs detected, 244 miRNAs commonly present, 24 (8%) miRNAs detected in cells only and 40 (13%) miRNAs detected in Hs578T EVs only. In addition, linear regression analysis was performed using C_T values to question the correlation between miRNAs detected in Hs578T cells and EVs. This analysis illustrated significant correlation of miRNA detected in both cells and EVs (r^2=0.72; p<0.0001) (Figure 3.8C).

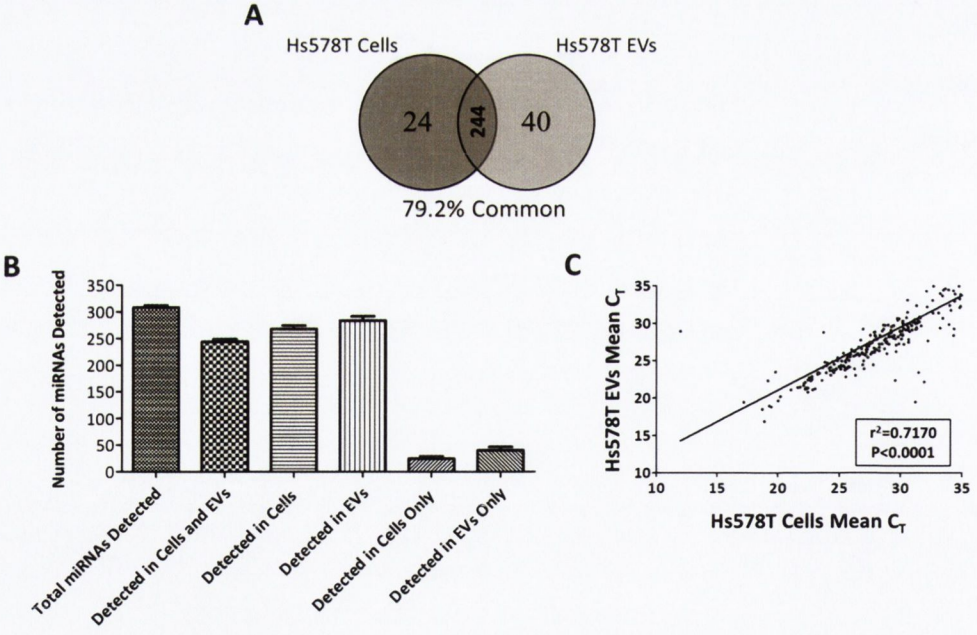

Figure 3.8: Analysis of the miRNA relationship between Hs578T cells and EVs taking C_T values of <35 as present and ≥35 as absent.

A: Venn diagram analysis illustrating the relationships between Hs578T cells and Hs578T EVs. **B:** Graphical representation of the numbers of miRNAs present in Hs578T cells and EVs. **C:** Linear regression analysis illustrating the mathematical relationship of the similarities of Hs578T cells and EVs. Results represent 3 biological repeats; ±SEM where appropriate.

Similarly, these analyses were also performed on Hs578Ts(i)$_8$ cells and EVs derived from them. Of the 271 miRNAs detected in Hs578Ts(i)$_8$ cells and/or their EVs, 203 of the miRNAs were found to be present in both cells and EVs. This corresponds to 74.9% similarity (Figure 3.9).

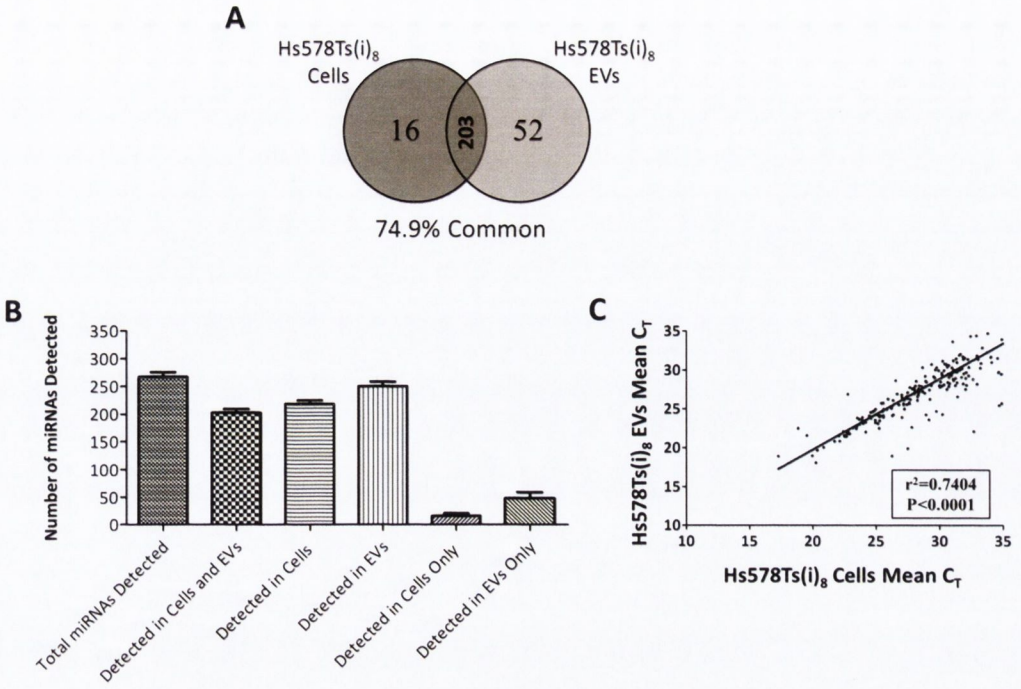

Figure 3.9: Analysis of the miRNA relationship between Hs578Ts(i)$_8$ cells and EVs taking C_T values of <35 as present and ≥35 as absent.

A: Venn diagram analysis illustrating the relationships between Hs578Ts(i)$_8$ cells and Hs578Ts(i)$_8$ EVs. **B:** Graphical representation of the numbers of miRNAs present in Hs578Ts(i)$_8$ cells and EVs. **C:** Linear regression analysis illustrating the mathematical relationship of the similarities of Hs578Ts(i)$_8$ cells and EVs. Results represent three biological repeats; ±SEM where appropriate.

3.3.5. miR-451, miR-122 and miR-142 are enriched in EVs compared to cells

Previous studies have observed that the miRNA content of EVs does not necesserally compliment the miRNA profile of their cells of origin, suggesting some miRNAs are shuttled to EVs for removal from the cell [235-237]. Taking C_T values of $C_T < 35$ to be present and $C_T \geq 35$ to be absent, here the miRNA contents of the EVs were compared to their cells of origin. Analysis determined that seven miRNAs were detected in Hs578T EVs but undectectable in their cells of origin. Analysing Hs578Ts(i)$_8$ EVs, 17 miRNAs were enriched in the EVs but undetected in their cells of origin. Taking both cell line derived EVs together, 3 of these miRNA were commonly present in both Hs578T EVs and Hs578Ts(i)$_8$ EVs but undectectable in their respective cells of origin. These 3 miRNAs are miR-451, miR-122 and miR-142-5p. This is illustrated in Figure 3.10 below. Specific results are for Hs578T cells and their EVs are displayed in Table 3.16. Specific results are for Hs578Ts(i)$_8$ cells and their EVs are displayed Table 3.17.

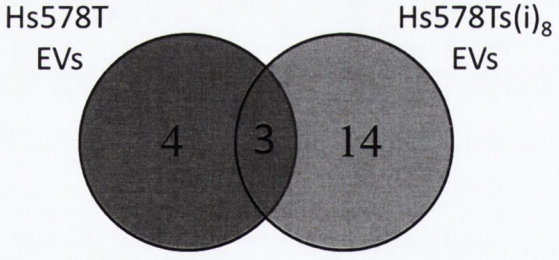

Figure 3.10: miRNAs commonly present in Hs578T and Hs578Ts(i)$_8$ EVs but not detected in their cells of origin.

Venn diagram reperesentation of the number of miRNAs detected in Hs578T EVs but not Hs578T cells, and Hs578Ts(i)$_8$ EVs and not Hs578Ts(i)$_8$ cells. Results represent three biological repeats, where miRNAs were scored as present if >35 C_T in all three replicates; and absent if ≥35 C_Ts in all three replicates.

Table 3.16: miRNAs detected in Hs578T EVs but undetectable in Hs578T cells

Results represent three biological repeats. P-values calculated by Student's t-test. Undetermined denotes no amplification after 40 PCR cycles.

miRNA	Cell Mean C_T	SEM	EV Mean C_T	SEM	p-value
miR-451	Undetermined	0.00E+00	26.1	4.14E-01	0.000005
miR-122	37.6	1.26E+00	27.1	3.15E-01	0.001
miR-142-5p	Undetermined	0.00E+00	30.0	2.35E-01	0.000002
miR-10b	Undetermined	0.00E+00	32.1	6.87E-01	0.0003
miR-450b-5p	38.3	1.67E+00	31.3	1.06E+00	0.02
miR-133b	Undetermined	0.00E+00	32.4	5.68E-01	0.0002
miR-616	Undetermined	0.00E+00	33.7	4.50E-01	0.0002

Table 3.17: miRNAs detected in Hs578Ts(i)$_8$ EVs but undetectable in Hs578Ts(i)$_8$ cells

Results represent three biological repeats. P-values calculated by Student's t-test. Undetermined denotes no amplification after 40 PCR cycles.

miRNA	Cell Mean C_T	SEM	EV Mean C_T	SEM	p-value
miR-451	Undetermined	0.00E+00	26.8	6.09E-01	0.00003
miR-122	Undetermined	0.00E+00	28.0	2.58E-01	0.000001
miR-139-3p	Undetermined	0.00E+00	28.7	5.05E-01	0.00002
miR-495	Undetermined	0.00E+00	29.0	6.82E-01	0.0001
miR-539	38.8	1.20E+00	29.2	3.95E-01	0.002
miR-379	Undetermined	0.00E+00	30.0	8.50E-01	0.0003
miR-411	Undetermined	0.00E+00	29.9	9.87E-01	0.0005
miR-382	Undetermined	0.00E+00	29.6	5.32E-01	0.00004
miR-370	Undetermined	0.00E+00	30.9	6.22E-01	0.0001
miR-346	Undetermined	0.00E+00	30.7	4.02E-01	0.00002
miR-142-5p	Undetermined	0.00E+00	31.0	7.34E-01	0.0003
miR-548b-5p	39.2	7.80E-01	40.0	0.00E+00	0.374
miR-371-3p	38.5	1.47E+00	33.5	5.73E-01	0.03
miR-410	Undetermined	0.00E+00	31.7	5.59E-01	0.0001
miR-219-2-3p	Undetermined	0.00E+00	32.7	9.81E-01	0.002
miR-1	39.8	1.56E-01	33.3	7.91E-01	0.001
miR-516b	Undetermined	0.00E+00	32.1	8.00E-01	0.0006

3.3.6. TLDA analysis of miRNA presence indicates that miRNA levels are reduced in more aggressive TNBC cells and EVs compared to non-aggressive counterpart

The miRNA detection differences between Hs578T cells and EVs was compared to Hs578Ts(i)$_8$ cells and EVs respectively to investigate if miRNAs are gained/lost with increasing aggression. Results demonstrated that miRNAs are typically lost with increasing aggression. Figure 3.11A(i) illustrates that 68% of the detected miRNAs are present in both Hs578T and Hs578Ts(i)$_8$ cells. This diagram shows that 268 miRNAs were detected in Hs578T cells, whereas, 219 miRNAs were detected in Hs578Ts(i)$_8$ cells, representing 49

fewer miRNAs present in the more aggressive cells. Figure 3.11A(ii) shows that 80% of miRNAs detected in EVs were present in both Hs578T EVs and Hs578Ts(i)$_8$ EVs. 284 miRNAs were detected in Hs578T EVs, whereas, 255 miRNAs were detected in Hs578Ts(i)$_8$ EVs, representing 29 fewer miRNAs present in the more aggressive EVs. A significant loss of miRNAs was observed in Hs578Ts(i)$_8$ cells compared to Hs578T cells (75% of the overall detected miRNAs; p=0.003, compared to 92% of the miRNAs present in Hs578T cells (p=0.02) (Figure 3.11B(i)). Similarly, significantly fewer miRNAs were detected in Hs578Ts(i)$_8$ EVs (85% of the overall detected miRNAs; p=0.00001) compared to 95% of the miRNAs present in Hs578T EVs (p=0.02) (Figure 3.11B(ii)).

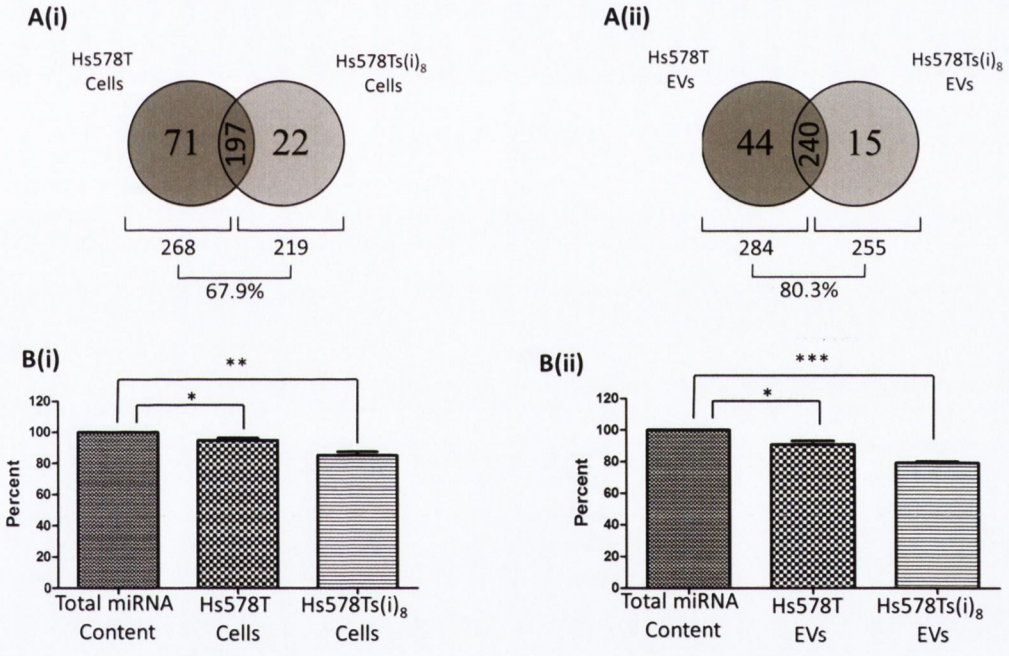

Figure 3.11: miRNA presence differences between Hs578T cells and EVs compared to Hs578Ts(i)$_8$ cells and EVs respectively.

A(i) Venn diagram representation of the numbers of miRNAs detected in Hs578T cells and Hs578Ts(i)$_8$ cells. **A(ii)** Venn diagram representation of the numbers of miRNAs detected in Hs578T EVs and Hs578Ts(i)$_8$ EVs. **B(i):** Graphical representation of the percentage of miRNAs detected in Hs578T and Hs578Ts(i)$_8$ cells and **B(ii)** EVs, illustrating a significant reduction in miRNA numbers in the more aggressive Hs578Ts(i)$_8$ cells and Hs578Ts(i)$_8$ EVs compared to Hs578T cells and EVs respectively. Results are displayed as n=3±SEM, where *=$p<0.05$, **=$p<0.01$, ***=$p<0.001$ (Student's t-test)

3.3.7. miRNAs are expressed at significantly altered levels in Hs578Ts(i)$_8$ cells and EVs versus Hs578T cells and EVs respectively

In order to identify potential miRNA biomarkers for TNBC progression, and/or to identify miRNAs that may be of therapeutic value in TNBC, the miRNA expression differences were analysed for all miRNAs detected. Fold changes of miRNA expression were calculated using the $\Delta\Delta C_T$ method as described in Section 3.2.6.4, normalising miRNA expression values to RNU48 as the endogenous control. Fold changes of > 2 fold were considered substantially altered, so were relevant for further analysis. Volcano plot analyses were performed to visualise an overall spread of the dysregulation of miRNAs in Hs578T(i)$_8$ cells and their EVs, compared to Hs578T cells and their EVs. This analysis allows the researcher to view a broad picture of miRNA presence in one graph, by plotting fold changes on the x-axis and p-values on the y-axis. Results indicate an overall tendency for miRNAs to be down-regulated in the more aggressive Hs578Ts(i)$_8$ cells (Figure 3.12A) and their EVs (Figure 3.12B), as the majority of miRNAs (individual miRNAs represented by a point on the graph) are observed in the >2 fold downregulated graph section. Four miRNAs were found to be significantly up-regulated in Hs578Ts(i)$_8$ cells, with 94 miRNAs significantly down-regulated miRNAs in Hs578Ts(i)$_8$ cells *versus* Hs578T cells. A similar tendency was observed in EVs. Although no miRNAs were significantly up-regulated in Hs578Ts(i)$_8$ EVs, 173 miRNAs were observed to be down-regulated in Hs578Ts(i)$_8$ EVs compared to Hs578T EVs. Individual fold change values for miRNAs are shown in Appendix IB, Table A2, Table A3 and Table A4.

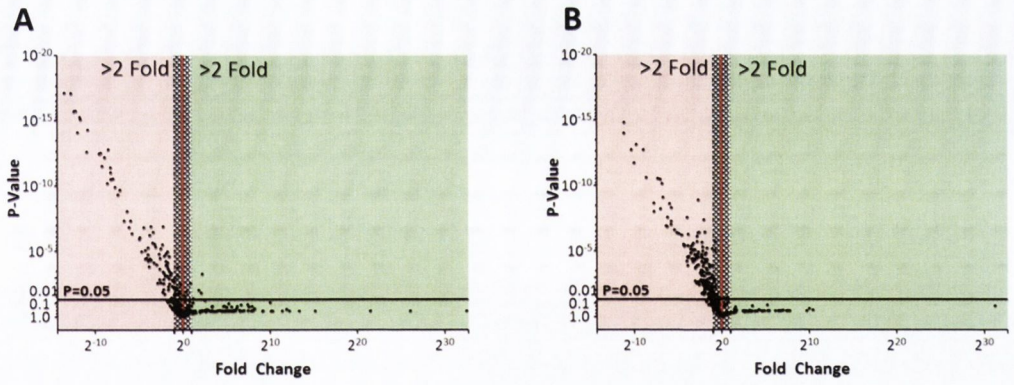

Figure 3.12: miRNA expression differences of Hs578Ts(i)$_8$ cells and EVs versus Hs578T cells and EVs.

Volcano plot analyses illustrating the spread of > 2 fold downregulated (pink) and > 2 fold upregulated (green) miRNAs in Hs578Ts(i)$_8$ cells and their compared to Hs578T cells and their EVs. **A:** 4 miRNAs significantly up-regulated, and 95 significantly down-regulated miRNAs in Hs578Ts(i)$_8$ cells *versus* Hs578T cells. **B:** 174 miRNAs were found to be significantly down-regulated in Hs578Ts(i)$_8$ EVs *versus* Hs578T EVs. Results represent three biological repeats.

Results displayed in Figure 3.13 graphically represent the fold changes observed in Hs578Ts(i)$_8$ cells compared to Hs578T cells; and Hs578Ts(i)$_8$ EVs compared to Hs578T EVs. Figure 3.13A shows the 4 miRNAs significantly up-regulated in Hs578Ts(i)$_8$ cells compared to Hs578T cells. For illustrative purposes, the top 20 down-regulated miRNAs are displayed for both cells (Figure 3.13B) and EVs (Figure 3.13C) where miR-370 and miR-134 are highlighted in green as they showed greatest fold change in cells and EVs respectively, and are the subject of further analysis later in this chapter.

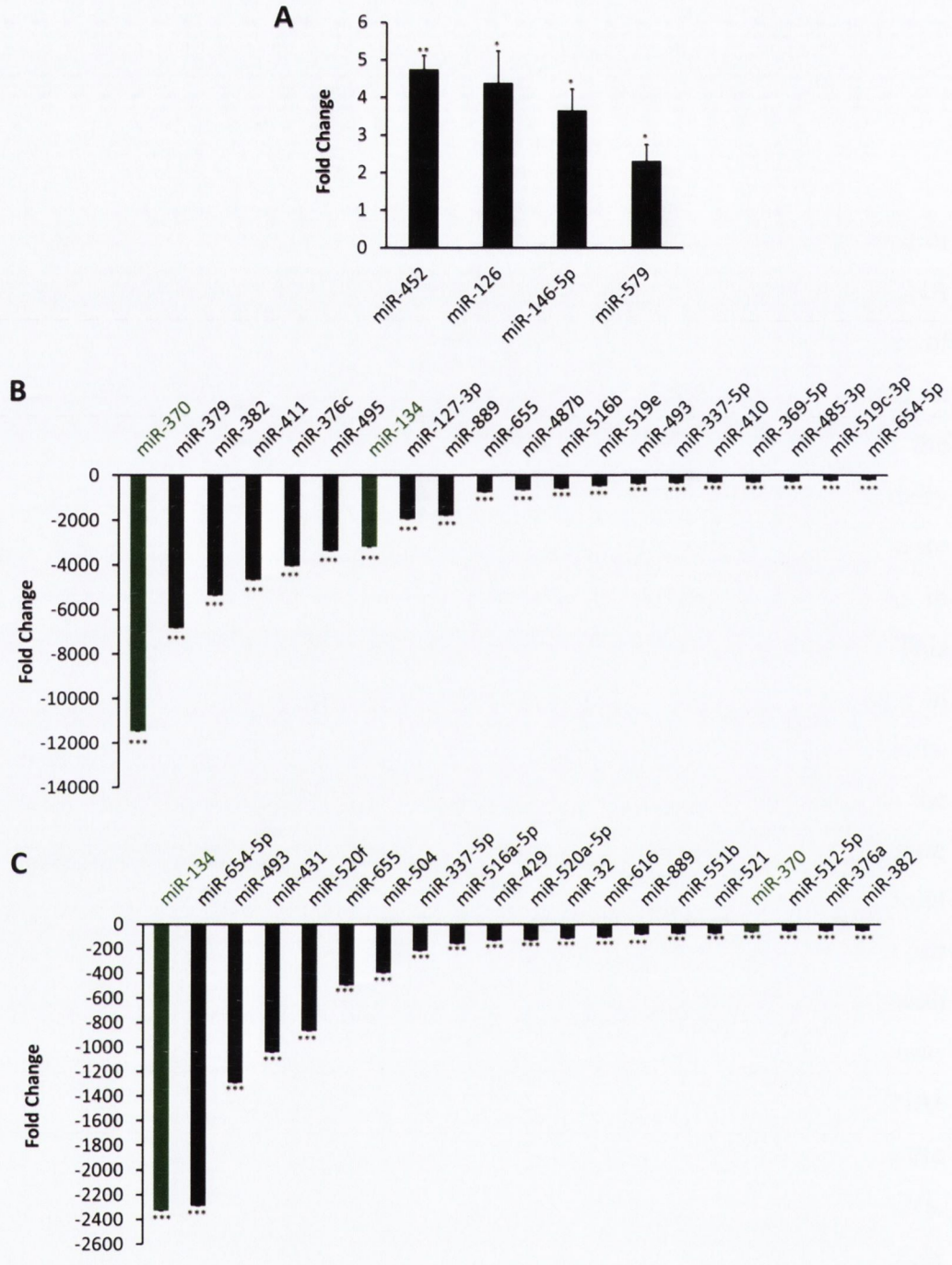

Figure 3.13: Graphical representation of the up- and down-regulated miRNAs in cells and EVs.

A: Significantly up-regulated miRNAs in Hs578Ts(i)$_8$ cells compared to Hs578T cells. **B:** The top 20 most significantly down-regulated in Hs578Ts(i)$_8$ cells compared to Hs578T cells. C: The top 20 most significantly down-regulated in Hs578Ts(i)$_8$ EVs compared to Hs578T EVs. Results are displayed as n=3±SEM, where *=$p<0.05$, **=$p<0.01$, ***=$p<0.001$ (Student's t-test)

3.3.8. Eighty-three miRNAs are commonly down-regulated in both Hs578Ts(i)$_8$ cells and EVs

To determine a relationship between the expression similarities of cells and EVs, the commonly down-regulated miRNAs in both cells and EVs were identified. Results of this analysis determined that 83 miRNAs are commonly down-regulated in both Hs578Ts(i)$_8$ cells and EVs, compared to Hs578T cells and Hs578T EVs respectively. Venn diagram analysis illustrates their relationship (Figure 3.14). A list of the commonly down-regulated miRNAs is shown in Table 3.18 below.

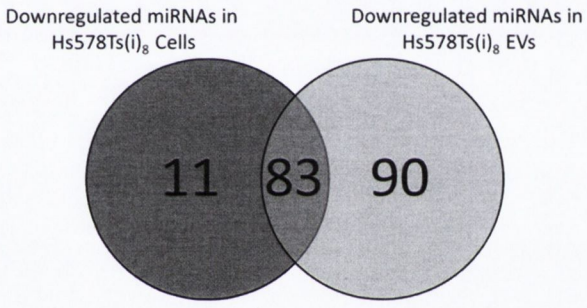

Figure 3.14: Venn diagram analysis illustrating 83 commonly down-regulated miRNAs in both Hs578Ts(i)$_8$ cells and EVs.

Results represent three biological repeats.

Table 3.18: miRNAs commonly down-regulated in both Hs578Ts(i)$_8$ cells and their EVs compared to Hs578T cells and their EVs respectively

Results represent three biological repeats.

miRNAs as listed based on fold change observed in Hs578Ts(i)$_8$ cells compared to Hs578T cells.

miR-370	miR-204	miR-518f	miR-183
miR-379	miR-376a	miR-520f	miR-145
miR-382	miR-486-5p	miR-494	miR-143
miR-411	miR-654-3p	miR-140-3p	miR-372
miR-376c	miR-433	miR-182	miR-24
miR-495	miR-515-3p	miR-519a	miR-195
miR-134	miR-512-5p	miR-23a	miR-199b-5p
miR-127-3p	miR-487a	miR-515-5p	miR-135b
miR-889	miR-375	miR-138	miR-500
miR-655	miR-371-3p	miR-486-3p	miR-323-3p
miR-487b	miR-299-5p	miR-31	miR-221
miR-516b	miR-518a-3p	miR-34c-5p	miR-199a-5p
miR-519e	miR-526b	miR-148b	miR-28-5p
miR-493	miR-525-3p	miR-518d-5p	miR-27a
miR-337-5p	miR-518c	miR-532-5p	miR-185
miR-410	miR-518e	miR-517a	miR-130b
miR-485-3p	miR-512-3p	miR-140-5p	miR-522
miR-519c-3p	miR-520g	miR-135a	miR-28-3p
miR-654-5p	miR-519d	miR-523	miR-152
miR-431	miR-517c	miR-324-5p	miR-27b
miR-539	miR-362-5p	miR-29c	

3.3.9. The ten most substantially down-regulated miRNAs in Hs578Ts(i)$_8$ cells and their EVs originate from the14q32 locus

Investigation of the chromosomal location for the miRNAs commonly down-regulated in Hs578Ts(i)$_8$ cells and Hs578Ts(i)$_8$ EVs indicated that the majority (51 of 83) of these miRNAs originate from two chromosomes; chromosome 19 (26 miRNAs) and chromosome 14 (25 miRNAs) (Figure 3.15A). Interestingly, nine of the top ten down-regulated miRNAs are encoded in the same locus (14q32.31), with the other miRNA (miR-370) in the neighbouring locus, 14q32.2, as illustrated in (Figure 3.15B(i), and chromosomal locations tabulated in Figure 3.15B(ii).

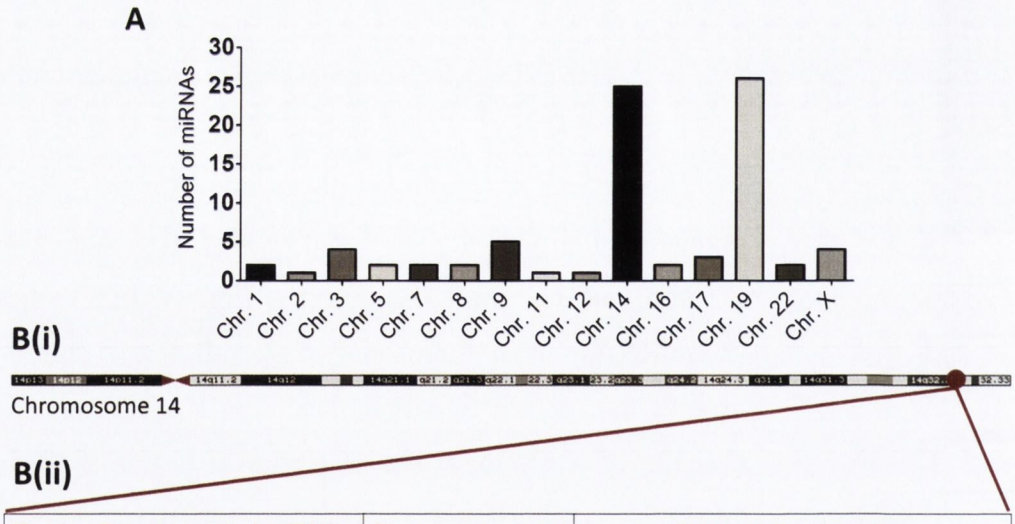

Top ten Downregulated miRNAs	Chromosome Loci	Chromosome Location
miR-370	14q32.2	14: 101,375,476-101,379,550
miR-379	14q32.31	14:101,490,403-101,486,469
miR-382	14q32.31	14: 101,518,643-101,522,718
miR-411	14q32.31	14: 101,487,662-101,491,757
miR-376c	14q32.31	14: 101,504,027-101,508,092
miR-495	14q32.31	14: 101,498,092-101,502,173
miR-134	14q32.31	14: 101,519,024-101,523,096
miR-127-3p	14q32.31	14: 101,347,316-101,351,412
miR-889	14q32.31	14: 101,512,238-101,516,316
miR-655	14q32.31	14: 101,513,887-101,517,983
miR-487b	14q32.31	14: 101,510,792-101,514,875

Figure 3.15: Chromosomal origins of the commonly down-regulated miRNAs found in the Hs578Ts(i)$_8$ cells and EVs.

A: Graphical representation of the chromosomal origins of the 83 commonly down-regulated miRNAs. **B(i):** Map of chromosome 14, indicating the location of the origin of the top ten down-regulated miRNAs found in Hs578Ts(i)$_8$ cells. **B(ii):**Table listing the exact locations of each of these miRNAs. Results are represent three biological repeats.

3.3.10. qPCR validated that miR-370, miR-134, miR-889 and miR-376c are all significantly down-regulated in Hs578Ts(i)$_8$ cells and EVs compared to Hs578T cells and EVs

Five miRNAs were identified from the eighty-three commonly down-regulated miRNAs identified in Hs578Ts(i)$_8$ cells and EVs as being of potential relevance as tumour suppressors in cancer. These miRNAs were selected for validation based on a number of factors: greatest fold change, relevance in literature and potential relevance based on the miRNA-protein target prediction software TargetScan Human Release 6.2. From this, the following miRNAs were selected for validation by qPCR: miR-370, miR-134, miR-889, miR-376c and miR-655.

Expression analysis was performed by qPCR using Taqman small RNA assays, and normalising C_T values to RNU48 (endogenous control) confirming that miR-370 is significantly down-regulated in Hs578Ts(i)$_8$ cells (1285.5 fold; $p=4.6x10^{-9}$) (Figure 3.16A) compared to Hs578T cells. Similarly, there was significant downregulation of miR-134 (428.6 fold; $p=8.9x10^{-11}$) (Figure 3.16B), miR-889 (362.2 fold; $p=2.5x10^{-11}$) (Figure 3.16C), miR-376c (339.2 fold; $p=5.7x10^{-11}$) (Figure 3.16D), miR-655 (384.1 fold; $p=6.5x10^{-12}$) (Figure 3.16E) in Hs578Ts(i)$_8$ cells compared to Hs578T cells.

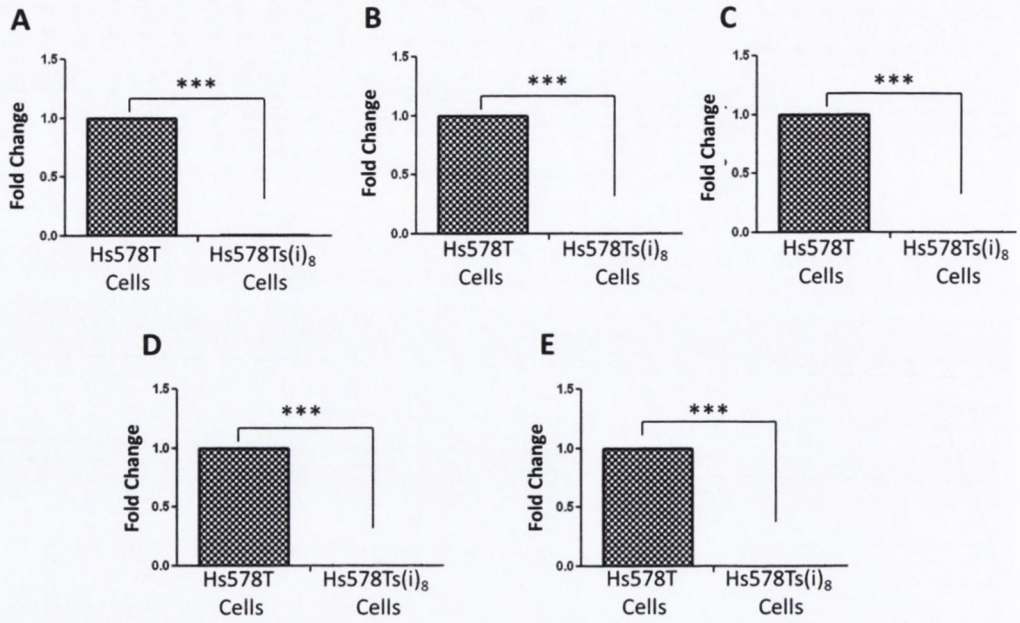

Figure 3.16: qPCR validation of miRNA expressions in Hs578Ts(i)$_8$ cells, compared to Hs578T cells.

A: miR-370. **B:** miR-134. **C:** miR-889. **D:** miR-376c. **E:** miR-655. Results are displayed as n=3±SEM, where *=p<0.05, **=p<0.01, ***=p<0.001 (Student's t-test).

Taqman small RNA assay validations performed on EV-RNA determined that miR-370 is significantly down-regulated in Hs578Ts(i)$_8$ EVs (33 fold; $p=4.6x10^{-7}$), compared to Hs578T EVs (Figure 3.17A). Similarly, miR-134 is significantly down-regulated in Hs578Ts(i)$_8$ EVs (59.1 fold; $p=3.0x10^{-9}$) (Figure 3.17B). miR-889 is significantly down-regulated in Hs578Ts(i)$_8$ EVs (17.4 fold; $p=9.8x10^{-7}$) (Figure 3.17C). miR-376c is significantly down-regulated in Hs578Ts(i)$_8$ EVs (12.8 fold; $p=1.2x10^{-6}$) (Figure 3.17D). Although miR-655 was confirmed to be significantly down-regulated in Hs578Ts(i)$_8$ cells, it was not found to be significantly down-regulated in Hs578Ts(i)$_8$ EVs ($p=0.45$) (Figure 3.17E) compared to Hs578T EVs.

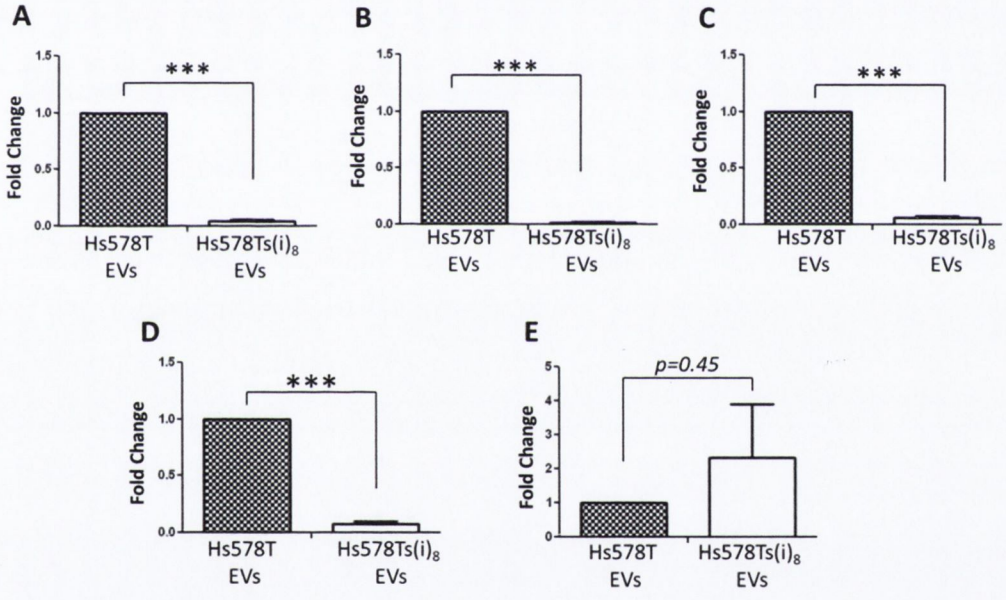

Figure 3.17: qPCR validation of miRNA expressions in Hs578Ts(i)$_8$ EVs, compared to Hs578T EVs.

A: miR-370 expression in Hs578Ts(i)$_8$ EVs . **B:** miR-134 expression in Hs578Ts(i)$_8$ EVs. **C:** miR-889 expression in Hs578Ts(i)$_8$ EVs. **D:** miR-376c expression in Hs578Ts(i)$_8$ EVs. **E:** miR-655 expression in Hs578Ts(i)$_8$ EVs. Results are displayed as n=3±SEM, where *=$p<0.05$, **=$p<0.01$, ***=$p<0.001$ (Student's t-test)

3.3.11. Transient transfection of Hs578Ts(i)$_8$ cells with miR-370 successfully reduces invasion and migration; independent of Smoothened (SMO)

Both TLDA and qPCR analyses showed that, of the 384 miRNAs evaluated, miR-370 is the greatest fold down-regulated miRNA in Hs578Ts(i)$_8$ cells compared to Hs578T cells. We therefore investigated the functional role of miR-370 when introduced back into Hs578Ts(i)$_8$ cells by transient transfection using lipofectamine, as described in Section 3.2.8. Post transfection of Hs578Ts(i)$_8$ cells with an NC mimic miRNA or miR-370 mimic miRNA, three functional analyses were performed:

(i) Proliferation
(ii) Migration
(iii) Invasion

Results demonstrate that miR-370 does not affect the growth rate of Hs578Ts(i)$_8$ cells (1.1 fold; p=0.06) (Figure 3.18A), but slightly reduces the migration by 1.2 fold (p=0.000001) (Figure 3.18B) and invasion by 1.1 fold (p=0.00000000004) (Figure 3.18C) of Hs578Ts(i)$_8$ cells. SMO, a protein involved in activating the hedgehog pathway, was predicted to be a target of miR-370 using the target prediction software, TargetScan Human Release 6.2. Immunoblotting analysis performed here suggests that this action is independent of miR-370-SMO interaction (Figure 3.18D(i)). Densitometry determined no significant differences between SMO expression in miR-370 mimic transfected Hs578Ts(i)$_8$ cells compared to NC mimic transfected Hs578Ts(i)$_8$ cells (p=0.41) (Figure 3.18D(ii)).

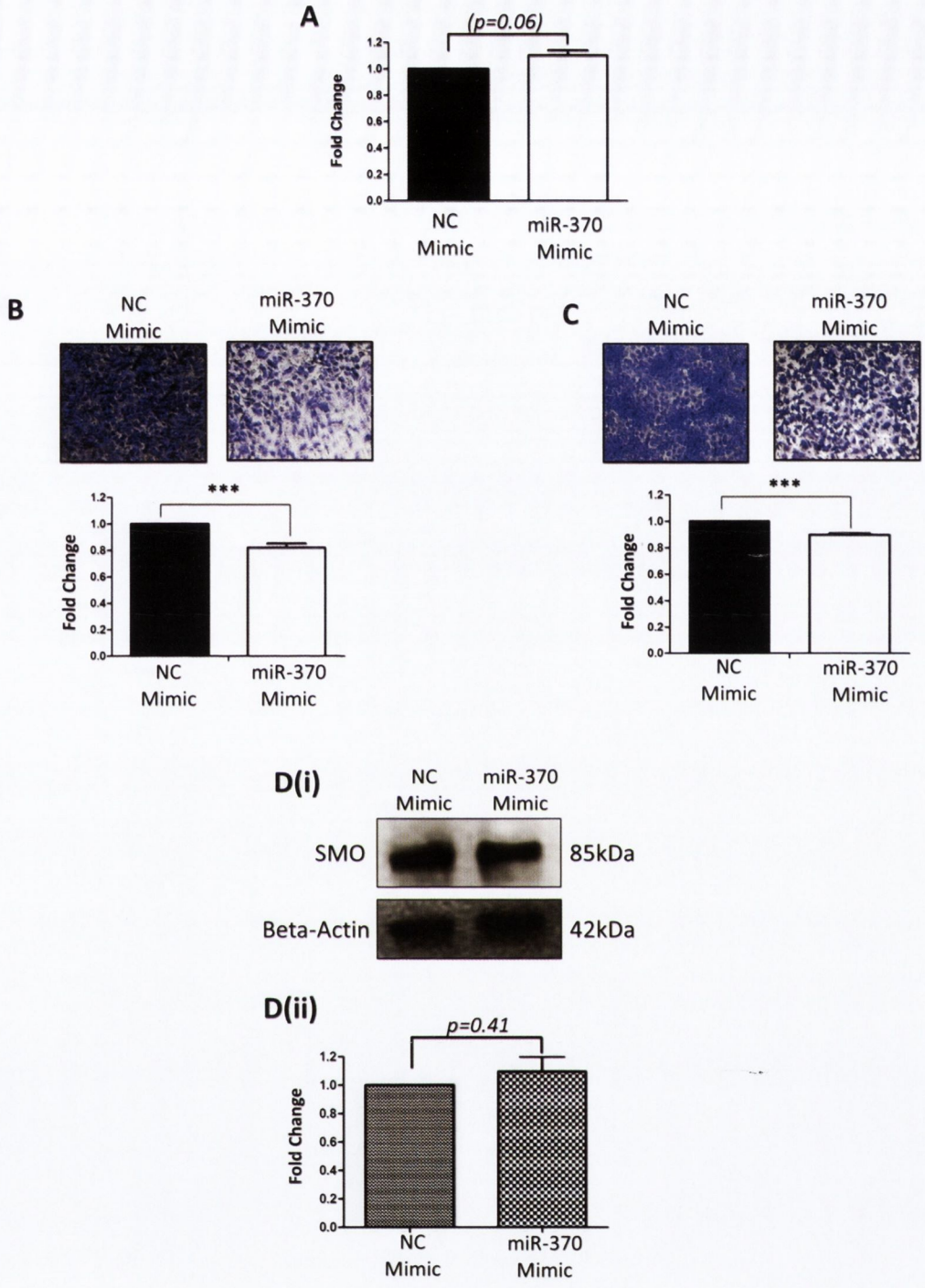

Figure 3.18: miR-370 slightly reduces the migration and invasion of Hs578Ts(i)$_8$ cells independent of targeting SMO protein levels.

A: Proliferation analysis showed no significant effect of miR-370 in Hs578Ts(i)$_8$ cells. **B**: miR-370 reduces the migration and **C:** invasion of Hs578Ts(i)$_8$ cells. **D:** miR-370 doesn't affect the expression of SMO in Hs578Ts(i)$_8$ cells as determined by **D(i)** immunoblotting investigation and confirmed by **D(ii)** densitometry of the immunoblot bands. Results are displayed as n=3±SEM, where *=$p<0.05$, **=$p<0.01$, ***=$p<0.001$ (Student's t-test).

3.3.12. STAT5B and Hsp90 are increased in Hs578Ts(i)$_8$ cells

The target prediction software, TargetScan Human Release 6.2, predicted that STAT5B is a target of miR-134, the second miRNA we assessed for its functional effects. As it has been previously reported that STAT5B induces the transcription of Hsp90 [301], we also became interested in any knock-on effects on Hsp90 expression. To determine the innate expression of STAT5B and Hsp90 in Hs578T and Hs578Ts(i)$_8$ cells, immunoblot analysis was performed in triplicate. Immunoblot analysis showed that Hs578Ts(i)$_8$ cells contain greater levels of both STAT5B (2.2 fold; p=0.01) (Figure 3.19A(i)) and Hsp90 (fold 2.6; p=0.03) (Figure 3.19A(ii)) than its parental, less aggressive variant, Hs578T cells.

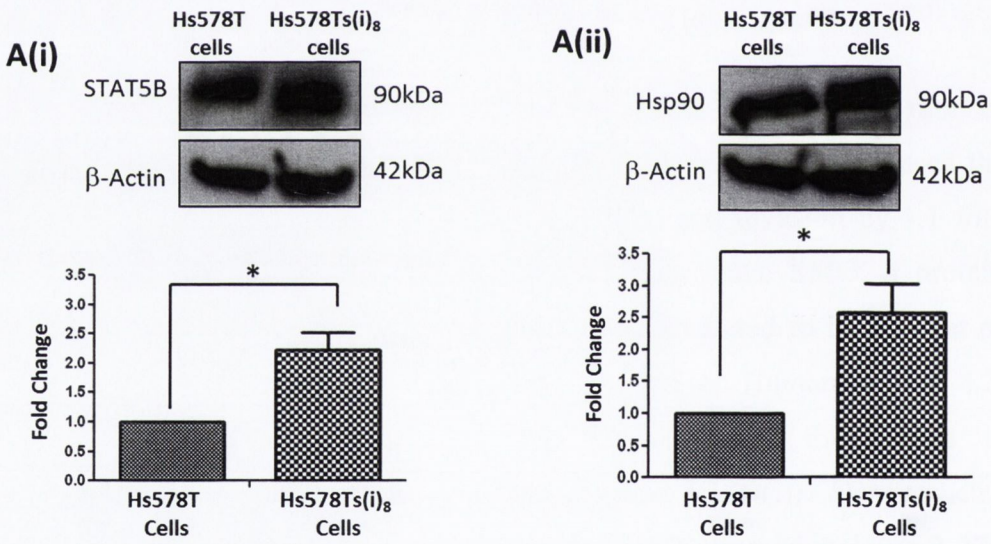

Figure 3.19: STAT5B and Hsp90 are increased in Hs578Ts(i)$_8$ cells and EVs. Hs578Ts(i)$_8$ cells.

Hs578T(i)$_8$ cells express greater levels of **A(i)** STAT5B and **A(ii)** Hsp90 compared to Hs578T cells. Results are displayed as n=3±SEM, where *=p<0.05, **=p<0.01, ***=p<0.001 (Student's t-test).

3.5.14 Transient transfection of Hs578Ts(i)$_8$ cells with miR-134 successfully reduces the levels of STAT5B, Hsp90 and Bcl-2 in Hs578Ts(i)$_8$ cells.

Upon transient transfection of Hs578Ts(i)$_8$ cells with miR-134 as determined by qPCR (Figure 3.20A), the expression of STAT5B, Hsp90 and Bcl-2 were significantly reduced (Figure 3.20B). Densitometry analysis indicated that STAT5B expression is reduced by expression by 2.2 fold ($p=0.008$), Hsp90 by 1.5 fold ($p=0.0001$) and Bcl-2 expression by 1.6 fold ($p= 0.000004$) (Figure 3.20C).

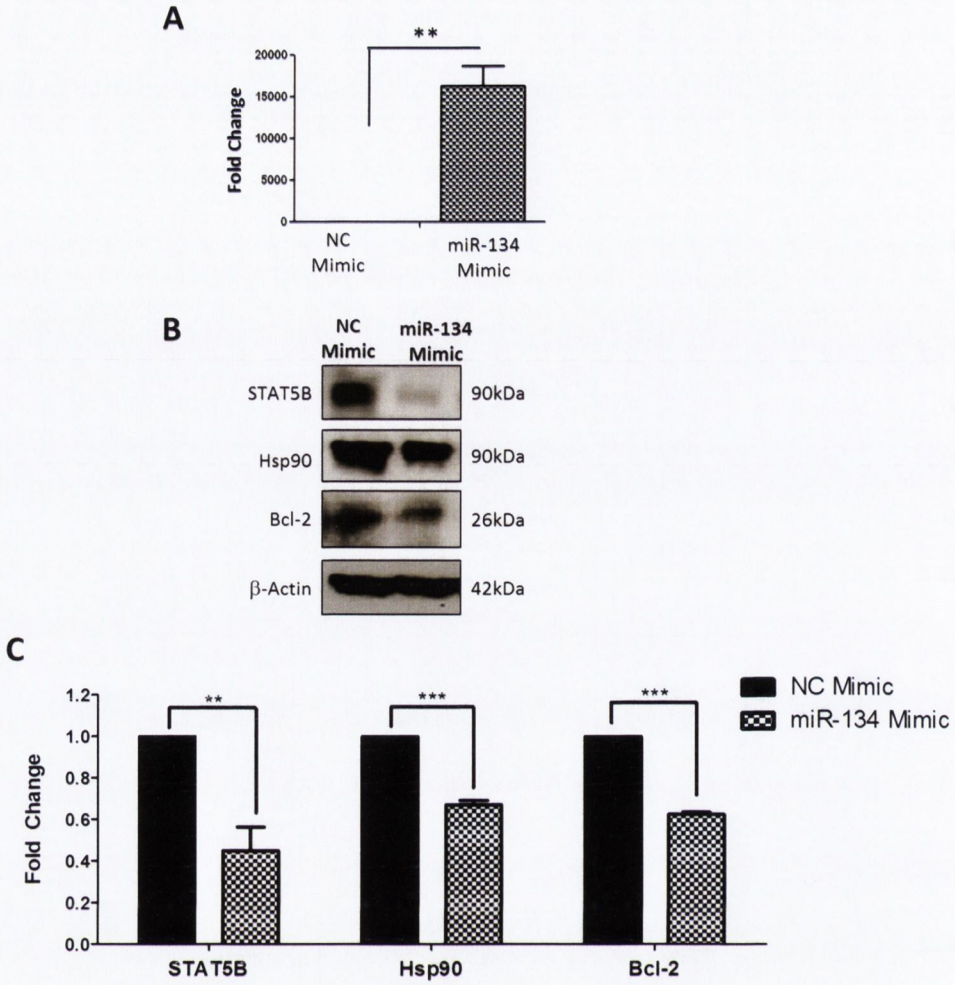

Figure 3.20: miR-134 mimic, compared to NC mimic reduces the expression of STAT5B, Hsp90 and Bcl-2 in Hs578Ts(i)$_8$ cells.

A: qPCR analysis determined successful uptake of miR-134 in Hs578Ts(i)$_8$ cells. **B:** Introduction of miR-134 reduced the levels of STAT5B, Hsp90 and Bcl-2 expression. **C:** Densitometry analysis of STAT5B, Hsp90 and Bcl-2 expression normalised to β-actin. Results are displayed as n=3±SEM, where *=$p<0.05$, **=$p<0.01$, ***=$p<0.001$ (Student's t-test).

3.3.15. miR-134 transfection reduces the proliferation, invasion and migration of Hs578Ts(i)$_8$ cells

In order to analyse the functional effects of miR-134 in aggressive TNBC cells, it was decided to analyse its effects on three hallmarks of cancer progression *i.e.* proliferation, migration and invasion. Results indicate that miR-134 reduces the proliferation of Hs578Ts(i)$_8$ cells by 2.2 fold (p=0.00004) (Figure 3.21A). Additionally, miR-134 apparently also reduces the migration of these cells by 1.4 fold (p=0.0002) (Figure 3.21B) and invasion by 1.3 fold (p=0.00002) (Figure 3.21C).

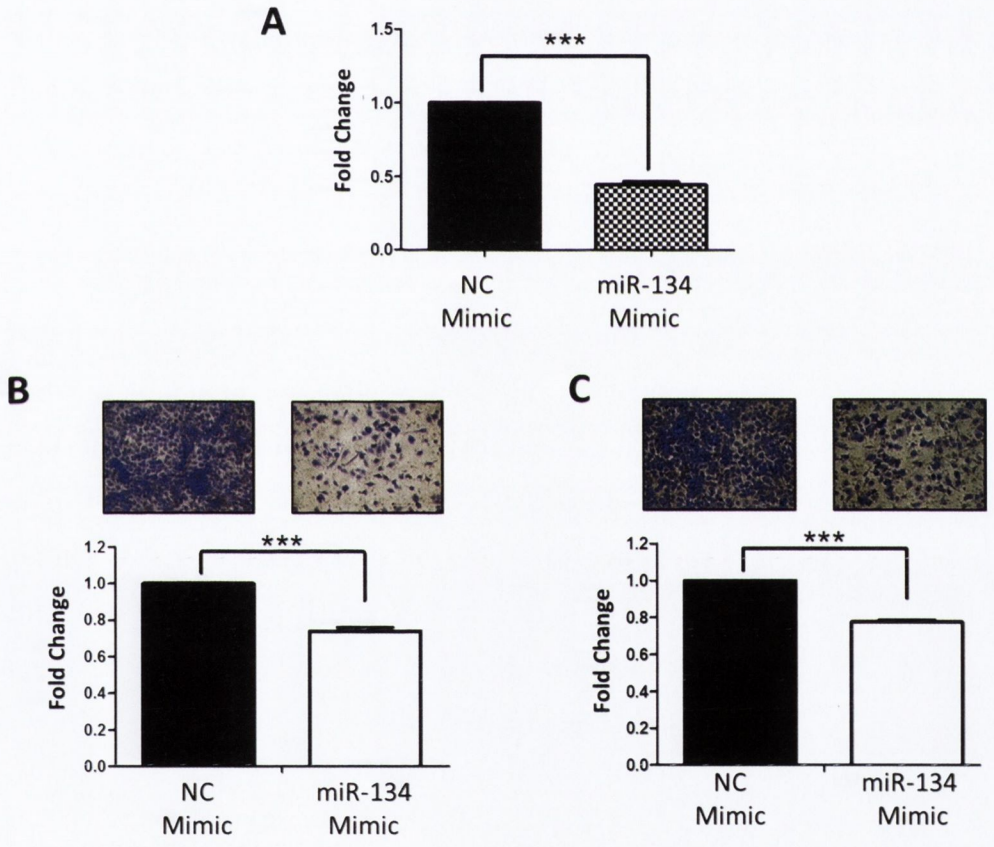

Figure 3.21: Effects of miR-134 on proliferation, migration and invasion.

A: Proliferation analysis demonstrating that miR-134, versus NC mimic, reduced Hs578Ts(i)$_8$ proliferation. **B:** Migration of Hs578Ts(i)$_8$ cells is reduced by miR-134 **C:** as well as reducing invasion of Hs578Ts(i)$_8$ cells. Results are displayed as n=3±SEM, where *=p<0.05, ***=p<0.001 (Student's t-test).

3.3.16. miR-134 augments cisplatin-induced apoptosis

As miR-134 transfection resulted in the down-regulation of Bcl-2 expression (Figure 3.20), an anti-apoptotic protein as detailed in Section 1.2.2, we analysed the effect of miR-134 transfection on apoptosis in combination with cisplatin treatment. First, we determined the effect of 15μM cisplatin on non-transfected (NT) cells. Under the same culture conditions used for transfection, Hs578Ts(i)$_8$ cells were treated with 15μM cisplatin for 24 hrs and apoptosis compared to non-treated Hs578Ts(i)$_8$ cells, as described in Section 3.2.12. Results show that after 24 hrs, 15μM cisplatin significantly increases Hs578Ts(i)$_8$ apoptosis from 4.6% in non-treated cells to 40.0% in cisplatin treated cells ($p=0.0002$). Representative scatter plots are shown for non-treated cells (Figure 3.22A(i)) and cisplatin treated cells (Figure 3.22A(ii)) are shown. Graphical representation of total apoptosis induction showing the difference between non-treated cells and 15μM cisplatin treated cells is shown in Figure 3.22B.

24 hrs following transfection of Hs578Ts(i)$_8$ with miR-134 or NC mimic, cells were treated with 15μM cisplatin for 24 hrs. Flow cytometry using Annexin-V-APC and PI indicated a 10%±3% increase ($p=0.017$) of apoptosis in response to cisplatin in miR-134 transfected cells *versus* NC mimic transfected cells. Representative scatter plots are shown for NC mimic (Figure 3.22C(i)) and miR-134 mimics (Figure 3.22C(ii)). Graphical representation of total apoptosis induction showing the difference between NC mimic and miR-134 mimic is shown in Figure 3.22D.

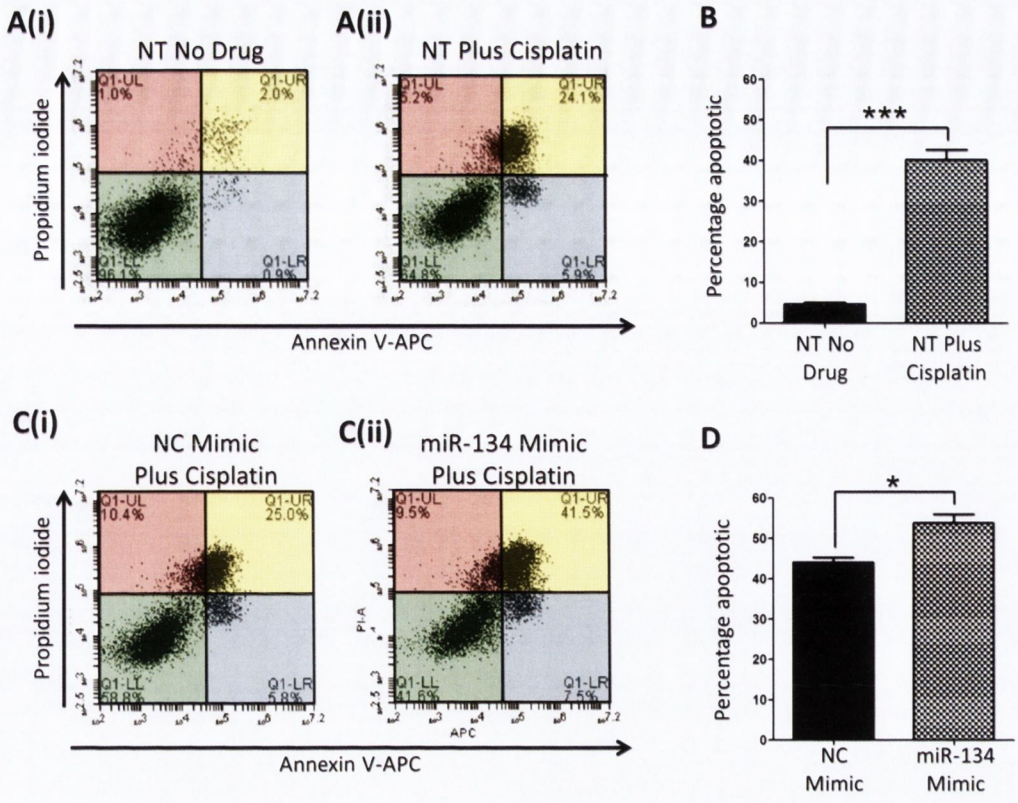

Figure 3.22: Cells transfected with miR-134 increased cisplatin induced apoptosis.

A: Representative Annexin V-APC and PI scatter plots for **A(i)** non-transfected (NT) and non-treated Hs578Ts(i)$_8$ cells and **A(ii)** non-transfected (NT) Hs578Ts(i)$_8$ cells treated with 15μM cisplatin. **B:** Graphical representation of total apoptotic cells detected in non-transfected, non-treated cells *versus* non-transfected cells plus 15μM cisplatin. **C:** Representative Annexin V-APC and PI scatter plots for **C(i)** Negative control (NC) mimic Hs578Ts(i)$_8$ cells treated with 15μM cisplatin and **C(ii)** miR-134 transfected Hs578Ts(i)$_8$ cells treated with 15μM cisplatin. **D:** Graphical representation of total apoptotic cells detected in NC mimic *versus* miR-134 transfected cells. Results are displayed as n=3±SEM, where *=$p<0.05$ & ***=$p<0.001$ (Student's t-test).

All flow-cytometry analyses were performed with the help of Dr. Vanesa Martinez

3.3.17. Effect of miR-134 compared to currently effective anti-Hsp90 molecules

[This analysis was performed with the help of Dr. Martina Gogarty]

As direct transfection of miR-134 was shown to successfully reduce the levels of Hsp90 within Hs578Ts(i)$_8$ cells (Figure 3.20), it was questioned whether miR-134 could add value to anti-Hsp90 drugs. To analyse this, the anti-proliferative effects of miR-134 was compared to the anti-Hsp90 compounds 17-AAG and PU-H71, as well as in combination with these compounds.

To investigate appropriate IC_{50} concentrations to use for the miR-134 plus Hsp90 inhibitor analyses, cell survival analyses were performed. The IC_{50} value of 17-AAG was found here to be approximately 70nM (Figure 3.23A), and 60nM to PU-H71 after 48 hrs exposure to Hs578Ts(i)$_8$ cells (Figure 3.23B).

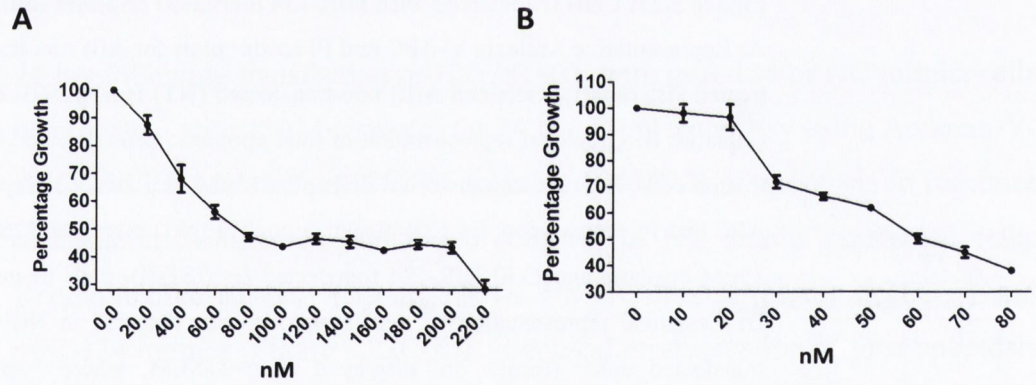

Figure 3.23: Survival curves for Hs578Ts(i)$_8$ cells to determine their IC_{50} concentrations to 17-AAG and PU-H71

Response of Hs578Ts(i)$_8$ cells to **A:** 17-AAG and **B:** PU-H71 drug concentrations after 48 hrs. Graphical representation of total apoptotic cells detected in NC mimic *versus* miR-134 transfected cells. Results are displayed as n=3±SEM

Results, here, show that NC mimic does not significantly affect the growth rate of Hs578Ts(i)$_8$ cells compared to NT cells (p=0.874). Results show that miR-134 (30nM) transfection, compared to NC mimic transfection, successfully reduced Hs578Ts(i)$_8$ proliferation by 2.21 fold (p=0.0004) (Figure 3.24A). This is comparable to the effects of anti-Hsp90 compounds, when NC mimic transfected Hs578Ts(i)$_8$ cells were treated. Specifically, anti-Hsp90 compounds reduced Hs578Ts(i)$_8$ proliferation by 2.7 fold with 17-AAG (70nM) (p=0.004) and 2.5 fold with PU-H71 (60nM) (p=0.01) (Figure 3.24A).

It was then questioned whether miR-134 can amplify the sensitivity of Hs578Ts(i)$_8$ cells to anti-Hsp90 compounds (17-AAG and PU-H71). Although miR-134 appears to increase the sensitivity of Hs578Ts(i)$_8$ cells to 17-AAG by 1.36 fold (p=0.02) and PU-H71 by 1.46 fold (p=0.002) (Figure 3.24B(i)), this observation is likely to be an effect of the growth suppressive effects of miR-134 on Hs578Ts(i)$_8$ cells (2.2 fold; p-0.0004), rather than directly mediating drug sensitivity (Figure 3.24B(ii)).

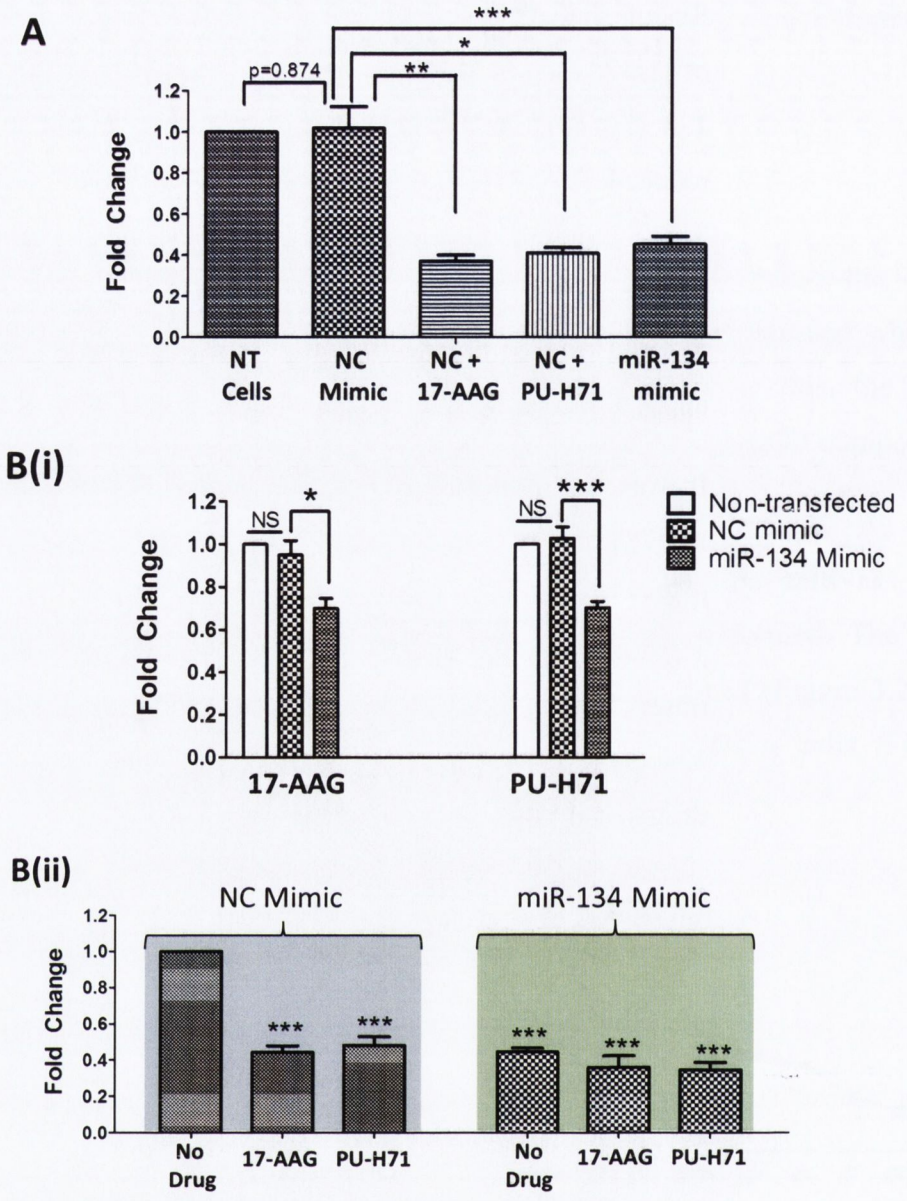

Figure 3.24: Effects of miR-134 on anti-Hsp90 treatments.

A: Comparison of the effects of miR-134 *versus* 17-AAG and PU-H71 to reduce Hs578Ts(i)$_8$ growth. **B(i):** Analysis of whether miR-134 amplifies the sensitivity of Hs578Ts(i)$_8$ cells to 17-AAG and PH-H71.**B(ii):** Graph illustrating the overall picture of the effects of miR-134 on drug sensitivity, clearly demonstrating that miR-134 reduces the proliferation of Hs578Ts(i)$_8$ cells. Results are displayed as n=3±SEM, where *=$p<0.05$, **=$p<0.01$, ***=$p<0.001$ (Student's t-test).

This analysis performed with the help of Dr. Martina Gogarty

3.3.18. miR-134 positive EVs reduce the expression of STAT5B and Hsp90

To investigate whether EVs could be manipulated for use as miRNA-therapeutic delivery vesicles, EVs were collected from the CM of miR-134 transfected cells or NC mimic transfected cells and applied to Hs578Ts(i)$_8$ cells to investigate whether they could reduce protein expression and/or cellular aggression. EVs (40μg) were collected from the conditioned medium of miR-134 transfected cells and applied to Hs578Ts(i)$_8$ cells, as described in Section 3.2.16.1. qPCR analysis determined that EVs from transfected cells are enriched, compared to NC mimic transfected cells, with miR-134 (1.8 fold; p=0.0007) and is protected within the EVs from the action of RNase (Figure 3.25A).

Addition of the miR-134-enriched EVs to Hs578Ts(i)$_8$ cells resulted in reduced levels of STAT5B and Hsp90 expression, as shown in Figure 3.25B. Densitometry analysis determined that miR-134-enriched EVs caused significantly reduced STAT5B expression by 1.6 fold; p=0.005 (Figure 3.25C(i)), and Hsp90 expression by 2.3 fold; p=0.04 (Figure 3.25C(ii)).

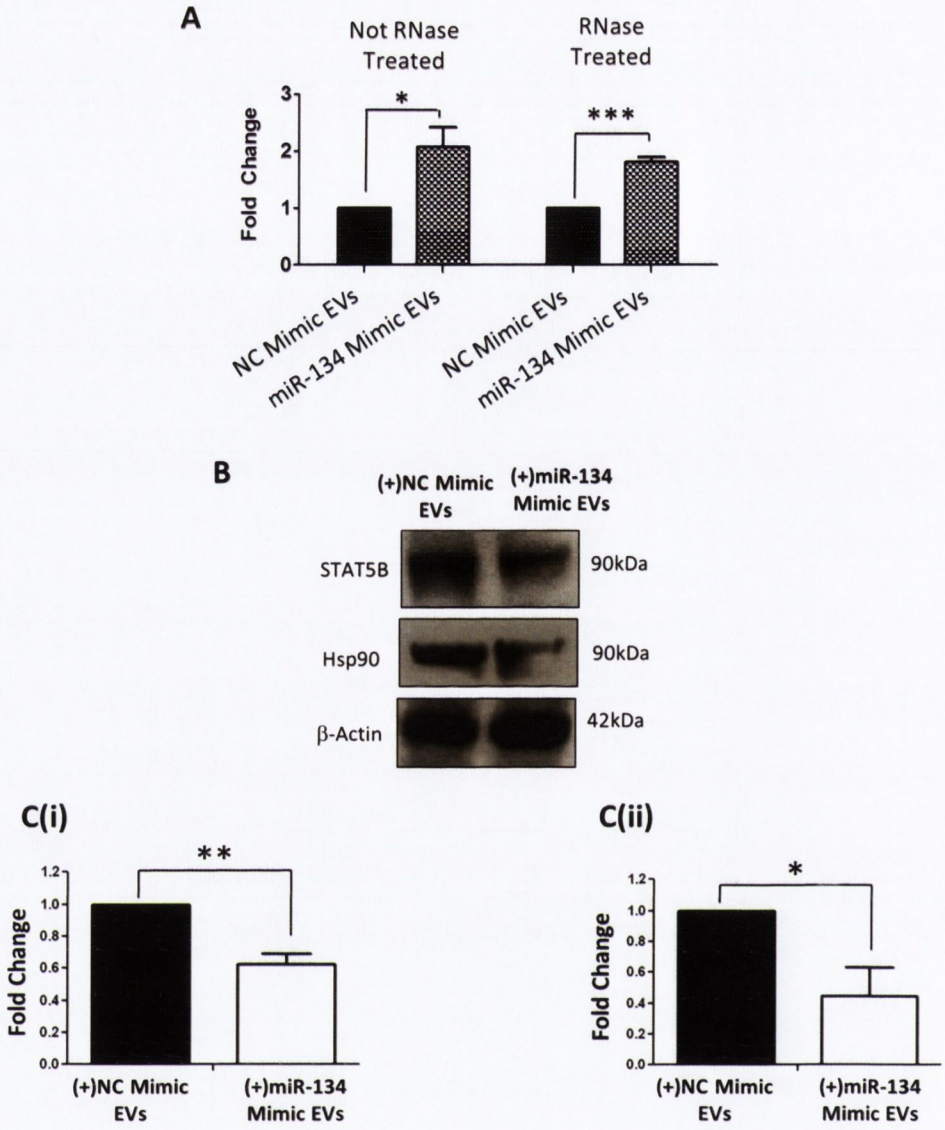

Figure 3.25: miR-134 positive EVs reduce the aggression of Hs578Ts(i)$_8$ cells.

A: qPCR analysis showed that miR-134 is enriched in EVs released by miR-134-transfected Hs578Ts(i)$_8$ cells, and that miR-134 is protected by the action of RNase. **B:** Upon treatment of Hs578Ts(i)$_8$ cells with miR-134 enriched EVs, the levels of STAT5B and Hsp90 are reduced, just as with direct transfection of miR-134 into Hs578Ts(i)$_8$ cells using lipofectamine. **C(i):** Densitometry analysis for STAT5B expression post miR-134-enriched EV treatment. **C(ii):** Densitometry analysis for Hsp90 expression post miR-134-enriched EV treatment. Results are displayed as n=3±SEM, where *=$p<0.05$ & **=$p<0.01$ (Student's t-test).

3.3.19. miR-134 enriched EVs reduce the levels of migration and invasion of Hs578Ts(i)$_8$ cells.

We elected to investigate whether the tumour suppressive effects of miR-134, observed in Figure 3.21, could be signalled through miR-134-enriched EVs. Here, we observe that 2μg of miR-134-enriched EVs do not significantly alter the proliferation of Hs578Ts(i)$_8$ cells (p=0.147) (Figure 3.26A). However, treating Hs578Ts(i)$_8$ cells with miR-134-enriched EVs successful reduced the migration by 1.2 fold (p=0.002) (Figure 3.26B) and invasion by 1.2 fold (p=0.009) (Figure 3.26C).

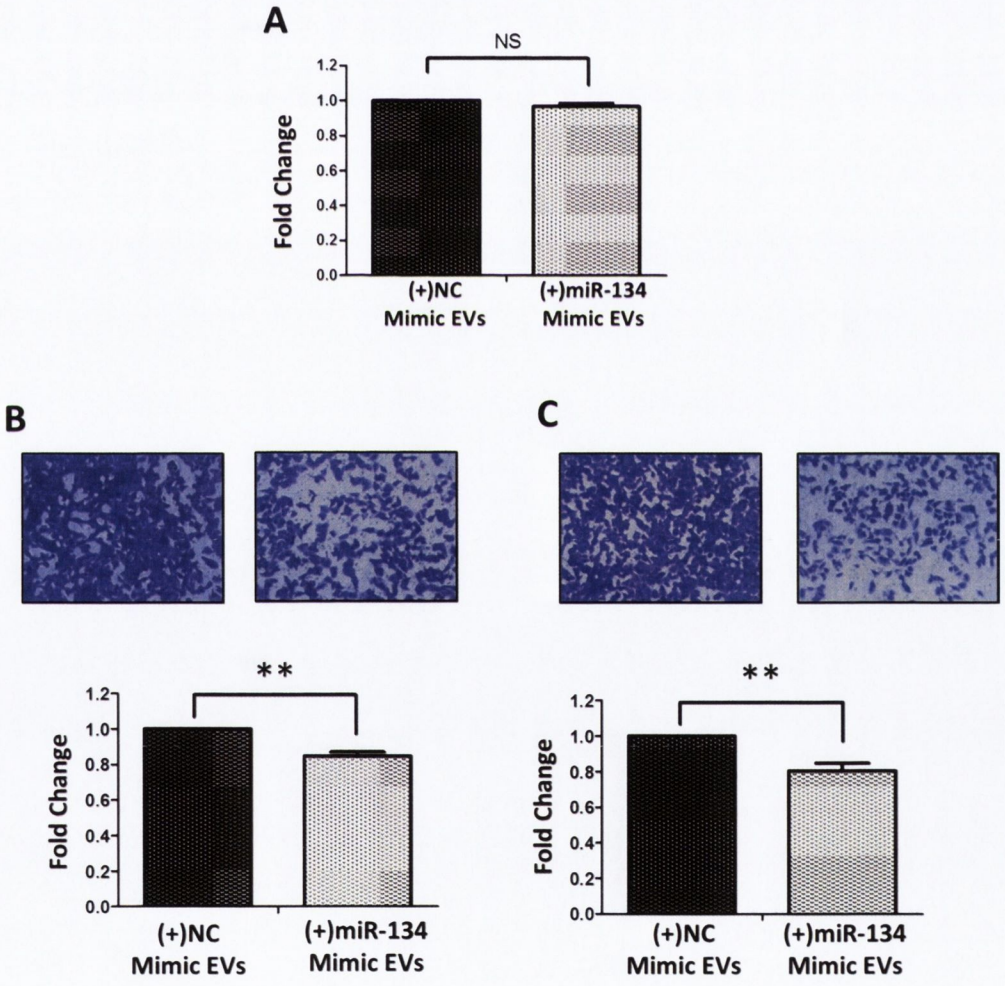

Figure 3.26: Effects of miR-134 enriched EVs on migration and invasion.

A: Proliferation of Hs578Ts(i)$_8$ cells is unaltered by miR-134 enriched EVs. **B:** Migration and **C:** invasion of Hs578Ts(i)$_8$ cells is reduced by miR-134 enriched EVs. Results are displayed as n=3±SEM, where **=p<0.01, (Student's t-test).

3.3.20. miR-134-enriched EVs do not significantly alter cisplatin-induced apoptosis

As direct miR-134 transfection results in increased apoptosis in the presence of 15μM cisplatin (Figure 3.22), we analysed the apoptotic effect of miR-134-enriched EVs in combination with cisplatin treatment. Following transfection of Hs578Ts(i)$_8$ with NC mimic or miR-134 mimic as detailed in Section 3.2.14, 5μg of EVs were collected from the conditioned medium and applied to Hs578Ts(i)$_8$ cells. Cells were treated with 15μM cisplatin and 5μg of EVs the following day and cultured for 24 hrs. Flow cytometry using Annexin-V-APC and PI showed that, under these conditions, miR-134-enriched EVs do not significantly alter cisplatin-induced apoptosis compared to the effect of EVs derived from NC-mimic transfected cells. Representative scatter plots are shown for NC-mimic EVs (Figure 3.27A(i)) and miR-134-EVs (Figure 3.27A(ii)). Graphical representation of total apoptosis induction with NC-EVs or miR-134-enriched EVs is shown in Figure 3.27B.

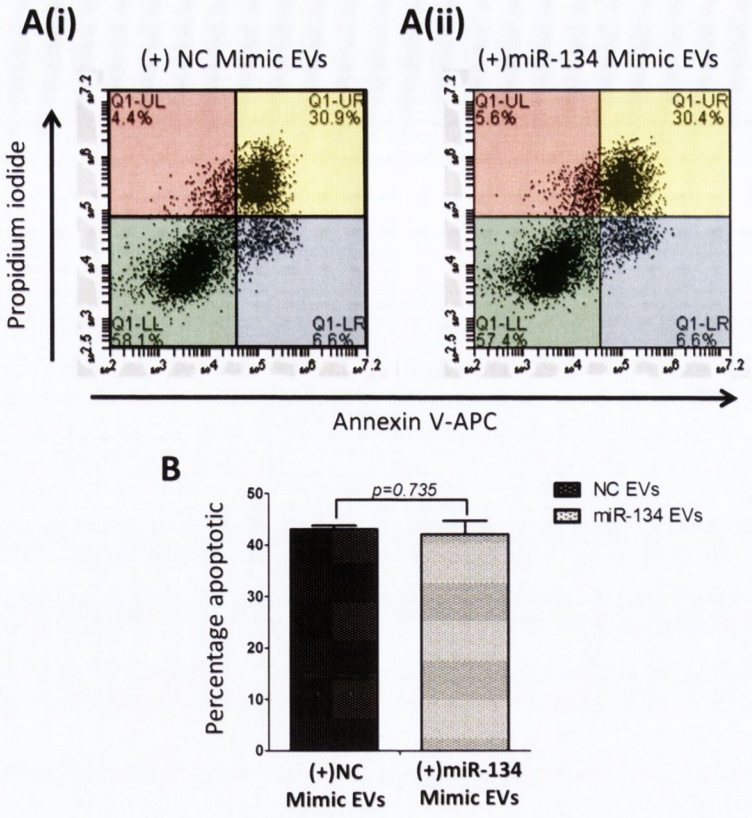

Figure 3.27: miR-134-enriched EVs do not significantly alter cisplatin-induced apoptosis. **A:** Representative Annexin-V-APC and PI scatter plots for **A(i)** NC-mimic EVs with Hs578Ts(i)$_8$ cells treated with 15μM cisplatin and **A(ii)** miR-134-enriched EVs with Hs578Ts(i)$_8$ cells treated with 15μM cisplatin. **B:** Graphical representation of total apoptotic cells detected in NC-mimic EV *versus* miR-134 EV treated cells. Results are displayed as n=3±SEM (Student's t-test).

All flow-cytometry analyses were performed with the help of Dr. Vanesa Martinez.

3.3.21. miR-134-enriched EVs significantly increase the sensitivity of Hs578Ts(i)$_8$ cells to 17-AAG and PU-H71

As we observed that miR-134 enriched EVs significantly reduce the expression of Hsp90 in Hs578Ts(i)$_8$ cells (Figure 3.25C(i)) and did not significantly alter the proliferation of Hs578Ts(i)$_8$ cells (Figure 3.26A), we opted to investigate whether such EVs could increase sensitivity to the anti-Hsp90 compounds 17-AAG and PU-H71, which have previously been shown to have efficiency in TNBC treatment [65]. Treating Hs578Ts(i)$_8$ cells with miR-134-enriched EVs significantly increased cellular sensitivity to anti-Hsp90 compounds,

independent on any proliferation altering effects of miR-134 enriched EVs as illustrated in Figure 3.26A.

Considering 17-AAG (Figure 3.28A), cells treated with miR-134-enriched EVs showed 4.1 fold toxicity (p=0.0000004) when treated with 70nM 17-AAG for 48 hrs. This is in comparison to 2.8 fold toxicity (p=0.00000007) with cells treated with NC-mimic EVs and 70nM 17-AAG for 48 hrs. Comparing the effects of NC-mimic EVs to miR-134-mimic EVs, a 1.5 fold (p=0.001) increase in sensitivity to 17-AAG is observed (Figure 3.28A).

Likewise, considering PU-H71 (Figure 3.28B), cells treated with miR-134 enriched EVs showed 4.5 fold toxicity (p=0.000004) when treated with 60nM PU-H71 for 48 hrs. This is in comparison to 2.2 fold toxicity (p=0.000007) with cells treated with NC-mimic EVs and 60nM PU-H71 for 48 hrs. Comparing the effects of NC-mimic EVs to miR-134-mimic EVs, a 2.1 fold (p= 0.0001) increase in sensitivity to PU-H71 is observed (Figure 3.28B).

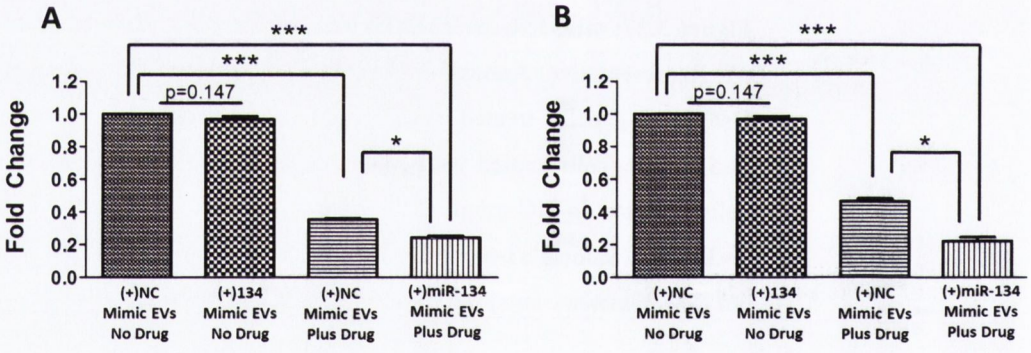

Figure 3.28: Effect of miR-134 enriched EVs in combination with anti-Hsp90 compounds. **A:** miR-134 enriched EVs increase Hs578Ts(i)$_8$ cells sensitivity to 17-AAG and **B:** PH-H71 compared to the effect of NC-mimic EVs. Results are displayed as n=3±SEM, where *=p<0.05 & ***=p<0.001 (Student's t-test).

3.5.22 dsDNA is present in Hs578T and Hs578Ts(i)$_8$ EVs.

Subsequent to DNA isolated from cells and EVs, the dsDNA quantification were analysed by Qubit quantification assay. dsDNA was successfully isolated from both Hs578T and Hs578Ts(i)$_8$ cells, with no significant difference between DNA isolated from 2x10^6 cells (Figure 3.29A). More interestingly, we observed that dsDNA is present in the EVs derived from both Hs578T and Hs578Ts(i)$_8$ cells, with significantly greater levels of dsDNA per µg present in Hs578T EVs (62.06ng) compared to Hs578Ts(i)$_8$ EVs (10.52ng) (p=0.003) (Figure 3.29B).

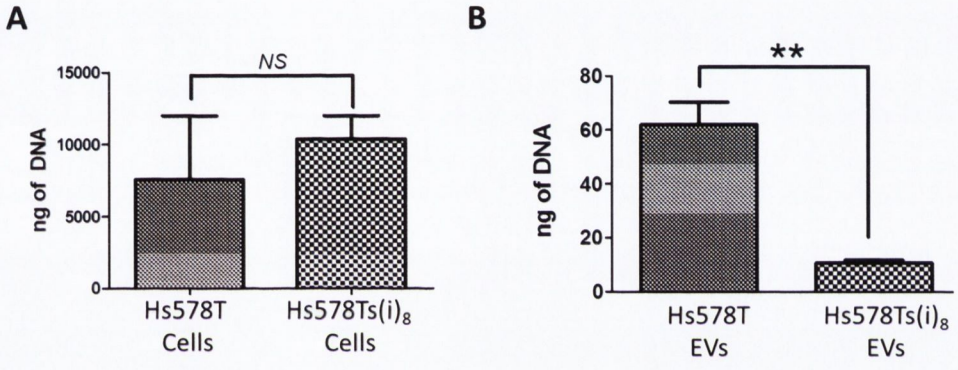

Figure 3.29: DNA is present in EVs.

A: Quantification of dsDNA obtained from 2x10^6 Hs578T and Hs578Ts(i)$_8$ cells. **B:** Quantification of dsDNA obtained from Hs578T and Hs578Ts(i)$_8$ EVs. Results are displayed as n=3±SEM, where *=p<0.05 (Student's t-test).

3.5.23 PHLPP2 is mutated in Hs578T and Hs578Ts(i)$_8$ cells and EVs

MALDI-TOF analyses of the mutations status of 284 different breast cancer associated SNPs, in a total of 49 genes, determined that PHLPP2 is mutated in all Hs578T cells (Figure 3.30A), Hs578T EVs (Figure 3.30B), Hs578Ts(i)$_8$ (Figure 3.30C) cells and Hs578Ts(i)$_8$ EVs (Figure 3.30D). The same mutation is observed in all samples, where the gene gains a cytosine. When transcribed, this mutation results in a change of amino acids from leucine to serine at codon 1016 (L1016S; T3047C).

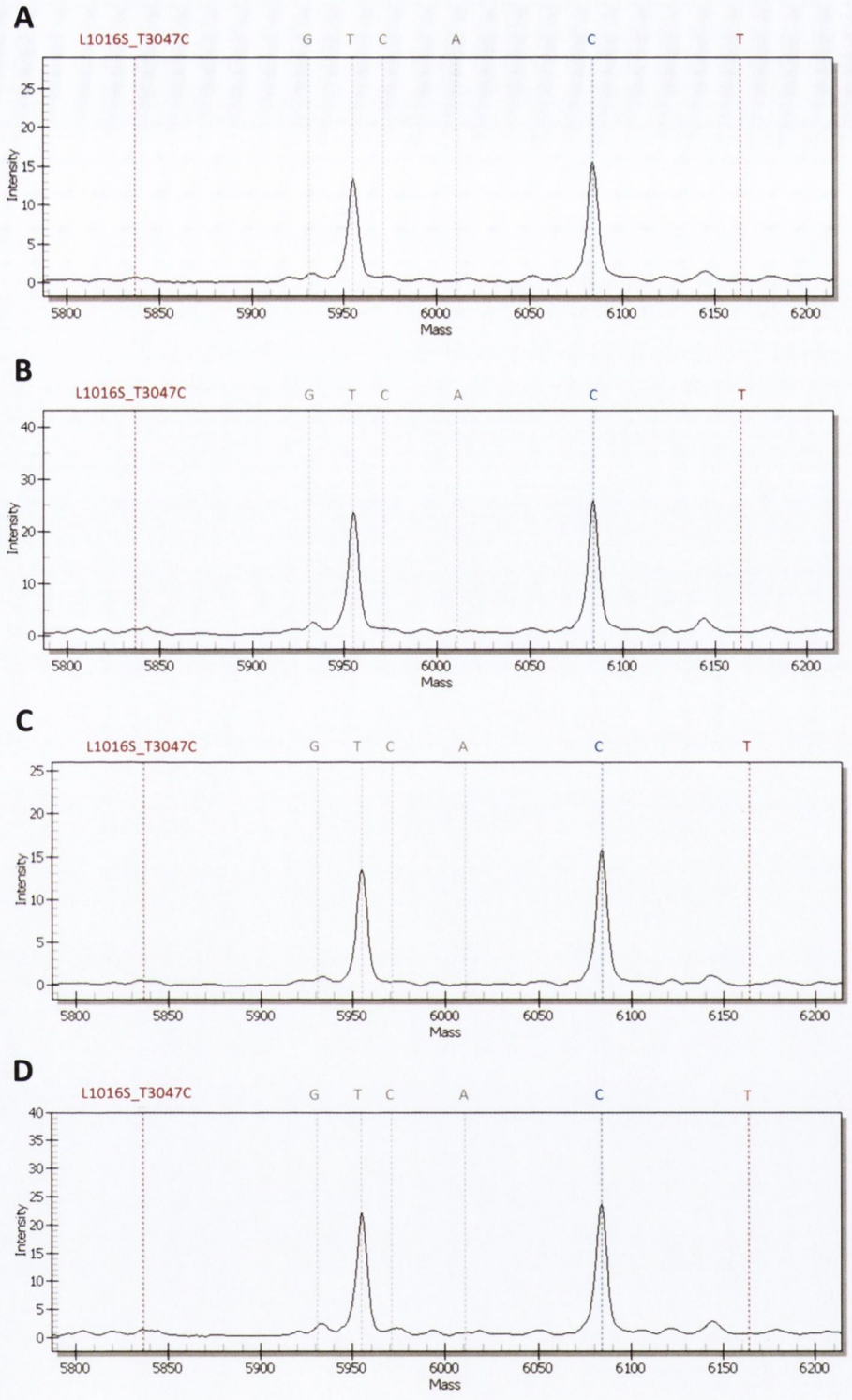

Figure 3.30: Detection of mutated PHLPP2 in all Hs578T and Hs578Ts(i)$_8$ cells and EVs by mass spectrometry.

A: Hs578T cells show a transition mutation through loss of thymine and gaining cytosine. **B:** Hs578T EVs also show a transition mutation through loss of thymine and gaining cytosine. The same transition mutation is observed in **C:** Hs578Ts(i)$_8$ cells and in **D:** Hs578Ts(i)$_8$ EVs. Results displayed represent three biological repeats.

All Sequenom analyses were performed with the help of Dr. Sinead Toomey in Beaumont Hospital, RCSI.

3.5.24 HRAS is mutated in Hs578T and Hs578Ts(i)$_8$ cells but not in their EVs

MALDI-TOF analyses showed that HRAS is mutated in Hs578T cells (Figure 3.31A) but not in Hs578T EVs (Figure 3.31B). Similarly, HRAS is mutated in Hs578Ts(i)$_8$ cells (Figure 3.31C) but not in Hs578Ts(i)$_8$ EVs (Figure 3.31D). Both mutations of HRAS are the same in both Hs578T and Hs578Ts(i)$_8$ cells, affecting codon 12 with a point insertion of adenine (G35A).

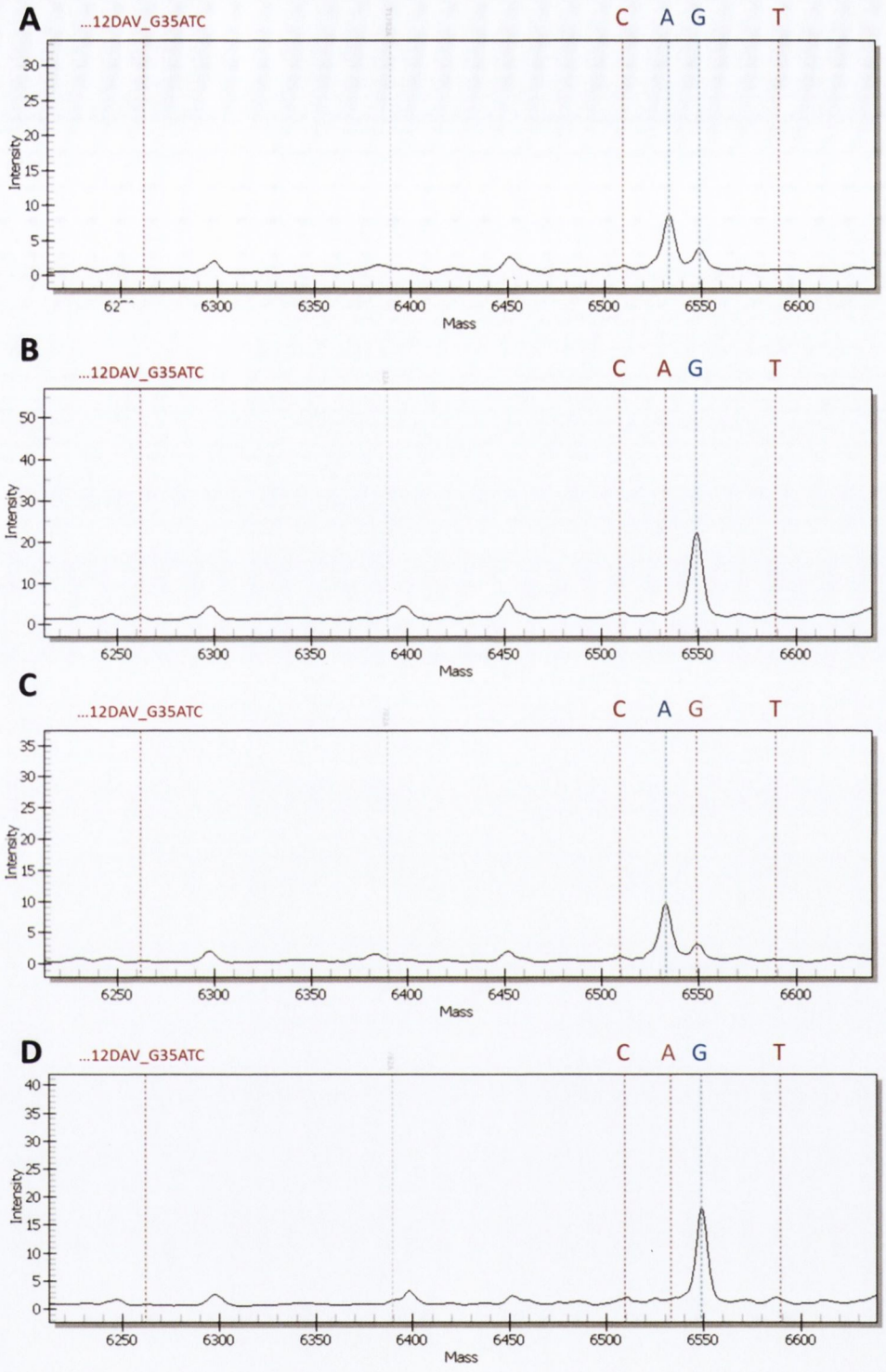

Figure 3.31: Detection of mutated HRAS in Hs578T and Hs578Ts(i)$_8$ cells but not in their EVs by mass spectrometry.

A: Hs578T cells show a point mutation through insertion of adenine. **B:** Hs578T EVs contain wild type HRAS. **C:** Hs578Ts(i)$_8$ cells show a point mutation through insertion of adenine. **D:** Hs578Ts(i)$_8$ EVs contain wild type HRAS. Results displayed represent three biological repeats.

All Sequenom analyses were performed with the help of Dr. Sinead Toomey in Beaumont Hospital, RCSI.

3.5.25 TP53 is mutated in Hs578Ts(i)$_8$ EVs only

Although TP53 was found to be present as wild type in in Hs578T cells (Figure 3.32A), Hs578T EVs (Figure 3.32B) and in Hs578Ts(i)$_8$ cells (Figure 3.32C), TP53 is mutated in Hs578Ts(i)$_8$ derived EVs (Figure 3.32D). In the Hs578Ts(i)$_8$ EVs, TP53 is mutated at codon 248. This mutation results in the insertion of a thymine (C742T).

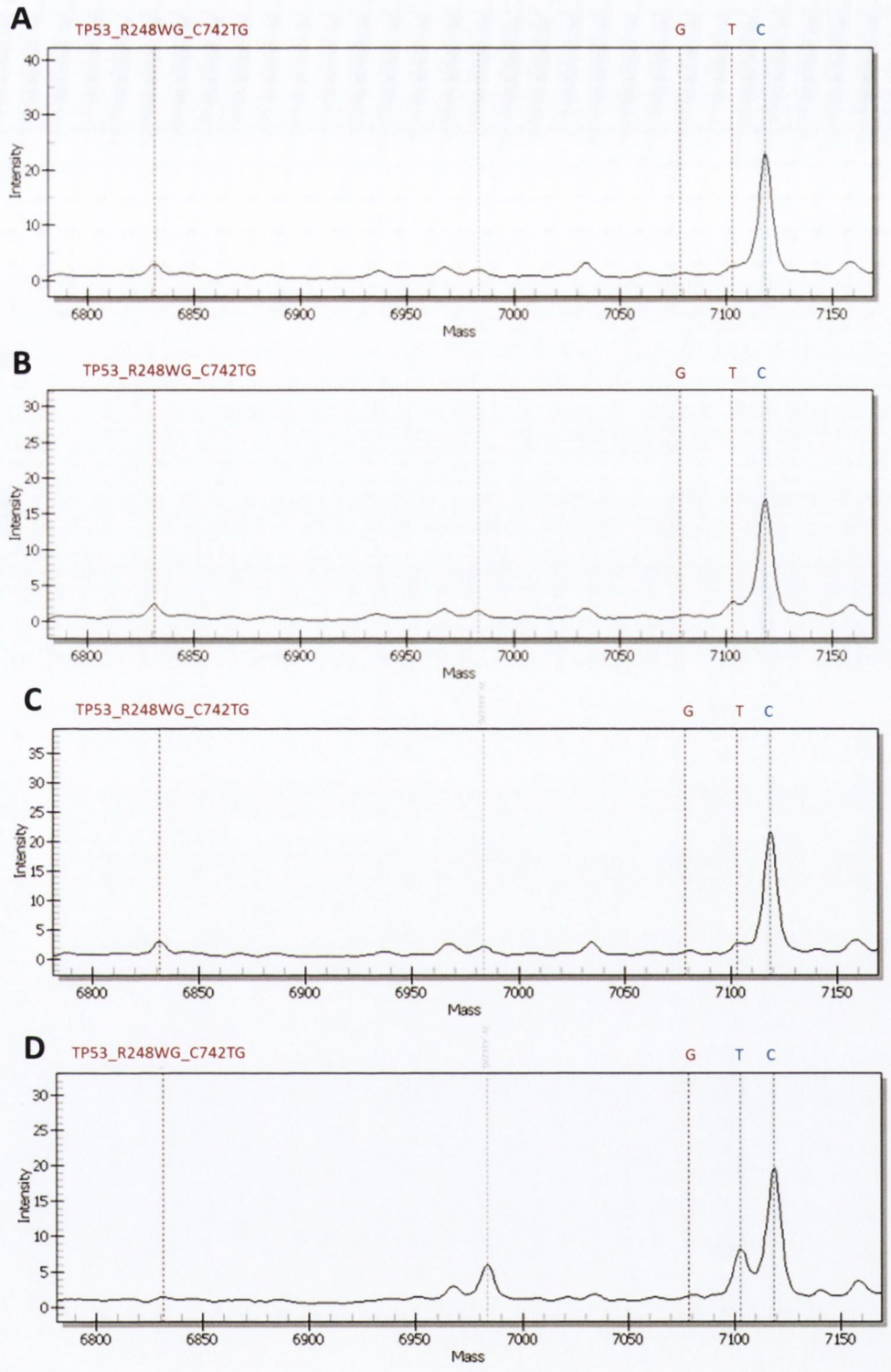

Figure 3.32: Detection of TP53 mutation in Hs578Ts(i)$_8$ EVs but not in cells by mass spectrometry.

A: Analysis of Hs578T cells shows wild type TP53. **B:** Analysis of Hs578Ts EVs shows wild type TP53. **C:** Analysis of Hs578Ts(i)$_8$ cells shows wild type TP53. **D:** Hs578Ts(i)$_8$ EVs contain a mutated version of TP53 due to a point mutation of a thymine insertion. Results displayed represent three biological repeats.

All Sequenom analyses were performed with the help of Dr. Sinead Toomey in Beaumont Hospital, RCSI.

3.5.26 Summary of SNP genotyping results

Table 3.19 below displays a summary of the mutations detected by performing MALDI-TOF analyses of the mutations status of 284 different breast cancer associated SNPs in 49 genes.

Table 3.19: Summary of DNA-SNP genotyping results

Results displayed represent biological repeats.

All Sequenom analyses were performed with the help of Dr. Sinead Toomey in Beaumont Hospital, RCSI.

Gene	Hs578T Cells	Hs578T EVs	Hs578Ts(i)$_8$ Cells	Hs578Ts(i)$_8$ EVs
PHLPP2	Mutated	Mutated	Mutated	Mutated
HRAS	Mutated	Wild Type	Mutated	Wild Type
TP53	Wild Type	Wild Type	Wild Type	Mutated

Results here represent mutations observed in all three biological repeats.

3.4. Discussion

Advancing on our previous analysis of EVs in TNBC [152], here we have more extensively investigated the relevance of EVs in the progression, detection and potential treatment of this disease. Our previous study demonstrated that TNBC EVs have the ability to mediate phenotypic alterations in recipient/secondary cells, conferring more aggressive phenotypes of breast cancer cells; in a manner indicative of the phenotypic traits of the originating cells [152]. We, therefore, investigated the DNA and miRNA content of these EVs to identify molecules that may be responsible for mediating these alterations and we questioned whether their miRNA content could be manipulated to reduce the aggressiveness of TNBC. We believe this to be the first study to profile the DNA and miRNA contents of both TNBC derived-EVs and cells to identify miRNAs which may have therapeutic potential in TNBC and to attempt to exploit these EVs as therapeutic miRNA delivery vesicles to reduce TNBC aggression and increase their drug sensitivity. Additionally, this is the first report detailing the significant relevance of miR-134 in TNBC, as well it's the potential as a tumour suppressor.

3.4.1 miRNA in EVs and cells

In this chapter, we have established the presence of total RNA (including miRNA) in the EVs from the TNBC cell line variants, Hs578T and Hs578Ts(i)$_8$. Once total RNA was isolated from Hs578T and Hs578Ts(i)$_8$ cells and their EVs using the miRNeasy mini kit, RNA yield and quality was measured using the NanoDrop ND-1000 spectrophotometer. The quality of the RNA isolated was of high quality, based the mean 260/280 ratios of 1.89 to 2.02, so was therefore ideal to proceed for use in global miRNA profiling analysis. No differences of total RNA presence was observed per $1x10^6$ Hs578T and Hs578Ts(i)$_8$ cells; however, results show that, per μg of EV isolated, Hs578Ts(i)$_8$ EVs carry 3 times greater total RNA compared to its less aggressive variant Hs578T EVs. This observation is in keeping with previous reports, that more aggressive cell derived EVs contain greater levels of total RNA [253].

qPCR analysis provides researchers with a numerical value, known as the cycle threshold (C_T), corresponding to the number of cycles that the samples underwent before the target gene/miRNA was detected. C_T values vary logarithmically with expression values [328]. To normalise miRNA expression data to calculate relative fold changes between sample sets, a number of low variance miRNAs are commonly used. As part of the TLDA kit, three of the commonly used endogenous control miRNAs are analysed; RNU48, RNU44 and MammU6, which allows the researcher to choose the most appropriate miRNA for normalising their global expression data, based on low variability C_T values. Here, we have chosen RNU48 as the most suitable endogenous control for normalising our expression data, as it showed the lowest variance between Hs578T and Hs578Ts(i)$_8$ EVs. However, either RNU44 or MammU6 would have been suitable for use as they were not expressed significantly differently between Hs578T and Hs578Ts(i)$_8$ cells and EVs.

Initial assessment of miRNA levels in cells and EVs focused on their overall content. To analyse this, C_T values of <35 C_T were regarded as being present, with all C_T values of ≥35 regarded as being absent from our samples. This analysis showed that miRNA profiles of EVs are highly representative of the miRNA profiles of their cells of origin. We observed that 79% of miRNAs detected in Hs578T cells and EVs were commonly present in both. Similarly from the Hs578Ts(i)$_8$ cells and EVs, 75% of miRNAs were commonly present in both. Strengthening this observation, linear regression analysis indicated strong correlation between miRNAs detected in cells and their EVs. This observation is consistent with previous publications. In a study analysing the mRNA and miRNA contents of cells and EVs derived from the A357 melanoma line and HEMa-LP human epidermal melanocyte cell line, Xiao *et al.* [228] observed strong correlation between the mRNA and miRNA presence in cells and their derived EVs [228]. miRNA presence in ovarian cancer sera-derived EVs have also been shown to be highly correlated to the miRNA presence of tumours from the same patient [244]. Strong correlation has also been observed in between tumours and EVs derived from peripheral blood of NSCLC patients [246]. This data suggests that the miRNA contents of EVs are strongly indicative of the miRNA profiles of their derivative tumours. Such an

observation supports the potential of EVs to be used a minimally invasive biomarkers.

Previous studies have reported a phenomenon of some miRNAs being enriched in their EVs, at the expense of diminishing the cells of these miRNAs. In a study analysing the miRNA expression of cells and EVs from breast cancer cells, Pigati *et al.* [237] observed miR-451 loss in all four aggressive breast cancer cells lines tested (MCF7, BT-20, SKBR3 and MDA-MB-231), yet their derived EVs were enriched with miR-451. Additionally, non-malignant mammary epithelial cells (MCF10A) and normal fibroblasts (IMR90) retained miR-451 in their cells. Such a finding suggests that miR-451 may have play an important role in breast cancer progression and may have value as a circulating biomarker for breast cancer progression [237] Additionally, in a study on 15 renal cell carcinoma patients, miR-451 has been identified as a potential serum based biomarker [329].

Our study has identified the same phenomenon, where miR-451 was not detected in either Hs578T or Hs578Ts(i)$_8$ cells, but was enriched in both of their derived EVs, further suggesting that miR-451 may have potential as an extracellular biomarker in breast cancer. Similarly, we have also identified miR-122 and miR-142-5p to be selectively incorporated into Hs578T and Hs578Ts(i)$_8$ EVs as the expense of their presence in their cells of origin. Interestingly, in a study on 195 hepatocellular carcinoma serum specimens, miR-122 has been identified as having potential as a circulating biomarker [330]. miR-122 has also been shown to have use as a circulating biomarker in gastric cancer, as part of a study on 12 gastric cancer serum specimens [331]. Similarly, miR-142-5p has shown potential as a circulating biomarker in pancreatic cancer [332] and osteosarcoma from analysing 18 tumours [333]. Of note, the apparent occurrence of selective miRNA trafficking into EVs, resulting in loss from the cells, was more common in the more aggressive Hs578Ts(i)$_8$ derived EVs, where 17 miRNAs were found to be present in Hs578Ts(i)$_8$ EVs but not in their cells of origin, suggesting that this occurrence may be more common in aggressive TNBC.

Taking C_T values of <35 to be present and ≥ 35 to be absent from samples, this study showed that miRNA presence is significantly reduced in the more

aggressive Hs578Ts(i)$_8$ cells and their derived EVs, when compared to Hs578T cells and their EVs. This observation concurs with previous observations that miRNAs are lost with increasing cancer aggression [334], subsequently allowing from dysregulated protein expression. Our observation also complements observations made by Gaur *et al* [335]. Gaur *et al.* examined the expression of 241 human miRNAs in the NCI-60 cell line panel, compared to normal tissues, confirming that most miRNAs are expressed at reduced levels in tumour cell lines compared to corresponding normal tissue [335]. This observation that miRNAs are generally reduced in Hs578Ts(i)$_8$ cells and EVs compared to Hs578T cells and EVs was well represented when the fold changes of miRNA expressions were calculated.

Comparing miRNA content of the cells and corresponding EVs from a pair of TNBC cell line variants *i.e.* Hs578T and its more aggressive isogenic subclone Hs578Ts(i)$_8$, revealed distinctly different miRNA fingerprints. Of particular interest to identifying a tumour suppressor miRNA, we observed that 94 miRNAs were >2 fold down-regulated in Hs578Ts(i)$_8$ cells compared to Hs578T cells; with 173 miRNAs >2 fold down-regulated in Hs578Ts(i)$_8$-derived EVs compared to Hs578T EV. Eighty-three of these miRNAs were commonly down-regulated in both cells and EVs of Hs578Ts(i)$_8$ compared to Hs578T. Although 4 miRNAs were observed to be up-regulated in Hs578Ts(i)$_8$ cells compared to HS578T cells, no miRNAs were found to be significantly up-regulated in Hs578Ts(i)$_8$ EVs compared to Hs578T EVs.

From this we identified a panel of miRNAs to be commonly down-regulated in both Hs578Ts(i)$_8$ cells and their EVs. Of these, miR-370 (from 14q32.2) showed the greatest down-regulation in cells and miR-134 (from 14q32.31) showed the greatest level of reduction in the Hs578Ts(i)$_8$-derived EVs. This suggests that loss, or at least reduced levels, of miR-370 and/or miR-134 may play an important role in mediating TNBC aggressiveness. Similar observations to this have recently been reported in other cancers where miR-370 was found to be significantly reduced in CML patients *versus* healthy controls (n=23), and transfection of miR-370 mimic, using lipofectamine 2000, increased the sensitivity of CML-K562 (myeloid leukaemia) cells to homoharringtonine (HHT) treatment and promoted apoptosis [336].

Similar to our observations, miR-134 levels were found to inversely correlate with the aggression of four NSCLC cell lines (A549, H1395, Calu1 and H1299) [337] and in osteosarcoma [338]. Additionally, miR-134 exerts anti-tumour effects in NSCLC, as well as playing a tumour suppressive role in hepatocellular carcinoma *in vivo* through down-regulating KRAS [339]. However, no such observation has been reported in breast cancer or TNBC to the best of our knowledge. Similar to other miRNA profiling studies performed on TNBC cells (MDA-MB-231 and MDA-MB-436), here we also identified miR-31 and miR-245 to be down-regulated in our aggressive Hs578Ts(i)$_8$ TNBC cells and their EVs, compared to Hs578T cells and their EVs. Although we did not observe, miR-15a, miR-126 and miR-200b to be down-regulated in our cells, we identified them to be present at reduced levels in our Hs578Ts(i)$_8$ EVs compared to Hs578T EVs [297]. Complimenting Roy *et al*'s [298] miRNA profiling study on Proline-glutamic acid- and leucine-rich protein 1(PELP1)-overexpressing and PELP1-underexpressing model cells, we also found that miR-200a is down-regulated in our aggressive breast cancer cells. However, neither of these studies identified miR-134 as being reduced in breast cancer.

We have also identified miR-106b to be significantly down-regulated in Hs578Ts(i)$_8$ EVs compared to Hs578T EVs. A similar observation has been previously reported, with miR-106b where it was observed to be reduced in breast cancer. Down-regulation of miR-106b was shown to be associated increased MMP2 expression in 50 breast cancer tumour tissues, which correlated with increased cell motility and invasion of SUM1315-bo cells [340]. Similarly, down-regulation of miR-125b has been consistently reported in breast cancers [84, 341-343] and has been reported to act as a tumour suppressor in breast cancer, by targeting the 3'-UTRs of ENPEP, CK2-α, CCNJ, and MEGF9 mRNAs in MCF7, MDA-MB-231, and HMEC cells [344]. Here, we identified miR-125b to be down-regulated in Hs578Ts(i)$_8$ EVs and miR-185, to be down-regulated in both cells and EVs. Interestingly, miR-185 has been observed to reduce tumour growth of HEK-293 cells (kidney cell line) in SCID mice [345].

It has been established that human miRNAs tend to be encoded by fragile chromosomal regions or genomic regions associated with cancer progression [346], as detailed in Chapter 1, Section 1.4.2.2. Notably, the ten most substantially down-regulated miRNAs in Hs578Ts(i)$_8$ cells all stem from the same chromosomal cluster of chromosome 14, 14q32, which has been identified as a region commonly deleted in cancer progression [347-352]. Specifically, such studies have shown that that 14q32 is frequently deleted in neuroblastoma. Analysing 54 primary neuroblastoma samples, Hoshi *et al.* [353] showed that there is substantial deletion of 14q32 in 17 of 54 (31%) neuroblastoma patients tested. Similarly, loss-of-heterogeneity at 14q32 was observed in 44% primary colorectal carcinomas, in a study on 66 primary colorectal carcinomas [348]. Allelic loss of 14q was observed in all stages of urinary bladder cancer of 285 primary carcinomas analysed [349]. Similar observations were seen in ovarian carcinomas [350], low and high-grade meningiomas [351], as well as in breast carcinomas [352]. Additionally, down-regulated miRNAs derived from this cluster have been strongly suggested to be involved in cancer progression [354-357], which suggests a possible malfunction of this fragile area of the genome in the more aggressive TNBC cells, Hs578Ts(i)$_8$. In gastrointestinal stromal tumours (GISTs), Haller *et al.* [354] globally profiled twelve GISTs to observe a high-degree of co-expression of 44 miRNAs clustered at 14q32.31. Interestingly, this study observed a significant correlation between low miR-134 and miR-370 expression with 14q loss which is associated with shorter disease free survival [354]. Similarly, Gattolliat *et al.* [355] observed that 15 of 17 miRNAs significantly down-regulated in high-risk neuroblastoma are encoded by the 14q.32.31 locus. In addition, expression analysis of two miRNAs encoded by 14q32.31 (miR-487b and miR-140) in 227 neuroblastoma tumours demonstrated that these two miRNAs are significantly reduced, and significantly associated with overall survival and disease free survival. Interestingly, high levels of genomic instability and loss of heterogeneity of 14q32 has been observed in BRCA2 mutated luminal breast cancers (n=30 ER+ tumour specimens), and may predict BRCA2 status in ER+ invasive ductal carcinomas [358].

To proceed with our analysis, five miRNAs from the 83 commonly down-regulated miRNAs were chosen for expression validation based on a three factors:

(i) Fold change of expression
(ii) Relevance in literature
(iii) Relevance based on target prediction (Targetscan Human Release 6.2)

From this we chose miR-370, miR-134, miR-376c, miR-889 and miR-655 for validation, all of which significantly validated as down-regulated in Hs578Ts(i)$_8$ cells compared to Hs578T cells. However, miR-655 did not significantly validate as being down-regulated in Hs578Ts(i)$_8$ EVs compared to Hs578T EVs. As miR-370 showed the greatest fold change reduction in Hs578Ts(i)$_8$ cells compared to Hs578T cells, and miR-134 showed the greatest fold change reduction in Hs578Ts(i)$_8$ EVs compared to Hs578T EVs, these miRNAs were chosen for functional analysis.

We analysed the functional relevance to miR-370 and miR-134 in the aggressive TNBC cell line Hs578Ts(i)$_8$, determining that both miRNAs have tumour suppressive qualities. Specifically, by analysing the tumour suppressive qualities of miR-370, we observed that transient transfection of Hs578Ts(i)$_8$ cells with miR-370 slightly reduced both migration and invasion of these cells, independent of affecting Hs578Ts(i)$_8$ proliferation, suggesting that it's loss may impact increased TNBC aggression. Target-prediction software, TargetScan Human, predicted SMO to be a target for miR-370 action. SMO is a protein involved in inducing the hedgehog signalling pathway. The hedgehog signalling pathway is essential for cellular processes during embryonic development, yet constitutive activation in adults induces tumourigenesis [359]. Furthermore, in a study on 123 paraffin embedded specimens, representing 83 primary breast carcinomas, 30 mammary hyperplasia and 10 normal tissues, SMO was observed to be increased at high histological grades; associated with advanced tumour stage and expressed at greater levels in TNBCs, compared to non TNBCs [360]. For these reasons, we felt it was relevant to investigate the effects of miR-370 on SMO. However, analysis here shows that miR-370 does not affect SMO expression in Hs578Ts(i)$_8$ cells.

Although miR-370-SMO interaction is not the responsible for the slight reduction of migration and invasion observed in this chapter, miR-370 may be targeting other proteins to result in these alterations. It has previously been observed that miR-370 reduces the expression of Forkhead box protein M1 (FOXM1) in myeloid leukaemia K562 [336, 361] and in HL60 cells [361]. As increased levels of FOXM1 has been associated with increased glioblastoma cell invasion [362], and as FOXM1 has been observed to be consistently increased in metastatic TNBCs (n=14 fresh frozen tumour tissues) [363], FOXM1 poses as an attractive protein for further miR-370 investigations.

We discovered that re-introducing miR-134 back into Hs578Ts(i)$_8$ cells, from where it has been substantially lost, resulted in significantly reduced levels of its predicted target protein, STAT5B, and associated proteins Hsp90 and Bcl-2. Of particular interest, it has been previously reported that STAT5B induces the transcription of Hsp90 [301]. Hsp90 is a molecular chaperone protein, widely expressed in breast cancer, and implicated to increase the survival of breast cancer cells by stabilising oncogenic proteins [364]. Hsp90 is also emerging as potential target for TNBC therapy [65], as detailed in Chapter 1, Section 1.3.3. In addition, inhibition of Hsp90 has been shown to result in the decreased expression of Bcl-2, allowing tumour cells to overcome apoptotic resistance [365]. However, pre-clinical studies in breast cancers has shown that HER2-overexpressing tumours are sensitive to Hsp90 inhibitors, such as 17-AAG and 17-DMAG, yet TNBC tumours show less sensitivity to the same inhibitors [366-368].

We therefore opted to investigate the efficiency of miR-134 to halt cell growth compared to anti-Hsp90 inhibitors, which showed that its effects are comparable to the 17-AAG and PU-H71, another Hsp90 inhibitor which has shown greater potency in TNBC [65]. In an attempt to increase TNBC sensitivity to Hsp90 inhibitors, we opted to combine transfection of miR-134 mimic with 17-AAG and PU-H71 treatment. Although increased sensitivity is apparent when miR-134 transfected cells are treated with anti-Hsp90 compounds, this is probably due to the decreased proliferation mediated by miR-134.

As Bcl-2 expression was also observed to be decreased upon miR-134 transfection, we opted to investigate its potential relevance as an apoptosis inducer in TNBC cells. Transfection of Hs578Ts(i)$_8$ cells in combination with cisplatin treatment, a commonly used chemotherapeutic in anti-TNBC strategies [369], increased TNBC cells sensitivity to apoptosis. This result suggests that miR-134 may have potential as an onco-suppressor when used in combination with chemotherapeutics such as cisplatin. This finding compliments previous observations that miR-195, miR-24-2 and miR-365-2 amplify the apoptotic effect of etoposide in MCF7 breast cancer cells by reducing Bcl-2 expression [11]. Further investigations of the effects of miR-134 in TNBC aggression led us to analysing its effects on migration and invasion. Although miR-134 appears to significantly reduce the invasion and migration of TNBC cells, it does not appear to give substantial benefit to migration and invasion over its effects on proliferation.

In addition to these findings, we demonstrate that, not only does direct miR-134 transfection have potential as a tumour suppressor, but EVs can also be manipulated into carrying miR-134 to act as therapeutic-miRNA delivery vesicles. Post-transfection of Hs578Ts(i)$_8$ cells with miR-134, the expelled EVs subsequently relay miR-134 from cell to cell, thus reducing the migration and invasion of recipient Hs578Ts(i)$_8$ cells (effects similar to direct transfection of miR-134 into the cells). As miR-134-enriched EVs also have the ability to reduce STAT5B and Hsp90 expression, we propose this function might be mediated through STAT5B→Hsp90 interactions. However, even though direct transfection of Hs578Ts(i)$_8$ cells with miR-134 reduced proliferation and increased cisplatin-mediated apoptosis, miR-134 enriched EVs do not significantly alter the proliferation or increase the apoptotic effect of cisplatin.

A summary of the effects of miR-134 by direct transfection compared to miR-134-enriched EVs is displayed in Table 3.20 below.

Table 3.20: Summary of the effects of miR-134 on Hs578Ts(i)$_8$ cells (miR-134 with lipofectamine *versus* miR-134 enriched EV)

Results displayed represent three biological repeats

Assay	miR-134 transfection by lipofectamine	miR-134-enriched EVs
Proliferation	Reduction	No effect
Migration	Reduction	Reduction
Invasion	Reduction	Reduction
Cisplatin-induced apoptosis	Increased sensitivity	No effect
17-AAG potency	No effect	Increased sensitivity
PU-H71 potency	No effect	Increased sensitivity

Observation that miR-134-enriched EVs do not alter Hs578Ts(i)$_8$ phenotypes in the same manner as direct miR-134 transfection using lipofectamine may be attributed to a number of reasons. The first explanation could be due to the difference of miR-134 load transmitted by both mechanisms. We have shown that direct transfection of miR-134 into Hs578Ts(i)$_8$ cells increases miR-134 presence substantially greater than the presence of miR-134 in EVs derived from the miR-134 transfected cells. This could allow for more efficient and sustained action of miR-134 in the cells. As observed in chapter 2 of this thesis, Hs578Ts(i)$_8$ derived EVs have the ability to substantially increase the aggressiveness of four breast cancer cells, as well as increasing the vasculogenesis of human epithelial cells. These observations are highly indicative that Hs578Ts(i)$_8$ EVs carry potent oncogenic factors, independent of miR-134. Although the EVs from miR-134 transfected cells carry miR-134, they may be carrying oncogenic signals which may negate or reduce the effects miR-134 in receiving cells by signalling for increased aggression. This may explain why miR-134 enriched may bestow different phenotypic alterations to secondary cells compared to direct miR-134 transfection. To overcome this limitation of using miR-134, EVs derived from a miR-134 transfected normal

cell line would minimise any oncogenic signals transmitted by EVs, to increase the effects of miR-134 enriched EVs for use as therapeutic delivery vesicles.

3.4.2 DNA in EVs

DNA SNP genotyping using the Sequenom massARRAY MALDI-TOF MS system, we have identified a number of DNA mutations in cells and EVs associated with breast cancer. Specifically, we identified a PHLPP2 mutation at codon 1016 in all Hs578T cells, Hs578T EVs, Hs578Ts(i)$_8$ cells and Hs578Ts(i)$_8$ EVs. A mutation of HRAS was identified at codon 12, resulting in the substitution of glycine to alanine, in both Hs578T and Hs578Ts(i)$_8$ cells, but wild type was present in their derived EVs. Interestingly, all Hs578T and Hs578Ts(i)$_8$ cells have wild type TP53, yet TP53 is mutated in Hs578Ts(i)$_8$ derived EVs, resulting in the insertion of threonine at codon 248. However, as reactions where >15% of the resultant mass ran in the mutant sites are scored as positive by the MassArray Analyser 4 software, this observation could be due to scoring accuracies of the genotyping platform.

Initial analysis focused in determining whether dsDNA is present in EVs derived from our TNBC cell line variants, Hs578T and Hs578Ts(i)$_8$ cells. Once DNA was isolated from Hs578T and Hs578Ts(i)$_8$ EVs using the QIAamp DNA mini kit, dsDNA was quantified using the Qubit dsDNA broad range kit, which is selective for dsDNA. Quantifications show that Hs578T EVs have substantially greater levels of dsDNA compared to Hs578Ts(i)$_8$ EVs. Previous reports has indicated that EVs from tumour cells, including GBM11/5 [253] and a panel of cancer cell lines [324] have increased levels of EV-DNA compared to to normal, fibroblast cells. The levels of DNA in EVs has been shown differ greatly between cancer cell lines [324], as we observed in this chapter, suggesting that EV-DNA concentrations in EVs may not be osicuated with the innate aggression of their cells of origin.

A non-synonymous mutation of PHLPP2 at codon 1016 in all Hs578T cell and EV variants was identified (L1016S). PHLPP2 has been shown to have relevance in breast cancer progression by binding to, and dephosphorylating the hydrophobic motif of Akt1 and Akt3. As PHLPP2 appears to play a role in

the inactivation of Akt, it has been strongly suggested that it may have a role as a tumour suppressor [370]. PHLPP2 acts to dephosphorylate the hydrophobic motif at Ser-473 in Akt1 to prevent activity of both Akt and protein kinase C (PKC) [371].

Here, we observed a polymorphism resulting in the substitution of a leucine to serine at codon 1016 of PHLPP2 in all cells and EVs. Through inactivation of the phosphatase activity of PHLPP2, this polymorphism has been shown to decrease apoptosis and increase the phosphorylation of Akt at Ser-473 in breast cancer cells, including Hs578T cells. Specifically, it has been observed that Hs578TBst cells (normal variant of Hs578T cells) are heterozygous at codon 1016 (Leu/Ser-1016) yet Hs578T cells are homozygous at this codon (Ser-1016). This observation correlates with increased Akt phosphorylation at Ser-473, as well as more prolonged phosphorylation than leucine variants. The same mutation of PHLPP2 was also reported in high grade breast cancer [371]. In addition to such observations, we observed that this mutation is conserved in the Hs578Ts(i)$_8$ cell variant.

Identification of the mutation present in Hs578T EVs and Hs578Ts(i)$_8$-derived EVs may have adverse consequences if communicated to neighbouring cells. As EVs have been shown to have the ability to transfer active DNA to cells [161, 249], transfer of L1016S mutated PHLPP2 could potentially lead to increased phosphorylation of Akt and PKC in receiving cells. In addition, as mutated PHLPP2 has been identified in EVs, reflecting the status of their cells of origin, this suggests that EVs from breast cancer patients may have potential relevance as a blood based DNA biomarker for breast cancer diagnosis. This is supported by previous observations the same polymorphism of PHLPP2 is observed in 13.5% of breast cancers [319]. As this mutation has knock-on effects for Akt activity, identification of mutated PHLPP2 in EVs may act as a biomarker for selection of appropriate breast cancer treatment regimens by using Akt pathway inhibitors. In support of the use of PHLPP2 as a blood-based biomarker for breast cancer detection, PHLPP2 has previously been shown to have promise as biomarkers in glioma and colorectal cancer, when 21 glioma tissue specimens and 14 colorectal cancer tissue specimens were analysed [372]. In addition to observing PHLPP2 mutated in Hs578T and

Hs578T cells, we also observed HRAS to be mutated in these cells. However, this mutation is not passed onto their derived EVs. As this study is interested in detecting the presence of mutated DNA sequences in EVs to help identify their mechanism of action, or to suggest their use as DNA blood-based biomarkers for breast cancer diagnosis, this observation does not substantially add to our investigations.

Sequenom MALDI-TOF analysis also identified the presence of mutated TP53 in Hs578Ts(i)$_8$ derived EVs, whereas wild type is present in their cells of origin. TP53 mutations are commonly observed in TNBCs [373], and these are suggested to be one of the central players in TNBC progression. As TP53 acts as a tumour suppressor in cells, loss of appropriate TP53 function is detrimental in cancer progression. As explained in Chapter 1, Section 1.2.2, TP53 is mutated and/or inactivated in approximately 50% of cancers [12]. Malfunctioning TP53 has major implications for impaired apoptosis regulation in cancer cells, by interaction with apoptosis associated proteins, such as: BAX, PUMA, NOXA and APAF-1 [4]. Therefore, the presence of mutated TP53 could be detrimental if communicated *via* EVs to secondary cells.

Observation of the presence of mutated TP53 in the EVs but not in the cells was highly surprising, and we are only in the position at the moment to speculate how this occurred. One explanation for this observation is that the Sequenom system scores reactions as positive, only where >15% of the resultant mass ran is mutated. This could suggest that Hs578Ts(i)$_8$ cells could carry the TP53 mutation, yet when its EVs are analysed, the mutated sequence become more enriched, crossing the 15% threshold, therefore scoring positive by Sequenom MALDI-TOF MS. Previously, a report detailed the presence of retrotransposon elements present in glioblastoma derived microvesicles. Observations from that report have indicated the presence of transposable elements allows for EVs to have reverse-transcriptase activity, suggesting that some of the DNA present in EVs represents cDNA [253]. As the presence of retrotransposable elements is commonly elevated in tumour cells, and its presence can lead to overall gene instability [374] this may explain why TP53 is mutated in our Hs578Ts(i)$_8$ EVs compared to their cells of origin. However,

the presence of retrotransposable elements in these EVs should be further investigated to substantiate this hypothesis.

3.5 Conclusion

This study provides evidence that the miRNA content is greatly altered in cells and EVs with increasing aggression and, although miRNA contents are substantially conserved in EVs from their cells of origin, there appears to be a phenomenon whereby some miRNAs are selectively incorporated into EVs and effectively eliminated from cells. We have observed a tendency for miRNA content to be vastly down-regulated in both aggressive cells and their EVs, with one of those miRNAs being miR-134. Here, miR-134 down-regulation is associated with increased aggressiveness. Functionally, miR-134 exerts its effects, at least in part, by targeting the translation of STAT5B. This subsequently reduces the levels of Hsp90 and Bcl-2. miR-134 appears to be as efficient as current anti-Hsp90 compounds in halting cell growth and, when used in combination with cisplatin, can increase cellular sensitivity to apoptosis. However, miR-134 transfection using lipofectamine does not appear to augment the effects of Hsp90 inhibitors (17-AAG and PU-H71 tested) over its effect on proliferation. Additionally, we provide evidence that EVs loaded with miR-134 reduce the aggressiveness of TNBC, suggesting they hold therapeutic value. This approach, however, requires optimisation if its true value is to be established, as these EVs are derived from aggressive TNBC cells, they may also be harbouring oncogenic signals to reduce the effectiveness of miR-134. Pilot analysis of DNA in EVs has shown that DNA is present in TNBC derived EVs. Regarding the potential use of EVs as DNA biomarkers, we have identified PHLPP2 to be mutated in Hs578T and Hs578Ts(i)$_8$ cells and their EVs, suggesting that EVs have potential for use as blood-based biomarkers to reflect mutated DNA sequences in their originating tumour cells.

Chapter 4

Investigation of the effects of sera-derived EVs and their use as miRNA blood-based biomarkers for breast cancer diagnosis

4. Abstract

Background: The presence of EVs has been observed in a wide range of biological fluids such as tumour ascites, semen, breast milk, urine, saliva and serum/plasma. The presence of EVs in such fluids has been attributed to having broad biological and diagnostic implications in human development and disease. Previously, we have shown that EVs from TNBC cell lines can increase the aggression of breast cancer cells (Chapter 2) and have distinctly different miRNA profiles (Chapter 3), depending on the innate aggressiveness of their cells of origin. We observed an overall tendency for miRNAs to be down-regulated with increased aggression. From this, we became interested in miR-134, miR-370, miR-376c, miR-889 and miR-655. Additionally, we observed miRNAs to be largely conserved in EVs from their cells of origin, suggesting that EV-miRNAs may have relevance as minimally-invasive biomarkers for cancer progression. Studies focused solely on the clinical relevance of EVs from breast cancer patients are limited, yet detailed analysis of their interactions, signalling and contents may lead researchers to discover their true value in a clinical setting. Therefore, this chapter aimed to solely investigate the phenotypic mediating effects, and the miRNA contents, of EVs derived from serum of breast cancer patients, compared to EVs derived from the sera of healthy individuals, to better elucidate the relevance of EVs in breast cancer.

Methods: EVs were isolated from 250µl of serum derived from breast cancer patients or healthy, age-matched donors by filtration and ultracentrifugation. Immunoblotting was used to detect the presence of PDC6I/Alix and TSG101. EVs from TNBC patients, ER+ patients or age matched healthy individuals were added to breast cancer cells to analyse their effects on proliferation (n=14), migration (n=8) and invasion (n=10). To clinically investigate the relevance of miR-134, miR-370 and miR-376c in breast cancer tumour tissues, publically available datasets from miRNA profiling studies were analysed. Additionally EVs were also isolated from 250µl of serum from healthy individuals, TNBC patients (n=14), ER+ patients (n=14) and HER2+ patients (n=4) for miRNA expression analysis. Total RNA was isolated from the sera-

EVs using the Qiagen miRNeasy mini kit. qPCR analysis was performed using TaqMan small RNA assays to determine the levels of miR-134, miR-370 and miR-376c in TNBC, ER+ and HER2+ sera-derived EVs compared to age-matched healthy control sera-EVs; and between breast cancer subtypes and cancer stages. Receiver operator characteristic (ROC) curves were used to determine their sensitivity as biomarkers. Additionally, miR-889 and miR-655 expression was analysed in EVs from the sera of TNBC patients compared to age-matched controls (n=9).

Results: EVs obtained from the sera of ER+ and TNBC patients increase the proliferation, migration and invasion of breast cancer cells *in vitro*, compared to the effects of EVs from healthy controls. Analysed by subtype, TNBC, but not ER+ sera-derived EVs, significantly increase secondary cell proliferation. Similarly, both ER+ and TNBC-derived sera-EVs increase cell migration and invasion, with no significant difference between subtypes. Sera-EVs from breast cancer specimens are enriched in RNA compared to sera-EVs from age-matched control specimens. Considering miRNA expression in breast tumours; miR-134, miR-370 and miR-376c are all significantly reduced in two gene-expression omnibus data-sets. Considering breast cancer sera-EVs, miR-134 (AUC: 0.73; p=0.001), miR-370 (AUC: 0.81; p=<0.0001) and miR-376c (AUC: 0.75; p=0.0006) are all present at significantly reduced levels in EVs derived from breast cancer sera compared to EVs derived from age-matched healthy control sera. Three miRNAs were found to be substantially reduced in stage 1 [miR-134 (AUC: 0.86; p=0.03), miR-370 (AUC: 0.86; p=0.03), miR-376c (AUC: 0.79; p=0.07)], and stage 3 breast cancers [miR-134 (AUC: 0.90; p=0.003), miR-370 (AUC: 1.00; p=0.0006) and miR-376c (AUC: 0.80; p=0.02)] compared to miRNA from age matched control sera-EVs. Neither miR-889 nor miR-655 from sera-EVs are sensitive for use as blood-based biomarkers.

Conclusions: Evaluating the effects of EVs derived from the sera of breast cancer patients has shown that they can increase the aggression of breast cancer cells *in vivo.* This suggests that these entities may act within breast cancer patients to aid in increased breast cancer aggression. The observation of vastly

down-regulated miR-134, miR-370 and miR-367c in breast cancer tumours compared to normal tissues and breast cancer derived sera-EVs compared to healthy control sera-EVs suggests clinical importance of these miRNAs, both functionally in tumour progression and as easily obtainable biomarkers for breast cancer. As these EV-miRNAs are present at significantly reduced levels in stage 1 breast cancers, these miRNAs may have relevance as biomarkers for detection of early breast cancer, and have significant potential when all EV-miRNAs are considered as biomarkers.

4.1. Introduction

Following on from findings in previous chapters utilising cell line models for tumour derived EVs, there was a need to validate these results in clinical specimens to determine whether such findings are applicable in a clinical context. In Chapter 2, we determined that EVs from TNBC cell lines have the ability to alter secondary cell phenotypes and increase the aggression of cell lines in a manner representative of the innate phenotypes of their originating cells [198]. Following on from these analyses, in Chapter 3 we showed that TNBC EVs contain miRNAs which may be responsible for such events. We observed the miRNA content to be largely conserved in EVs compared to their donor cells, suggesting that EVs may represent miniature miRNA-maps of their donor tumour cells which could allow for their use as a minimally-invasive method for detecting, monitoring and predicting treatment response in breast cancer. Additionally, In Chapter 2 we observed a large number of miRNAs to be commonly down-regulated in both aggressive cells and their derived EVs. These included: miR-134, miR-370, miR-376c, miR-655 and miR-889. From this we became very much interested in a select few of these miRNAs for use as biomarkers. To clinically evaluate these observations, we obtained sera from breast cancer patients and healthy controls to validate our cell line functional investigations and differential miRNA expression findings.

Breast cancer diagnosis, at present, relies upon detection and analysis of a growth typically reported initially by a patient and referred to a clinic by their general practitioner. Unfortunately, as there is no reliable blood-based assessment available, biopsies must be taken from all referred patients. Not only is this an invasive, stressful and uncomfortable procedure for a patient to experience, it also means those with breast cancer experience a lack of prioritisation due to excess strain on the health care system [239]. Tumour markers found in serum, such as carcinoembryonic antigen in colorectal cancer [375] and carbohydrate antigen 19-9 in pancreatic cancer [376] are commonly used as easily obtainable biomarkers in diagnostic assays [377, 378]. However, carcinoembryonic antigen is insensitive for this purpose in breast cancer [379]. Growth factors, such as VEGF and basic fibroblast growth factor have been

investigated as potential blood-based biomarkers in cancer [380], however their use is limited due to their insensitivity to detect cancer early [381]. For these reasons there is urgent requirement for blood-based minimally-invasive biomarkers for breast cancer diagnosis.

Circulating nucleic acids, including extracellular miRNAs in blood, hold promise for clinical application for breast cancer detection and prediction [239]. As the miRNA content present in serum is reflective of the expression levels in the originating tumour specimens [382], circulating miRNAs are receiving much attention as blood-based cancer diagnostics. Recently, Gao *et al.* [383] observed that the expression levels of miR-21 in tumour specimens, as well as freely circulating in plasma, can be used as a predictive biomarker for disease free survival and response to platinum-based chemotherapeutic treatment in patients with NSCLC (n=32) [383]. Of relevance to breast cancer, circulating miR-125b is associated with chemoresistance in breast cancer in a study on 56 breast cancer patients with invasive ductal carcinoma and pre-operative neoadjuvant chemotherapy [342]. Additionally, miR-630 has been recently proposed to have potential as a circulating predictive biomarker for therapeutic response of HER2 overexpressing breast cancer cells *in vitro* [384].

Although peripheral blood, serum and plasma are rich sources of miRNA, it can be difficult to discriminate between disease-specific miRNA biomarkers from those constitutively expressed in both healthy and diseased individuals. Of concern, circulating ribonucleases place freely circulating miRNAs at risk of degradation, which may substantially diminish the sensitivity and specificity of freely circulating miRNA biomarker assays [385].

Since the first observation of miRNAs in EVs seven years ago, their relevance as blood-based biomarkers has been investigated [154]. Progression in the area of EV research is leading to more standardised protocols for their isolation, overcoming some of the limitations of circulating miRNA biomarker research. This may allow for more reliable approaches to circulating miRNA biomarker discovery and detection [385]. Our observation that EVs act as a protective barrier against the action of RNase (Section 3.3.18.), which has also been observed in other studies [224], suggests that EV-miRNA is more stable than freely circulating miRNA. This observation suggests that EVs have potential as

a robust entity from which to analyse miRNAs in the clinic. As EVs are released by most cells in culture [386], it suggests that all species of miRNAs could theoretically be detected in circulation [381].

Attempts to identify EV based miRNA biomarkers have led to a number of studies dedicated to investigating the miRNA profile of EVs derived from the sera of cancer patients. In an ovarian cancer analysis, a team investigated the miRNA profile of sera derived EVs (n=50) and primary tumour cell cultures (n=6) compared to age-matched healthy control sera-EV miRNA profiles. This analysis showed that the levels of eight miRNAs, previously determined to be of diagnostic value in ovarian cancer, were expressed in a similar manner in both primary cell cultures and sera-derived EVs, exhibiting correlation of 0.71 to 0.90 for miRNAs between cells and EVs [244].

Similarly, miRNA profiling of 742 miRNAs was performed on prostate cancer sera-EVs (n=78) to identify differences in control (n=28), non-metastatic and metastatic prostate cancer. In that study, 12 miRNAs were present at different levels in prostate cancer patients compared with controls, including 9 in patients without metastases compared to controls. Additionally, 11 miRNAs were found to be significantly increased, and one miRNA significantly decreased in sera-derived EVs when from patients with metastases compared with those without metastases. Comparing non-metastatic to metastatic patient sera-EVs, determined that 15 miRNAs were significantly up-regulated and one down-regulated. This study supports the hypothesis that circulating miRNAs, associated with EVs have potential as an aid in cancer diagnosis, by differentiating between healthy and cancer patients, as well as allowing for the detection of occult micro-metastases in prostate cancer [387]. miRNA analysis was performed on EVs from 27 lung adenocarcinoma patients, determining that EVs derived from cancer patient sera contained >2 fold concentration of miRNA compared to healthy controls sera-EVs [246]. Similarly, oesophageal squamous cell carcinoma analysis showed different levels of miRNAs in cancer patients (n=101) *versus* age matched controls (n=46), with 6 miRNAs significantly up-regulated and 5 miRNAs significantly down-regulated in oesophageal squamous cell carcinoma sera-EVs compared to healthy control sera-EVs [388]. miRNAs derived from sera-EVs are also showing potential in

other cancers, such as colon cancer [389], acute myeloid leukaemia [390], and glioblastoma [155].

Although investigations have been performed on the relevance of circulating miRNAs in breast cancer detection [391-394], investigation into the clinical relevance of EV-miRNA in breast cancer detection and monitoring are somewhat limited. Advancing on our previous studies, this chapter aimed to investigate the relevance of circulating EVs in clinical specimens, not only to determine whether they may have an influence on breast cancer metastasis, but to also investigate whether they hold promise as circulating miRNA biomarkers for breast cancer detection and progression, while investigating novel findings reported in Chapter 3 of this thesis.

4.2. Materials and Methods

4.2.1 Serum specimens

All sera specimens from ER+, HER2+, and fourteen of the sera specimens from TNBC patients, were obtained from St. James' Hospital (SJH), Dublin, where ethics approval was granted. Ten of the serum specimens from TNBC patients and their healthy controls were obtained from Asterand Biobank (Asterand UK). All other age-matched control sera specimens were obtained from St. Vincent's University Hospital, Dublin, where ethics approval was granted. Written, informed consent was sought and obtained from all participants involved in this study. A breakdown of the specimens used for each analysis, and sources, are shown in Table 4.1, Table 4.2 and Table 4.3.

Table 4.1: Serum specimens from ER+ patients used in this chapter (n=23)									
Specimen ID	Source	Phenotypic assay			miRNA presence assay				
		HCC1954 Proliferation	HCC1954 Migration	HCC1954 Invasion	miR-134	miR-370	mir-376c	miR-889	miR-655
ER 1	SJH	X	X	X	✓	✓	✓	X	X
ER 2	SJH	X	X	X	✓	✓	✓	X	X
ER 3	SJH	X	X	X	✓	✓	✓	X	X
ER 4	SJH	X	X	X	✓	✓	✓	X	X
ER 5	SJH	X	X	X	✓	✓	✓	X	X
ER 6	SJH	X	X	X	✓	✓	✓	X	X
ER 7	SJH	X	X	X	✓	✓	✓	X	X
ER 8	SJH	X	X	X	✓	✓	✓	X	X
ER 9	SJH	X	X	X	✓	✓	✓	X	X
ER 10	SJH	X	X	X	✓	✓	✓	X	X
ER 11	SJH	X	X	X	✓	✓	✓	X	X
ER 12	SJH	X	X	X	✓	✓	✓	X	X
ER 13	SJH	X	X	X	✓	✓	✓	X	X
ER 14	SJH	X	X	X	✓	✓	✓	X	X
ER 15	SJH	✓	X	✓	X	X	X	X	X
ER 16	SJH	✓	✓	X	X	X	X	X	X
ER 17	SJH	✓	✓	✓	X	X	X	X	X
ER 18	SJH	✓	✓	X	X	X	X	X	X

Table 4.1Continsued (ER+ specimens used)									
Specimen ID	**Source**	**Phenotypic assay**			**miRNA presence assay**				
		HCC1954 Proliferation	HCC1954 Migration	HCC1954 Invasion	miR-134	miR-370	mir-376c	miR-889	miR-655
ER 19	SJH	✓	X	X	X	X	X	X	X
ER 20	SJH	✓	X	✓	X	X	X	X	X
ER 21	SJH	✓	✓	✓	X	X	X	X	X
ER 23	SJH	X	X	✓	X	X	X	X	X

Table 4.2: Serum specimens from TNBC patients used in this chapter (n=24)										
Specimen ID	Source	Phenotypic assay				miRNA presence assay				
		HCC1954 Proliferation	HCC1954 Migration	HCC1954 Invasion	SKBR3 Invasion	miR-134	miR-370	mir-376c	miR-889	miR-655
TNBC 1	Asterand	x	x	x	✓	✓	✓	✓	✓	✓
TNBC 2	Asterand	x	x	x	✓	✓	✓	✓	✓	✓
TNBC 3	Asterand	x	x	x	✓	✓	✓	✓	✓	✓
TNBC 4	Asterand	x	x	x	✓	✓	✓	✓	✓	✓
TNBC 5	Asterand	x	x	x	✓	✓	✓	✓	✓	✓
TNBC 6	Asterand	x	x	x	✓	✓	✓	✓	✓	✓
TNBC 7	Asterand	x	x	x	✓	✓	✓	✓	✓	✓
TNBC 8	Asterand	x	x	x	✓	✓	✓	✓	✓	✓
TNBC 9	Asterand	x	x	x	✓	✓	✓	✓	✓	✓
TNBC 10	Asterand	x	x	x	✓	✓	✓	✓	x	x
TNBC 11	SJH	x	x	x	x	✓	✓	✓	x	x
TNBC 12	SJH	x	x	x	x	✓	✓	✓	x	x
TNBC 13	SJH	x	x	x	x	✓	✓	✓	x	x
TNBC 14	SJH	x	x	x	x	✓	✓	✓	x	x
TNBC 15	SJH	✓	✓	✓	x	x	x	x	x	x
TNBC 16	SJH	✓	x	✓	x	x	x	x	x	x
TNBC 17	SJH	✓	✓	✓	x	x	x	x	x	x
TNBC 18	SJH	✓	x	x	x	x	x	x	x	x

Table 4.2 Continued (TNBC specimens used)										
Specimen ID	Source	Phenotypic assay				miRNA presence assay				
		HCC1954 Proliferation	HCC1954 Migration	HCC1954 Invasion	SKBR3 Invasion	miR-134	miR-370	mir-376c	miR-889	miR-655
TNBC 19	SJH	✓	X	X	X	X	X	X	X	X
TNBC 20	SJH	✓	✓	✓	X	X	X	X	X	X
TNBC 21	SJH	✓	X	X	X	X	X	X	X	X
TNBC 22	SJH	X	✓	✓	X	X	X	X	X	X
TNBC 23	SJH	X	X	X	✓	X	X	X	X	X
TNBC 24	SJH	X	X	X	✓	X	X	X	X	X

Table 4.3: Serum specimens from HER2+ patients used in this chapter (n=4)						
Specimen ID	Source	miR-134 PCR	miR-370 PCR	mir-376c PCR	miR-889 PCR	miR-655 PCR
HER2 1	SJH	✓	✓	✓	X	X
HER2 2	SJH	✓	✓	✓	X	X
HER2 3	SJH	✓	✓	✓	X	X
HER2 4	SJH	✓	✓	✓	X	X

4.2.2 Isolation of EVs from serum specimens

EVs were isolated from 250µl aliquots of serum from TNBC, ER+ and HER2+ breast cancer patients and age-matched healthy controls. Serum specimens were diluted in 5ml of sterile PBS prior to being centrifuged at 2,000g for 10 mins at 4°C and filtered through 0.45µm syringe filters (PAL; Cat. #:4564). The specimens were then transferred to sterile 8ml polyallomer ultracentrifuge tubes (Backman-coulter: Cat. #: 358649) and subsequently ultracentrifuged at 110,000g for 75 mins at 4°C on a SW41Ti swinging bucket rotor. EV pellets were washed in sterile PBS and ultracentrifugation repeated. Pellets were resuspended in 100µl of sterile PBS for use in functional assays, 200µl of sterile PBS for RNA isolation, or resuspended in 20µl of cell extraction buffer (Invitrogen, Cat. #: FNN0011), as described below for immunoblotting. EV quantities were determined using the Bio-Rad protein assay (Bio-Rad; Cat. #: 500-0006) as described in Section 2.2.2.1.

4.2.3 Immunoblotting

EV specimens were collected as detailed in Section 0, and resuspended in 20µl of cell extraction buffer (Invitrogen, Cat. #: FNN0011) with protease inhibitor (Roche; Cat. #: 05892970001) and phosphatase inhibitors as appropriate (Roche; Cat. #: 04906837001). Lysate suspensions were then incubated 3 times on ice for 10 mins vortexing for 15 secs between each 10 min incubation. Lysates were then centrifuged using a bench-top centrifuge at 13,000g for 15mins at 4°C. Any residual pellet was discarded, as the supernatant represents the protein lysate fraction. Protein quantities were determined using the Bio-Rad protein assay (Bio-Rad; Cat. #: 500-0006) as described in Section 2.2.2.1.

Proteins were made up to the desired concentrations at which point appropriate volume of 4X loading buffer was added to the sample, then placed at 95°C for 5 mins and incubated on ice until loading the gel wells. 30µg of EV-specimen lysates were resolved on 12.5% SDS gels and transferred to PVDF membranes (Bio-Rad laboratories, Cat. #: 162-0177) by semi-dry transfer at 25V for 30 mins. Blots were washed 3 times (5 mins each) with wash buffer (PBS + 0.1% Tween-20 (Sigma-Aldrich, Cat. #: P2287)); then blocked in 5% (w/v) non-fat

milk in PBS + 0.1% Tween (Bio-Rad laboratories; Cat. #: 170-6404) for 1 hr, washed 3 times and incubated overnight at 4°C, gently rocking with primary antibodies for: PDC6I/Alix (Rabbit; 1:1000; Abcam; Cat. #: ab76608) and TSG101 (Mouse; 1:1000; Abcam; Cat. #:ab83). Blots were subsequently washed 3 times for 5 mins in washing buffer. Membranes were then incubated with the appropriate horseradish peroxidase-conjugated secondary antibodies *i.e.* anti-mouse (Cell Signalling, Cat. #: 7074; 1:1000 dilution) or anti-rabbit (Cell Signalling, Cat. #: 7076; 1:1000 dilution) for 1 hr at room temperature. Protein bands were visualised by chemiluminescence (ThemoFisher: Cat. #: 34080). Detection was performed with a Chemidoc exposure system (Bio-Rad Laboratories).

4.2.4 Cell culture

HCC1954 and SKBR3 cells were cultured as previously described in Section 2.2.1.

4.2.5 Proliferation assay

HCC1954 cells were seeded in triplicate at equal densities (2 x 10^3 cells/well) in 96-well culture plates. 2µg of EVs from either breast cancer patients (ER+ or TNBC) or age matched controls were added upon seeding in complete 10% dFBS DMEM medium. Cells were allowed to grow for 72 hrs, when cell growth was measured using the acid phosphatase method, as described in Section 3.2.10.1.

4.2.6 Migration assay

To assess the influences of EVs on motility using wound healing assays, $3x10^5$ HCC1954 cells/well were seeded in a 24 well plate and allowed to grow to confluency for 24 hrs. When confluent, cell monolayers were scratched with a 200µl pipette tip and gently washed twice using DMEM to remove floating cells. Medium was then replaced with 1% dFBS DMEM medium and 10µg of EVs from breast cancer patients or age matched control were applied to each well, as appropriate. The resulting wounded areas were monitored by phase

contrast microscopy and measurements determined using Olympus Cell^A Image Acquisition Software 24 and 48 hrs post-scratching and EV treatments.

4.2.7 Invasion Assay

Invasion assays were performed using 8μm pore size 24-well transwell chambers (Unitech, Cat. #: 353097). Prior to seeding, transwell chambers were coated with 100μl of 1:10 ECM (Sigma-Aldrich, Cat. #: E1270) diluted in DMEM, and left at 4°C overnight. Two hrs prior to seeding the assay, ECM-coated inserts were placed at 37°C, subsequently washed 3 times with DMEM in preparation of seeding cells. Medium containing 10% dFBS (500μl) was added to each well below the insert. SKBR3 ($5x10^4$) or HCC1954 ($2.5x10^4$) cells, in 500μl complete 10% dFBS medium, were added to each insert. 5 hrs later, when cells had attached, medium within the inserts was replaced with medium containing 1% dFBS and 15μg of patients or control serum-derived EVs, in equal volumes. After 72 hrs, medium was removed, inside of the insert wiped twice with PBS-soaked Q-tip, and stained with 1% crystal violet (Sigma-Aldrich, Cat. #: C6158). Crystal violet staining was solubilised in 10% acetic acid and absorbance was measured at 595nm on a FlouStar Optima microplate reader (BMG Labtech). Effects of TNBC derived sera-EVs on SKBR3 invasion was performed with the help of Dr. Sweta Rani.

4.2.8 Isolation of total RNA from serum derived EVs

Total RNA was isolated from EVs derived from serum specimens using the Qiagen miRNeasy mint kit according to manufacturer's instructions and eluted in 15μl of nuclease-free water. RNA concentration was determined using a Nanodrop spectrophotometer ND-1000.

4.2.9 Assessment of miRNA expression in breast cancer tumours

Expression levels of miR-134, miR-370 and miR-376c in breast tumours and matched normal breast tissue were determined using two publically-available tumour datasets by Gene expression omnibus (GEO) (http://www.ncbi.nlm.nih.gov/geo/) *(note: miR-889 or miR-655 were not*

represented in either of these datasets). Specifically GEO accession GSE26659 [395] is comprised of a total of 77 breast tumour specimens obtained from patients who underwent primary surgical treatment and 17 normal breast tissue specimens obtained from mammoplastic reductions. GEO accession GSE40525 [396] consists of breast tumour specimens (n=61) including ER+ (n=47), HER2+ (n=6) and TNBC (n=8) with 56 control tissues obtained from matched adjacent peri-tumoural normal breast tissues. miRNA expression values were determined using GEO2R [397].

4.2.10 Real-time quantitative reverse-transcription PCR

In order to validate key findings from the miRNA profiling on clinical specimens, qPCR was performed for specific miRNAs of interest. All of the TaqMan miRNA assays (miR-134: Assay ID: 001186; miR-655: Assay ID: 001612; miR-376c: Assay ID: 002122; miR-889: Assay ID: 002202) were purchased from Applied Biosystems. cDNA sysnthesis was performed using TaqMan miRNA Reverse Transcription assays kit (Applied Biosystems; 4366597) according to manufacturer's instructions. Reverse transcriptions were performed on 10ng of total RNA from breast cancer derived sera-EVs and healthy control sera-EVs. RT master mix was made up according to Table 4.4 below: Levels of miR-134 in sera-EVs was performed with the help of Dr. Sweta Rani. Levels of the other miRNAs was performed with the help of Ms. Melissa Daly.

Table 4.4: Master mix components for reverse transcription

Component	Volume per reaction
100mM dNTPs (with dTTP)	0.15µl
Multiscribe™ reverse transcriptase, 50 U/µl	1.00µl
10X reverse transcription buffer	1.50µl
RNase inhibitor	0.19µl
Nuclease free water	4.16µl
5X reverse transcription primer	3.00µl
Total volume	**10.00**µl

RT was performed under the following conditions:

Table 4.5: Program used for reverse transcription		
Step	**Time**	**Temperature**
Hold	30 mins	16°C
Hold	30 mins	42°C
Hold	5 mins	85°C
Hold	∞	4°C

Once completed, cDNA was placed in labelled nuclease-free Eppendorfs and stored at -20°C. qPCR was performed using TaqMan microRNA assay kit (Applied Biosystems; 4427975), using 1.33µl of cDNA product from reverse transcription. qPCR master mix was made up according to Table 4.6 below:

Table 4.6: Master mix components for reverse transcription	
Component	**Master mix volume per reaction**
TaqMan small RNA assay (20X) (primer)	1.99µl
Product from RT reaction (cDNA)	1.33µl
TaqMan universal PCR master mix II (2X), no UNG	10.00µl
Nuclease free water	7.67µl
Total volume	**20.00µl**

qPCR was performed using the ViiA™ 7 real time PCR system (Life Technologies) using the following program:

Table 4.7: Master mix components for reverse transcription		
Step	Time	Temperature
Hold	10 mins	95°C
40 cycles	15 secs	95°C
	60 secs	60°C

4.2.11 Normalisation of miRNA levels in serum EVs

Relative quantities of miRNAs were calculated using the ΔC_T method. This was performed by subtracting the C_T value of the patient specimens for each miRNA from the corresponding C_T value for the healthy individual, to give a ΔC_T value. Fold changes were calculated by $2^{(-\Delta C_T)}$. An outline of how this was calculated is shown in Table 4.8 below.

Table 4.8: miRNA fold change of expression calculation using ΔC_T method

Calculation	Definition
C_T	Cycle threshold where miRNA is detected
ΔC_T	C_T of patient *(minus)* C_T of healthy individual
$2^{(-\Delta CT)}$	Fold change

4.2.12 Statistical analyses

Statistical analysis for fold changes were performed in Microsoft Excel, where p-values were generated using Student's T-tests, with $p<0.05$ considered as statistically significant. GraphPad Prism 5.0 was used for graph generation. To assess sensitivity and specificity, ROC curves were created using relative quantification (RQ) values of miRNA expressions. ROC curves were generated by GraphPad Prism 5.0, which determined area under curve (AUC), confidence intervals (CI), standard errors and p-values as previously described [398]. Blume [399] has defined AUC as: "AUC is the probability that a randomly selected observation from one population scores less on the test than a randomly selected observation from the other population. If the AUC is one (or zero) then the test discriminated perfectly, but if the AUC is one-half (0.5) then the test has no discriminative ability whatsoever". To determine minimum number of specimens required to perform accurate ROC curve analysis, help was obtained from Dr. Karsten Hokamp, Bioinformatics Research Officer, TCD. Minimum specimen numbers were calculated using the online tool "StatsToDo: Computer program to calculate specimen size requirements for estimating a single receiver operating characteristics" [400].

4.3. Results

4.3.1 EVs were isolated from control and patient sera

Immunoblot analysis was performed and detected the presence of two proteins accepted as markers of EVs, PDC6I/Alix and TSG101 (Figure 4.1A).

EV quantities expelled from control and breast cancer sera were similar, showing no significant differences in quantities obtained per 1 ml of sera from age-matched controls *versus* sera from patients with TNBC or ER+ breast cancer (p=0.915), control sera *versus* sera from patients with TNBC (p=0.605), or control sera *versus* sera from patients with ER+ breast cancer (p=0.795). Similary, no difffeences of EV quantities per 1 ml of sera was observed between patients with TNBC or ER+ breast cancer (p=0.511) (Figure 4.1B).

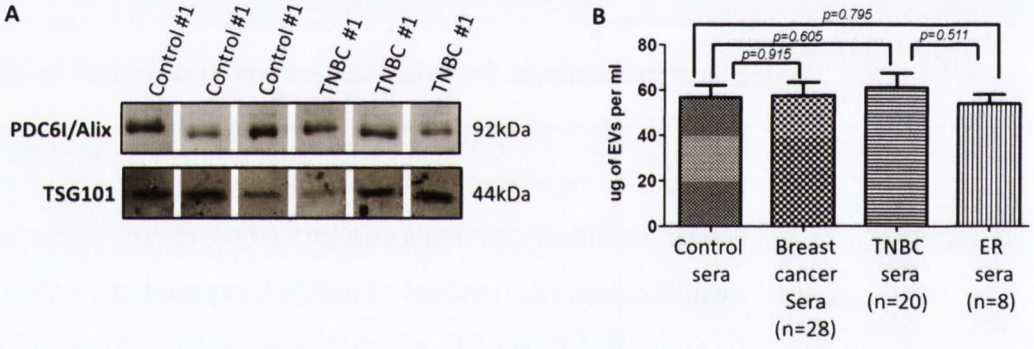

Figure 4.1: EVs were successfully isolated from control and TNBC serum.

A: Immunoblot analysis determined the presence of EV markers, PDC6I/Alix and TSG101 post filtration and ultracentrifugation of 250µl of serum specimens. **B:** Protein quantification of EVs determined no significant differences in EVs isolated from from sera of breast cancer parients compared to age-matched controls. Results are displayed as mean±SEM, where (Student's t-test).

4.3.2 EVs from breast cancer sera increase cellular proliferation

To analyse effects on proliferation, 2μg of EVs (ER+, TNBC or healthy individual derived) were added to $2x10^3$ HCC1954 cells and allowed to culture for 72 hrs. Individual replicate results are shown in Figure 4.2A. This analysis demonstrated that EVs from breast cancer specimens increase the rate of proliferation of HCC1954 cells compared to the effects of age-matched healthy control EVs by 1.2 fold; p=0.004 (Figure 4.2B). Analysing results based on subtype determined that EVs derived from TNBC patients significantly increase the rate of HCC1954 proliferation by 1.2 fold (p=0.03) (Figure 4.2C); yet EVs from ER+ patients do not significantly increase HCC1954 proliferation (p=0.08) (Figure 4.2D). Comparing the effects of EV from TNBC patients to EVs from ER+ patients TNBC showed no significant difference between the subtypes (p=0.91) (Figure 4.2E). Results displayed below represent EVs derived from the specimens defined in Table 4.1 and Table 4.2.

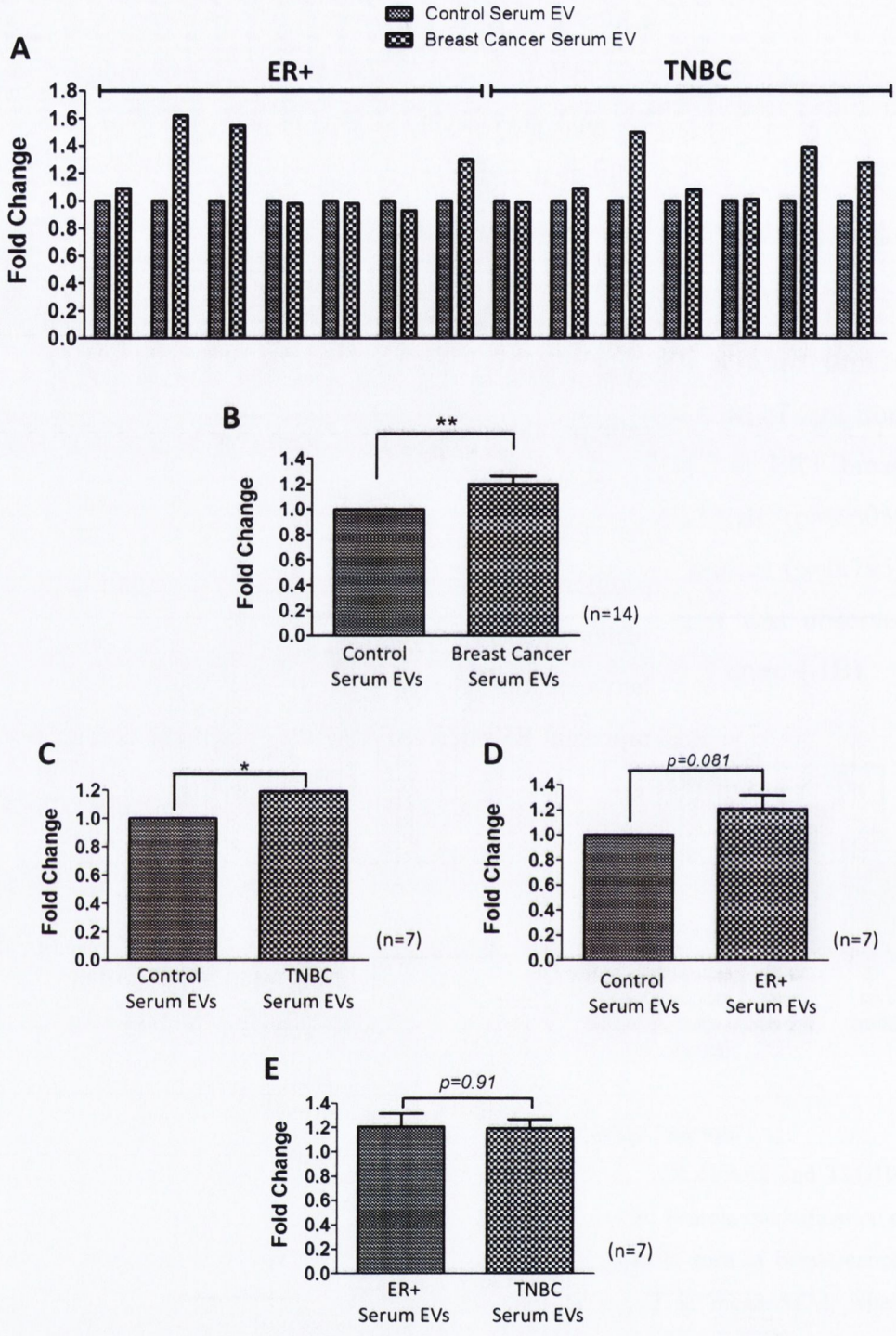

Figure 4.2: Breast cancer sera-EVs increase the proliferation of HCC1954 cells, compared to EVs from aged-matched healthy controls.

A: Graphical representation of the individual replicate values obtained from this proliferation analysis. **B:** Taking results together, EVs from TNBC and ER+ subtypes increase proliferation of HCC1954 cells. **C:** EVs derived from TNBC patient serum significantly increase the proliferation of HCC1954 cells. **D:** EVs derived from ER+ patient serum specimens do not significantly increase the rate of HCC1954 proliferation. **E:** Comparing the effects of EVs from ER+ and TNBC patient sera, no significant difference in proliferation was observed. Results are displayed as mean±SEM, where *=$p<0.05$, **=$p<0.01$ (Student's t-test).

4.3.3 EVs from breast cancer sera increase cellular motility

To assess their effects on migration, once HCC1954 cells became confluent, 10μg of EVs derived from TNBC patient, ER+ patient or age-matched control sera were applied to scratched cells. Migration was measured by photographing wound closure in 1% FBS DMEM after 24 and 48 hrs. Graphical representation of individual replicates is represented in Figure 4.3A and representative images in Figure 4.3B. Here, EVs from breast cancer specimens increase the rate of migration of HCC1954 cells compared to the effects of age matched healthy controls after 24 and 48 hrs by 1.6 ($p=0.00001$) and 1.9 fold ($p=0.0007$) respectively (Figure 4.3C).

Analysing results based on subtype determined that EVs from sera of TNBC patients significantly increase migration by 1.6 fold ($p=0.006$) and 1.6 fold ($p=0.001$) after 24 and 48 hrs respectively (Figure 4.3D). Similarly, ER+ EVs increase migration by 1.6 fold ($p=0.002$) and 2.2 fold ($p=0.02$) after 24 and 48 hrs, respectively (Figure 4.3E). Comparing the effects of TNBC *versus* ER+ EVs determined no significant difference between the subtypes after either 24 ($p=0.87$) or 48 ($p=0.19$) hrs (Figure 4.3F). Results displayed below represent EVs derived from the specimens defined in Table 4.1 and Table 4.2.

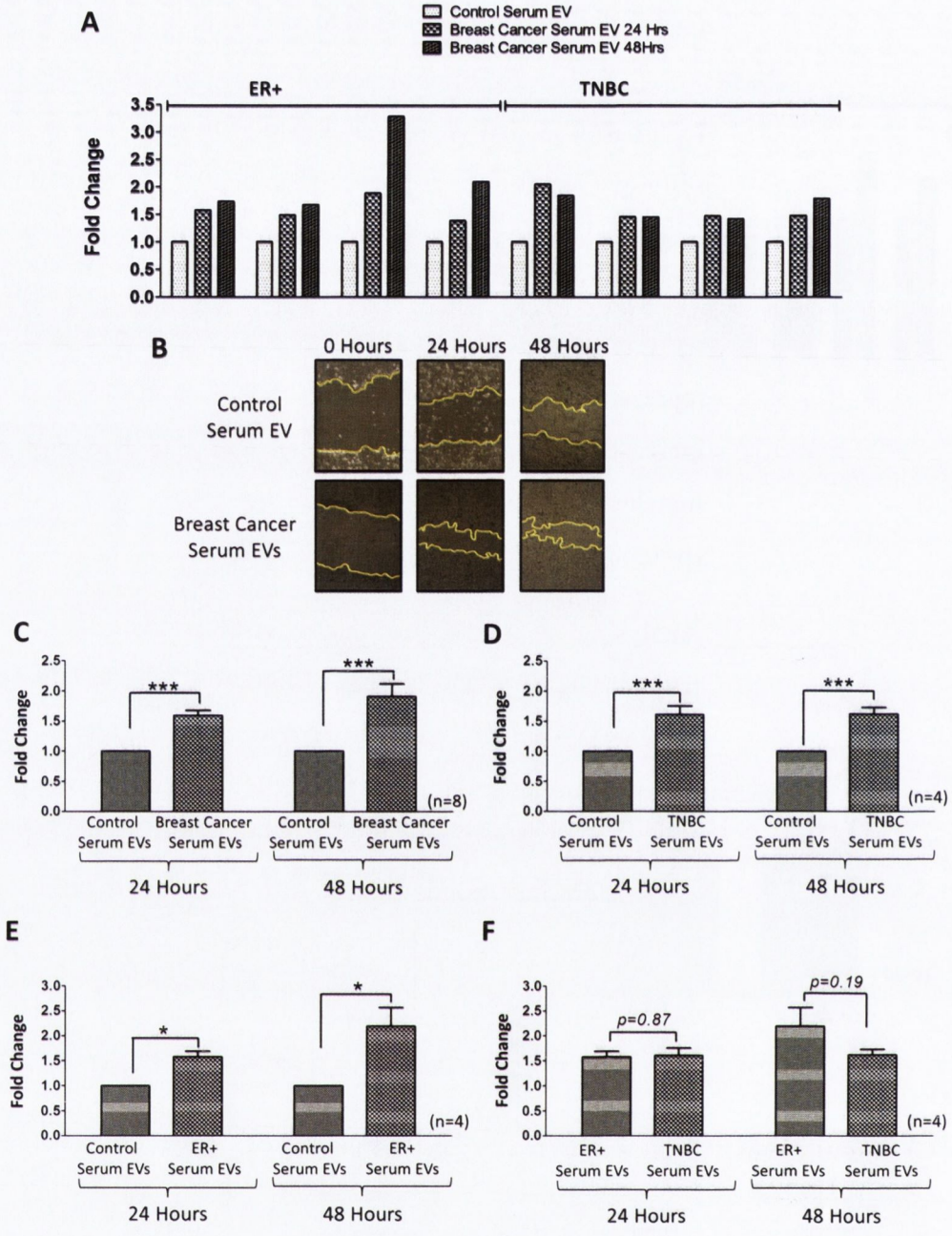

Figure 4.3: Breast cancer derived sera-EVs increase the migration of breast cancer cells. **A:** Graphical representation of the individual replicate values obtained from this migration analysis for 24 and 48 hrs post treatment with EVs. **B:** Representative images of wound healing pictures from 0, 24 and 48 hrs. **C:** Taking results together, EVs from TNBC and ER+ patient subtypes significantly increase migration of HCC1954 cells after 24 and 48 hrs. **D:** EVs derived from TNBC patient serum significantly increase the migration of HCC1954 cells after 24 and 48 hrs. **E:** Similarly, EVs derived from ER+ patient serum significantly increase the migration of HCC1954 cells after 24 and 48 hrs. **F:** Comparing the effects of EVs from ER+ and TNBC patient sera, no significant difference in migration was observed between subtypes. Results are displayed as mean±SEM, where *=$p<0.05$, ***=$p<0.001$ (Student's t-test).

4.3.4 EVs from breast cancer sera increase the invasive capacity of HCC1954 and SKBR3 cells

To assess their effects on invasion, HCC1954 cells were treated with 15μg of EVs from breast cancer patients or healthy donors and allowed to culture for 72 hrs in ECM coated transwell chambers (8μm pores). Graphical representation of individual replicates is represented in Figure 4.4A(i). Here, EVs from breast cancer specimens increase the rate of invasion of HCC1954 cells compared to age matched healthy controls, by 1.5 fold ($p=0.00008$) (Figure 4.4A(ii)). Analysed based on subtype determined that EVs from TNBC patient sera significantly increase the rate of HCC1954 invasion by 1.4 fold ($p=0.02$) (Figure 4.4B(i) & Figure 4.4B(ii)) and EVs from ER+ patient sera increase invasion by 1.6 fold ($p=0.003$) (Figure 4.4C(i) and Figure 4.4C(ii)). Comparing the effects of TNBC *versus* ER+ patient sera-derived EVs determined no significant difference between the subtypes ($p=0.58$) (Figure 4.4D). Results displayed below represent EVs derived from the specimens defined in Table 4.1 and Table 4.2.

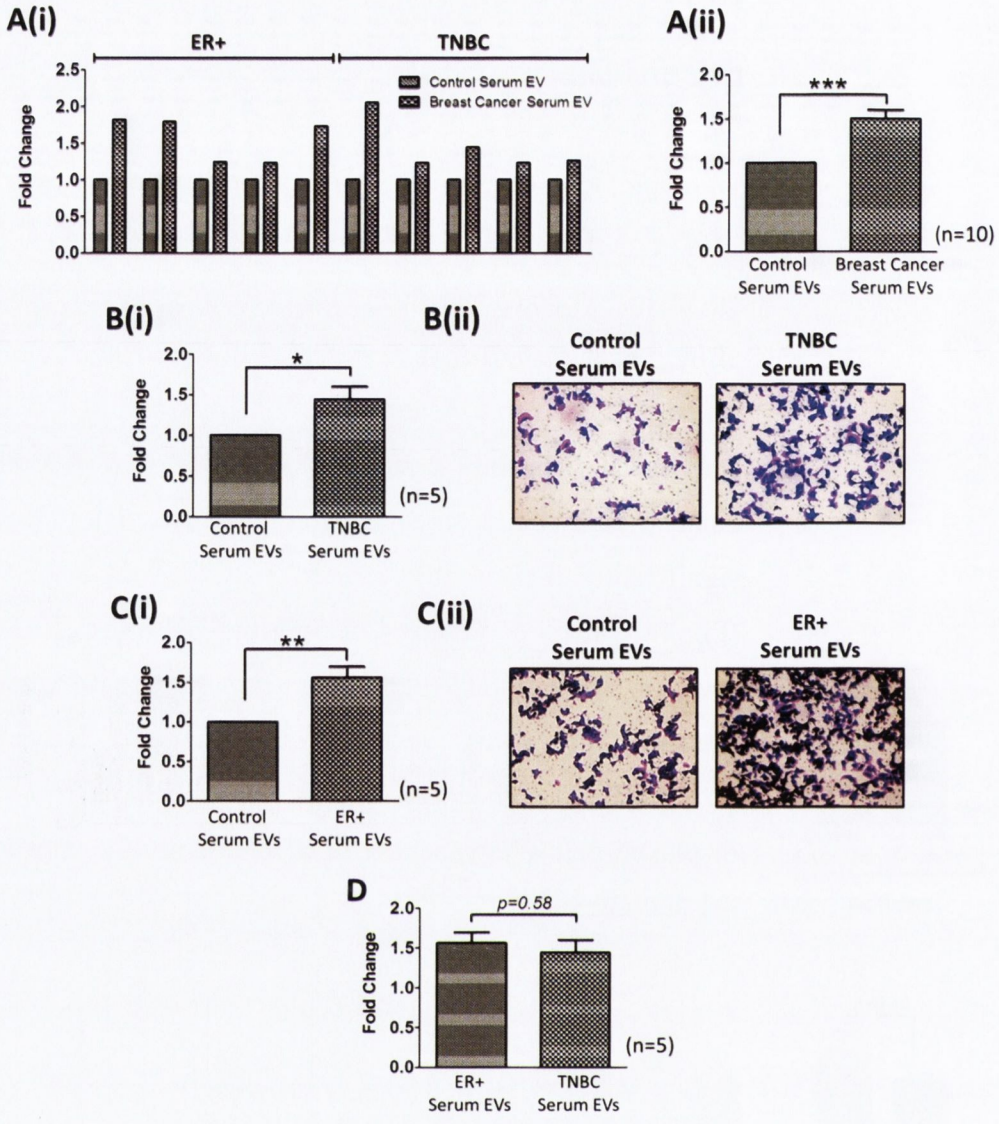

Figure 4.4: Breast cancer derived serum EVs increase the invasion of breast cancer cells. **A(i):** Graphical representation of the individual replicate values obtained from this invasion analysis. **A(ii):** Analysing results together, EVs from TNBC and ER+ subtypes increase invasion of HCC1954 cells. **B(i):** EVs derived from TNBC serum significantly increase the invasion of HCC1954 cells with **B(ii):** representative crystal violet stained invaded cell images. **C(i):** EVs derived from ER+ serum specimens significantly increase the rate of HCC1954 invasion with **C(ii):** representative crystal violet stained invaded cell images. **D:** Comparing the effects of EVs from ER+ and TNBC sera, no significant difference in invasion was observed. Results are displayed as mean±SEM, where *=$p<0.05$, **=$p<0.01$, ***=$p<0.001$ (Student's t-test).

As the primary interest of this Ph.D is the relevance TNBC derived EVs, and a greater volume of serum was available to us from the Asterand Biobank, further investigation was performed to analyse the potential of TNBC to increase the aggression of another breast cancer cell line, SKBR3. EVs were isolated from 12 TNBC sera specimens and applied to SKBR3 cells to analyse their effects on invasion compared to EVs derived from healthy control donor sera. Results illustrating individual sera replicates *versus* their age matched control demonstrate that all specimens, albeit slightly in some cases, increase the invasion of secondary cells (Figure 4.5A). TNBC serum-EVs induced significantly greater (2.2 fold; p=0.01) invasion of recipient cells, as illustrated in Figure 4.5B(i). Representative crystal violet stained cell images in Figure 4.5B(ii). Results displayed below represent EVs derived from the specimens defined in Table 4.2.

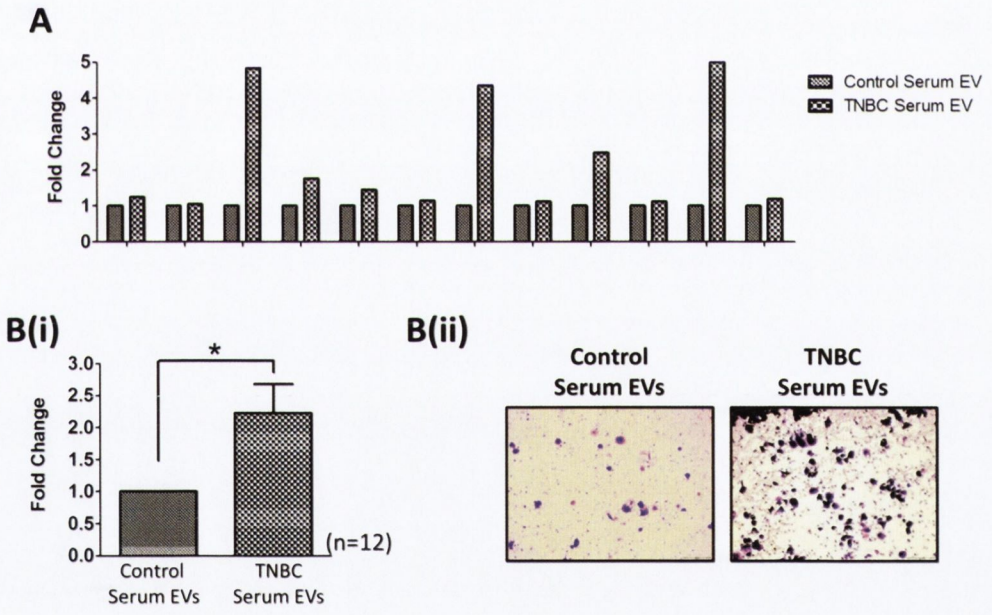

Figure 4.5: TNBC sera derived EVs increase the invasion of SKBR3 cells.

A: Graphical representation of the individual replicate values obtained from this invasion analysis. **B(i):** EVs derived from TNBC serum significantly increase the invasion of SKBR3 cells with **B(ii):** representative crystal violet stained invaded cell images. Results are displayed as mean±SEM, where *=$p<0.05$, (Student's t-test).

Effects of TNBC EVs on SKBR3 invasion was performed with the help of Dr. Sweta Rani.

4.3.5 EVs derived from breast cancer sera are enriched in total RNA

Once the RNAs was isolated from EVs derived from 250µl of serum, total RNA was quantified using the NanoDrop 1000 spectrophotometer. Figure 4.6A displays total RNA quantifications obtained from 69 breast cancer serum EV specimens *versus* 6 age-matched healthy control serum EV specimens. Results are displayed as ng of RNA obtained EVs derived from 1ml of serum. A mean quantification of 596.8ng of total RNA was obtained from healthy control derived EVs and 1534.5ng of total RNA obtained from breast cancer-derived serum EVs ($p=8.2x10^{-21}$). This represents a 2.6 fold increase in RNA obtained from breast cancer sera-EVs.

Based on subtypes, RNA levels are significantly increased in EV-RNA derived from ER+ ($p=6x10^{-20}$), HER2+ ($p=1x10^{-4}$) and TNBC ($p=6x10^{-18}$) breast cancer patients (Figure 4.6A(ii)). RNA presence is increased in EVs from TNBC patients compared to EVs from ER+ patients ($p=4.3x10^{-8}$), but insignificantly increased compared to EVs from HER2+ patients (p=0.07). No significant difference of RNA presence is observed between ER+ and HER2+ patient-derived sera EVs (p=0.961).

RNA was isolated from 11 of the serum specimens from breast cancer patients, to investigate whether the increased RNA presence of breast cancer sera-EVs is represented in total serum. No significant difference between RNA obtained from healthy individuals and breast cancer patients is observed (p=0.539) (Figure 4.6B(i)), although, for the same 11 specimens, RNA is significantly increased in breast cancer-derived sera-EVs ($p=4.0x10^{-6}$) (Figure 4.6B(ii)). Although RNA presence does not differ between total-sera and EVs from healthy individuals (p=0.247), RNA presence is significantly increased in sera derived -EVs from breast cancer patients compared to total serum from the same patients ($p=3.2x10^{-6}$) (Figure 4.6C).

This data also indicates that, based on ROC analysis, RNA concentrations in EVs derived from breast cancer serum are significantly sensitive to discriminate patients with breast cancer, from healthy individuals. This data is presented in Table 4.9.

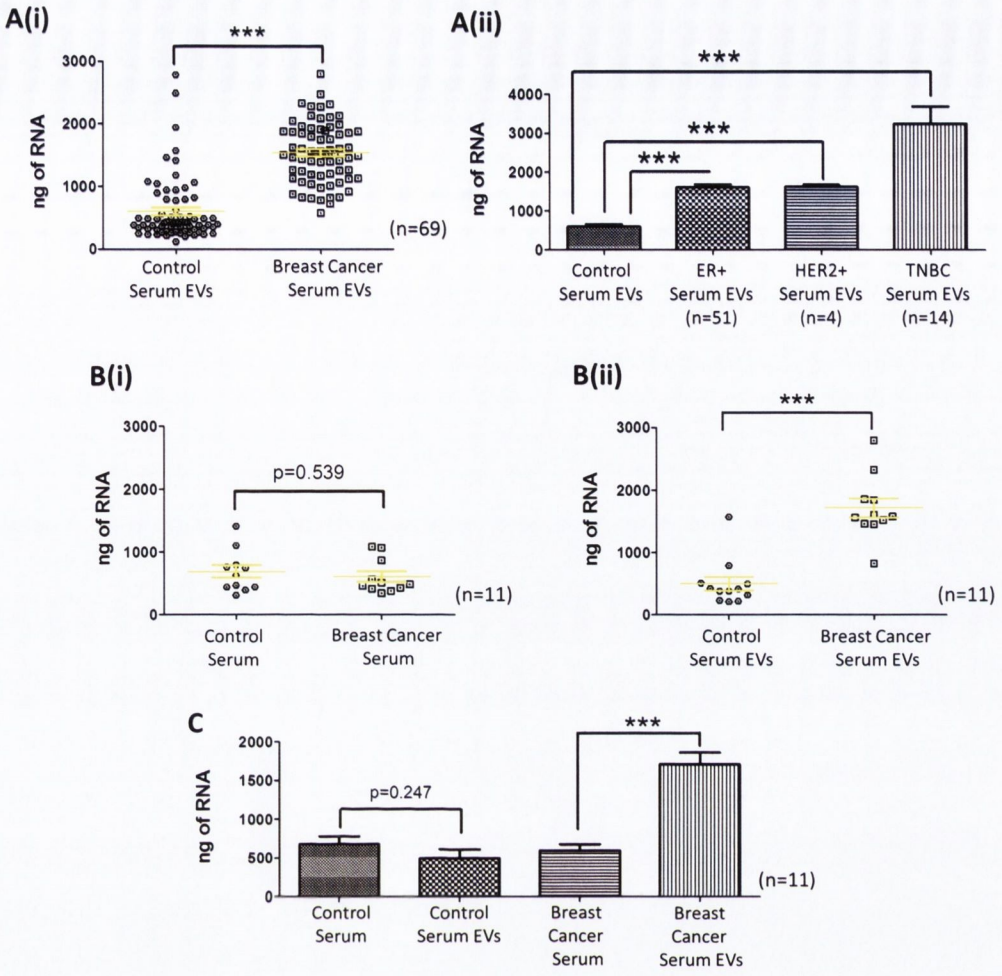

Figure 4.6: Breast cancer derived serum EVs are enriched in miRNA compared to control serum EVs.

A(i): Total RNA quantification obtained from EVs derived from 1ml of serum (n=68) with **A(i)** quantifications separated by breast cancer subtype. **B(i):** Total RNA quantification from total-serum, representing total RNA obtained per ml of serum **B(ii):** Total RNA quantification obtained EVs derived from 1ml of serum, from the same eleven specimens analysed for total serum miRNA. **C:** Comparison of the yields of RNA obtained from total serum *versus* serum derived EVs. Results are displayed as mean±SEM, where *=$p<0.05$, **=$p<0.01$, ***=$p<0.001$(Student's t-test)

Table 4.9: Sensitivity of EV-RNA concentrations to discriminate healthy individuals from those with breast cancer

	All subtypes (n=69)	ER+ (n=51)	HER2 (n=4)	TNBC (n=14)
AUC	0.92	0.93	0.95	0.88
Standard Error	0.03	0.03	0.03	0.07
95% CI	0.87 to 0.97	0.87 to 0.98	0.90 to 1.00	0.74 to 1.02
p-value	<0.0001	<0.0001	0.002	<0.0001

4.3.6 MammU6, miR-16, RNU44 and RNU48 are not effective endogenous controls for serum-EV miRNA analysis

To determine the most suitable endogenous/normalisation control to use for the miRNA expression analysis in EVs derived from serum, a number of miRNAs were analysed for stable expression between healthy and breast cancer derived EVs. This was performed as some of the commonly used endogenous controls have been previously discovered to be differentially expressed in cancers, meaning that they are inappropriate for use as endogenous controls [328]. Here, C_T values were compared for four commonly used endogenous controls; MammU6, miR-16, RNU44 and RNU48. None of these miRNAs can be used to normalise miRNAs levels for this study. Analysing C_T values, MammU6 is detected significantly differently between healthy control derived EVs and breast cancer derived EVs ($p=0.02$) (Figure 4.7A). miR-16 showed differences in levels, and almost reached significance between healthy and breast cancer sera ($p=0.05$) (Figure 4.7B). RNU44 was not expressed in any specimen (Figure 4.7C). Although RNU48 expression did not significantly differ between control and breast cancer sera, RNU48 was not detected in one control and one breast cancer specimen (Figure 4.7D).

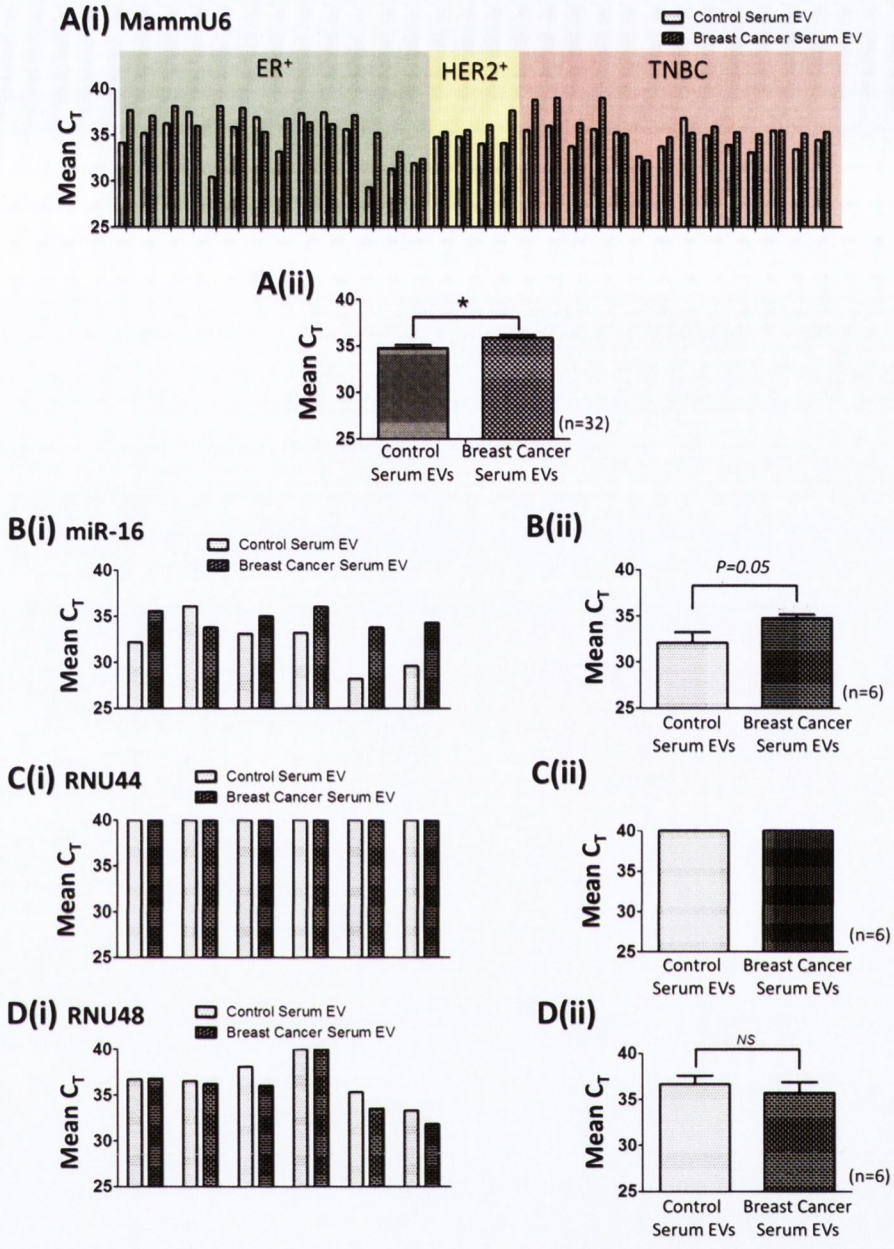

Figure 4.7: Commonly used endogenous controls are not expressed equally in healthy derived EVs and breast cancer derived EVs .

A(i): MammU6 levels in 32 breast cancer and age matched control specimens, **A(ii):** data correlated together to determine a significant difference between MammU6 levels in healthy donor serum EVs and breast cancer serum EVs. **B(i):** miR-16 levels in six breast cancer specimens and age mached controls, **B(ii):** data correlated together. Although no statistical difference is observed between control and breast cancer specimens, a mean difference of 2.7 C_T values was determined. **C(i):** RNU44 levels in six breast cancer and age matched control specimens, **C(ii):** data correlated together in determining RNU44 was not detected in either control or breast cancer serum EVs. **D(i):** RNU48 levels in six breast cancer and age matched control specimens, **D(ii):** data correlated together to determine no significant difference between MammU6 levels in healthy donor serum EVs and breast cancer serum EVs. Results are displayed as mean±SEM, where *=$p<0.05$ (Student's t-test).

4.3.7 miR-134 is significantly down-regulated in breast tumours, compared to normal tissue, and breast-cancer sera-EVs, compared to age-matched control sera-EVs.

To determine if miRNA expression findings discovered in Chapter 2 have translational potential in a clinical setting, a number of analyses were performed, including bioinformatical scrutiny of publicaly-available datasets for miRNA expression in breast cancer tumours, as detailed in Section 0. Two miRNA datasets are reported here, GSE26659 and GSE40525. miR-134 was found present at significantly reduced levels in breast cancer tumours compared to normal tissue, as determined by both datasets; GSE26650 ($p=0.0001$) (Figure 4.8A) and GSE40525 ($p=0.000000003$) (Figure 4.8B). As information was available from the GSE40525 dataset regarding breast cancer subtypes, expression values were compared based on subtype. This analysis showed that miR-134 is present at significantly reduced levels in ER+ tumours ($n=47$; $p=0.000001$), HER2+ tumours ($n=6$; $p=0.04$) and TNBC tumours ($n=8$; $p=0.01$), compared to normal tissue (Figure 4.8B). Levels of miR-134 did not differ between subtypes.

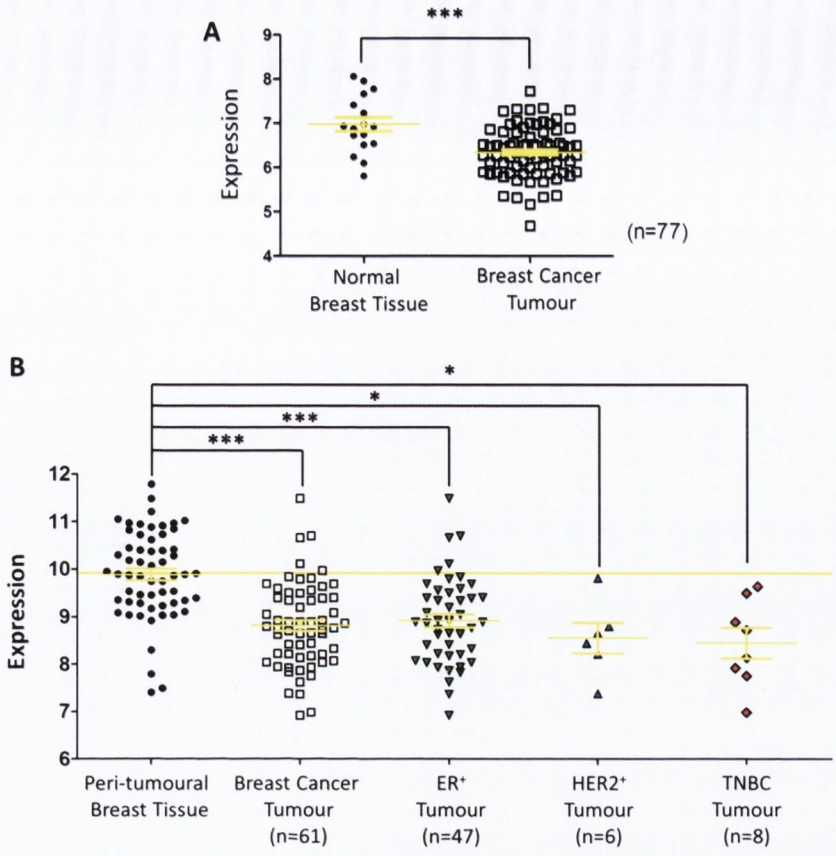

Figure 4.8: Compared to normal tissue, miR-134 is present at significantly reduced levels in breast cancer tumours (GSE26659 & GSE40525).

A: GSE26659: Analysing ductal breast carcinoma biopsies from GSE26659, miR-134 was found to be present at significantly reduced levels (n=77) compared to 17 normal tissues from mammoplastic reductions. **B:** Similarly, analying GSE40525 miR-134 is present at significantly reduced levels in primary breast cancer tumours when all subtypes were analysed together (n=61) as part of another dataset. When subtypes were analysed seperately, miR-134 is present at significantly reduced levels in ER+ (n=47), HER2+ (n=6) and TNBC (n=8) primary breast cancer tumours. Results are displayed as mean±SEM, where *=$p<0.05$, ***=$p<0.001$(Student's t-test).

qPCR analysis was performed on miRNA isolated from ER+ (n=14), HER2+ (n=4) and TNBC (n=14) sera-EVs, as listed in Table 4.1, Table 4.2, and Table 4.3.

As no suitable endogenous control was identified for normaising miRNA levels (Figure 4.7), C_T values were normalised using the ΔC_T method, by subtracting the C_T value of the patient specimens for each miRNA from the corresponding C_T value for the healthy individuals. Fold changes were calculated by $2^{(-\Delta C_T)}$. This is detailed in Section 0.

Graphical representation of all fold changes determined for all breast cancer sera-EV is illustrated in Figure 4.9A. This graph shows that miR-134 is down-regulated in 23 of the 32 (71.9%) breast cancer EVs analysed. Analysing all breast cancer subtypes together, miR-134 is significantly reduced by 6.3 fold (p=0.003) in EVs derived from breast cancer serum EVs (n=32) (Figure 4.9B), with an AUC value of 0.73 (p=0.01) (Table 4.10).

When analysed in each breast cancer subtype, we observed that miR-134 is down-regulated in 10 of 14 (71.4%) ER+ serum EVs compared to EVs from healthy control sera. Overall, miR-134 is significanty reduced in EVs derived from ER+ sera by 5.7 fold (p=0.048) (Figure 4.9C(i)), with an AUC of 0.75 (p=0.02) (Table 4.10). Although miR-134 is reduced in all EVs derived from HER2+ sera, the 11.1 fold is not significant (p=0.143) (Figure 4.9C(ii)). However, AUC analysis determined an AUC of 1.00 (p=0.02) (Table 4.10). Additionally, miR-134 was observed to be down-regulated in 9 of 14 TNBC specimens (64.3%) and the mean fold change of 6.5 reduction is not significant (p=0.105) compared to age-matched healthy control sera-EVs (Figure 4.9C(iii). Additionally, the AUC of 0.64 was also insignificant for TNBC (p=0.198) (Table 4.10). Mean C_T values are presented in Appendix IC, Table A5 of this thesis.

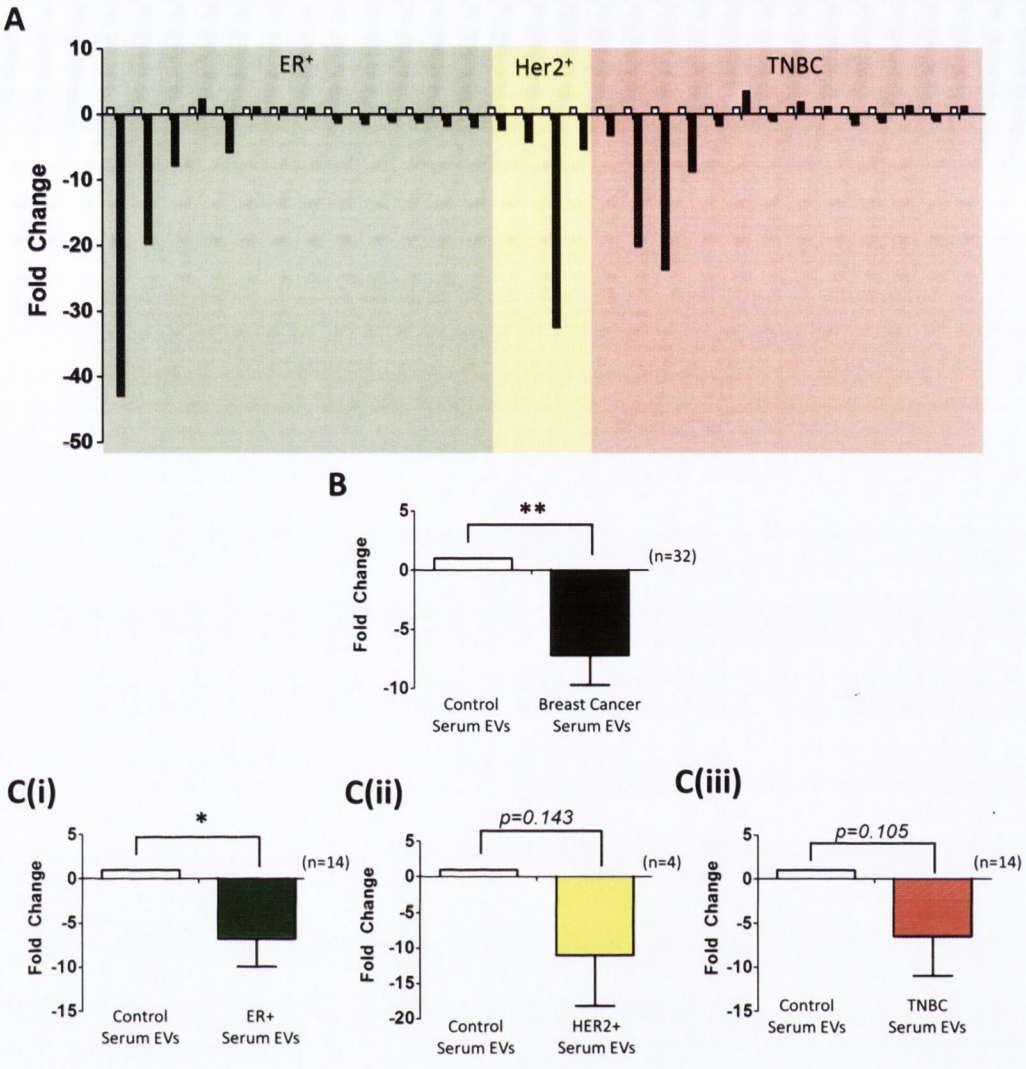

Figure 4.9: miR-134 is significantly down-regulated in breast cancer serum derived serum EVs compared to age-matched healthy control sera-EVs

A: Graphical representation of the expression fold changes of the 32 breast cancer specimens analysed for miR-134 expression *versus* age-matched controls, indicating the subtypes of each specimen. **B:** Graphical representation of the mean±SEM fold change of miR-134 in the 32 breast cancer specimen. **C(i):** Fold change of miR-134 in the 14 ER+ EV specimens, **C(ii)** 4 HER2+ EV specimens; and **C(iii):** 14 TNBC EV specimens. Results are displayed as mean±SEM, where *=$p<0.05$, **=$p<0.01$ (Student's t-test)

Levels of miR-134 in sera-EVs from TNBC patients was performed with the help of Dr. Sweta Rani. Levels of the other miRNAs were performed with the help of Ms Melissa Daly

Table 4.10: AUC values for miR-134						
Subtype	**No. specimens analysed**	**Min. no. specimens rqd.**	**AUC**	**Standard error**	**95% CI**	**p-value**
All subtypes	32	21	0.73	0.08	0.58 to 0.86	0.001
ER+	14	11	0.75	0.11	0.53 to 0.96	0.02
HER2+	4	3	1.00	0.00	1.00 to 1.00	0.02
TNBC	14	10	0.64	0.13	0.59 to 0.89	0.198

4.3.8 miR-370 is significantly down-regulated in breast tumours, compared to normal tissue, and breast-cancer EVs, compared to age-matched control EVs.

Once again, the same two tumour miRNA datasets were scrutinised for miRNA expression, this time for miR-370 expression as miR-370 showed the greatest fold change, down-regulated from *in vitro* miRNA expression analysis of Hs578T and Hs578Ts(i)$_8$ cells (Figure 3.13B). Expression analysis determined that miR-370 is present at significantly reduced levels in breast cancer tumours, observed in both tumour miRNA datasets, GSE26650 (p=0.0000000002) (Figure 4.10A) and GSE40525 (p=0.002) (Figure 4.10B). Analysis of miR-370 expression from the dataset GSE26650, sugested miR-370 is non-detectable in 39 of the 77 (50.6%) breast cancer tumours analysed, compared to normal tissue.

Breaking down the GSE40525 dataset into subtypes showed that miR-370 is present at significantly reduced levels in ER+ tumours (n=47; p=0.02) and TNBC tumours (n=8; p=0.003), but not in HER2+ tumours (n=6; p=0.279) (Figure 4.10B), compared to peri-tumoural normal tissue. Levels of miR-370 did not differ between subtypes.

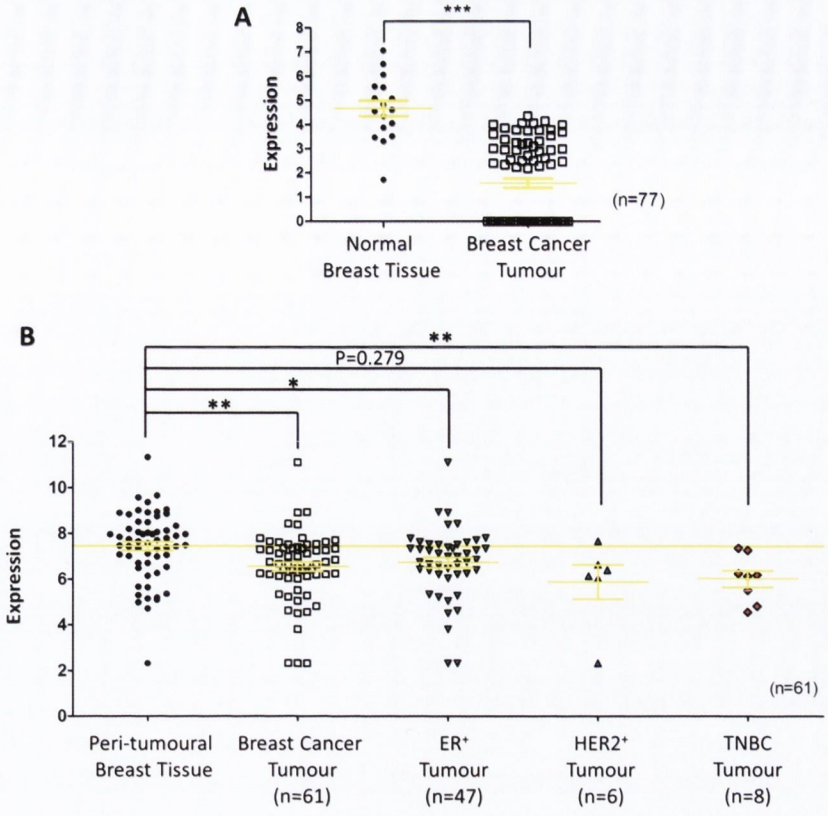

Figure 4.10: miR-370 is present at significantly reduced levels in breast cancer tumours compared to normal tissue (GSE26659 & GSE40525).

Using the publically available datasets GSE26659 and GSE40525, miR-370 expression was questioned. **A:** GSE26659**:** Analysing ductal breast carcinoma biopsies, miR-370 is present at significantly reduced levels (n=77) compared to 17 normal tissues from mammoplastic reductions. **B:** Similarly, miR-370 is present at significantly reduced levels in primary breast cancer tumours when all subtypes were analysed together (n=61) as part of another dataset. When subtypes were analysed seperately, miR-370 is present at significantly reduced levels in ER+ (n=47) and TNBC (n=8), but not significantly reduced in HER2+ primary breast cancer tumours (n=6). Results are displayed as mean±SEM, where *=$p<0.05$, **=$p<0.01$, ***=$p<0.001$ (Student's t-test).

qPCR analysis was performed on miRNA isolated from ER+ (n=14), HER2+ (n=4) and TNBC (n=14) sera-EVs, as listed in Table 4.1, Table 4.2, and Table 4.3.

Graphical representation of all fold changes determined for all breast cancer sera-EV is illustrated in Figure 4.11A. This graph shows that miR-370 is down-regulated in 26 of the 32 (81.3%) breast cancer EVs analysed, compared to age-matched healthy control EVs. Taking all breast cancer subtypes together, miR-370 is significantly down-regulated by 52.0 fold (p=0.008) in EVs derived from breast cancer serum EVs (n=32) (Figure 4.11B), with an AUC of 0.81 (p=<0.0001) (Table 4.11).

When analysed per subtype, we observed that miR-370 is down-regulated in 11 of 14 (78.6%) ER+ sera-EVs, however the mean change of 57.0 fold did not reach significance (p=0.079) (Figure 4.11C(i)). Although the fold change was insignificant, a significant AUC value of 0.79 was found (p=0.01) (Table 4.11). Similarly, all HER2+ sera-EV specimens analysed showed miR-370 down-regulation, yet the mean fold change reduction of 62.5 fold was not significant (p=0.207) ((Figure 4.11C(ii)). While the fold change was insignificant, a significant AUC value of 1.00 was calculated (p=0.02) (Table 4.11). Similarly, miR-370 was observed to be down-regulated in 11 of 14 (78.6%) TNBC specimens, yet the mean fold change of 44.0 fold was not significant (p=0.144) (Figure 4.11C(iii)). A significant AUC value of 0.79 was calculated for miR-370 in TNBC (p=0.01) (Table 4.11).

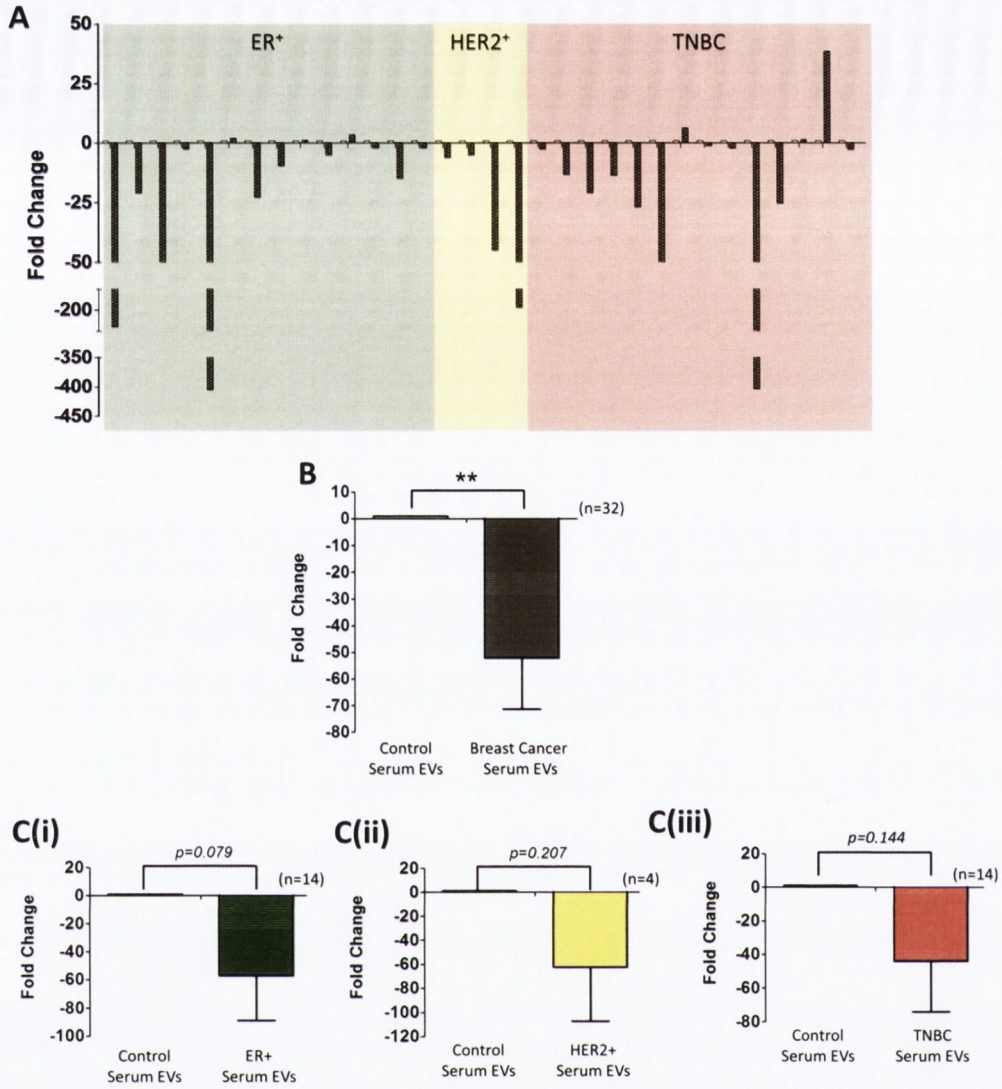

Figure 4.11: miR-370 is significantly down-regulated in breast cancer sera-EVs compared to age-matched control sera-EVs .

A: Graphical representation of the expression fold changes of the 32 breast cancer specimens analysed for miR-370 expression *versus* age-matched controls, indicating the subtypes of each specimen. **B:** Graphical representation of the mean±SEM fold change of miR-370 in the 32 breast cancer specimen. **C(i):** Fold change of miR-370 in the 14 ER+ EV specimens, **C(ii)** 4 HER2+ EV specimens; and **C(iii):** 14 TNBC EV specimens. Results are displayed as mean±SEM, where **=$p<0.01$ (Student's t-test).

Levels of miRNAs in sera-EVs was performed with the help of Ms Melissa Daly

Table 4.11: AUC values for miR-370						
Subtype	**No. of specimens analysed**	**Min. no. of specimens rqd.**	**AUC**	**Standard error**	**95% CI**	**p-value**
All subtypes	32	21	0.81	0.07	0.68 to 0.95	<0.0001
ER+	14	12	0.79	0.11	0.57 to 1.00	0.01
HER2+	4	3	1.00	0.00	1.00 to 1.00	0.02
TNBC	14	10	0.79	0.11	0.57 to 1.00	0.01

4.3.9 miR-376c is significantly down-regulated in breast tumours, compared to normal tissue, and breast-cancer EVs, compared to age-matched control EVs.

Expression analysis determined that miR-376c is present at significantly reduced levels in breast cancer tumours compared to normal tissue, determined by both tumour-miRNA datasets, GSE26650 (p=0.00000001) (Figure 4.12A) and GSE40525 (p=0.00002) (Figure 4.12B). Breaking down the GSE40525 dataset into subtypes showed that miR-376c is present at significantly reduced levels in ER+ tumours (n=47; p=0.002) and HER2+ tumours (n=6; p=0.02). However, miR-376c is not present at significantly reduced levels in TNBC tumours compared to normal tissues (n=8; p=0.07) (Figure 4.12B). Levels of miR-376c did not differ between subtypes.

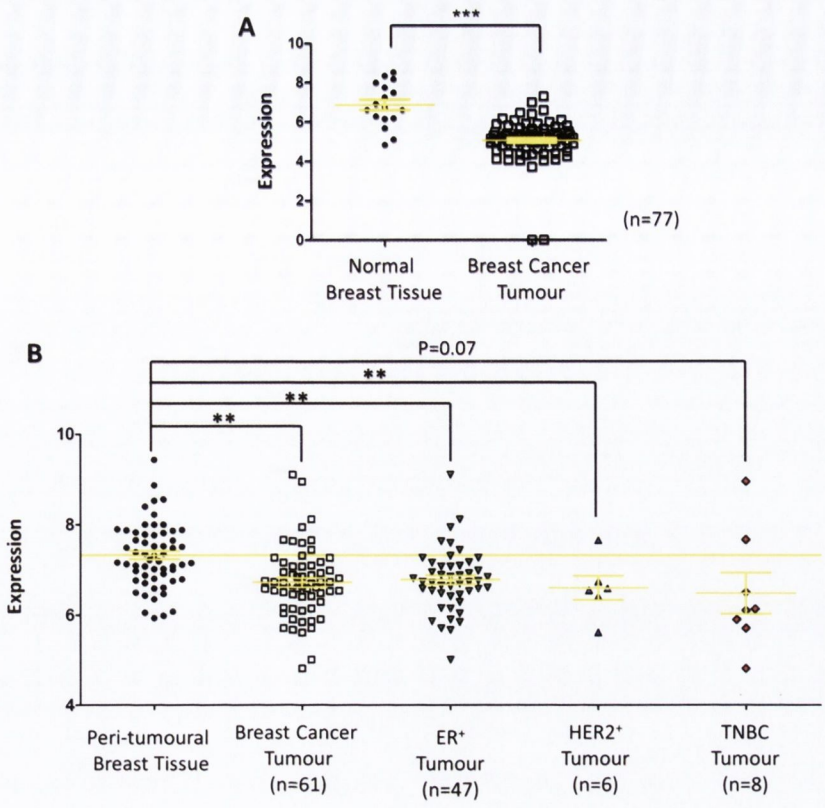

Figure 4.12: miR-376c is present at significantly reduced levels in breast cancer tumours compared to normal tissue (GSE26659 & GSE40525).

Using the publically available datasets GSE26659 and GSE40525, miR-376c expression was questioned, **A:** GSE26659**:** Analysing ductal breast carcinoma biopsies, miR-376c is present at significantly reduced levels (n=77) compared to 17 normal tissues from mammoplastic reductions. **B:** GSE40525: Similarly, miR-376c is present at significantly reduced levels in primary breast cancer tumours when all subtypes were analysed together (n=61) as part of another dataset. When subtypes were analysed seperately, miR-376c is not present at significantly reduced levels in TNBC (n=8), but is significantly reduced in ER+ (n=47) and HER2+ primary breast cancer tumours (n=6). Results are displayed as mean±SEM, where **=$p<0.01$, ***=$p<0.001$ (Student's t-test)

qPCR analysis was performed on miRNA isolated from ER+ (n=14), HER2+ (n=4) and TNBC (n=14) sera-EVs, as listed in Table 4.1, Table 4.2, and Table 4.3.

Graphical representation of all fold changes determined for all breast cancer sera-EV is illustrated in Figure 4.13A. This graph shows that miR-376c is down-regulated in 23 of the 32 (71.9%) breast cancer EVs analysed compared to sera-EVs from healthy individuals. Taking all breast cancer subtypes together, miR-376c is significantly down-regulated by 6.8 fold (p=0.0006) in EVs derived from breast cancer serum EVs (n=32) (Figure 4.13B), with a AUC value of 0.75 (p=0.0006) (Table 4.12).

When analysed by subtype, we observed that miR-376c is down-regulated in 9 of 14 (64.3%) ER+ serum EVs, with a mean fold change of 8.2 fold reduction observed (p=0.050) (Figure 4.13C(i)) and an AUC of 0.71 (p=0.05) (Table 4.12). Similarly, 3 of 4 (75.0%) HER2+ specimens tested showed down-regulation of miR-376c, and is significantly down-regulated by 2.5 fold (p=0.03) (Figure 4.13C(ii)), yet an AUC of 0.71 is insignificant (p=0.248) (Table 4.12). Considering TNBC, 11 of the 14 (78.6%) specimens tested showed down-regulation of miR-376c, corresponding to a significant fold change reduction of 6.6 fold (p=0.002) (Figure 4.13C(iii)) and a significant AUC of 0.79 (p=0.01) (Table 4.12).

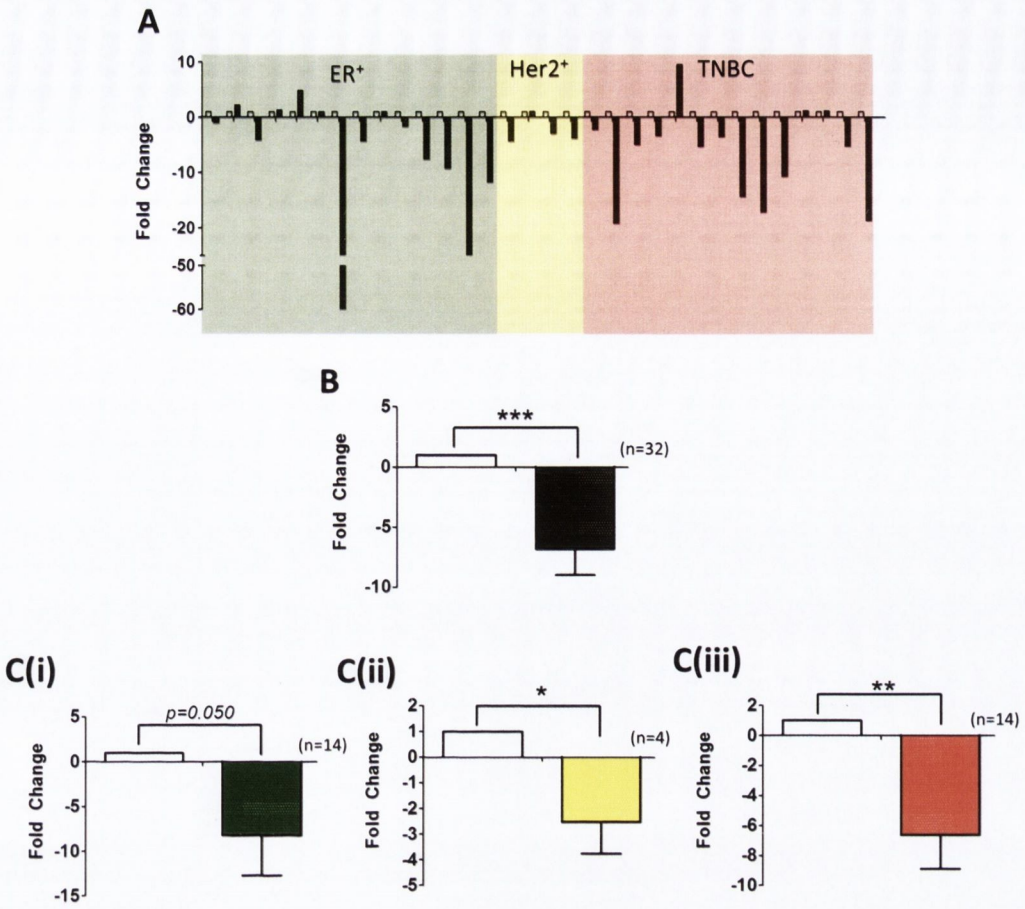

Figure 4.13: miR-376c is significantly down-regulated in breast cancer sera-EVs compared to age-matched control sera-EVs .

A: Graphical representation of the expression fold changes of the 32 breast cancer specimens analysed for miR-376c expression *versus* age-matched controls, indicating the subtypes of each specimen. **B:** Graphical representation of the mean±SEM fold change of miR-376c in the 32 breast cancer specimen. **C(i):** Fold change of miR-376c in the 14 ER+ EV specimens, **C(ii)** 4 HER2+ EV specimens; and **C(iii):** 14 TNBC EV specimens. Results are displayed as mean±SEM, where *=$p<0.05$, **=$p<0.01$, ***=$p<0.001$ (Student's t-test).

Levels of miRNAs in sera-EVs was performed with the help of Ms Melissa Daly

Table 4.12: AUC values for miR-376c						
Subtype	**No. of specimens analysed**	**Min. no. of specimens rqd.**	**AUC**	**Standard error**	**95% CI**	**p-value**
All subtypes	32	20	0.75	0.07	0.60 to 0.90	0.0006
ER+	14	12	0.71	0.11	0.49 to 0.94	0.05
HER2+	4	3	0.75	0.22	0.44 to 1.17	0.248
TNBC	14	10	0.79	0.11	0.57 to 1.00	0.01

4.3.10 Analysed together, miR-370 and miR-376c are vastly reduced in breast cancer serum EVs

To investigate whether sera-EV derived miR-134, miR-370 and miR-376c could be used in combination for breast cancer diagnosis, we analysed the specificity and sensitivity of using these three together. Attempts to combine the use for miR-134, miR-370 and miR-376c were statistically limited by too few specimen numbers. For statistical use of these three miRNAs together, a minimum specimen number of 70 patients and 70 controls are required. However, 32 patients and 32 controls were analysed as part of this study. See Section 0 for statistical methods used.

However, for use of miR-370 and miR-376c, enough specimens were used for statistical accuracy, based on AUC and standard error values obtained. As miR-134 showed an insignificant AUC value of 0.64 (p=0.198) (Table 4.10) in TNBC derived sera-EVs, miR-370 and miR-376c were analysed alone to see if they increase AUC and significance values. Results show that miR-370 and miR-376c alone increase the sensitivity to AUC 0.79 (p=0.0002) (Table 4.13).

Table 4.13: AUC values for miR-370 and miR-376c in TNBC derived sera-EVs						
Subtype	**No. of specimens analysed**	**Min. no. of specimens rqd.**	**AUC**	**Standard error**	**95% CI**	**p-value**
All subtypes	32	17	0.79	0.08	0.63 to 0.94	0.0002

Analysing all breast cancer subtypes together, all three miRNAs were down-regulated in 17 of 32 (53.1%) specimens. At least two miRNAs were down-regulated in 24 of 32 (75.0%) of specimens, and at least one of the miRNAs down-regulated in 31 of 32 (96.9%) of specimens.

All three miRNAs were down-regulated in 6 of 14 (42.9%) of ER+ patient derived specimens, with two miRNAs down-regulated in 11 of 14 (78.9%) ER+ patient derived specimens. 13 of 14 (92.9%) ER+ patient derived specimens had at least one of the miRNAs down-regulated.

Similarly, all three miRNAs were down-regulated in 3 of 4 (75.0%) of HER2+ patient derived specimens, with at least 2 miRNAs down-regulated in all 4 specimens analysed.

Taking TNBC alone, 7 of the 14 specimens (50.0%) showed down-regulation of all three miRNAs. Of the TNBC patient derived specimens analysed, 9 of 14 (64.3%) showed down-regulation of at least two miRNAs with all 14 specimens showing down-regulation of at least one of the miRNAs. These findings are displayed in Table 4.14 below.

Table 4.14: miRNA levels in EVs from TNBC, ER+ and HER2+ patient sera compared to EVs from sera of age-matched controls			
Legend:	Red: Down-regulated		
	Green: Up-regulated		
Specimen Subtype	***miR-134 fold change***	***miR-370 fold change***	***miR-376c fold change***
ER	-42.92	-239.41	-1.02
ER	-19.71	-20.91	2.19
ER	-7.83	-81.01	-4.12
ER	2.30	-2.52	1.31
ER	-5.78	-405.44	4.83
ER	1.08	1.83	1.00
ER	1.09	-22.67	-59.88
ER	1.00	-9.43	-4.35
ER	-1.25	1.14	1.00
ER	-1.48	-5.02	-1.67
ER	-1.16	3.41	-7.60
ER	-1.24	-1.93	-9.25
ER	-1.76	-14.73	-25.66
ER	-1.97	-1.93	-11.78
HER2	-2.33	-6.07	-4.32
HER2	-4.19	-4.98	1.04
HER2	-32.53	-44.78	-2.96
HER2	-5.33	-194.06	-3.86
TNBC	-3.20	-2.46	-2.22
TNBC	-20.16	-13.18	-19.20
TNBC	-60.95	-20.93	-4.96
TNBC	-8.77	-13.51	-3.34
TNBC	3.51	-26.79	9.55
TNBC	-1.07	-149.53	-5.27
TNBC	1.77	6.18	-3.55
TNBC	1.10	-1.06	-14.32
TNBC	-1.68	-2.19	-17.19
TNBC	-1.25	-404.03	-10.73
TNBC	1.18	-25.21	1.14
TNBC	-1.10	1.31	1.14
TNBC	1.13	38.39	-5.23
TNBC	-1.76	-2.60	-18.73

4.3.11 Levels miR-134, miR-370 and miR-376c in serum EVs from stage 1, 2 and 3 breast cancers compared to age-matched healthy control sera-EVs

miR-134, miR-370 and miR-376c levels were investigated in breast cancer stages 1 (n=7), 2 (n=14) and 3 (n=10) compared to levels in age-matched control sera-EVs.

Results show that miR-134 is significantly down-regulated in EVs derived in stage 1 breast cancer sera-EVs by 1.6 fold (p=0.005), compared to age-matched healthy control derived-sera-EVs. Although miR-134 expression in stage 2 derived sera-EVs showed a 7.81 fold reduction, statistical significance was just not reached (p=0.08). Additionally, miR-134 is significantly down-regulated in stage 3 breast cancer sera-EVs by 7.8 fold (p=0.006) (Figure 4.14A), compared to age-matched healthy control derived-sera-EVs.

Similarly, such an analysis was performed for miR-370 in sera derived EVs. Results show that miR-370 is reduced in all breast cancer stages compared to age-matched healthy controls. Specifically, we observed miR-370 to be reduced by 139.8 fold (p=0.07) in stage 1 derived sera-EVs; 7.15 fold (p=0.130) in stage 2; and by 35.5 fold (p=0.08) in stage 3 derived sera-EVs (Figure 4.14B).

miR-376c analysis determined that miR-376c is significantly down-regulated in EVs derived from stage 1, 2 and 3 sera compared to age-matched healthy controls. Specifically, miR-376c is significantly down-regulated in stage 1 sera-EVs by 7.4 fold (p=0.05); in stage 2 by 8.4 fold (p=0.04); and in stage 3 sera-EVs by 4.8 fold (p=0.03) (Figure 4.14C).

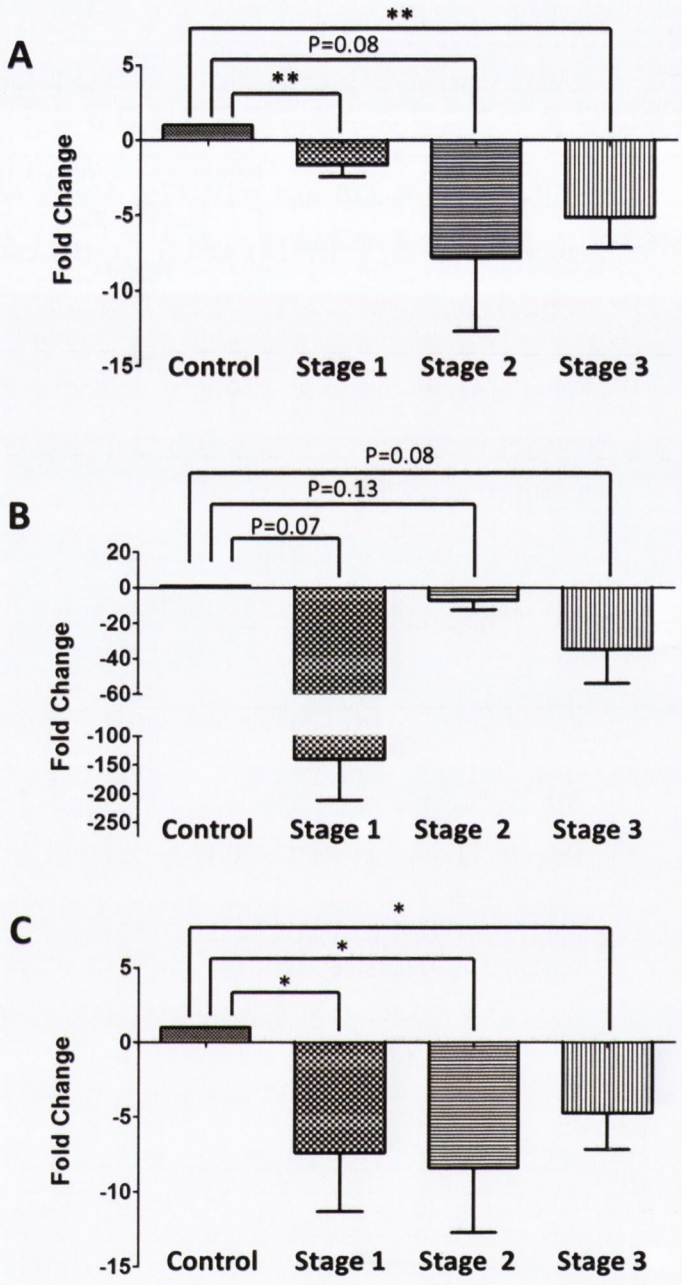

Figure 4.14: Fold change of miRNA expression for stages 1, 2 and 3 of breast cancer compared to age-matched healthy control sera-EVs.

A: Fold changes of miR-134 levels, comparing stage 1, stage 2 and stage 3 of breast cancer progression. **B:** Fold changes of miR-370 levels, comparing stage 1, stage 2 and stage 3 of breast cancer progression. **C:** Fold changes of miR-376c levels, comparing stage 1, stage 2 and stage 3 of breast cancer progression. Results are displayed as mean±SEM, where *=$p<0.05$, **=$p<0.01$ (Student's t-test).

Considering the sensitivity and specificity of these sera derived EV-miRNAs for use as biomarkers in stage 1, 2 and 3 breast cancers, ROC analysis was performed (Table 4.15). Calculating the AUC of miR-134 expression determined values of 0.86 (p=0.03), 0.54 (p=0.748) and 0.90 (p=0.003) for stage 1, 2 and 3 breast cancer derived EVs respectively Table 4.15.

Although specific mean fold changes for miR-370 were insignificant at each stage, ROC curves determined the AUC for stage 1 miR-370 expression to be 0.86 (p=0.03); 0.64 (p=0.198) for stage 2; and 1.00 (p=0.0006) for stage 3 derived sera-EVs Table 4.15.

ROC analysis for the sensitivity of EV-miR-376c to discriminate healthy individuals from breast cancer patients determined AUCs of 0.79 (p=0.07) for stage 1; 0.68 (p=0.108) for stage 2; and 0.80 (p=0.02) for stage 3 derived sera-EVs Table 4.15.

Table 4.15: AUC results for miR-134, miR-370 and miR-376c from stages 1-3							
miRNA	**Stage**	**No. of specimens analysed**	**Min. no. of specimens rqd.**	**AUC**	**Standard error**	**95% CI**	**p-value**
miR-134	1	7	5	0.86	0.13	0.60 to 1.11	0.03
	2	14	11	0.54	0.13	0.28 to 0.79	0.748
	3	10	6	0.90	0.10	0.71 to 0.86	0.003
miR-370	1	7	5	0.86	0.13	0.60 to 1.12	0.03
	2	14	10	0.64	0.13	0.39 to 0.89	0.198
	3	10	3	1.00	0.00	1.00 to 1.00	0.0006
miR-376c	1	7	6	0.79	0.15	0.50 to 1.17	0.07
	2	14	11	0.68	0.12	0.44 to 0.92	0.108
	3	10	7	0.80	0.13	0.55 to 1.05	0.02

4.3.12 miR-889 and miR-655 are not significantly altered in TNBC derived sera-EVs

To investigate the relevance of two other miRNAs found to be downregulated in Hs578Ts(i)$_8$ cells compared to Hs578T cells (see Section 3.3.10) for use as EV-based biomarkers, a preliminary investigation was performed using nine TNBC specimens compared to age-matched healthy control sera-EVs to assess levels of miR-889 and miR-655. Results demonstrated that miR-889 is down-regulated in 5 of 9 (55.6%) TNBC specimens (Figure 4.15A(i)). There was no significant difference of expression between TNBC and control sera-EVs ($p=0.400$) (Figure 4.15 (ii)). Similarly, miR-655 is down-regulated in 6 of 9 (66.7%) TNBC specimens (Figure 4.15B(i)). There was no significant difference of expression between TNBC and control sera-EVs ($p=0.07$) (Figure 4.15B(ii)). AUC values were calculated by ROC analysis all determined insignificant and are displayed in Table 4.16 below.

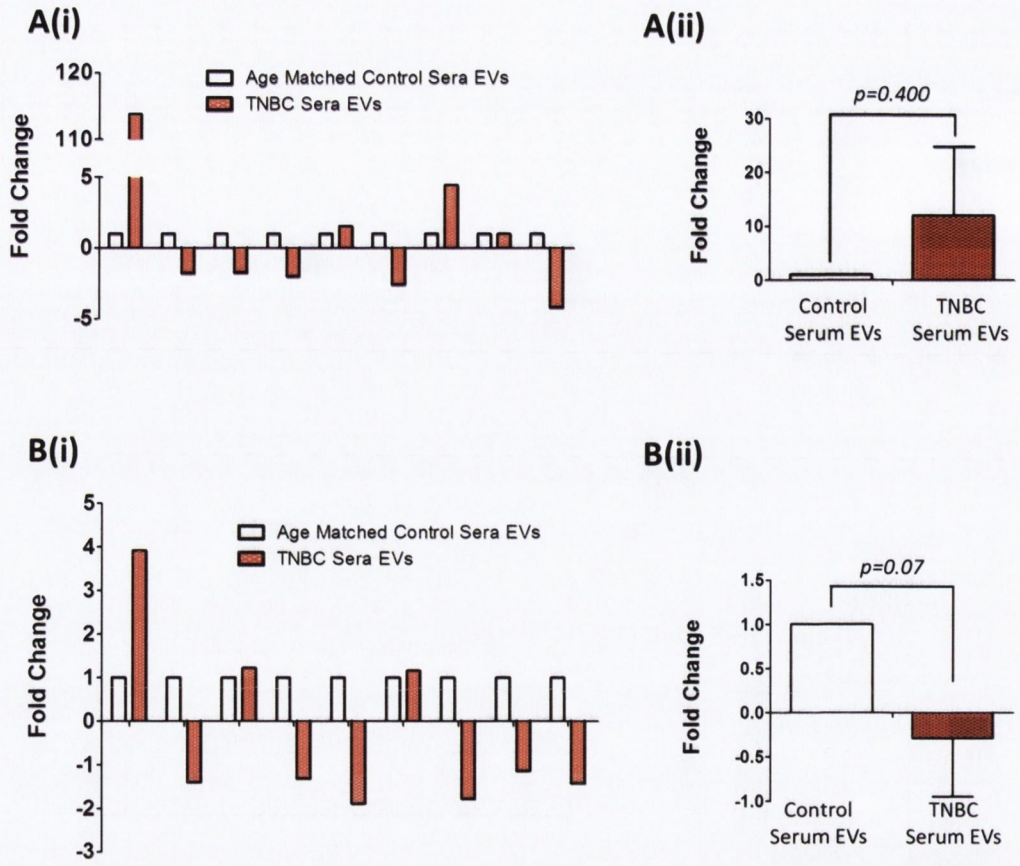

Figure 4.15: Expression of miR-889 and miR-655 in TNBC sera-derived EVs.

A(i): Expression of miR-889 in nine TNBC sera derived EVs compared to EVs derived from healthy control sera with **A(ii)** mean±SEM fold change of miR-889 in the nine TNBC EV specimens. **B(i):** Expression of miR-655 in nine TNBC sera derived EVs compared to EVs derived from healthy control sera with **A(ii)** mean±SEM fold change of miR-655 in the nine TNBC EV specimens. Results are displayed as mean±SEM (Student's t-test).

Table 4.16: AUC values for miR-889 and miR-655 in TNBC serum EVs

miRNA	No. of specimens analysed	Min. no. of specimens rqd.	AUC	Standard error	95% CI	p-value
miR-889	9	7	0.61	0.16	0.30 to 0.92	0.427
miR-655	9	7	0.67	0.16	0.36 to 0.97	0.233

4.4. Discussion

Tumour development and subsequent metastasis requires complex communication between cancer cells and their surrounding environment. One of the mechanisms used by cancer cells to communicate oncogenic messages from cell-to-cell, including transfer of miRNAs, is by release and uptake of EVs [401]. Here, EVs were isolated from the sera of breast cancer patients and from age-matched healthy controls to analyse if they bestow any phenotypic alterations to secondary cells, and to investigate their potential use as blood-based biomarkers. Isolation of EVs from breast cancer sera was confirmed by immunoblot detection of exosome/EV protein markers, PDC6I/Alix and TSG101.

Although previous reports have suggested that EVs are present in greater levels in cancer patients compared to healthy individuals, as shown in an ovarian cancer study using 50 ovarian cancer patients compared to 10 controls [244], our study here of EVs from TNBC patients compared to healthy controls found no substantial differences in EV quantities between these populations of cancer specimens. Similar to the ovarian cancer study, a more recent report on 40 breast cancer patient sera specimens have shown a significant increase of EVs from breast cancer patients compared to 10 healthy control sera [402]. These differing observations may be due to the different methods used for EV isolation and/or quantification. Specifically, in the study on ovarian cancer sera-derived EVs, a modified magnetic activated cell sorting (MACS) using epithelial cell adhesion molecule to selectively isolate EVs from epithelial tumours [244]. As the ovarian cancer study specifically isolated tumour derived-EVs, this could account for the increased levels of EVs detected circulating in sera, compared to our analysis which was not interested in selectively obtaining tumour derived EVs. Similarly, the study on breast cancer sera-derived EVs isolated their EVs using the commercially available kit, ExoQuick, and quantified their EVs based on acetylcholinesterase activity [402]. Such findings suggest that alternative isolation procedures and/or EV quantification methods can account for differing levels of EVs obtained from sera specimens.

Moving on from previous analyses using cell line models for tumour derived EVs, in this chapter we investigated whether EVs have a more clinical relevance in breast cancer progression. Here, we analysed the effects of TNBC and ER+ sera-derived EVs to investigate whether the functional effects induced by TNBC EVs are comparable to the effects induced by EVs derived from ER+ breast cancer sera, or whether they are subtype specific. Due to limited numbers and volumes of sera from HER2+ patients available, we chose to reserve sera-specimens from HER2+ patients for miRNA analysis later in this chapter. We observed that treating cells with EVs derived from TNBC and ER+ serum specimens increase the aggressiveness of secondary cells, similar to the effects of cell line obtained EVs. Specifically, TNBC derived serum EVs significantly increase the rates of secondary cell proliferation, migration and invasion. Although ER+ derived EVs were not observed to significantly increase the proliferation of secondary cells, they have the ability to stimulate migration and invasion of secondary cells. As the relevance of TNBC derived EVs are of the most interest to this Ph.D, and as sera-was available for further analysis using TNBC patient derived EVs, we opted to investigate whether the observation that EVs from TNBC sera can increase the invasion of another breast cancer cell line, SKBR3. This observation supports our observation that EVs from the sera of TNBC patients can increase breast cancer cell invasion, compared to the effects of age-matched control derived sera-EVs. As migration and invasion are key events in cancer metastasis [1], and as these EVs are derived from breast cancer patients, these results support the hypothesis that EVs may promote tumour growth and increase the metastatic potential of tumours from both breast cancer subtypes in cancer patients.

Quantification of RNA from EVs derived from breast cancer sera, compared to age-matched healthy control derived sera-EVs, showed a significant increase of RNA per μg of EVs isolated, complementing our previous observation that RNA is increased in Hs578Ts(i)$_8$ EVs compared to Hs578T EVs. This result demonstrated that EVs from the sera of breast cancer patients are enriched in RNA, compared to the sera- of age matched healthy controls. When analysed by subtype, the same finding was observed. This observation is in keeping with a previous report that EVs from tumour cells, compared to normal fibroblast, can be substantially increased in RNA depending on cancer type. Specifically,

Balaj *et al.* [253] observed that, compared to the EVs from the normal fibroblast cell lines HF19 and HF29, medulloblastoma cell line-derived EVs (D384, D425, D458) had 120 to 310 fold greater levels of RNA, glioblastoma cell line-derived EVs (203 and 11/5) had 2.8 to 6.5 fold levels of RNA, yet the one melanoma cell line-derived EVs (Yumel 0106) analysed showed no difference between the normal fibroblast cell derived EVs .This suggests that the levels of RNA in EVs are cancer specific.

Similar to these observations, we have also observed that EVs from breast cancer sera have 2.3 fold greater levels of RNA. Not only this, but we have observed that RNA levels in EVs may be breast cancer subtype specific, as EVs derived from TNBC patients showed 2 fold increased levels of RNA compared to ER+ and HER2+ sera-derived EVs, although HER2+ and ER EV-RNA levels did not differ. To analyse whether EV-RNA levels are sensitive to discriminate healthy individuals from cancer patients, we performed ROC analyses to determine the AUC. ROC analysis is commonly used to assess the diagnostic ability of a test to discriminate between healthy and diseased populations. ROC analysis determined an AUC value, indicative of the tests overall diagnostic ability [399].

In recent years, miRNAs have shown great potential for use as diagnostic and prognostic biomarkers in breast cancer [84, 85, 391, 403]. Such expression profiling, using clinical specimens, have primarily focused on investigating the miRNA expression in either peripheral blood [404] or in cell-free serum or plasma [382]. However, this approach has limitations, including degradation of freely circulating miRNAs by ribonuceases and lack of standardised protocols for expression analyses [385].

To clinically evaluate our *in vitro* findings that miR-134, miR-370 and miR-376c are all significantly reduced in aggressive TNBC cells and their derived EVs (see Section 3.3.10), we analysed their levels in breast cancer tumours and in EVs derived from breast cancer patients *versus* age matched healthy controls. Using two publically available-datasets, as described in Section 0, we discovered that all three miRNAs are present at significantly reduced levels in primary breast cancer tumours, suggesting that loss of their expression is important in breast cancer progression, thus clinically supporting our previous

observations. Once validated as having clinical relevance in tumour specimens, we investigated the relevance of these miRNAs from EVs derived from breast cancer patients. Complementing the tumour observation in publically-available datasets, all three miRNAs are significantly down-regulated in sera-EVs compared to healthy control derived EVs, suggesting that the miRNA content of EVs is concurrent with the miRNA profile of tumour cells.

We show that miR-134 is significantly reduced by 7 fold, miR-370 by 52 fold and miR-376c by 7 fold in breast cancer sera-EVs compared to EVs from age-matched control derived EVs. Further statistical analysis to analyse the sensitivity and specificity of each of these miRNAs to discriminate cancer patients from healthy individuals, we performed ROC analyses to determine the AUC. ROC analysis determined that these miRNAs in serum EVs can discriminate sensitively between individuals with breast cancer and those without, however this may be subtype specific as miR-134 does not have sensitive discriminatory capability to detect TNBCs and miR-376c cannot distinguish between healthy individuals and those with HER2+ breast cancer. Analysis of levels of miR-889 or miR-655 in breast cancer sera-derived EVs compared to age-matched control sera-derived EVs suggests that they have no use as potential blood-based biomarkers in TNBC diagnosis.

Observation that these miRNAs are sensitive to detect breast cancer presence, and are significantly reduced in breast cancer, they may provide desirable, blood derived biomarkers for breast cancer diagnoses bypassing invasive procedure used to obtain tumour biopsies, which could allow for reduced discomfort for patients.

As information was available to use regarding breast cancer stages, we questioned whether these miRNAs in sera-EVs are altered during breast cancer progression. We find here that, not only can these miRNAs discriminate between breast cancer and healthy patients; ROC analysis has shown that miR-134 and miR-370 are sensitive for use as blood-based biomarkers for early stage breast cancer. As 1 year survival rates for stage 1 breast cancers are 99% in Ireland, and 92.1% for 5 year survival, this findings may have benefit in preventing premature death caused by breast cancer. In comparison, stage 2 breast cancers show 97.8% survival 1 year post diagnosis, but deviates more

substantially from stage 1 breast cancer at 5 year survival, which is 84.1% [405]. In addition to detecting early stage breast cancer, all EV-miRNAs are highly sensitive to detection stage 3 breast cancers with miR-370 showing the greatest sensitivity for discrimination.

To the best of our knowledge, these observations have not been speculated before in breast cancer, yet a limited number of reports have suggested that these miRNAs have use as circulating biomarkers in cancer. In lung adenocarcinoma, miR-134 has been observed to be present at significantly reduced levels in malignant pleural effusions compared to benign pleural effusions, and has sensitivity for use as a biomarker. This finding suggests that miR-134 may have diagnostic value in differentiation between lung adenocarcinoma associated malignant pleural effusion and benign pleural effusions [406]. Although that study did not analyse the specific source of the miRNAs (*i.e.* whether freely circulating in pleural fluid specimens or bound with EVs), it complements our hypothesis that circulating miR-134 is an attractive miRNA for use as a blood-based biomarker. Additionally, it also suggests that miR-134 may play a wider role in diagnosing other cancer types, not only breast cancer. miR-376c has been shown to have potential as a serum based biomarker for early detection of gastric cancer [407]. Although our study suggests that detection of reduced levels of miR-376c in serum derived EVs has potential as a biomarker for breast cancer diagnosis, Song *et al.* demonstrated that miR-376c is present in significantly increased levels in serum from gastric cancer patients [407]. Perhaps, differential miR-376c expression is cancer specific. To the best of our knowledge, circulating miR-370 has not been previously implicated as a biomarker in cancer, so represents a novel discovery for use as a blood-based biomarker for cancer detection.

4.5. Conclusion

In conclusion, this chapter has observed that EVs derived from both TNBC and ER+ patients increased the aggression of breast cancer cells *in vivo*, with no significant differences between EVs from the two subtypes. Interestingly, we have observed that EVs from breast cancer patient sera are enriched with RNA, in a manner which may be subtype specific as EVs from TNBC patients have substantially more RNA than other ER+ and HER2+ subtypes. We have also observed the down-regulation of miR-134, miR-370 and miR-376c in both breast cancer tumours and in EVs derived from breast cancer serum. Specifically, analysing expression values based in breast cancer stage show that miR-134 and miR-370 from sera-EVs may have diagnostic value when differentiating between healthy individuals and those with early stage breast cancer. Similarly, miR-134, miR-370 and miR-376c from sera-EVs may also have diagnostic relevance for distinguishing stage 3 breast cancer from healthy individuals. Rather than being subtype specific and sensitive, these miRNAs appear to have sensitivity to detect breast cancer stages in all subtypes analysed. These findings, especially this pertaining to stage 1 breast cancer detection, suggest they have value in the diagnosis of early stage breast cancers through blood-based diagnostics.

A summary of the major findings in this chapter are illustrated in Figure 4.16 below.

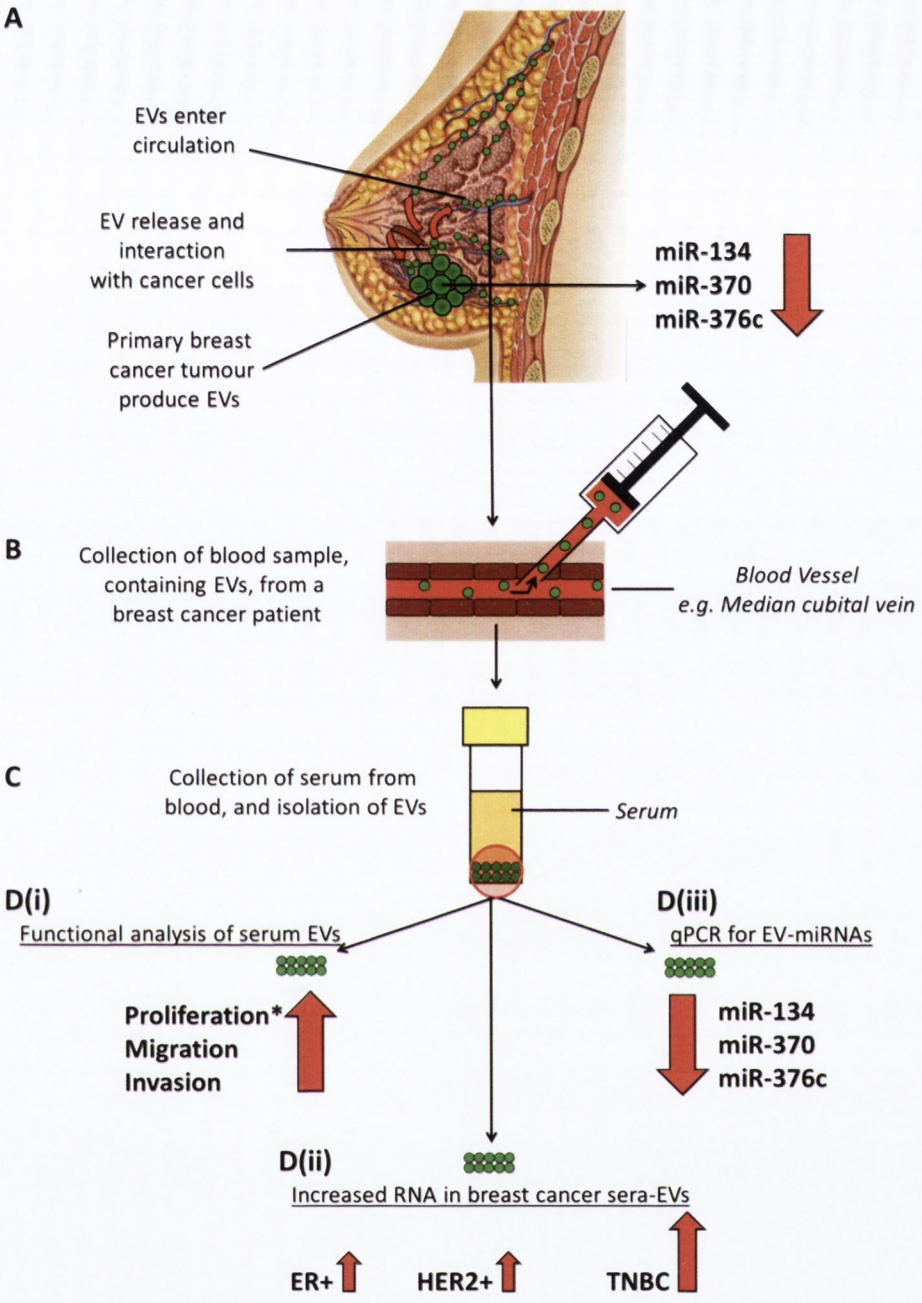

Figure 4.16: Summary of the major findings in this chapter.

A: Upon primary tumour establishment, tumour cells have reduced levels of miR-134, miR-370 and miR-376c. Additionally, tumour derived EVs interact with the surrounding cancer cells and enter the circulatory system. **B:** Intercepting these tumour derived EVs by taking a blood specimen allows for the **C:** collection of EVs from the serum fraction of the whole blood. **D(i):** Treating cancer cells with these tumour derived EVs have been shown, here, to increase their proliferation*, migration and invasion. **D(ii):** RNA levels are substantially increased in breast cancer –derived EVs compared to sera-EVs of healthy individuals. **(iii):** Once isolated, miRNA can be extracted from the EVs and subjected to qPCR analysis to determine miR-134, miR-370 and/or miR-376c expression levels for prognostic purposes.

**proliferation significantly increased from EVs from TNBC patients, not from EVs from ER+ patients.*

Chapter 5

5. Final Discussion and Conclusions

5.1. Discussion

The objective of this Ph.D was to investigate the relevance of EVs in TNBC progression, treatment and diagnosis. To study this, a number of approaches were taken. First, this Ph.D aimed to determine whether TNBC derived EVs could influence TNBC progression, by analysing their effects on phenotypes associated with cancer metastasis. Secondly, EV miRNA and DNA contents were analysed to see whether their signals could be intercepted for use as circulating biomarkers, and to identify potential tumour suppressors. From this, we hoped to re-introduce down-regulated miRNAs back into the cells and manipulate the miRNA content of the EVs communicate therapeutic signals. Subsequently, to investigate their sensitivity for use as circulating miRNA blood-based biomarkers, we aimed to evaluate whether these findings have translational potential by analysing EVs derived from breast cancer patients.

Prior to this Ph.D, the field of exosomes and microvesicles (EVs) research was gaining much speed, with their presence being implicated to have importance in cancer progression. However, limited reports were performed investigating their relevance in breast cancer. Additionally, we know of no other studies investigating their relevance in TNBC, except for studies reported in this thesis. To begin, we opted to establish whether EVs have any functional influences in cancer progression. We were lucky enough to have a pair of isogenic TNBC cell line variants, ideal for an analysis focused on the influence of EVs in TNBC metastasis. Specifically, Hughes *et al.* [278] generated an aggressive TNBC cell line variant, Hs578Ts(i)$_8$, from the Hs578T TNBC cell line to have increased invasive capability and ability to form tumours in nude mice. We opted to investigate their derived EVs for two reasons:

(i) We were interested in the influence of TNBC EVs in TNBC progression and aggression, which the Hs578Ts(i)$_8$ cells represent

(ii) Many studies prior to this Ph.D reported having concerns about the use of suitable controls for use when analysing the functional effects of EVs. To overcome this limitation, we believed that using EVs derived from cell line variants would overcome this concern, providing more realistic representations of the effects of EVs, comparing more aggressive derived EVs to less aggressive.

Chapter 2 determined that EVs derived from TNBC cell lines (Hs578Ts(i)$_8$ and MDA-MB-231) increase the aggression of all breast cancer cells treated with these EVs, in a manner representing the innate phenotypes of the cells of origin. Specifically, EVs derived from aggressive TNBC cells can increase the proliferation, migration, invasion and vasculogenesis of secondary cells. In additionally, pilot *in vivo* analysis suggests that EVs from TNBC cells may influence pre-metastatic niche development. Taking all these results together, these findings implicate EVs in playing detrimental roles in cancer progression. Specifically, the data suggests that EVs from more aggressive cancers can increase the metastatic potential of tumour cells. Not only have this, but TNBC-derived EVs may also play an influential role in the nature of TNBC metastatic spread, by preparing the pre-metastatic niche, and having the ability to enter the brain, crossing the BBB.

The phenotypic altering effects of cell line-derived EVs were clinically validated in Chapter 4, when EVs from the sera of TNBC patients were assessed for their phenotype altering capabilities, compared to EVs from the sera of healthy controls. EVs from the sera of patients diagnosed with TNBC can increase tumour growth, migration and invasion of tumour cells *in vitro.* Investigation whether these events are subtype-specific, we determined that EVs from ER+ patients also increase migration and invasion, with no significant effect on proliferation. These findings suggest that tumour derived-EVs may act in both TNBC and ER+ patients in a similar manner, to promote cancer aggression.

As Chapter 2 established that TNBC-EVs may actually have relevance in TNBC progression, we wondered what was within the EVs which may be

mediating these effects. Therefore, in Chapter 3 we primarily focused on the miRNA contents of the EVs by globally profiling both Hs578T and Hs578Ts(i)$_8$ cells and EVs. This analysis gave the potential to elucidate a spectrum of important information, including:

(i) Identification of EV-associated miRNA which may be responsible for the increasing the aggression of receiving cells
(ii) Discovery of key miRNAs lost in TNBC aggression, which may have tumour suppressive qualities
(iii) Detection of circulating miRNAs for use as minimally-invasive biomarkers to aid in TNBC diagnosis and/or monitor progression

Global miRNA profiling of the cells and EVs produced quite a few observations. First of all, linear regression analysis determined that the miRNA content of EVs is highly representative cells of origin, suggesting that EVs could potentially be used a blood based biomarkers, to give information about the originating TNBC tumour cells. Interestingly we also observed some miRNAs to be selectively incorporated into EVs, at the expense of their presence in the cells. Comparing the miRNA profiles of the more aggressive cells and their derivative EVs to their isogenic parent cells and EVs demonstrated mass downregulation and loss of miRNA levels, which supplied us with eighty-three possible tumour suppressors from the cell analysis alone. Based on the miRNA expression profiling of the cells and EVs, along with scrutinisation of miRNA-target prediction software to determine potential tumour-suppressive miRNAs, we became interested in five miRNAs which were commonly down-regulated in both the Hs578Ts(i)$_8$ cells and EVs :miR-134, miR-370, miR-376c, miR-889 and miR-665. By having the ability to reduce TNBC aggression, we discovered that miR-134 and miR-370 have tumour suppressive qualities.

Specifically, observation that miR-134 and miR-370 can reduce both migration and invasion are novel observations which suggest that their loss is an important event in increasing metastatic potential of TNBC. A lot more information was gathered regarding the effects of miR-134 in events associated with metastasis. Specifically, immunoblot analysis confirmed miRNA target prediction algorithms that miR-134 reduces the expression of STAT5B.

However, it is the knock-on effects of reducing STAT5B expression which we became most interested in. As STAT5B regulates the transcription of Hsp90, which in turn mediates Bcl-2 expression, we hypothesised the discovery of a central player in TNBC aggression. Immunoblot analysis confirmed that introduction of miR-134 back into Hs578Ts(i)$_8$ cells reduces all STAT5B, Hsp90 and Bcl-2 expression. Functionally, these expression differences correlated with substantially reduced proliferation. Of relevance to miR-134 reduction of reduced Bcl-2 expression, we observed that combination treatment of miR-134 with cisplatin significantly increased cisplatin-induced apoptosis, suggesting that this approach to TNBC treatment may be valuable.

In addition to these observations we successfully manipulated EVs into carrying miR-134 from cell to cell, which reduced the expression of both STAT5B and Hsp90 in receiving cells. These miR-134 containing EVs also had functional relevance, by way of reducing both migration and invasion of receiving cells. In addition, as miR-134 contain EVs did not significantly alter proliferation, we observed that they have the ability to significantly increase the potency of two anti-Hsp90 inhibitors, 17-AAG and PU-H71. Such observations are strongly suggesting that miR-134, encapsulated within EVs, have sound therapeutic value, which should be investigated further. These *in vitro* observations suggest treatment of patients with miR-134 enriched EVs could reduce metastatic potential of TNBC cells, as well as potentially act as combination therapies with anti-Hsp90 compounds.

To bring the miRNA profiling results into a setting which may be directly beneficial to patients in the breast cancer clinic, we elected to investigate whether some of the commonly down-regulated miRNAs from the cell analysis was relevant in EVs derived the serum of patients diagnosed with breast cancer. To begin to establish whether some of these miRNAs may have relevance in breast cancer progression, we analysed their expression in breast cancer tumours using publically available datasets. This analysis determined that miR-134, miR-370 and miR-376c are all significantly reduced in breast cancer tumours, so had high relevance for EV-based analysis. We determined, by qPCR expression analysis that miR-134, miR-370 and miR-376c all have value as EV-based minimally-invasive cancer diagnostic biomarkers.

Specifically, we observed that both miR-134 and miR-370 are sensitive to discriminate between healthy individuals and those with stage 1 breast cancer. It was also observed that miR-370 and miR-376c are sensitive to distinguish stage 3 breast cancer from healthy individuals.

5.2 Conclusion

In conclusion, this Ph.D thesis presents research investigating the relevance of EVs in TNBC progression, signalling, treatment and diagnosis. This research has determined that EVs play an influential role in increasing TNBC aggression by relaying oncogenic signals from cell-to-cell, specifically miRNAs and mutated DNA were evaluated here. We observed that TNBC derived EVs are highly representative of their originating tumour cells, and pose as very attractive vesicles for blood-based diagnostics. Specifically, this research discovered that both miR-134 and miR-370 act as tumour suppressors in TNBC cells. In addition, combinational therapy using miR-134 with cisplatin treatment may have therapeutic value, by increasing cisplatin-induced apoptosis. We have also observed that EVs can be manipulated into transmitting functional miR-134 from cell-to-cell, subsequently reducing target protein expression, aggression and increasing efficacy of anti-Hsp90 compounds. Not only did this body of work determine tumour suppressive qualities of these miRNAs, but we also discovered their reduced expression in breast cancer tumours. Determining that miR-134 and miR-370 in EVs are sensitive to discriminate healthy individuals from stage 1 breast cancer patients; and that miR-134, miR-370 and miR-376c can discriminate stage 3 from healthy individuals suggests that these miRNAs, encapsulated with EVs, may have value as blood-based breast cancer diagnostics.

5.3 Future directions

5.3.1 Do Hs578Ts(i)$_8$ EVs increase cellular movement *in vivo*?

In order to fully elucidate the relevance of TNBC EVs *in vivo* a follow on experiment from the one reported in Chapter 2, Section 2.3.10, is warranted. As results in Chapter 2 demonstrate that EVs from more aggressive derived cells increase the aggression of breast cancer cells *in vitro* and hone towards areas commonly affected in breast cancer metastasis *in vivo*, a more detailed *in vivo* analysis should be performed to determine their effects on altering the metastatic potential of tumour cells. As Hughes *et al.* [278] demonstrated that Hs578Ts(i)$_8$ cells can form tumours *in vivo*, these cells are an ideal model to assess. According to a previous publication using melanoma derived EVs [206], to assess whether TNBC EVs could increase Hs578Ts(i)$_8$ cellular movement in mice, mice would be pre-treated three times with either Hs578T or Hs578Ts(i)$_8$ derived EVs. In tangent with the third treatment of EVs, luciferase-labelled Hs578Ts(i)$_8$ cells would be injected and movement assessed by IVIS to see if Hs578Ts(i)$_8$ EVs increase cell movement compared to Hs578T EVs. An outline of proposed groups is outlined in Table 5.1 below.

Table 5.1: Outline of proposed *in vivo* analysis

Group	Assessment	Number of mice
Group 1.1	Hs578T(i)$_8$ EVs plus Hs578T(i)$_8$ cells	n=10
Group 1.2	Hs578T EVs + Hs578T(i)$_8$ cells	n=10
Group 1.3	Hs578T(i)$_8$ EVs	n=10
Group 1.4	Hs578T EVs	n=10
Group 1.5	Hs578Ts(i)$_8$ cells	n=10
Group 1.6	No cells and no Evs	n=10

5.3.2 Can TNBC derived EVs influence the phenotypes of normal cells

To assess whether EVs derived from TNBC can and alter the phenotypes of normal cells analyses should be carried out using EVs derived from the TNBC cell line variants, Hs578T and Hs578Ts(i)$_8$ on normal cells (e.g. MCF10A cells). Such an analysis would establish whether TNBC-derived EVs can influence non-cancerous cells to aid in TNBC progression by recruiting healthy cells.

5.3.3 More in-depth investigating using a larger panel of TNBC cell lines

To strengthen the observations made in this thesis that TNBC-derived EVs can increase the aggression of secondary cells; this analysis should be expanded using a larger panel of TNBC cell-derived EVs.

5.3.4 Is miR-134 a potential tumour suppressor in other breast cancer subtypes?

Chapter 3 determined that miR-134 can act as a tumour suppressor in Hs578Ts(i)$_8$ cells and can increase cisplatin-mediated apoptosis. Scrutinising publically-available miRNA breast cancer datasets in Chapter 4, demonstrated that miR-134 expression is significantly reduced in TNBC, ER+ and HER2+ breast cancers, suggesting that miR-134 has importance in these subtypes too. Assessing the tumour suppressive qualities of miR-134 in other breast cancer subtypes, as well as its ability to amplify the effect of chemotherapeutics, may lead to discovering the full potential of miR-134 as a breast cancer therapeutic, not only in TNBC.

5.3.5 Relevance of miR-370 and miR-376c as tumour suppressors

Chapter 3 showed that miR-370 can reduce the invasion and migration of TNBC cells, and Chapter 4 determined that is it significantly reduced in breast cancer tumours. However, the mechanism of action was not discovered. Further analysis should be performed to elucidate its mechanism of action as this thesis suggests that it may be a desirable tumour suppressor. Although no

functional work has been performed using miR-376c as a tumour suppressor, observation of its down-regulation in breast cancer tumours suggests it may have an important role in breast cancer progression. The relevance of using these miRNAs within EVs as therapeutic strategies is also warranted.

5.3.6 Assessing the relevance of miR-134 *in vivo*

To further investigate the relevance of miR-134 to act as a tumour suppressor, this study should move on to analyse whether it can suppress tumour growth *in vivo*. To perform this, stably transfected miR-134 cell lines should be generated and implanted into mice models to assess tumour growth compared to NC mimic stable transfected cells. Assessing the ability of miR-134 to amplify cisplatin and/or anti-Hsp90 drug potency should be performed as part of such a study to see if such combinational treatments are beneficial.

5.3.7 Further investigation of the ability of EVs to carry miRNA therapeutics

Chapter 3 determined that EVs derived from miR-134 transfected cells, compared to EVs from NC-mimic transfected cells, have the ability to reduce the expression of target proteins in secondary Hs578Ts(i)$_8$ cells and to reduce their cellular aggressiveness. Although this analyses showed that EVs can be manipulated into carrying miRNA therapeutic signals, this should be further investigated to analyse if increasing the load of miR-134 within the EVs can amplify their therapeutic potential. Utilising other mechanisms of miRNA transfection into EVs may determine the true potential of miR-134 in EVs to act as a therapeutic approach in breast cancer. If this analysis is successfully optimised, this study could move into mice models to investigate whether miRNA manipulated EVs have the ability to reduce tumour growth and increase the potency of chemotherapeutics.

5.3.8 Is total serum a reliable approach to circulating miRNA biomarker discovery?

Findings generated in Chapter 4 suggest that sera-derived EVs have potential for used a minimally-invasive blood-based miRNA biomarkers for detection of early stage breast cancer. To assess whether total serum is as efficient for use a source of miRNAs, miRNA expression analysis for miR-134, miR-370 and miR-376c should be investigated in a larger cohort of sera-specimens. Findings from such an analysis would aid in deciding the most efficient protocol for use in a clinical setting for breast cancer diagnosis *i.e.* total serum *versus* serum EVs.

5.3.9 Relevance of PHLPP2 mutation in TNBC-EVs

SNP genotyping of TNBC cells and EVs identified the presence of mutated PHLPP2 (L1016S) in both cells and EVs. As it has been previously discovered that this mutation of PHLPP2 has relevance in breast cancer [319, 371], the functional and diagnostic implications should be further investigated in EVs. Specifically, L1016S mutated PHLPP2 has been shown to dephosphorylate Akt1 and Akt3 to inactivate Akt and PKC to reduce apoptosis in breast cancer cells [371]. To investigate whether this is a potential mechanism of action of the EVs analysed in this thesis should be investigated. This could be performed by treating secondary breast cancer cells with EVs derived from Hs578T and/or Hs578Ts(i)$_8$ cells to determine whether Akt phosphorylation is reduced and apoptosis affected. As Hs578TBst had been previously shown to be wild-type for this mutation [370], the effects of these EVs could be directly compared to the mutated Hs578T and Hs578Ts(i)$_8$ derived EVs. To investigate the clinical relevance and biomarker potential of this observation, EVs should be isolated from patients' sera and assessed for the presence/absence of this mutation.

5.3.10 Relevance of TP53 mutation Hs578Ts(i)$_8$ TNBC-EVs

Similar to the functional knock-on implications of PHLPP2 mutations in TNBC derived EVs, the relevance of mutated TP53 in Hs578Ts(i)$_8$ EVs should be investigated. Chapter 3 identified TP53 to be mutated in Hs578Ts(i)$_8$ EVs. This may have profound implications as in cancer progression and biomarker discovery. Investigations should be performed to determine the mechanistic implications of mutated TP53 transfer within receiving cells. As Hs578T derived EVs have wild-type TP53, the effects can be direct compared between the two cell line variants. Clinically, investigations should be carried out on EVs from TNBC sera to determine if this observation is clinically relevant in metastatic spread an in biomarker discovery. As the TP53 mutation was observed in the EVs, but not in their cells of origin, any potential explanation, such as the presence of transposable elements should be investigation to explain this phenomenon.

5.3.11 Relevance EV enclosed DNA mutations in breast cancer

As this Ph.D has determined that mutations can be identified in breast cancer derived EVs, studies could be extended to investigate whether this is a more common phenomenon in breast cancer progression, which could aid in breast cancer diagnosis. For example, as mutations are frequently observed in therapeutic-resistant breast cancer [408], investigating whether mutations are carried in EVs derived from breast cancer resistant cells/patients, may lead to discovery of a minimally-invasive biomarker to monitor breast cancer therapeutic resistance.

6. References

1. Weinberg, R.A., *The Biology of Cancer*. 2006: Garland Science.
2. *Cancer in Ireland 2013: Annual report of the National Cancer Registry* 2013, National Cancer Registry: National Cancer Registry.
3. Pani, G., T. Galeotti, and P. Chiarugi, *Metastasis: cancer cell's escape from oxidative stress.* Cancer Metastasis Rev, 2010. **29**(2): p. 351-78.
4. Fernald, K. and M. Kurokawa, *Evading apoptosis in cancer.* Trends Cell Biol, 2013. **23**(12): p. 620-33.
5. Wong, R.S., *Apoptosis in cancer: from pathogenesis to treatment.* J Exp Clin Cancer Res, 2011. **30**: p. 87.
6. Raffo, A.J., et al., *Overexpression of bcl-2 protects prostate cancer cells from apoptosis in vitro and confers resistance to androgen depletion in vivo.* Cancer Res, 1995. **55**(19): p. 4438-45.
7. Del Bufalo, D., et al., *Bcl-2 overexpression enhances the metastatic potential of a human breast cancer line.* FASEB J, 1997. **11**(12): p. 947-53.
8. Zhao, M., et al., *Apigenin inhibits proliferation and induces apoptosis in human multiple myeloma cells through targeting the trinity of CK2, Cdc37 and Hsp90.* Mol Cancer, 2011. **10**: p. 104.
9. Mandal, M. and R. Kumar, *Bcl-2 expression regulates sodium butyrate-induced apoptosis in human MCF-7 breast cancer cells.* Cell Growth Differ, 1996. **7**(3): p. 311-8.
10. Cimmino, A., et al., *miR-15 and miR-16 induce apoptosis by targeting BCL2.* Proc Natl Acad Sci U S A, 2005. **102**(39): p. 13944-9.
11. Singh, R. and N. Saini, *Downregulation of BCL2 by miRNAs augments drug-induced apoptosis--a combined computational and experimental approach.* J Cell Sci, 2012. **125**(Pt 6): p. 1568-78.
12. Feki, A. and I. Irminger-Finger, *Mutational spectrum of p53 mutations in primary breast and ovarian tumors.* Crit Rev Oncol Hematol, 2004. **52**(2): p. 103-16.
13. Weis, S.M. and D.A. Cheresh, *Pathophysiological consequences of VEGF-induced vascular permeability.* Nature, 2005. **437**(7058): p. 497-504.
14. Hellberg, C., A. Ostman, and C.H. Heldin, *PDGF and vessel maturation.* Recent Results Cancer Res, 2010. **180**: p. 103-14.
15. Franco, O.E., et al., *Cancer associated fibroblasts in cancer pathogenesis.* Semin Cell Dev Biol, 2010. **21**(1): p. 33-9.
16. Gonda, T.A., et al., *Molecular biology of cancer-associated fibroblasts: can these cells be targeted in anti-cancer therapy?* Semin Cell Dev Biol, 2010. **21**(1): p. 2-10.
17. Xing, F., J. Saidou, and K. Watabe, *Cancer associated fibroblasts (CAFs) in tumor microenvironment.* Front Biosci (Landmark Ed), 2010. **15**: p. 166-79.
18. Demaria, S., et al., *Cancer and inflammation: promise for biologic therapy.* J Immunother, 2010. **33**(4): p. 335-51.
19. Grivennikov, S.I., F.R. Greten, and M. Karin, *Immunity, inflammation, and cancer.* Cell, 2010. **140**(6): p. 883-99.
20. Steeg, P.S., *Tumor metastasis: mechanistic insights and clinical challenges.* Nat Med, 2006. **12**(8): p. 895-904.
21. Folgueras, A.R., et al., *Matrix metalloproteinases in cancer: from new functions to improved inhibition strategies.* Int J Dev Biol, 2004. **48**(5-6): p. 411-24.
22. Overall, C.M. and O. Kleifeld, *Towards third generation matrix metalloproteinase inhibitors for cancer therapy.* Br J Cancer, 2006. **94**(7): p. 941-6.
23. Liling Wan, K.P.Y.K., *Tumor metastasis: moving new biological insights into the clinic.* Nature Medicine, 2013. **19**: p. 1450–1464.
24. Goswami, S., et al., *Macrophages promote the invasion of breast carcinoma cells via a colony-stimulating factor-1/epidermal growth factor paracrine loop.* Cancer Res, 2005. **65**(12): p. 5278-83.
25. Polyak, K., *Heterogeneity in breast cancer.* J Clin Invest, 2011. **121**(10): p. 3786-8.
26. Perou, C.M., et al., *Molecular portraits of human breast tumours.* Nature, 2000. **406**(6797): p. 747-52.
27. Carey, L., et al., *Triple-negative breast cancer: disease entity or title of convenience?* Nat Rev Clin Oncol, 2010. **7**(12): p. 683-92.

28. Sorlie, T., et al., *Gene expression patterns of breast carcinomas distinguish tumor subclasses with clinical implications.* Proc Natl Acad Sci U S A, 2001. **98**(19): p. 10869-74.
29. Sorlie, T., et al., *Repeated observation of breast tumor subtypes in independent gene expression data sets.* Proc Natl Acad Sci U S A, 2003. **100**(14): p. 8418-23.
30. Herschkowitz, J.I., et al., *Identification of conserved gene expression features between murine mammary carcinoma models and human breast tumors.* Genome Biol, 2007. **8**(5): p. R76.
31. Charafe-Jauffret, E., et al., *Gene expression profiling of breast cell lines identifies potential new basal markers.* Oncogene, 2006. **25**(15): p. 2273-84.
32. Parker, J.S., et al., *Supervised risk predictor of breast cancer based on intrinsic subtypes.* J Clin Oncol, 2009. **27**(8): p. 1160-7.
33. Nielsen, T.O., et al., *Immunohistochemical and clinical characterization of the basal-like subtype of invasive breast carcinoma.* Clin Cancer Res, 2004. **10**(16): p. 5367-74.
34. Coates, A.S., et al., *Five years of letrozole compared with tamoxifen as initial adjuvant therapy for postmenopausal women with endocrine-responsive early breast cancer: update of study BIG 1-98.* J Clin Oncol, 2007. **25**(5): p. 486-92.
35. Arimidex, T.A.o.i.C.T.G., et al., *Effect of anastrozole and tamoxifen as adjuvant treatment for early-stage breast cancer: 100-month analysis of the ATAC trial.* Lancet Oncol, 2008. **9**(1): p. 45-53.
36. Goss, P.E., et al., *Efficacy of letrozole extended adjuvant therapy according to estrogen receptor and progesterone receptor status of the primary tumor: National Cancer Institute of Canada Clinical Trials Group MA.17.* J Clin Oncol, 2007. **25**(15): p. 2006-11.
37. Metzger-Filho, O., et al., *Dissecting the heterogeneity of triple-negative breast cancer.* J Clin Oncol, 2012. **30**(15): p. 1879-87.
38. Rastelli, F., et al., *Triple-negative breast cancer: current state of the art.* Tumori, 2010. **96**(6): p. 875-88.
39. Blows, F.M., et al., *Subtyping of breast cancer by immunohistochemistry to investigate a relationship between subtype and short and long term survival: a collaborative analysis of data for 10,159 cases from 12 studies.* PLoS Med, 2010. **7**(5): p. e1000279.
40. Foulkes, W.D., et al., *Disruption of the expected positive correlation between breast tumor size and lymph node status in BRCA1-related breast carcinoma.* Cancer, 2003. **98**(8): p. 1569-77.
41. Heitz, F., et al., *Triple-negative and HER2-overexpressing breast cancers exhibit an elevated risk and an earlier occurrence of cerebral metastases.* Eur J Cancer, 2009. **45**(16): p. 2792-8.
42. Liedtke, C., et al., *Response to neoadjuvant therapy and long-term survival in patients with triple-negative breast cancer.* J Clin Oncol, 2008. **26**(8): p. 1275-81.
43. Crown, J., J. O'Shaughnessy, and G. Gullo, *Emerging targeted therapies in triple-negative breast cancer.* Ann Oncol, 2012. **23 Suppl 6**: p. vi56-65.
44. Criscitiello, C., et al., *Understanding the biology of triple-negative breast cancer.* Ann Oncol, 2012. **23 Suppl 6**: p. vi13-8.
45. Lehmann, B.D., et al., *Identification of human triple-negative breast cancer subtypes and preclinical models for selection of targeted therapies.* J Clin Invest, 2011. **121**(7): p. 2750-67.
46. Kreike, B., et al., *Gene expression profiling and histopathological characterization of triple-negative/basal-like breast carcinomas.* Breast Cancer Res, 2007. **9**(5): p. R65.
47. Creighton, C.J., et al., *Residual breast cancers after conventional therapy display mesenchymal as well as tumor-initiating features.* Proc Natl Acad Sci U S A, 2009. **106**(33): p. 13820-5.
48. Hennessy, B.T., et al., *Characterization of a naturally occurring breast cancer subset enriched in epithelial-to-mesenchymal transition and stem cell characteristics.* Cancer Res, 2009. **69**(10): p. 4116-24.
49. Han, W., et al., *DNA copy number alterations and expression of relevant genes in triple-negative breast cancer.* Genes Chromosomes Cancer, 2008. **47**(6): p. 490-9.
50. Andre, F., et al., *Molecular characterization of breast cancer with high-resolution oligonucleotide comparative genomic hybridization array.* Clin Cancer Res, 2009. **15**(2): p. 441-51.

51. Yoshida, K. and Y. Miki, *Role of BRCA1 and BRCA2 as regulators of DNA repair, transcription, and cell cycle in response to DNA damage.* Cancer Sci, 2004. **95**(11): p. 866-71.
52. Vollebergh, M.A., et al., *An aCGH classifier derived from BRCA1-mutated breast cancer and benefit of high-dose platinum-based chemotherapy in HER2-negative breast cancer patients.* Ann Oncol, 2011. **22**(7): p. 1561-70.
53. Carey, L.A., et al., *The triple negative paradox: primary tumor chemosensitivity of breast cancer subtypes.* Clin Cancer Res, 2007. **13**(8): p. 2329-34.
54. Ashworth, A., *A synthetic lethal therapeutic approach: poly(ADP) ribose polymerase inhibitors for the treatment of cancers deficient in DNA double-strand break repair.* J Clin Oncol, 2008. **26**(22): p. 3785-90.
55. Byrski, T., et al., *Response to neoadjuvant therapy with cisplatin in BRCA1-positive breast cancer patients.* Breast Cancer Res Treat, 2009. **115**(2): p. 359-63.
56. D'Ippolito, E. and M.V. Iorio, *MicroRNAs and triple negative breast cancer.* Int J Mol Sci, 2013. **14**(11): p. 22202-20.
57. Rouleau, M., et al., *PARP inhibition: PARP1 and beyond.* Nat Rev Cancer, 2010. **10**(4): p. 293-301.
58. de Ruijter, T.C., et al., *Characteristics of triple-negative breast cancer.* J Cancer Res Clin Oncol, 2011. **137**(2): p. 183-92.
59. O'Shaughnessy, J., et al., *Iniparib plus chemotherapy in metastatic triple-negative breast cancer.* N Engl J Med, 2011. **364**(3): p. 205-14.
60. Harari, P.M., *Epidermal growth factor receptor inhibition strategies in oncology.* Endocr Relat Cancer, 2004. **11**(4): p. 689-708.
61. Nechushtan H. Steinberg H, P.T., *Prelimenary results of a phase I/II of a combination of cetuximab and taxane for triple negative breast cancer patients [abstract].* J Clin Oncol, 2009. **27**((suppl; abstr e12018)).
62. Carey, L.A., et al., *TBCRC 001: randomized phase II study of cetuximab in combination with carboplatin in stage IV triple-negative breast cancer.* J Clin Oncol, 2012. **30**(21): p. 2615-23.
63. Gartner, E.M., et al., *A phase II study of 17-allylamino-17-demethoxygeldanamycin in metastatic or locally advanced, unresectable breast cancer.* Breast Cancer Res Treat, 2012. **131**(3): p. 933-7.
64. Yan, C., et al., *The targeted inhibition of mitochondrial Hsp90 overcomes the apoptosis resistance conferred by Bcl-2 in Hep3B cells via necroptosis.* Toxicol Appl Pharmacol, 2013. **266**(1): p. 9-18.
65. Caldas-Lopes, E., et al., *Hsp90 inhibitor PU-H71, a multimodal inhibitor of malignancy, induces complete responses in triple-negative breast cancer models.* Proc Natl Acad Sci U S A, 2009. **106**(20): p. 8368-73.
66. Lee, R.C., R.L. Feinbaum, and V. Ambros, *The C. elegans heterochronic gene lin-4 encodes small RNAs with antisense complementarity to lin-14.* Cell, 1993. **75**(5): p. 843-54.
67. Esquela-Kerscher, A. and F.J. Slack, *Oncomirs - microRNAs with a role in cancer.* Nat Rev Cancer, 2006. **6**(4): p. 259-69.
68. Bartel, D.P., *MicroRNAs: genomics, biogenesis, mechanism, and function.* Cell, 2004. **116**(2): p. 281-97.
69. Miska, E.A., *How microRNAs control cell division, differentiation and death.* Curr Opin Genet Dev, 2005. **15**(5): p. 563-8.
70. Rajewsky, N., *L(ou)sy miRNA targets?* Nat Struct Mol Biol, 2006. **13**(9): p. 754-5.
71. Rajewsky, N., *microRNA target predictions in animals.* Nat Genet, 2006. **38 Suppl**: p. S8-13.
72. Macfarlane, L.A. and P.R. Murphy, *MicroRNA: Biogenesis, Function and Role in Cancer.* Curr Genomics, 2010. **11**(7): p. 537-61.
73. Calin, G.A. and C.M. Croce, *MicroRNA signatures in human cancers.* Nat Rev Cancer, 2006. **6**(11): p. 857-66.
74. Calin, G.A. and C.M. Croce, *MicroRNA-cancer connection: the beginning of a new tale.* Cancer Res, 2006. **66**(15): p. 7390-4.
75. Iorio, M.V., et al., *MicroRNA signatures in human ovarian cancer.* Cancer Res, 2007. **67**(18): p. 8699-707.
76. Hennessy, E. and L. O'Driscoll, *Molecular medicine of microRNAs: structure, function and implications for diabetes.* Expert Rev Mol Med, 2008. **10**: p. e24.

77. Borchert, G.M., W. Lanier, and B.L. Davidson, *RNA polymerase III transcribes human microRNAs.* Nat Struct Mol Biol, 2006. **13**(12): p. 1097-101.
78. Perron, M.P. and P. Provost, *Protein interactions and complexes in human microRNA biogenesis and function.* Front Biosci, 2008. **13**: p. 2537-47.
79. Zhang, H., et al., *Single processing center models for human Dicer and bacterial RNase III.* Cell, 2004. **118**(1): p. 57-68.
80. Han, J., et al., *The Drosha-DGCR8 complex in primary microRNA processing.* Genes Dev, 2004. **18**(24): p. 3016-27.
81. Griffiths-Jones, S., et al., *miRBase: microRNA sequences, targets and gene nomenclature.* Nucleic Acids Res, 2006. **34**(Database issue): p. D140-4.
82. Chen, P.S., J.L. Su, and M.C. Hung, *Dysregulation of microRNAs in cancer.* J Biomed Sci, 2012. **19**: p. 90.
83. Mulrane, L., et al., *miRNA dysregulation in breast cancer.* Cancer Res, 2013. **73**(22): p. 6554-62.
84. Iorio, M.V., et al., *MicroRNA gene expression deregulation in human breast cancer.* Cancer Res, 2005. **65**(16): p. 7065-70.
85. Blenkiron, C., et al., *MicroRNA expression profiling of human breast cancer identifies new markers of tumor subtype.* Genome Biol, 2007. **8**(10): p. R214.
86. Sempere, L.F., et al., *Altered MicroRNA expression confined to specific epithelial cell subpopulations in breast cancer.* Cancer Res, 2007. **67**(24): p. 11612-20.
87. Janssen, E.A., et al., *Biologic profiling of lymph node negative breast cancers by means of microRNA expression.* Mod Pathol, 2010. **23**(12): p. 1567-76.
88. Volinia, S., et al., *Breast cancer signatures for invasiveness and prognosis defined by deep sequencing of microRNA.* Proc Natl Acad Sci U S A, 2012. **109**(8): p. 3024-9.
89. Dvinge, H., et al., *The shaping and functional consequences of the microRNA landscape in breast cancer.* Nature, 2013. **497**(7449): p. 378-82.
90. Zhang, L., et al., *microRNAs exhibit high frequency genomic alterations in human cancer.* Proc Natl Acad Sci U S A, 2006. **103**(24): p. 9136-41.
91. Zhang, Y., et al., *miR-125b is methylated and functions as a tumor suppressor by regulating the ETS1 proto-oncogene in human invasive breast cancer.* Cancer Res, 2011. **71**(10): p. 3552-62.
92. Png, K.J., et al., *MicroRNA-335 inhibits tumor reinitiation and is silenced through genetic and epigenetic mechanisms in human breast cancer.* Genes Dev, 2011. **25**(3): p. 226-31.
93. Khoshnaw, S.M., et al., *Loss of Dicer expression is associated with breast cancer progression and recurrence.* Breast Cancer Res Treat, 2012. **135**(2): p. 403-13.
94. Grelier, G., et al., *Prognostic value of Dicer expression in human breast cancers and association with the mesenchymal phenotype.* Br J Cancer, 2009. **101**(4): p. 673-83.
95. Melo, S.A., et al., *A TARBP2 mutation in human cancer impairs microRNA processing and DICER1 function.* Nat Genet, 2009. **41**(3): p. 365-70.
96. Melo, S.A., et al., *A genetic defect in exportin-5 traps precursor microRNAs in the nucleus of cancer cells.* Cancer Cell, 2010. **18**(4): p. 303-15.
97. Martello, G., et al., *A MicroRNA targeting dicer for metastasis control.* Cell, 2010. **141**(7): p. 1195-207.
98. Schmeier, S., et al., *dPORE-miRNA: polymorphic regulation of microRNA genes.* PLoS One, 2011. **6**(2): p. e16657.
99. Hu, Z., et al., *Common genetic variants in pre-microRNAs were associated with increased risk of breast cancer in Chinese women.* Hum Mutat, 2009. **30**(1): p. 79-84.
100. Shen, J., et al., *A functional polymorphism in the miR-146a gene and age of familial breast/ovarian cancer diagnosis.* Carcinogenesis, 2008. **29**(10): p. 1963-6.
101. Yang, R., et al., *A genetic variant in the pre-miR-27a oncogene is associated with a reduced familial breast cancer risk.* Breast Cancer Res Treat, 2010. **121**(3): p. 693-702.
102. Preskill, C. and J.B. Weidhaas, *SNPs in microRNA binding sites as prognostic and predictive cancer biomarkers.* Crit Rev Oncog, 2013. **18**(4): p. 327-40.
103. Tchatchou, S., et al., *A variant affecting a putative miRNA target site in estrogen receptor (ESR) 1 is associated with breast cancer risk in premenopausal women.* Carcinogenesis, 2009. **30**(1): p. 59-64.
104. Paranjape, T., et al., *A 3'-untranslated region KRAS variant and triple-negative breast cancer: a case-control and genetic analysis.* Lancet Oncol, 2011. **12**(4): p. 377-86.

105. Zhu, S., et al., *MicroRNA-21 targets tumor suppressor genes in invasion and metastasis.* Cell Res, 2008. **18**(3): p. 350-9.
106. Yan, L.X., et al., *MicroRNA miR-21 overexpression in human breast cancer is associated with advanced clinical stage, lymph node metastasis and patient poor prognosis.* RNA, 2008. **14**(11): p. 2348-60.
107. Qian, B., et al., *High miR-21 expression in breast cancer associated with poor disease-free survival in early stage disease and high TGF-beta1.* Breast Cancer Res Treat, 2009. **117**(1): p. 131-40.
108. Ma, L., J. Teruya-Feldstein, and R.A. Weinberg, *Tumour invasion and metastasis initiated by microRNA-10b in breast cancer.* Nature, 2007. **449**(7163): p. 682-8.
109. Ma, L., et al., *Therapeutic silencing of miR-10b inhibits metastasis in a mouse mammary tumor model.* Nat Biotechnol, 2010. **28**(4): p. 341-7.
110. Huang, Q., et al., *The microRNAs miR-373 and miR-520c promote tumour invasion and metastasis.* Nat Cell Biol, 2008. **10**(2): p. 202-10.
111. Tavazoie, S.F., et al., *Endogenous human microRNAs that suppress breast cancer metastasis.* Nature, 2008. **451**(7175): p. 147-52.
112. Lynch, J., et al., *MiRNA-335 suppresses neuroblastoma cell invasiveness by direct targeting of multiple genes from the non-canonical TGF-beta signalling pathway.* Carcinogenesis, 2012. **33**(5): p. 976-85.
113. Xu, Y., et al., *MicroRNA-335 acts as a metastasis suppressor in gastric cancer by targeting Bcl-w and specificity protein 1.* Oncogene, 2012. **31**(11): p. 1398-407.
114. Scott, G.K., et al., *Coordinate suppression of ERBB2 and ERBB3 by enforced expression of micro-RNA miR-125a or miR-125b.* J Biol Chem, 2007. **282**(2): p. 1479-86.
115. Iorio, M.V., et al., *microRNA-205 regulates HER3 in human breast cancer.* Cancer Res, 2009. **69**(6): p. 2195-200.
116. Wu, H., S. Zhu, and Y.Y. Mo, *Suppression of cell growth and invasion by miR-205 in breast cancer.* Cell Res, 2009. **19**(4): p. 439-48.
117. Lee, J.Y., et al., *Loss of the polycomb protein Mel-18 enhances the epithelial-mesenchymal transition by ZEB1 and ZEB2 expression through the downregulation of miR-205 in breast cancer.* Oncogene, 2014. **33**(10): p. 1325-35.
118. Aydogdu, E., et al., *MicroRNA-regulated gene networks during mammary cell differentiation are associated with breast cancer.* Carcinogenesis, 2012. **33**(8): p. 1502-11.
119. Hurteau, G.J., et al., *Overexpression of the microRNA hsa-miR-200c leads to reduced expression of transcription factor 8 and increased expression of E-cadherin.* Cancer Res, 2007. **67**(17): p. 7972-6.
120. Howe, E.N., D.R. Cochrane, and J.K. Richer, *Targets of miR-200c mediate suppression of cell motility and anoikis resistance.* Breast Cancer Res, 2011. **13**(2): p. R45.
121. Piovan, C., et al., *Oncosuppressive role of p53-induced miR-205 in triple negative breast cancer.* Mol Oncol, 2012. **6**(4): p. 458-72.
122. Wang, C., et al., *MicroRNA-203 suppresses cell proliferation and migration by targeting BIRC5 and LASP1 in human triple-negative breast cancer cells.* J Exp Clin Cancer Res, 2012. **31**: p. 58.
123. Sossey-Alaoui, K., et al., *WAVE3, an actin remodeling protein, is regulated by the metastasis suppressor microRNA, miR-31, during the invasion-metastasis cascade.* Int J Cancer, 2011. **129**(6): p. 1331-43.
124. Valastyan, S., et al., *A pleiotropically acting microRNA, miR-31, inhibits breast cancer metastasis.* Cell, 2009. **137**(6): p. 1032-46.
125. Korner, C., et al., *MicroRNA-31 sensitizes human breast cells to apoptosis by direct targeting of protein kinase C epsilon (PKCepsilon).* J Biol Chem, 2013. **288**(12): p. 8750-61.
126. Mackiewicz, M., et al., *Identification of the receptor tyrosine kinase AXL in breast cancer as a target for the human miR-34a microRNA.* Breast Cancer Res Treat, 2011. **130**(2): p. 663-79.
127. Taylor, M.A., et al., *TGF-beta upregulates miR-181a expression to promote breast cancer metastasis.* J Clin Invest, 2013. **123**(1): p. 150-63.
128. Bisso, A., et al., *Oncogenic miR-181a/b affect the DNA damage response in aggressive breast cancer.* Cell Cycle, 2013. **12**(11): p. 1679-87.

129. Liu, H., et al., *Expression and regulatory function of miRNA-182 in triple-negative breast cancer cells through its targeting of profilin 1.* Tumour Biol, 2013. **34**(3): p. 1713-22.
130. Kawakami, S. and M. Hashida, *Targeted delivery systems of small interfering RNA by systemic administration.* Drug Metab Pharmacokinet, 2007. **22**(3): p. 142-51.
131. Seto, A.G., *The road toward microRNA therapeutics.* Int J Biochem Cell Biol, 2010. **42**(8): p. 1298-305.
132. Seow, Y. and M.J. Wood, *Biological gene delivery vehicles: beyond viral vectors.* Mol Ther, 2009. **17**(5): p. 767-77.
133. Alvarez-Erviti, L., et al., *Delivery of siRNA to the mouse brain by systemic injection of targeted exosomes.* Nat Biotechnol, 2011. **29**(4): p. 341-5.
134. Pan, B.T. and R.M. Johnstone, *Fate of the transferrin receptor during maturation of sheep reticulocytes in vitro: selective externalization of the receptor.* Cell, 1983. **33**(3): p. 967-78.
135. Harding, C., J. Heuser, and P. Stahl, *Endocytosis and intracellular processing of transferrin and colloidal gold-transferrin in rat reticulocytes: demonstration of a pathway for receptor shedding.* Eur J Cell Biol, 1984. **35**(2): p. 256-63.
136. Raposo, G., et al., *B lymphocytes secrete antigen-presenting vesicles.* J Exp Med, 1996. **183**(3): p. 1161-72.
137. Raposo, G. and W. Stoorvogel, *Extracellular vesicles: exosomes, microvesicles, and friends.* J Cell Biol, 2013. **200**(4): p. 373-83.
138. Booth, A.M., et al., *Exosomes and HIV Gag bud from endosome-like domains of the T cell plasma membrane.* J Cell Biol, 2006. **172**(6): p. 923-35.
139. Blanchard, N., et al., *TCR activation of human T cells induces the production of exosomes bearing the TCR/CD3/zeta complex.* J Immunol, 2002. **168**(7): p. 3235-41.
140. Zitvogel, L., et al., *Eradication of established murine tumors using a novel cell-free vaccine: dendritic cell-derived exosomes.* Nat Med, 1998. **4**(5): p. 594-600.
141. Heijnen, H.F., et al., *Activated platelets release two types of membrane vesicles: microvesicles by surface shedding and exosomes derived from exocytosis of multivesicular bodies and alpha-granules.* Blood, 1999. **94**(11): p. 3791-9.
142. Raposo, G., et al., *Accumulation of major histocompatibility complex class II molecules in mast cell secretory granules and their release upon degranulation.* Mol Biol Cell, 1997. **8**(12): p. 2631-45.
143. van Niel, G., et al., *Intestinal epithelial cells secrete exosome-like vesicles.* Gastroenterology, 2001. **121**(2): p. 337-49.
144. Fauré, J., et al., *Exosomes are released by cultured cortical neurones.* Mol Cell Neurosci, 2006. **31**(4): p. 642-8.
145. Février, B. and G. Raposo, *Exosomes: endosomal-derived vesicles shipping extracellular messages.* Curr Opin Cell Biol, 2004. **16**(4): p. 415-21.
146. Rodrigues, M.L., et al., *Extracellular vesicles produced by Cryptococcus neoformans contain protein components associated with virulence.* Eukaryot Cell, 2008. **7**(1): p. 58-67.
147. Zhou, Q., et al., *Immune-related microRNAs are abundant in breast milk exosomes.* Int J Biol Sci, 2012. **8**(1): p. 118-23.
148. Gallo, A., et al., *The majority of microRNAs detectable in serum and saliva is concentrated in exosomes.* PLoS One, 2012. **7**(3): p. e30679.
149. Runz, S., et al., *Malignant ascites-derived exosomes of ovarian carcinoma patients contain CD24 and EpCAM.* Gynecol Oncol, 2007. **107**(3): p. 563-71.
150. Keller, S., et al., *CD24 is a marker of exosomes secreted into urine and amniotic fluid.* Kidney Int, 2007. **72**(9): p. 1095-102.
151. Sullivan, R., et al., *Role of exosomes in sperm maturation during the transit along the male reproductive tract.* Blood Cells Mol Dis, 2005. **35**(1): p. 1-10.
152. O'Brien, K., et al., *Exosomes from triple-negative breast cancer cells can transfer phenotypic traits representing their cells of origin to secondary cells.* European Journal of Cancer, 2013.
153. Thery, C., *Exosomes: secreted vesicles and intercellular communications.* F1000 Biol Rep, 2011. **3**: p. 15.
154. Valadi, H., et al., *Exosome-mediated transfer of mRNAs and microRNAs is a novel mechanism of genetic exchange between cells.* Nat Cell Biol, 2007. **9**(6): p. 654-9.

155. Skog, J., et al., *Glioblastoma microvesicles transport RNA and proteins that promote tumour growth and provide diagnostic biomarkers.* Nat Cell Biol, 2008. **10**(12): p. 1470-6.
156. Ge, R., et al., *Exosomes in Cancer Microenvironment and Beyond: have we Overlooked these Extracellular Messengers?* Cancer Microenviron, 2012. **5**(3): p. 323-32.
157. Sun, D., et al., *A novel nanoparticle drug delivery system: the anti-inflammatory activity of curcumin is enhanced when encapsulated in exosomes.* Mol Ther, 2010. **18**(9): p. 1606-14.
158. Lakhal, S. and M.J. Wood, *Exosome nanotechnology: an emerging paradigm shift in drug delivery: exploitation of exosome nanovesicles for systemic in vivo delivery of RNAi heralds new horizons for drug delivery across biological barriers.* Bioessays, 2011. **33**(10): p. 737-41.
159. Maguire, C.A., et al., *Microvesicle-associated AAV vector as a novel gene delivery system.* Mol Ther, 2012. **20**(5): p. 960-71.
160. Gajos-Michniewicz, A., M. Duechler, and M. Czyz, *MiRNA in melanoma-derived exosomes.* Cancer Lett, 2014.
161. Cai, J., et al., *Extracellular vesicle-mediated transfer of donor genomic DNA to recipient cells is a novel mechanism for genetic influence between cells.* J Mol Cell Biol, 2013. **5**(4): p. 227-38.
162. Pap, E., E. Pallinger, and A. Falus, *The role of membrane vesicles in tumorigenesis.* Crit Rev Oncol Hematol, 2011. **79**(3): p. 213-23.
163. Kharaziha, P., et al., *Tumor cell-derived exosomes: A message in a bottle.* Biochim Biophys Acta, 2012. **1826**(1): p. 103-11.
164. Ludwig, A.K. and B. Giebel, *Exosomes: small vesicles participating in intercellular communication.* Int J Biochem Cell Biol, 2012. **44**(1): p. 11-5.
165. Vlassov, A.V., et al., *Exosomes: Current knowledge of their composition, biological functions, and diagnostic and therapeutic potentials.* Biochim Biophys Acta, 2012. **1820**(7): p. 940-8.
166. Hosseini-Beheshti, E., et al., *Exosomes as biomarker enriched microvesicles: characterization of exosomal proteins derived from a panel of prostate cell lines with distinct AR phenotypes.* Mol Cell Proteomics, 2012. **11**(10): p. 863-85.
167. van Balkom, B.W., et al., *Exosomes and the kidney: prospects for diagnosis and therapy of renal diseases.* Kidney Int, 2011. **80**(11): p. 1138-45.
168. Di Fiore, P.P., S. Polo, and K. Hofmann, *When ubiquitin meets ubiquitin receptors: a signalling connection.* Nat Rev Mol Cell Biol, 2003. **4**(6): p. 491-7.
169. Katzmann, D.J., et al., *Multivesicular body sorting: ubiquitin ligase Rsp5 is required for the modification and sorting of carboxypeptidase S.* Mol Biol Cell, 2004. **15**(2): p. 468-80.
170. van Niel, G., et al., *Dendritic cells regulate exposure of MHC class II at their plasma membrane by oligoubiquitination.* Immunity, 2006. **25**(6): p. 885-94.
171. Piper, R.C. and D.J. Katzmann, *Biogenesis and function of multivesicular bodies.* Annu Rev Cell Dev Biol, 2007. **23**: p. 519-47.
172. Yeo, S.C., et al., *Vps20p and Vta1p interact with Vps4p and function in multivesicular body sorting and endosomal transport in Saccharomyces cerevisiae.* J Cell Sci, 2003. **116**(Pt 19): p. 3957-70.
173. Fisher, R.D., et al., *Structure and ubiquitin binding of the ubiquitin-interacting motif.* J Biol Chem, 2003. **278**(31): p. 28976-84.
174. von Schwedler, U.K., et al., *The protein network of HIV budding.* Cell, 2003. **114**(6): p. 701-13.
175. de Gassart, A., et al., *Lipid raft-associated protein sorting in exosomes.* Blood, 2003. **102**(13): p. 4336-44.
176. Géminard, C., et al., *Degradation of AP2 during reticulocyte maturation enhances binding of hsc70 and Alix to a common site on TFR for sorting into exosomes.* Traffic, 2004. **5**(3): p. 181-93.
177. Theos, A.C., et al., *A lumenal domain-dependent pathway for sorting to intralumenal vesicles of multivesicular endosomes involved in organelle morphogenesis.* Dev Cell, 2006. **10**(3): p. 343-54.
178. Savina, A., et al., *Rab11 promotes docking and fusion of multivesicular bodies in a calcium-dependent manner.* Traffic, 2005. **6**(2): p. 131-43.

179. Ostrowski, M., et al., *Rab27a and Rab27b control different steps of the exosome secretion pathway.* Nat Cell Biol, 2010. **12**(1): p. 19-30; sup pp 1-13.
180. Hsu, C., et al., *Regulation of exosome secretion by Rab35 and its GTPase-activating proteins TBC1D10A-C.* J Cell Biol, 2010. **189**(2): p. 223-32.
181. Gross, J.C., et al., *Active Wnt proteins are secreted on exosomes.* Nat Cell Biol, 2012. **14**(10): p. 1036-45.
182. Lima, L.G., et al., *Tumor-derived microvesicles modulate the establishment of metastatic melanoma in a phosphatidylserine-dependent manner.* Cancer Lett, 2009. **283**(2): p. 168-75.
183. Del Conde, I., et al., *Tissue-factor-bearing microvesicles arise from lipid rafts and fuse with activated platelets to initiate coagulation.* Blood, 2005. **106**(5): p. 1604-11.
184. Pilzer, D., et al., *Emission of membrane vesicles: roles in complement resistance, immunity and cancer.* Springer Semin Immunopathol, 2005. **27**(3): p. 375-87.
185. D'Souza-Schorey, C. and J.W. Clancy, *Tumor-derived microvesicles: shedding light on novel microenvironment modulators and prospective cancer biomarkers.* Genes Dev, 2012. **26**(12): p. 1287-99.
186. Muralidharan-Chari, V., et al., *ARF6-regulated shedding of tumor cell-derived plasma membrane microvesicles.* Curr Biol, 2009. **19**(22): p. 1875-85.
187. Di Vizio, D., et al., *Oncosome formation in prostate cancer: association with a region of frequent chromosomal deletion in metastatic disease.* Cancer Res, 2009. **69**(13): p. 5601-9.
188. Cocucci, E., G. Racchetti, and J. Meldolesi, *Shedding microvesicles: artefacts no more.* Trends Cell Biol, 2009. **19**(2): p. 43-51.
189. Johnstone, R.M., *Exosomes biological significance: A concise review.* Blood Cells Mol Dis, 2006. **36**(2): p. 315-21.
190. Muralidharan-Chari, V., et al., *Microvesicles: mediators of extracellular communication during cancer progression.* J Cell Sci, 2010. **123**(Pt 10): p. 1603-11.
191. Denzer, K., et al., *Follicular dendritic cells carry MHC class II-expressing microvesicles at their surface.* J Immunol, 2000. **165**(3): p. 1259-65.
192. Mallegol, J., et al., *T84-intestinal epithelial exosomes bear MHC class II/peptide complexes potentiating antigen presentation by dendritic cells.* Gastroenterology, 2007. **132**(5): p. 1866-76.
193. Gatti, S., et al., *Microvesicles derived from human adult mesenchymal stem cells protect against ischaemia-reperfusion-induced acute and chronic kidney injury.* Nephrol Dial Transplant, 2011. **26**(5): p. 1474-83.
194. Ratajczak, J., et al., *Embryonic stem cell-derived microvesicles reprogram hematopoietic progenitors: evidence for horizontal transfer of mRNA and protein delivery.* Leukemia, 2006. **20**(5): p. 847-56.
195. Wolfers, J., et al., *Tumor-derived exosomes are a source of shared tumor rejection antigens for CTL cross-priming.* Nat Med, 2001. **7**(3): p. 297-303.
196. Liu, C., et al., *Murine mammary carcinoma exosomes promote tumor growth by suppression of NK cell function.* J Immunol, 2006. **176**(3): p. 1375-85.
197. Al-Nedawi, K., et al., *Intercellular transfer of the oncogenic receptor EGFRvIII by microvesicles derived from tumour cells.* Nat Cell Biol, 2008. **10**(5): p. 619-24.
198. O'Brien, K., et al., *Exosomes from triple-negative breast cancer cells can transfer phenotypic traits representing their cells of origin to secondary cells.* Eur J Cancer, 2013. **49**(8): p. 1845-59.
199. Al-Nedawi, K., et al., *Endothelial expression of autocrine VEGF upon the uptake of tumor-derived microvesicles containing oncogenic EGFR.* Proc Natl Acad Sci U S A, 2009. **106**(10): p. 3794-9.
200. Sidhu, S.S., et al., *The microvesicle as a vehicle for EMMPRIN in tumor-stromal interactions.* Oncogene, 2004. **23**(4): p. 956-63.
201. Hendrix, A., et al., *An ex(o)citing machinery for invasive tumor growth.* Cancer Res, 2010. **70**(23): p. 9533-7.
202. Wieckowski, E.U., et al., *Tumor-derived microvesicles promote regulatory T cell expansion and induce apoptosis in tumor-reactive activated CD8+ T lymphocytes.* J Immunol, 2009. **183**(6): p. 3720-30.
203. Garnier, D., et al., *Cancer cells induced to express mesenchymal phenotype release exosome-like extracellular vesicles carrying tissue factor.* J Biol Chem, 2012. **287**(52): p. 43565-72.

204. Roccaro, A.M., et al., *BM mesenchymal stromal cell-derived exosomes facilitate multiple myeloma progression.* J Clin Invest, 2013. **123**(4): p. 1542-55.
205. Yang, L., et al., *Bladder cancer cell-derived exosomes inhibit tumor cell apoptosis and induce cell proliferation in vitro.* Mol Med Rep, 2013. **8**(4): p. 1272-8.
206. Hood, J.L., R.S. San, and S.A. Wickline, *Exosomes released by melanoma cells prepare sentinel lymph nodes for tumor metastasis.* Cancer Res, 2011. **71**(11): p. 3792-801.
207. Khan, S., et al., *Survivin is released from cancer cells via exosomes.* Apoptosis, 2011. **16**(1): p. 1-12.
208. Zhang, H.G., et al., *A membrane form of TNF-alpha presented by exosomes delays T cell activation-induced cell death.* J Immunol, 2006. **176**(12): p. 7385-93.
209. Safaei, R., et al., *Abnormal lysosomal trafficking and enhanced exosomal export of cisplatin in drug-resistant human ovarian carcinoma cells.* Mol Cancer Ther, 2005. **4**(10): p. 1595-604.
210. Yin, J., et al., *Secretion of annexin A3 from ovarian cancer cells and its association with platinum resistance in ovarian cancer patients.* J Cell Mol Med, 2012. **16**(2): p. 337-48.
211. Suetsugu, A., et al., *Imaging exosome transfer from breast cancer cells to stroma at metastatic sites in orthotopic nude-mouse models.* Adv Drug Deliv Rev, 2013. **65**(3): p. 383-90.
212. Yang, M., et al., *Microvesicles secreted by macrophages shuttle invasion-potentiating microRNAs into breast cancer cells.* Mol Cancer, 2011. **10**: p. 117.
213. Higginbotham, J.N., et al., *Amphiregulin exosomes increase cancer cell invasion.* Curr Biol, 2011. **21**(9): p. 779-86.
214. Antonyak, M.A., et al., *Cancer cell-derived microvesicles induce transformation by transferring tissue transglutaminase and fibronectin to recipient cells.* Proc Natl Acad Sci U S A, 2011. **108**(12): p. 4852-7.
215. Ciravolo, V., et al., *Potential role of HER2-overexpressing exosomes in countering trastuzumab-based therapy.* J Cell Physiol, 2012. **227**(2): p. 658-67.
216. Kaplan, R.N., et al., *VEGFR1-positive haematopoietic bone marrow progenitors initiate the pre-metastatic niche.* Nature, 2005. **438**(7069): p. 820-7.
217. Sceneay, J., M.J. Smyth, and A. Moller, *The pre-metastatic niche: finding common ground.* Cancer Metastasis Rev, 2013. **32**(3-4): p. 449-64.
218. Peinado, H., et al., *Melanoma exosomes educate bone marrow progenitor cells toward a pro-metastatic phenotype through MET.* Nat Med, 2012. **18**(6): p. 883-91.
219. Jung, T., et al., *CD44v6 dependence of premetastatic niche preparation by exosomes.* Neoplasia, 2009. **11**(10): p. 1093-105.
220. Rana, S., K. Malinowska, and M. Zoller, *Exosomal tumor microRNA modulates premetastatic organ cells.* Neoplasia, 2013. **15**(3): p. 281-95.
221. Takahashi, Y., et al., *Visualization and in vivo tracking of the exosomes of murine melanoma B16-BL6 cells in mice after intravenous injection.* J Biotechnol, 2013. **165**(2): p. 77-84.
222. Takino, T., et al., *Controlled biodistribution of highly lipophilic drugs with various parenteral formulations.* J Drug Target, 1993. **1**(2): p. 117-24.
223. Montecalvo, A., et al., *Mechanism of transfer of functional microRNAs between mouse dendritic cells via exosomes.* Blood, 2012. **119**(3): p. 756-66.
224. Koga, Y., et al., *Exosome can prevent RNase from degrading microRNA in feces.* J Gastrointest Oncol, 2011. **2**(4): p. 215-22.
225. Hannafon, B.N. and W.Q. Ding, *Intercellular Communication by Exosome-Derived microRNAs in Cancer.* Int J Mol Sci, 2013. **14**(7): p. 14240-69.
226. Umezu, T., et al., *Leukemia cell to endothelial cell communication via exosomal miRNAs.* Oncogene, 2013. **32**(22): p. 2747-55.
227. Grange, C., et al., *Microvesicles released from human renal cancer stem cells stimulate angiogenesis and formation of lung premetastatic niche.* Cancer Res, 2011. **71**(15): p. 5346-56.
228. Xiao, D., et al., *Identifying mRNA, microRNA and protein profiles of melanoma exosomes.* PLoS One, 2012. **7**(10): p. e46874.
229. Fabbri, M., et al., *MicroRNAs bind to Toll-like receptors to induce prometastatic inflammatory response.* Proc Natl Acad Sci U S A, 2012. **109**(31): p. E2110-6.

230. Batagov, A.O., V.A. Kuznetsov, and I.V. Kurochkin, *Identification of nucleotide patterns enriched in secreted RNAs as putative cis-acting elements targeting them to exosome nano-vesicles.* BMC Genomics, 2011. **12 Suppl 3**: p. S18.
231. Gibbings, D.J., et al., *Multivesicular bodies associate with components of miRNA effector complexes and modulate miRNA activity.* Nat Cell Biol, 2009. **11**(9): p. 1143-9.
232. Irion, U. and D. St Johnston, *bicoid RNA localization requires specific binding of an endosomal sorting complex.* Nature, 2007. **445**(7127): p. 554-8.
233. Yao, B., et al., *Defining a new role of GW182 in maintaining miRNA stability.* EMBO Rep, 2012. **13**(12): p. 1102-8.
234. Kosaka, N., et al., *Secretory mechanisms and intercellular transfer of microRNAs in living cells.* J Biol Chem, 2010. **285**(23): p. 17442-52.
235. Kogure, T., et al., *Intercellular nanovesicle-mediated microRNA transfer: a mechanism of environmental modulation of hepatocellular cancer cell growth.* Hepatology, 2011. **54**(4): p. 1237-48.
236. Ohshima, K., et al., *Let-7 microRNA family is selectively secreted into the extracellular environment via exosomes in a metastatic gastric cancer cell line.* PLoS One, 2010. **5**(10): p. e13247.
237. Pigati, L., et al., *Selective release of microRNA species from normal and malignant mammary epithelial cells.* PLoS One, 2010. **5**(10): p. e13515.
238. Elmore, J.G., et al., *Screening mammograms by community radiologists: variability in false-positive rates.* J Natl Cancer Inst, 2002. **94**(18): p. 1373-80.
239. Friel, A.M., et al., *Relevance of circulating tumor cells, extracellular nucleic acids, and exosomes in breast cancer.* Breast Cancer Res Treat, 2010. **123**(3): p. 613-25.
240. Viale, G., M. Ghioni, and M.G. Mastropasqua, *Traditional molecular markers and response to adjuvant endocrine or trastuzumab-based therapies.* Curr Opin Oncol, 2010. **22**(6): p. 541-6.
241. Koga, K., et al., *Purification, characterization and biological significance of tumor-derived exosomes.* Anticancer Res, 2005. **25**(6A): p. 3703-7.
242. Andre, F., et al., *Malignant effusions and immunogenic tumour-derived exosomes.* Lancet, 2002. **360**(9329): p. 295-305.
243. Valenti, R., et al., *Human tumor-released microvesicles promote the differentiation of myeloid cells with transforming growth factor-beta-mediated suppressive activity on T lymphocytes.* Cancer Res, 2006. **66**(18): p. 9290-8.
244. Taylor, D.D. and C. Gercel-Taylor, *MicroRNA signatures of tumor-derived exosomes as diagnostic biomarkers of ovarian cancer.* Gynecol Oncol, 2008. **110**(1): p. 13-21.
245. Chan, J.A., A.M. Krichevsky, and K.S. Kosik, *MicroRNA-21 is an antiapoptotic factor in human glioblastoma cells.* Cancer Res, 2005. **65**(14): p. 6029-33.
246. Rabinowits, G., et al., *Exosomal microRNA: a diagnostic marker for lung cancer.* Clin Lung Cancer, 2009. **10**(1): p. 42-6.
247. Tanaka, Y., et al., *Clinical impact of serum exosomal microRNA-21 as a clinical biomarker in human esophageal squamous cell carcinoma.* Cancer, 2013. **119**(6): p. 1159-67.
248. Tauro, B.J., et al., *Comparison of ultracentrifugation, density gradient separation, and immunoaffinity capture methods for isolating human colon cancer cell line LIM1863-derived exosomes.* Methods, 2012. **56**(2): p. 293-304.
249. Waldenstrom, A., et al., *Cardiomyocyte microvesicles contain DNA/RNA and convey biological messages to target cells.* PLoS One, 2012. **7**(4): p. e34653.
250. Guescini, M., et al., *C2C12 myoblasts release micro-vesicles containing mtDNA and proteins involved in signal transduction.* Exp Cell Res, 2010. **316**(12): p. 1977-84.
251. Guescini, M., et al., *Astrocytes and Glioblastoma cells release exosomes carrying mtDNA.* J Neural Transm, 2010. **117**(1): p. 1-4.
252. Kahlert, C., et al., *Identification of Double-stranded Genomic DNA Spanning All Chromosomes with Mutated KRAS and p53 DNA in the Serum Exosomes of Patients with Pancreatic Cancer.* J Biol Chem, 2014. **289**(7): p. 3869-75.
253. Balaj, L., et al., *Tumour microvesicles contain retrotransposon elements and amplified oncogene sequences.* Nat Commun, 2011. **2**: p. 180.
254. Herrera, M.B., et al., *Human liver stem cell-derived microvesicles accelerate hepatic regeneration in hepatectomized rats.* J Cell Mol Med, 2010. **14**(6B): p. 1605-18.

255. Cantaluppi, V., et al., *Microvesicles derived from endothelial progenitor cells protect the kidney from ischemia-reperfusion injury by microRNA-dependent reprogramming of resident renal cells.* Kidney Int, 2012. **82**(4): p. 412-27.
256. Cantaluppi, V., et al., *Microvesicles derived from endothelial progenitor cells enhance neoangiogenesis of human pancreatic islets.* Cell Transplant, 2012. **21**(6): p. 1305-20.
257. Fonsato, V., et al., *Human liver stem cell-derived microvesicles inhibit hepatoma growth in SCID mice by delivering antitumor microRNAs.* Stem Cells, 2012. **30**(9): p. 1985-98.
258. Yeo, R.W., et al., *Mesenchymal stem cell: an efficient mass producer of exosomes for drug delivery.* Adv Drug Deliv Rev, 2013. **65**(3): p. 336-41.
259. André, F., et al., *Exosomes as potent cell-free peptide-based vaccine. I. Dendritic cell-derived exosomes transfer functional MHC class I/peptide complexes to dendritic cells.* J Immunol, 2004. **172**(4): p. 2126-36.
260. Andaloussi S EL., et al., *Extracellular vesicles: biology and emerging therapeutic opportunities.* Nat Rev Drug Discov, 2013. **12**(5): p. 347-57.
261. Zhang, Y., et al., *Secreted monocytic miR-150 enhances targeted endothelial cell migration.* Mol Cell, 2010. **39**(1): p. 133-44.
262. Wahlgren, J., et al., *Plasma exosomes can deliver exogenous short interfering RNA to monocytes and lymphocytes.* Nucleic Acids Res, 2012. **40**(17): p. e130.
263. Ohno, S., et al., *Systemically injected exosomes targeted to EGFR deliver antitumor microRNA to breast cancer cells.* Mol Ther, 2013. **21**(1): p. 185-91.
264. Shtam, T.A., et al., *Exosomes are natural carriers of exogenous siRNA to human cells in vitro.* Cell Commun Signal, 2013. **11**: p. 88.
265. Escudier, B., et al., *Vaccination of metastatic melanoma patients with autologous dendritic cell (DC) derived-exosomes: results of thefirst phase I clinical trial.* J Transl Med, 2005. **3**(1): p. 10.
266. Morse, M.A., et al., *A phase I study of dexosome immunotherapy in patients with advanced non-small cell lung cancer.* J Transl Med, 2005. **3**(1): p. 9.
267. Dai, S., et al., *Phase I clinical trial of autologous ascites-derived exosomes combined with GM-CSF for colorectal cancer.* Mol Ther, 2008. **16**(4): p. 782-90.
268. Gyorgy, B., et al., *Membrane vesicles, current state-of-the-art: emerging role of extracellular vesicles.* Cell Mol Life Sci, 2011. **68**(16): p. 2667-88.
269. Carey, L.A., *Through a glass darkly: advances in understanding breast cancer biology, 2000-2010.* Clin Breast Cancer, 2010. **10**(3): p. 188-95.
270. Anders, C.K. and L.A. Carey, *Biology, metastatic patterns, and treatment of patients with triple-negative breast cancer.* Clin Breast Cancer, 2009. **9 Suppl 2**: p. S73-81.
271. Lin, N.U., et al., *Sites of distant recurrence and clinical outcomes in patients with metastatic triple-negative breast cancer: high incidence of central nervous system metastases.* Cancer, 2008. **113**(10): p. 2638-45.
272. Dent, R., et al., *Pattern of metastatic spread in triple-negative breast cancer.* Breast Cancer Res Treat, 2009. **115**(2): p. 423-8.
273. Arnedos, M., et al., *Triple-negative breast cancer: are we making headway at least?* Ther Adv Med Oncol, 2012. **4**(4): p. 195-210.
274. Perou, C.M., *Molecular stratification of triple-negative breast cancers.* Oncologist, 2011. **16 Suppl 1**: p. 61-70.
275. Battke, C., et al., *Tumour exosomes inhibit binding of tumour-reactive antibodies to tumour cells and reduce ADCC.* Cancer Immunol Immunother, 2011. **60**(5): p. 639-48.
276. Lau, C.S. and D.T. Wong, *Breast cancer exosome-like microvesicles and salivary gland cells interplay alters salivary gland cell-derived exosome-like microvesicles in vitro.* PLoS One, 2012. **7**(3): p. e33037.
277. Prat, A., et al., *Phenotypic and molecular characterization of the claudin-low intrinsic subtype of breast cancer.* Breast Cancer Res, 2010. **12**(5): p. R68.
278. Hughes, L., et al., *Characterisation of breast cancer cell lines and establishment of a novel isogenic subclone to study migration, invasion and tumourigenicity.* Clin Exp Metastasis, 2008. **25**(5): p. 549-57.
279. Rani, S., et al., *Isolation of exosomes for subsequent mRNA, MicroRNA, and protein profiling.* Methods Mol Biol, 2011. **784**: p. 181-95.
280. Frisch, S.M. and R.A. Screaton, *Anoikis mechanisms.* Curr Opin Cell Biol, 2001. **13**(5): p. 555-62.

281. Wang, J., et al., *Design of Barbiturate-Nitrate Hybrids that Inhibit MMP-9 Activity and Secretion.* Journal of Medicinal Chemistry, 2012. **55**(5): p. 2154-2162.
282. Grossmann, J., *Molecular mechanisms of "detachment-induced apoptosis-Anoikis".* Apoptosis, 2002. 7(3): p. 247-260.
283. Zhan, M., H. Zhao, and Z.C. Han, *Signalling mechanisms of anoikis.* Histol Histopathol, 2004. **19**(3): p. 973-83.
284. Reddig, P.J. and R.L. Juliano, *Clinging to life: cell to matrix adhesion and cell survival.* Cancer Metastasis Rev, 2005. **24**(3): p. 425-39.
285. Valentinis, B., et al., *Anti-apoptotic signaling of the IGF-I receptor in fibroblasts following loss of matrix adhesion.* Oncogene, 1999. **18**(10): p. 1827-36.
286. Noda, T., et al., *Induction of apoptosis of detached oral squamous cell carcinoma cells by safingol. Possible role of Bim, focal adhesion kinase and endonuclease G.* Apoptosis, 2009. **14**(3): p. 287-97.
287. Kioi M, V.H., Schultz G, Hoffman RM, Harsh GR, Brown JM., *Inhibition of vasculogenesis, but not angiogenesis, prevents the recurrence of glioblastoma after irradiation in mice.* J Clin Invest, 2010. **120**(3): p. 694-705.
288. Simionescu DT, S.A., *Vasculogenesis and Angiogenesis – from Embryonic Development to regenerative Medicine*, ed. S.A. Simionescu DT. 2011, New York: InTech - Open Access Publisher.
289. Roomi, M.W., et al., *Patterns of MMP-2 and MMP-9 expression in human cancer cell lines.* Oncol Rep, 2009. **21**(5): p. 1323-33.
290. Rakha, E.A. and S. Chan, *Metastatic triple-negative breast cancer.* Clin Oncol (R Coll Radiol), 2011. **23**(9): p. 587-600.
291. Bondar, V.M. and D.J. McConkey, *Anoikis is regulated by BCL-2-Independent pathways in human prostate carcinoma cells.* Prostate, 2002. **51**(1): p. 42-49.
292. Overall, C.M. and O. Kleifeld, *Tumour microenvironment - opinion: validating matrix metalloproteinases as drug targets and anti-targets for cancer therapy.* Nat Rev Cancer, 2006. **6**(3): p. 227-39.
293. Chen, K. and N. Rajewsky, *The evolution of gene regulation by transcription factors and microRNAs.* Nat Rev Genet, 2007. **8**(2): p. 93-103.
294. Turchinovich, A., et al., *Characterization of extracellular circulating microRNA.* Nucleic Acids Res, 2011. **39**(16): p. 7223-33.
295. Corcoran, C., et al., *Intracellular and extracellular microRNAs in breast cancer.* Clin Chem, 2011. **57**(1): p. 18-32.
296. Zhang JP, Z.C., Xu L, Gong J, Fang JH, Zhuang SM., *MicroRNA-148a suppresses the epithelial-mesenchymal transition and metastasis of hepatoma cells by targeting Met/Snail signaling.* Oncogene, 2013. **Advance Online Publication**.
297. Li, Y., et al., *Ratio of miR-196s to HOXC8 messenger RNA correlates with breast cancer cell migration and metastasis.* Cancer Res, 2010. **70**(20): p. 7894-904.
298. Roy, S.S., et al., *Significance of PELP1/HDAC2/miR-200 regulatory network in EMT and metastasis of breast cancer.* Oncogene, 2013.
299. Chan, J.K., et al., *The inhibition of miR-21 promotes apoptosis and chemosensitivity in ovarian cancer.* Gynecol Oncol, 2014. **132**(3): p. 739-44.
300. Stoorvogel, W., *Functional transfer of microRNA by exosomes.* Blood, 2012. **119**(3): p. 646-8.
301. Perotti, C., et al., *Heat shock protein-90-alpha, a prolactin-STAT5 target gene identified in breast cancer cells, is involved in apoptosis regulation.* Breast Cancer Res, 2008. **10**(6): p. R94.
302. Du, W., et al., *STAT5 isoforms regulate colorectal cancer cell apoptosis via reduction of mitochondrial membrane potential and generation of reactive oxygen species.* J Cell Physiol, 2012. **227**(6): p. 2421-9.
303. Buettner, R., L.B. Mora, and R. Jove, *Activated STAT signaling in human tumors provides novel molecular targets for therapeutic intervention.* Clin Cancer Res, 2002. **8**(4): p. 945-54.
304. Pleasance, E.D., et al., *A comprehensive catalogue of somatic mutations from a human cancer genome.* Nature, 2010. **463**(7278): p. 191-6.
305. Alexandrov, L.B., et al., *Signatures of mutational processes in human cancer.* Nature, 2013. **500**(7463): p. 415-21.
306. Pfeifer, G.P., *Environmental exposures and mutational patterns of cancer genomes.* Genome Med, 2010. **2**(8): p. 54.

307. Lichtenstein, P., et al., *Environmental and heritable factors in the causation of cancer--analyses of cohorts of twins from Sweden, Denmark, and Finland.* N Engl J Med, 2000. **343**(2): p. 78-85.
308. Silva Idos, S., et al., *Birth size and breast cancer risk: re-analysis of individual participant data from 32 studies.* PLoS Med, 2008. **5**(9): p. e193.
309. Zaman, K., et al., *[Breast cancer and obesity, a dangerous relation].* Rev Med Suisse, 2012. **8**(342): p. 1101-4.
310. Cheung, K.L., *Endocrine therapy for breast cancer: an overview.* Breast, 2007. **16**(4): p. 327-43.
311. Ford, D., et al., *Genetic heterogeneity and penetrance analysis of the BRCA1 and BRCA2 genes in breast cancer families. The Breast Cancer Linkage Consortium.* Am J Hum Genet, 1998. **62**(3): p. 676-89.
312. Teschendorff, A.E. and C. Caldas, *The breast cancer somatic 'muta-ome': tackling the complexity.* Breast Cancer Res, 2009. **11**(2): p. 301.
313. Greenman, C., et al., *Patterns of somatic mutation in human cancer genomes.* Nature, 2007. **446**(7132): p. 153-8.
314. Wood, L.D., et al., *The genomic landscapes of human breast and colorectal cancers.* Science, 2007. **318**(5853): p. 1108-13.
315. Shah, S.P., et al., *Mutational evolution in a lobular breast tumour profiled at single nucleotide resolution.* Nature, 2009. **461**(7265): p. 809-13.
316. Thomas, R.K., et al., *High-throughput oncogene mutation profiling in human cancer.* Nat Genet, 2007. **39**(3): p. 347-51.
317. Stephens, P.J., et al., *Complex landscapes of somatic rearrangement in human breast cancer genomes.* Nature, 2009. **462**(7276): p. 1005-10.
318. Ding, L., et al., *Genome remodelling in a basal-like breast cancer metastasis and xenograft.* Nature, 2010. **464**(7291): p. 999-1005.
319. Santarpia, L., et al., *Mutation profiling identifies numerous rare drug targets and distinct mutation patterns in different clinical subtypes of breast cancers.* Breast Cancer Res Treat, 2012. **134**(1): p. 333-43.
320. !!! INVALID CITATION !!!
321. Stratton, M.R., P.J. Campbell, and P.A. Futreal, *The cancer genome.* Nature, 2009. **458**(7239): p. 719-24.
322. Pfeifer, G.P. and A. Besaratinia, *Mutational spectra of human cancer.* Hum Genet, 2009. **125**(5-6): p. 493-506.
323. Gabriel, S., L. Ziaugra, and D. Tabbaa, *SNP genotyping using the Sequenom MassARRAY iPLEX platform.* Curr Protoc Hum Genet, 2009. **Chapter 2**: p. Unit 2 12.
324. Thakur, B.K., et al., *Double-stranded DNA in exosomes: a novel biomarker in cancer detection.* Cell Res, 2014.
325. Grimson, A., et al., *MicroRNA targeting specificity in mammals: determinants beyond seed pairing.* Mol Cell, 2007. **27**(1): p. 91-105.
326. Workman, P. and M.V. Powers, *Chaperoning cell death: a critical dual role for Hsp90 in small-cell lung cancer.* Nat Chem Biol, 2007. **3**(8): p. 455-7.
327. Livak, K.J. and T.D. Schmittgen, *Analysis of relative gene expression data using real-time quantitative PCR and the 2(-Delta Delta C(T)) Method.* Methods, 2001. **25**(4): p. 402-8.
328. Qureshi, R. and A. Sacan, *A novel method for the normalization of microRNA RT-PCR data.* BMC Med Genomics, 2013. **6 Suppl 1**: p. S14.
329. Redova, M., et al., *Circulating miR-378 and miR-451 in serum are potential biomarkers for renal cell carcinoma.* J Transl Med, 2012. **10**: p. 55.
330. Koberle, V., et al., *Serum microRNA-1 and microRNA-122 are prognostic markers in patients with hepatocellular carcinoma.* Eur J Cancer, 2013. **49**(16): p. 3442-9.
331. Chen, Q., et al., *Plasma miR-122 and miR-192 as potential novel biomarkers for the early detection of distant metastasis of gastric cancer.* Oncol Rep, 2014. **31**(4): p. 1863-70.
332. Xia, S., et al., *[Application of miRNAs in the occurrence and early diagnosis of pancreatic cancer].* Zhonghua Wai Ke Za Zhi, 2014. **52**(3): p. 198-201.
333. Jones, K.B., et al., *miRNA signatures associate with pathogenesis and progression of osteosarcoma.* Cancer Res, 2012. **72**(7): p. 1865-77.
334. Lu, J., et al., *MicroRNA expression profiles classify human cancers.* Nature, 2005. **435**(7043): p. 834-8.

335. Gaur, A., et al., *Characterization of microRNA expression levels and their biological correlates in human cancer cell lines.* Cancer Res, 2007. **67**(6): p. 2456-68.
336. Zhou, M., et al., *MiR-370 sensitizes chronic myeloid leukemia K562 cells to homoharringtonine by targeting Forkhead box M1.* J Transl Med, 2013. **11**: p. 265.
337. Li, J., et al., *miR-134 inhibits epithelial to mesenchymal transition by targeting FOXM1 in non-small cell lung cancer cells.* FEBS Lett, 2012. **586**(20): p. 3761-5.
338. Aaron L Sarver, V.T., Milcah C Scott, Anne-Marie Cleton-Jansen, Pancras CW Hogendoorn, Jaime F Modiano, Subbaya Subramanian, *MicroRNAs at the human 14q32 locus have prognostic significance in osteosarcoma.* Orphanet Journal of Rare Diseases, 2013. **8**(7).
339. Yin C, W.P., Xu WP, Yang Y, Zhang Q, Ning BF, Zhang PP, Zhou WP, Xie WF, Chen WS, Zhang X., *Hepatocyte nuclear factor-4α reverses malignancy of hepatocellular carcinoma through regulating miR-134 in the DLK1-DIO3 region.* Hepatology, 2013. .
340. Ni, X., et al., *Downregulation of miR-106b induced breast cancer cell invasion and motility in association with overexpression of matrix metalloproteinase 2.* Cancer Sci, 2014. **105**(1): p. 18-25.
341. Akhavantabasi, S., et al., *miR-125b targets ARID3B in breast cancer cells.* Cell Struct Funct, 2012. **37**(1): p. 27-38.
342. Wang, H., et al., *Circulating MiR-125b as a marker predicting chemoresistance in breast cancer.* PLoS One, 2012. **7**(4): p. e34210.
343. Mattie, M.D., et al., *Optimized high-throughput microRNA expression profiling provides novel biomarker assessment of clinical prostate and breast cancer biopsies.* Mol Cancer, 2006. **5**: p. 24.
344. Feliciano, A., et al., *miR-125b acts as a tumor suppressor in breast tumorigenesis via its novel direct targets ENPEP, CK2-alpha, CCNJ, and MEGF9.* PLoS One, 2013. **8**(10): p. e76247.
345. Imam, J.S., et al., *MicroRNA-185 suppresses tumor growth and progression by targeting the Six1 oncogene in human cancers.* Oncogene, 2010. **29**(35): p. 4971-9.
346. Calin, G.A., et al., *Human microRNA genes are frequently located at fragile sites and genomic regions involved in cancers.* Proc Natl Acad Sci U S A, 2004. **101**(9): p. 2999-3004.
347. Takayama, H., et al., *Deletion mapping of chromosomes 14q and 1p in human neuroblastoma.* Oncogene, 1992. **7**(6): p. 1185-9.
348. Bando, T., et al., *Loss of heterozygosity of 14q32 in colorectal carcinoma.* Cancer Genet Cytogenet, 1999. **111**(2): p. 161-5.
349. Chang, W.Y., et al., *Novel suppressor loci on chromosome 14q in primary bladder cancer.* Cancer Res, 1995. **55**(15): p. 3246-9.
350. Bandera, C.A., et al., *Deletion mapping of two potential chromosome 14 tumor suppressor gene loci in ovarian carcinoma.* Cancer Res, 1997. **57**(3): p. 513-5.
351. Tse, J.Y., et al., *Loss of heterozygosity of chromosome 14q in low- and high-grade meningiomas.* Hum Pathol, 1997. **28**(7): p. 779-85.
352. Kerangueven, F., et al., *Genome-wide search for loss of heterozygosity shows extensive genetic diversity of human breast carcinomas.* Cancer Res, 1997. **57**(24): p. 5469-74.
353. Hoshi, M., et al., *Detailed deletion mapping of chromosome band 14q32 in human neuroblastoma defines a 1.1-Mb region of common allelic loss.* Br J Cancer, 2000. **82**(11): p. 1801-7.
354. Haller, F., et al., *Localization- and mutation-dependent microRNA (miRNA) expression signatures in gastrointestinal stromal tumours (GISTs), with a cluster of co-expressed miRNAs located at 14q32.31.* J Pathol, 2010. **220**(1): p. 71-86.
355. Gattolliat, C.H., et al., *Expression of miR-487b and miR-410 encoded by 14q32.31 locus is a prognostic marker in neuroblastoma.* Br J Cancer, 2011. **105**(9): p. 1352-61.
356. Bray, I., et al., *Widespread dysregulation of MiRNAs by MYCN amplification and chromosomal imbalances in neuroblastoma: association of miRNA expression with survival.* PLoS One, 2009. **4**(11): p. e7850.
357. Lowery, A.J., et al., *MicroRNA signatures predict oestrogen receptor, progesterone receptor and HER2/neu receptor status in breast cancer.* Breast Cancer Res, 2009. **11**(3): p. R27.

358. Pecuchet, N., et al., *Loss of heterozygosity at 13q13 and 14q32 predicts BRCA2 inactivation in luminal breast carcinomas.* Int J Cancer, 2013. **133**(12): p. 2834-42.
359. Pasca di Magliano, M. and M. Hebrok, *Hedgehog signalling in cancer formation and maintenance.* Nat Rev Cancer, 2003. **3**(12): p. 903-11.
360. Tao, Y., et al., *Overexpression of Hedgehog signaling molecules and its involvement in triple-negative breast cancer.* Oncol Lett, 2011. **2**(5): p. 995-1001.
361. Zhang, X., et al., *The tumor suppressive role of miRNA-370 by targeting FoxM1 in acute myeloid leukemia.* Mol Cancer, 2012. **11**: p. 56.
362. Wang, S., et al., *CXCL12-induced upregulation of FOXM1 expression promotes human glioblastoma cell invasion.* Biochem Biophys Res Commun, 2014. **447**(1): p. 1-6.
363. Craig, D.W., et al., *Genome and transcriptome sequencing in prospective metastatic triple-negative breast cancer uncovers therapeutic vulnerabilities.* Mol Cancer Ther, 2013. **12**(1): p. 104-16.
364. Workman, P., et al., *Drugging the cancer chaperone HSP90: combinatorial therapeutic exploitation of oncogene addiction and tumor stress.* Ann N Y Acad Sci, 2007. **1113**: p. 202-16.
365. Gallerne, C., A. Prola, and C. Lemaire, *Hsp90 inhibition by PU-H71 induces apoptosis through endoplasmic reticulum stress and mitochondrial pathway in cancer cells and overcomes the resistance conferred by Bcl-2.* Biochim Biophys Acta, 2013. **1833**(6): p. 1356-66.
366. Munster, P.N., et al., *Inhibition of heat shock protein 90 function by ansamycins causes the morphological and functional differentiation of breast cancer cells.* Cancer Res, 2001. **61**(7): p. 2945-52.
367. Hollingshead, M., et al., *In vivo antitumor efficacy of 17-DMAG (17-dimethylaminoethylamino-17-demethoxygeldanamycin hydrochloride), a water-soluble geldanamycin derivative.* Cancer Chemother Pharmacol, 2005. **56**(2): p. 115-25.
368. Eiseman, J.L., et al., *Pharmacokinetics and pharmacodynamics of 17-demethoxy 17-[[(2-dimethylamino)ethyl]amino]geldanamycin (17DMAG, NSC 707545) in C.B-17 SCID mice bearing MDA-MB-231 human breast cancer xenografts.* Cancer Chemother Pharmacol, 2005. **55**(1): p. 21-32.
369. Silver, D.P., et al., *Efficacy of neoadjuvant Cisplatin in triple-negative breast cancer.* J Clin Oncol, 2010. **28**(7): p. 1145-53.
370. Brognard, J., et al., *PHLPP and a second isoform, PHLPP2, differentially attenuate the amplitude of Akt signaling by regulating distinct Akt isoforms.* Mol Cell, 2007. **25**(6): p. 917-31.
371. Brognard, J., et al., *Common polymorphism in the phosphatase PHLPP2 results in reduced regulation of Akt and protein kinase C.* J Biol Chem, 2009. **284**(22): p. 15215-23.
372. Agarwal, N.K., et al., *PHLPP2 suppresses the NF-kappaB pathway by inactivating IKKbeta kinase.* Oncotarget, 2014. **5**(3): p. 815-23.
373. Turner, N., et al., *Targeting triple negative breast cancer: is p53 the answer?* Cancer Treat Rev, 2013. **39**(5): p. 541-50.
374. Daskalos, A., et al., *Hypomethylation of retrotransposable elements correlates with genomic instability in non-small cell lung cancer.* Int J Cancer, 2009. **124**(1): p. 81-7.
375. Tiernan, J.P., et al., *Carcinoembryonic antigen is the preferred biomarker for in vivo colorectal cancer targeting.* Br J Cancer, 2013. **108**(3): p. 662-7.
376. Bauer, T.M., et al., *Carbohydrate antigen 19-9 is a prognostic and predictive biomarker in patients with advanced pancreatic cancer who receive gemcitabine-containing chemotherapy: a pooled analysis of 6 prospective trials.* Cancer, 2013. **119**(2): p. 285-92.
377. Sorokin, J.J., et al., *A clinical comparison of two radioimmunoassays for carcinoembryonic antigen (CEA).* Immunol Commun, 1972. **1**(1): p. 11-24.
378. Charpin, C., et al., *Carcinoembryonic antigen (CEA) and carbohydrate determinant 19-9 (CA 19-9) localization in 121 primary and metastatic ovarian tumors: an immunohistochemical study with the use of monoclonal antibodies.* Int J Gynecol Pathol, 1982. **1**(3): p. 231-45.
379. Guadagni, F., et al., *A re-evaluation of carcinoembryonic antigen (CEA) as a serum marker for breast cancer: a prospective longitudinal study.* Clin Cancer Res, 2001. **7**(8): p. 2357-62.

380. Nguyen, M., *Angiogenic factors as tumor markers.* Invest New Drugs, 1997. **15**(1): p. 29-37.
381. Wang, J., et al., *Tumor-associated circulating microRNAs as biomarkers of cancer.* Molecules, 2014. **19**(2): p. 1912-38.
382. Tsujiura, M., et al., *Circulating microRNAs in plasma of patients with gastric cancers.* Br J Cancer, 2010. **102**(7): p. 1174-9.
383. Gao, W., et al., *MiRNA-21: a biomarker predictive for platinum-based adjuvant chemotherapy response in patients with non-small cell lung cancer.* Cancer Biol Ther, 2012. **13**(5): p. 330-40.
384. Corcoran, C., et al., *miR-630 targets IGF1R to regulate response to HER-targeting drugs and overall cancer cell progression in HER2 over-expressing breast cancer.* Mol Cancer, 2014. **13**: p. 71.
385. Cheng, L., et al., *Exosomes provide a protective and enriched source of miRNA for biomarker profiling compared to intracellular and cell-free blood.* J Extracell Vesicles, 2014. **3**.
386. Thery, C., L. Zitvogel, and S. Amigorena, *Exosomes: composition, biogenesis and function.* Nat Rev Immunol, 2002. **2**(8): p. 569-79.
387. Bryant, R.J., et al., *Changes in circulating microRNA levels associated with prostate cancer.* Br J Cancer, 2012. **106**(4): p. 768-74.
388. Takeshita, N., et al., *Serum microRNA expression profile: miR-1246 as a novel diagnostic and prognostic biomarker for oesophageal squamous cell carcinoma.* Br J Cancer, 2013. **108**(3): p. 644-52.
389. Ogata-Kawata, H., et al., *Circulating Exosomal microRNAs as Biomarkers of Colon Cancer.* PLoS One, 2014. **9**(4): p. e92921.
390. Tanaka, M., et al., *Down-regulation of miR-92 in human plasma is a novel marker for acute leukemia patients.* PLoS One, 2009. **4**(5): p. e5532.
391. Heneghan, H.M., N. Miller, and M.J. Kerin, *Circulating microRNAs: promising breast cancer Biomarkers.* Breast Cancer Res, 2011. **13**(1): p. 402; author reply 403.
392. Heneghan, H.M., et al., *MicroRNAs as Novel Biomarkers for Breast Cancer.* J Oncol, 2009. **2009**: p. 950201.
393. Zhu, W., et al., *Circulating microRNAs in breast cancer and healthy subjects.* BMC Res Notes, 2009. **2**: p. 89.
394. Roth, C., et al., *Circulating microRNAs as blood-based markers for patients with primary and metastatic breast cancer.* Breast Cancer Res, 2010. **12**(6): p. R90.
395. Cimino, D., et al., *miR148b is a major coordinator of breast cancer progression in a relapse-associated microRNA signature by targeting ITGA5, ROCK1, PIK3CA, NRAS, and CSF1.* Faseb Journal, 2013. **27**(3): p. 1223-1235.
396. Biagioni, F., et al., *miR-10b*, a master inhibitor of the cell cycle, is down-regulated in human breast tumours.* EMBO Mol Med, 2012. **4**(11): p. 1214-29.
397. Barrett, T., et al., *NCBI GEO: archive for functional genomics data sets--update.* Nucleic Acids Res, 2013. **41**(Database issue): p. D991-5.
398. Rani S, G.K., Crown J, O'Byrne K, O'Driscoll L, *Global analysis of serum microRNAs as potential biomarkers for lung adenocarcinoma.* Cancer Biology and Therapy, 2013. **14**(12): p. 1104-1112.
399. Blume, J.D., *Bounding Sample Size Projections for the Area Under a ROC Curve.* J Stat Plan Inference, 2009. **139**(1): p. 711-721.
400. *StatsToDo: Computer program to calculate sample size requirements for estimating a single receiver operating characteristics*. 2014 14 July 2014]; Available from: https://www.statstodo.com/SSiz1ROC_Pgm.php.
401. Tian, T., et al., *Visualizing of the cellular uptake and intracellular trafficking of exosomes by live-cell microscopy.* J Cell Biochem, 2010. **111**(2): p. 488-96.
402. Khan, S., et al., *Early diagnostic value of survivin and its alternative splice variants in breast cancer.* BMC Cancer, 2014. **14**: p. 176.
403. Lowery, A.J., et al., *MicroRNAs as prognostic indicators and therapeutic targets: potential effect on breast cancer management.* Clin Cancer Res, 2008. **14**(2): p. 360-5.
404. Vaz, C., et al., *Analysis of microRNA transcriptome by deep sequencing of small RNA libraries of peripheral blood.* BMC Genomics, 2010. **11**: p. 288.
405. *Breast Cancer Incidence, Mortality, Treatment and Survival in Ireland: 1994-2009* 2012: National Cancer Registry Ireland

406. Shin, Y.M., et al., *Diagnostic Value of Circulating Extracellular miR-134, miR-185, and miR-22 Levels in Lung Adenocarcinoma-Associated Malignant Pleural Effusion.* Cancer Res Treat, 2014. **46**(2): p. 178-85.
407. Song, M.Y., et al., *Identification of serum microRNAs as novel non-invasive biomarkers for early detection of gastric cancer.* PLoS One, 2012. **7**(3): p. e33608.
408. Robinson, D.R., et al., *Activating ESR1 mutations in hormone-resistant metastatic breast cancer.* Nat Genet, 2013. **45**(12): p. 1446-51.

Appendix I

A: List of all genes and SNPs analysed in cells and EVs

Table A1: List of all genes and SNPs analysed in cells and EVs	
Gene	**AA Change**
AKT1	E17K
AKT1	E49K
AKT1	G173R
AKT1	K179M
AKT2	E17K
AKT2	G175R
AKT3	E17K
AKT3	G171R
ALK	L560F
ALK	A877S
ALK	D1091N
ALK	M1166R
ALK	I1171N
ALK	F1174C/S/L/L/I/V
ALK	F1245C/L/V/I
ALK	R1275Q/L
APC	R1114X
APC	E1306X
APC	E1338X
APC	Q1367X
APC	E1379X
APC	Q1429X
APC	R1450X
BRAF	R444Q
BRAF	R462I
BRAF	I463S
BRAF	G464E/V/A/R
BRAF	G466R/E/V/A
BRAF	G469A/E/R/V
BRAF	V471F
BRAF	Y472S
BRAF	E586K
BRAF	D587A/E
BRAF	I592M/V
BRAF	D594E/V/G

Gene	AA Change
BRAF	F595L/L/L/S
BRAF	G596R
BRAF	L597R/R/Q/V
BRAF	T599I
BRAF	V600E/A/G/L/M
BRAF	K601E/N/N
BRAF	S605N
BRAF	G615R
CDK4	R24C/H
CDKN1B	P117S
CDKN2A	R58X
CDKN2A	E61X
CDKN2A	E69X
CDKN2A	R80X
CDKN2A	H83Y
CDKN2A	E88X
CTNNB1	A13T
CTNNB1	A21T
CTNNB1	V22A
CTNNB1	D32A/G/V/H/N/Y
CTNNB1	S33A/P/T
CTNNB1	G34E/V/A/R/R
CTNNB1	I35N/S/T
CTNNB1	H36P/R/Y
CTNNB1	S37A/P/T/C/F/Y
CTNNB1	T41A/P/S/I/N/S
CTNNB1	S45A/P/T/C/F/Y
DDR2	R105S
DDR2	N456S
DDR2	T533K
EGFR	V689M
EGFR	N700D
EGFR	E709A/V/G/K/Q
EGFR	G719A/D/C/S/R
EGFR	S720T/P
EGFR	D761N/Y
EGFR	V769L/M
EGFR	T783A

Gene	AA Change
EGFR	A839T
EGFR	K846R
EGFR	L858M/R
EGFR	L861Q/R
EGFR	G863D
EGFR	H870R
EGFR	E884K
ERBB2	S310F/Y
ERBB2	L755S
ERBB2	G776S/V
ERBB2	D769H
ERBB2	V777A/L/M
ERBB2	V842I
ERBB2	H878Y
FBXO4	S8R
FBXO4	S12L
FBXO4	L23Q
FBXO4	P76T
FBXW7	R465C/H/L
FBXW7	R479G/Q/L
FBXW7	R505C/S/H/L/P
FBXW7	S582L
FGFR1	S125L
FGFR1	P252T
FGFR2	S252W
FGFR2	Y375C
FGFR2	N549K/K
FGFR3	R248C
FGFR3	S249C
FGFR3	G370C
FGFR3	S371C
FGFR3	Y373C
FGFR3	G380R
FGFR3	A391E
FGFR3	K650E/Q/M/T
FGFR3	G697C
GNA11	Q209L/P
GNA11	R183C

Gene	AA Change
GNAS	R201H/S/C
GNAS	Q227H/L/R
GNAQ	Q209L/P/R
HRAS	G12S/R/C/D/A/V
HRAS	G13S/R/C
HRAS	Q61H/H/Q/K/L/P/R
HRAS	E62G
IDH1	G70D
IDH1	R132C/G/S/H/L
IDH1	V178I
IDH2	R172G/W/M/K/S
KIT	M552L
KIT	Y553N
KIT	W557G/R/R
KIT	K558N/R
KIT	V559A/D/G/I
KIT	V560D/A
KIT	G565R
KIT	N566D
KIT	Y568D
KIT	V569G
KIT	P573L
KIT	F584S
KIT	L576P
KIT	E561K
KIT	K642E
KIT	V654A
KIT	T670I
KIT	D716N
KIT	D816E/H/N/Y/G/V/A
KIT	D820E/E/H/Y/A/G/
KIT	N822K/N/K/Y/H
KIT	Y823D/N
KRAS	G12D/A/V/S/R/C
KRAS	G13D/A/V/S/R/C/
KRAS	L19F/F
KRAS	Q22K
KRAS	T58I

Gene	AA Change
KRAS	A59T/G/E
KRAS	G60D
KRAS	Q61E/K/X/H/H/Q/L/P/R
KRAS	A146P/T
MAP2K1	F53C/S
MAP2K1	Q56P
MAP2K1	K57N
MAP2K1	P124L/T/S
MAP2K1	E203K/Q
MAP2K2	E207K/Q
MAP2K2	R388Q
MAP3K13	P373S
MAP3K13	S694L
MAP3K13	R880C
MAP3K13	A882S
MET	E168D
MET	N375S
MET	R970C
MET	T1010I
MET	H1112R/L/Y
MET	H1124D
MET	M1131T
MET	Y1248C/H/D
MET	Y1253D
MET	M1268T
MLH1	V384D
MYC	P57S
MYC	T58A
NCOR1	R108X
NCOR1	Q313X
NCOR1	E379X
NCOR1	I1422S
NCOR1	Q1792X
NRAS	G12D/A/V/S/R/C
NRAS	G13D/A/V/S/R/C
NRAS	A18T

Gene	AA Change
NRAS	Q61E/K/X/H/H/Q/R/P/L
PDGFRA	V561D
PDGFRA	N659K/Y
PDGFRA	D842Y/N/V
PDGFRA	D846Y
PDGFRA	Y849C
PDGFRA	D1071N
PHLPP2	L1016S
PIK3CA	R38H
PIK3CA	Q60K
PIK3CA	R88Q
PIK3CA	K111N
PIK3CA	G118D
PIK3CA	N345K
PIK3CA	S405F
PIK3CA	E418K
PIK3CA	C420R
PIK3CA	E453K
PIK3CA	P539R
PIK3CA	E542K/Q/V/G
PIK3CA	E545D/K/Q/A/V/G
PIK3CA	Q546H/E/K/L/P/R
PIK3CA	C901F
PIK3CA	F909L/L
PIK3CA	M1004I
PIK3CA	G1007R
PIK3CA	Y1021C/H/N
PIK3CA	R1023Q
PIK3CA	T1025A/S/I/T
PIK3CA	A1035T/V
PIK3CA	M1043I/I/I/V
PIK3CA	A1046V
PIK3CA	H1047R/L/Y
PIK3CA	G1049R
PIK3CA	I1058F
PIK3CA	H1065L
PIK3R1	M326I
PIK3R1	G376R

Gene	AA Change
PIK3R1	D560Y
PIK3R1	N564D
PTEN	R130L/P/Q/X
PTEN	R173C/H
PTEN	R233X
PTEN	R335X
PTPN11	A72D/V/T
PTPN11	E69K
PTPN11	E76A/G/V/Q/K
RB1	E137X
RB1	L199X
RB1	R320X
RB1	R358X
RB1	R455X
RB1	R552X
RB1	R556X
RB1	R579X
RB1	C706F
RB1	E748X
RET	C634R/W/Y
RET	A664D
RET	E768D
RET	M918T
SMARCD	Q539X
SMARCD	D391H
SMARCD	Q504X
SOS1	R248H
SOS1	R688Q
SOS1	H888Q
SRC	Q531X
STK11	Q37X
STK11	Q170X
STK11	D194N/Y/V
STK11	G196V
STK11	E199X/K
STK11	P281L
STK11	W332X
STK11	F354L

Gene	AA Change
TBX3	Y163X
TBX3	W197X
TP53	V143A
TP53	R175H/P/L
TP53	C176F
TP53	I195S
TP53	R196X
TP53	R213X/L
TP53	Y220C/S/H/N
TP53	Y234H/N/D/C
TP53	M237I
TP53	G245D/A/S/C/R
TP53	R248Q/P/L/W/G
TP53	R273C/H/P/L/S
TP53	D281G/H/Y
TP53	R282W
TP53	R306X
VHL	P81S
VHL	L85P
VHL	L89H
VHL	L158Q/V
VHL	R161X
VHL	R167W

B: Individual fold change values for miRNAs in Hs578Ts(i)$_8$ cells and their EVs, compared to Hs578T cells and their EVs.

Table A2: Significantly up-regulated miRNAs in Hs578Ts(i)$_8$ cell compared to Hs578T cells

Results are displayed as n=3 biological repeats. P-values calculated by Student's t-test.

miRNA	Mean Fold Change	SEM	p-Value
miR-452	4.8	0.370	0.001
miR-126	4.4	0.841	0.02
miR-146-5p	3.7	0.569	0.01
miR-579	2.30	0.440	0.04

Table A3: Significantly down-regulated miRNAs in Hs578Ts(i)$_8$ cellss compared to Hs578Tcells			
miRNA	**Mean Fold Change**	**SEM**	**p-value**
miR-370	-11464	3.40E-05	8.00E-18
miR-379	-6830.8	3.46E-05	8.56E-18
miR-382	-5363.8	7.64E-05	2.04E-16
miR-411	-4668.1	7.50E-05	1.90E-16
miR-376c	-4050.3	1.94E-04	8.44E-15
miR-495	-3375.8	9.87E-05	5.71E-16
miR-134	-3201.9	1.08E-04	8.32E-16
miR-127-3p	-1952	4.53E-04	2.54E-13
miR-889	-1789.1	1.72E-04	5.24E-15
miR-655	-744.66	4.89E-04	3.46E-13
miR-487b	-660.1	4.75E-04	3.07E-13
miR-516b	-592.26	8.46E-04	3.09E-12
miR-519e	-484.7	5.76E-04	6.66E-13
miR-493	-388.06	1.79E-03	6.26E-11
miR-337-5p	-359.14	4.07E-04	1.67E-13
miR-410	-302.71	8.95E-04	3.91E-12
miR-369-5p	-300.83	1.11E-03	9.35E-12
miR-485-3p	-293.79	1.50E-03	3.07E-11
miR-519c-3p	-245.77	1.47E-03	2.86E-11
miR-654-5p	-211.34	2.11E-03	1.21E-10
miR-431	-167.11	2.96E-03	4.74E-10
miR-376b	-143.76	2.39E-03	2.03E-10
miR-539	-103.98	9.27E-03	4.61E-08
miR-376a	-81.93	6.08E-03	8.61E-09
miR-486-5p	-71.13	1.23E-02	1.46E-07
miR-654-3p	-62.59	9.19E-03	4.57E-08
miR-615-3p	-56.54	1.61E-02	4.34E-07
miR-433	-31.66	2.03E-02	1.16E-06
miR-582-5p	-30.3	1.88E-02	8.51E-07
miR-409-5p	-26.37	3.50E-02	1.04E-05
miR-515-3p	-22.19	1.20E-02	1.48E-07
miR-512-5p	-19.73	4.74E-02	3.68E-05
miR-548b-5p	-19.65	3.26E-02	8.26E-06
miR-501-3p	-17.75	4.60E-02	3.33E-05
miR-487a	-15.94	3.89E-02	1.75E-05

miRNA	Mean Fold Change	SEM	p-value
miR-375	-15.75	2.87E-02	5.28E-06
miR-371-3p	-15.53	5.15E-02	5.40E-05
miR-299-5p	-14.59	6.62E-02	1.48E-04
miR-518a-3p	-13.87	1.64E-02	5.80E-07
miR-526b	-13.57	4.65E-02	3.74E-05
miR-525-3p	-12.66	1.10E-02	1.24E-07
miR-518c	-12.39	4.87E-02	4.63E-05
miR-518e	-10.99	2.25E-02	2.22E-06
miR-512-3p	-10.58	1.40E-02	3.42E-07
miR-520g	-9.81	5.36E-02	7.43E-05
miR-519d	-9.28	2.34E-02	2.84E-06
miR-517c	-8.66	2.62E-02	4.60E-06
miR-518f	-7.96	5.70E-02	1.05E-04
miR-520f	-7.49	1.30E-01	2.60E-03
miR-494	-6.56	3.44E-02	1.61E-05
miR-140-3p	-6.33	1.07E-01	1.40E-03
miR-182	-6.25	6.63E-02	2.24E-04
miR-519a	-6.08	4.08E-02	3.37E-05
miR-23a	-5.79	1.22E-01	2.47E-03
miR-515-5p	-5.76	2.64E-02	6.23E-06
miR-138	-5.02	2.15E-02	3.12E-06
miR-486-3p	-4.98	1.90E-01	1.35E-02
miR-31	-4.77	9.57E-03	1.29E-07
miR-34c-5p	-4.74	7.10E-02	3.73E-04
miR-148b	-4.61	1.61E-01	8.29E-03
miR-518d-5p	-4.55	1.20E-01	2.92E-03
miR-532-5p	-4.54	9.86E-02	1.38E-03
miR-517a	-4.44	7.36E-02	4.60E-04
miR-140-5p	-4.33	3.39E-02	2.25E-05
miR-135a	-4.21	2.02E-01	1.94E-02
miR-523	-4.06	8.10E-02	7.44E-04
miR-204	-3.82	4.15E-02	5.88E-05
miR-183	-3.82	4.95E-02	1.18E-04
miR-145	-3.75	2.93E-02	1.52E-05
miR-143	-3.6	7.78E-02	7.50E-04
miR-372	-3.43	7.71E-02	7.81E-04
miR-24	-3.42	4.89E-02	1.32E-04

miRNA	Mean Fold Change	SEM	p-value
miR-195	-3.35	2.57E-02	1.07E-05
miR-199b-5p	-3.31	4.16E-02	7.38E-05
miR-135b	-3.22	5.40E-02	2.18E-04
miR-500	-3.15	1.43E-01	8.92E-03
miR-744	-3.14	1.22E-01	5.06E-03
miR-323-3p	-3.01	8.10E-02	1.18E-03
miR-221	-2.95	2.99E-02	2.48E-05
miR-199a-5p	-2.89	1.02E-01	3.01E-03
miR-28-5p	-2.88	5.75E-02	3.43E-04
miR-27a	-2.7	6.54E-02	6.52E-04
has-miR-155	-2.66	6.48E-02	6.53E-04
miR-185	-2.63	2.14E-01	4.43E-02
miR-130b	-2.49	5.71E-02	4.66E-04
miR-139-5p	-2.49	1.94E-01	3.66E-02
miR-522	-2.46	2.08E-01	4.65E-02
miR-28-3p	-2.3	7.37E-02	1.56E-03
miR-152	-2.3	9.90E-02	4.68E-03
miR-324-5p	-2.17	7.34E-02	1.82E-03
miR-362-5p	-2.14	1.85E-01	4.49E-02
miR-29c	-2.06	7.11E-02	1.93E-03
miR-652	-2.01	9.24E-02	5.54E-03
miR-27b	-2	1.39E-01	2.27E-02

Table A4: Significantly down-regulated miRNAs in Hs578Ts(i)$_8$ EVs compared to Hs578T EVs			
miRNA	**Mean Fold Change**	**SEM**	**p-value**
miR-134	-2330.51	2.03E-04	1.03E-14
miR-654-5p	-2288.97	1.27E-04	1.54E-15
miR-493	-1290.95	4.21E-04	1.89E-13
miR-431	-1041.03	7.51E-04	1.91E-12
miR-520f	-869.67	3.34E-04	7.48E-14
miR-655	-495.05	4.20E-04	1.88E-13
miR-504	-394.69	1.42E-03	2.47E-11
miR-337-5p	-216.51	4.35E-03	2.20E-09
miR-516a-5p	-158.67	1.47E-03	2.86E-11
miR-429	-130.96	1.52E-03	3.32E-11
miR-520a-5p	-128.24	5.59E-03	6.05E-09
miR-32	-113.12	1.84E-03	7.15E-11
miR-616	-105.75	3.36E-03	7.93E-10
miR-889	-82.07	1.17E-02	1.19E-07
miR-551b	-75.80	1.22E-02	1.38E-07
miR-521	-73.82	8.03E-03	2.63E-08
miR-370	-62.51	4.44E-03	2.49E-09
miR-512-5p	-55.40	1.10E-02	9.40E-08
miR-376a	-54.84	9.55E-03	5.37E-08
miR-382	-54.20	5.27E-03	4.98E-09
miR-135a	-42.72	1.38E-02	2.42E-07
miR-485-3p	-34.93	1.56E-02	3.98E-07
miR-376c	-29.75	1.62E-02	4.75E-07
miR-516b	-23.74	1.70E-02	5.90E-07
miR-526b	-20.75	2.53E-02	3.00E-06
miR-520e	-20.04	2.64E-02	3.54E-06
miR-519e	-19.78	2.72E-02	4.03E-06
miR-518c	-19.00	2.64E-02	3.60E-06
miR-329	-16.03	5.25E-02	5.76E-05
miR-539	-15.69	7.63E-03	2.64E-08
miR-487b	-15.39	4.35E-02	2.78E-05
miR-296-3p	-14.88	6.34E-02	1.24E-04
miR-518d-5p	-14.53	4.46E-02	3.11E-05
miR-379	-14.45	2.63E-02	3.80E-06
miR-127-3p	-14.40	1.59E-02	5.12E-07
miR-525-3p	-13.61	4.22E-02	2.55E-05

miRNA	Mean Fold Change	SEM	p-value
miR-520a-3p	-11.70	3.58E-02	1.39E-05
miR-515-5p	-11.69	3.02E-02	7.08E-06
miR-34c-5p	-11.04	2.62E-02	4.12E-06
miR-518f	-10.76	4.63E-02	3.99E-05
miR-323-3p	-10.06	2.37E-02	2.84E-06
miR-495	-10.02	4.53E-02	3.78E-05
miR-487a	-9.95	5.17E-02	6.39E-05
miR-518a-3p	-9.80	3.13E-02	8.78E-06
miR-519d	-9.69	2.27E-02	2.46E-06
miR-512-3p	-9.30	3.04E-02	8.05E-06
miR-517c	-8.82	4.83E-02	5.16E-05
miR-519a	-8.48	3.72E-02	1.87E-05
miR-502-5p	-8.32	1.19E-01	1.81E-03
miR-518e	-8.29	2.99E-02	7.99E-06
miR-211	-8.15	6.66E-02	1.91E-04
miR-411	-8.14	6.49E-02	1.74E-04
miR-143	-7.97	4.43E-02	3.87E-05
miR-410	-7.86	3.74E-02	1.99E-05
miR-450a	-7.40	1.31E-01	2.71E-03
miR-517a	-7.38	4.12E-02	3.04E-05
miR-520b	-7.25	5.90E-02	1.27E-04
miR-23a	-7.13	1.62E-02	7.47E-07
miR-34a	-7.11	2.03E-02	1.86E-06
miR-200a	-6.96	1.27E-01	2.51E-03
miR-548d-3p	-6.94	1.26E-01	2.48E-03
miR-545	-6.86	1.26E-01	2.45E-03
miR-145	-6.66	1.36E-02	3.95E-07
miR-31	-6.65	3.51E-02	1.72E-05
miR-299-5p	-6.60	1.21E-01	2.15E-03
miR-140-3p	-6.50	4.01E-02	2.99E-05
miR-221	-6.47	3.20E-03	1.23E-09
miR-371-3p	-6.37	5.56E-02	1.10E-04
miR-520g	-6.34	3.15E-02	1.17E-05
miR-22	-6.20	1.19E-01	2.13E-03
miR-362-3p	-6.18	1.20E-01	2.20E-03
miR-138	-5.99	1.31E-02	3.69E-07
miR-519c-3p	-5.98	1.37E-01	3.67E-03
miR-140-5p	-5.56	7.76E-02	4.54E-04

miRNA	Mean Fold Change	SEM	p-value
miR-96	-5.37	1.05E-01	1.50E-03
miR-522	-5.18	6.75E-02	2.80E-04
miR-195	-5.11	7.13E-02	3.53E-04
miR-500	-4.95	8.41E-02	6.88E-04
miR-597	-4.95	3.70E-02	2.73E-05
miR-155	-4.93	3.35E-02	1.86E-05
miR-23b	-4.91	4.54E-02	6.21E-05
miR-377	-4.89	2.03E-01	1.72E-02
miR-887	-4.86	2.02E-01	1.71E-02
miR-27a	-4.85	7.57E-02	4.67E-04
miR-515-3p	-4.82	1.10E-01	1.98E-03
miR-183	-4.81	6.66E-02	2.87E-04
miR-486-3p	-4.80	2.01E-01	1.69E-02
miR-204	-4.79	1.93E-02	2.13E-06
miR-182	-4.73	3.78E-02	3.11E-05
miR-24	-4.73	3.82E-02	3.26E-05
miR-654-3p	-4.66	1.15E-01	2.43E-03
miR-501-5p	-4.62	1.16E-01	2.48E-03
miR-28-5p	-4.56	2.35E-02	4.92E-06
miR-433	-4.53	2.81E-02	1.00E-05
miR-136	-4.43	1.03E-01	1.69E-03
miR-146a	-4.41	1.02E-01	1.63E-03
miR-199b-5p	-4.40	5.42E-02	1.40E-04
miR-135b	-4.38	1.29E-01	3.93E-03
miR-199a-5p	-4.24	1.06E-01	1.95E-03
miR-532-5p	-4.19	6.92E-02	3.88E-04
miR-130b	-4.17	4.71E-02	8.61E-05
miR-525-5p	-4.16	6.86E-03	3.98E-08
miR-193a-3p	-4.15	2.04E-01	2.06E-02
miR-502-3p	-4.09	1.76E-01	1.27E-02
miR-449b	-4.09	1.11E-01	2.42E-03
miR-27b	-4.08	8.24E-02	7.87E-04
miR-671-3p	-4.07	1.08E-01	2.19E-03
miR-383	-3.97	1.47E-01	6.96E-03
miR-29b	-3.91	1.58E-01	9.32E-03
miR-301b	-3.83	1.27E-01	4.37E-03
miR-886-3p	-3.83	1.81E-01	1.51E-02
miR-517b	-3.82	9.91E-02	1.73E-03

miRNA	Mean Fold Change	SEM	p-value
miR-222	-3.82	1.15E-02	3.56E-07
miR-494	-3.80	3.83E-02	4.30E-05
miR-15b	-3.72	3.05E-02	1.79E-05
miR-215	-3.54	3.91E-02	5.19E-05
miR-28-3p	-3.46	2.77E-02	1.36E-05
miR-29a	-3.45	1.13E-01	3.27E-03
miR-523	-3.43	5.45E-02	2.02E-04
miR-185	-3.39	4.10E-02	6.72E-05
miR-199a-3p	-3.38	9.79E-02	1.98E-03
miR-532-3p	-3.31	4.02E-02	6.42E-05
miR-33b	-3.31	1.22E-01	4.61E-03
miR-152	-3.29	6.78E-02	5.09E-04
miR-320	-3.24	2.18E-02	5.89E-06
miR-454	-3.23	1.39E-01	7.69E-03
miR-362-5p	-3.23	8.91E-02	1.50E-03
miR-574-3p	-3.22	3.58E-02	4.29E-05
miR-486-5p	-3.22	5.77E-02	2.81E-04
miR-218-	-3.19	1.02E-01	2.55E-03
miR-374b	-3.07	1.34E-01	7.28E-03
miR-455-5p	-3.05	1.35E-01	7.64E-03
miR-511	-2.97	1.78E-01	2.03E-02
miR-154	-2.94	1.75E-01	1.95E-02
miR-21	-2.94	1.82E-01	2.23E-02
miR-490-3p	-2.93	1.73E-01	1.90E-02
miR-372	-2.93	1.75E-01	1.98E-02
miR-674	-2.93	1.73E-01	1.90E-02
miR-148b	-2.91	8.10E-02	1.25E-03
miR-891a	-2.91	1.71E-01	1.85E-02
miR-871	-2.90	1.70E-01	1.82E-02
miR-660	-2.86	2.17E-01	3.99E-02
miR-625	-2.83	1.11E-01	4.28E-03
miR-16	-2.74	9.41E-02	2.51E-03
miR-484	-2.72	4.13E-02	1.06E-04
miR-455-3p	-2.68	6.11E-02	5.10E-04
miR-142-3p	-2.66	1.99E-01	3.51E-02
miR-636	-2.63	6.01E-02	4.97E-04
miR-324-5p	-2.62	4.51E-02	1.64E-04
miR-122	-2.61	1.31E-01	9.18E-03

miRNA	Mean Fold Change	SEM	p-value
miR-30b	-2.54	7.32E-02	1.16E-03
miR-576-3p	-2.54	1.76E-01	2.62E-02
miR-106b	-2.48	1.74E-01	2.65E-02
miR-374a	-2.45	1.77E-01	2.90E-02
miR-579	-2.40	1.72E-01	2.74E-02
let-7e	-2.39	1.38E-01	1.35E-02
miR-29c	-2.38	2.08E-01	4.97E-02
miR-301a	-2.36	1.06E-01	5.50E-03
miR-451	-2.30	1.90E-01	4.07E-02
miR-130a	-2.25	1.35E-01	1.47E-02
miR-375	-2.23	1.58E-01	2.48E-02
miR-25	-2.21	3.77E-02	1.30E-04
miR-345	-2.19	8.54E-02	3.14E-03
miR-125b	-2.18	9.48E-02	4.63E-03
miR-159a	-2.18	1.78E-01	3.85E-02
miR-342-3p	-2.16	6.23E-02	9.93E-04
miR-328	-2.13	1.71E-02	6.49E-06
miR-30c	-2.12	1.06E-01	7.44E-03
miR-423-5p	-2.12	5.52E-02	6.69E-04
miR-335	-2.10	1.06E-01	7.73E-03
let-7b	-2.08	3.57E-02	1.30E-04
miR-128	-2.04	1.15E-01	1.15E-02
let-7c	-2.01	1.22E-01	1.48E-02

C: C_T values obtained as part of miR-134, miR-370 and miR-376c expression in sera EVs

Table A5: C_T values obtained for miR-134 in healthy individuals and breast cancer patients sera-EVs			
Subtype	**Experiment ID**	**Healthy Donor C_T Value**	**Breast Cancer C_T**
TNBC	TNBC 1	35.77	37.45
TNBC	TNBC 2	31.29	35.62
TNBC	TNBC 3	31.97	37.90
TNBC	TNBC 4	35.24	38.38
TNBC	TNBC 5	33.25	31.44
TNBC	TNBC 6	33.28	33.38
TNBC	TNBC 7	33.70	32.88
TNBC	TNBC 8	33.40	33.26
TNBC	TNBC 9	33.56	34.31
TNBC	TNBC 10	33.19	33.51
TNBC	TNBC 11	33.92	33.68
TNBC	TNBC 12	33.60	33.74
TNBC	TNBC 13	34.11	33.93
TNBC	TNBC 14	34.82	35.63
ER	ER 1	31.71	37.14
ER	ER 2	33.19	37.49
ER	ER 3	33.29	36.26
ER	ER 4	36.08	34.88
ER	ER 5	33.76	36.29
ER	ER 6	29.85	29.73
ER	ER 7	30.14	30.01
ER	ER 8	29.82	29.82
ER	ER 9	29.55	29.87
ER	ER 10	29.60	30.17
ER	ER 11	29.27	29.49
ER	ER 12	29.24	29.55
ER	ER 13	28.90	29.71
ER	ER 14	28.93	29.91
HER2	HER2 1	32.52	33.74
HER2	HER2 2	34.51	36.58
HER2	HER2 3	34.98	40.00
HER2	HER2 4	34.77	37.19

Table A6: C_T values obtained for miR-370 in healthy individuals and breast cancer patients sera-EVs			
Subtype	**Experiment ID**	**Healthy Donor C_T Value**	**Breast Cancer C_T**
TNBC	TNBC 1	38.06	39.36
TNBC	TNBC 2	32.92	36.63
TNBC	TNBC 3	35.61	40.00
TNBC	TNBC 4	36.24	40.00
TNBC	TNBC 5	35.26	40.00
TNBC	TNBC 6	29.81	37.04
TNBC	TNBC 7	36.86	34.24
TNBC	TNBC 8	39.09	39.18
TNBC	TNBC 9	38.57	39.70
TNBC	TNBC 10	26.45	35.11
TNBC	TNBC 11	35.20	39.86
TNBC	TNBC 12	36.51	36.12
TNBC	TNBC 13	38.12	32.86
TNBC	TNBC 14	35.69	37.07
ER	ER 1	31.42	39.32
ER	ER 2	34.77	39.15
ER	ER 3	28.83	35.17
ER	ER 4	37.45	38.78
ER	ER 5	31.34	40.00
ER	ER 6	33.11	32.23
ER	ER 7	35.45	39.95
ER	ER 8	29.44	32.68
ER	ER 9	31.99	31.80
ER	ER 10	35.80	38.13
ER	ER 11	40.00	38.23
ER	ER 12	29.88	30.83
ER	ER 13	31.02	34.90
ER	ER 14	35.36	36.31
HER2	HER2 1	30.39	32.99
HER2	HER2 2	34.01	36.33
HER2	HER2 3	34.52	40.00
HER2	HER2 4	31.26	38.86

Table A7: C_T values obtained for miR-376c in healthy individuals and breast cancer patients sera-EVs			
Subtype	**Experiment ID**	**Healthy Donor C_T Value**	**Breast Cancer C_T**
TNBC	TNBC 1	38.85	40.00
TNBC	TNBC 2	35.74	40.00
TNBC	TNBC 3	37.69	40.00
TNBC	TNBC 4	36.98	38.72
TNBC	TNBC 5	35.62	32.36
TNBC	TNBC 6	33.67	36.07
TNBC	TNBC 7	34.14	35.97
TNBC	TNBC 8	33.92	37.76
TNBC	TNBC 9	33.98	38.08
TNBC	TNBC 10	31.51	34.93
TNBC	TNBC 11	35.00	34.81
TNBC	TNBC 12	36.72	36.52
TNBC	TNBC 13	34.00	36.39
TNBC	TNBC 14	31.58	35.81
ER	ER 1	39.97	40.00
ER	ER 2	39.77	38.63
ER	ER 3	37.50	39.54
ER	ER 4	39.37	38.98
ER	ER 5	39.02	36.74
ER	ER 6	40.00	40.00
ER	ER 7	33.15	39.05
ER	ER 8	35.79	37.91
ER	ER 9	40.00	40.00
ER	ER 10	37.98	38.72
ER	ER 11	35.78	38.70
ER	ER 12	34.88	38.09
ER	ER 13	34.25	38.93
ER	ER 14	35.78	39.34
HER2	HER2 1	37.89	40.00
HER2	HER2 2	40.00	39.95
HER2	HER2 3	38.44	40.00
HER2	HER2 4	38.05	40.00

Appendix II

Publications, presentations and awards

Research articles:

Exosomes from triple-negative breast cancer cells can transfer phenotypic traits representing their cells of origin to secondary cells

O'Brien K, Rani S, Corcoran C, Wallace R, Hughes L, Friel AM, McDonnell S, Crown J, Radomski MW, O'Driscoll L.

European Journal of Cancer, 2013, May: 49(8): 1845-59

Docetaxel-resistance in prostate cancer: evaluating associated phenotypic changes and potential for resistance transfer via exosomes

Corcoran C, Rani S, **O'Brien K**, O'Neill A, Prencipe M, Sheikh R, Webb G, McDermott R, Watson W, Crown J, O'Driscoll L.

PLoS One. 2012;7(12):e50999. 2012 Dec 10.

Book chapter:

Isolation of exosomes for subsequent mRNA, microRNA, and protein profiling

Rani S, **O'Brien K**, Kelleher FC, Corcoran C, Germano S, Radomski MW, Crown J, O'Driscoll L.

Methods in Molecular Biology *2011;784:181-95.*

Published abstracts

miR-134 transported in extracellular vesicles reduces triple-negative breast cancer aggression

O'Brien K, Corcoran C, Rani, Crown J, Radomski M and O'Driscoll L

Journal of extracellular vesicles: 2014; Volume 3; Page 57

The relevance of exosomal-miRNAs in triple-negative breast cancer progression

O'Brien K, Corcoran C, Rani S, McDonnell S, Hughes L, Radomski M, Crown J and O'Driscoll L.

Journal of extracellular vesicles: 2013; Volume 2; Page 122

Can exosomes influence triple negative breast cancer metastasis?

O'Brien K, Rani S, Wallace R, McDonnell S, Hughes L, Radomski M and O'Driscoll L.

Journal of extracellular vesicles: 2012; Supplement 1; Page 74; Abstract 27

Exosomes: potential regulators and biomarkers of prostate cancer progression
Corcoran C, Rani S, **O'Brien K**, O'Neill A, Prencipe M, Crown J, Watson W and O'Driscoll L.
Journal of extracellular vesicles: 2012; Supplement 1; Page 76, Abstract 32

The relevance of exosomes in prostate cancer and their potential to confer docetaxel resistance to secondary cells
Corcoran C, Rani S, O'Neill A, Principe M, O'Brien A, **O'Brien K**, Crown J, Watson WG, O'Driscoll L.
Cancer Research: 2012; Volume 72; Issue 8; Supplement 1; Abstract 794.

Generation and characterisation of neratinib-resistant breast cancer cell line variants
Breslin S, Rani S, Corcoran C, **O'Brien K**, O'Driscoll L.
European Journal of Cancer: 2012; Volume 48; Supplement 6; Pages 32-33; Abstract 103

Triple-negative breast cancer cells may transfer phenotypic characteristics via exosomes
Rani S, **O'Brien K**, McDonnell S, Hughes L, Friel AM, Radomski MW, Crown J, O'Driscoll L.
European Journal of Cancer: 2011; Volume 47; Supplement 1*;* Page 143; Abstract 1166

Investigating naturally-occurring nano-sized exosomes in cancer
O'Brien K, Rani S, McDonnell S, Hughes L, Radomski MW, O'Driscoll L.
Journal of Pharmacy and Pharmaceutical Sciences: 2011; Volume 13; No.3; Page 209

Investigating the mechanisms of docetaxel resistance in prostate cancer
C Corcoran, S Rani, **O'Brien K**, O'Neill A, Watson W, O'Driscoll L.
Journal of Pharmacy and Pharmaceutical Sciences: 2011. Volume 13; No.3; Page 213

Awards

Young investigators award obtained for best poster presentation
2nd annual International Society for Extracellular Vesicles conference 2013
Boston, USA

Awarded travel grant from Trinity College Dublin to present at the Annual International Society for Extracellular Vesicles (ISEV) meeting, Boston, USA

First prize awarded for best oral presentation
Annual Irish Association of Cancer Research meeting 2013
Dublin, Ireland

First prize awarded for best oral presentation
Annual Irish Association of Cancer Research meeting 2012
Belfast, N.Ireland

Local meetings, national and international conference presentations

Oral presentations:

Exosomes in TNBC
Triple negative breast cancer meeting
St. Vincent's University Hospital; 2013

Functional characterisation, profiling and therapeutic manipulation of breast cancer derived exosomes
Invited speaker for a research seminar in the Lab of Dr. Clotilde Théry
Institut Curie, Paris; 2013

Exosomal miRNAs in triple-negative breast cancer progression and treatment
Dublin microRNA day
Dublin; 2013

Harnessing exosomes/microvesicles as microRNA therapeutic delivery vesicles in triple-negative breast cancer

European network on microvesicles and exosomes in health and disease (ME-HAD) inaugural meeting
Trinity College Dublin; 2013

Exosomal miRNAs in triple-negative breast cancer
All Ireland Schools of Pharmacy Conference
University of Ulster, Belfast; 2013

Exosomal miRNAs: potential communicators in triple-negative breast cancer
Irish Association for Cancer Research Annual meeting
Dublin; 2013

Can triple-negative breast cancer cells transfer aggressive phenotypic characteristics via exosomes?
Scientific advisory board review of MTCI
Dublin 2012

The relevance of triple-negative breast cancer-derived exosomes in the transfer of aggressive phenotypic characteristics
All Ireland Schools of Pharmacy Conference
University College Cork; 2012

Assessing the Influence of exosomes in triple-negative breast cancer
Irish Association for Cancer Research Annual meeting
Belfast; 2012

Triple-negative breast cancer cells can transfer phenotypic characteristics via exosomes
Exosomes and Microvesicles
Orlando, Florida; 2011

Investigating naturally-occurring circulating nano-sized exosomes in cancer
All Ireland Schools of Pharmacy Conference
Royal College of Surgeons, Dublin; 2011

Poster presentations:

The Relevance of Exosomal-miRNAs in Triple-negative Breast Cancer Progression
International Society for Extracellular Vesicles annual scientific meeting
Boston, MA; 2013

Can Exosomes influence Triple-negative breast cancer metastasis?
International Society for Extracellular Vesicles annual scientific meeting
Gothenburg, Sweden; 2012

Circulating exosomes in Triple-negative breast cancer; are these treasure chests of minimally-invasive biomarkers?
All Ireland Schools of Pharmacy Conference
Royal College of Surgeons Dublin; 2011

Senior sophister student project supervision

September 2013-October 2013

Position: Co-supervisor of senior sophister pharmacy student (Lisa Coffey B.Sc (Pharm.))
Title: Evaluation of the influence of exosomes *in vivo* in priming the pre-metastatic niche for breast cancer metastasis

September 2012-October 2012

Position: Co-supervisor of senior sophister pharmacy student (Chi Keung Wan B.Sc (Pharm.))
Title: "Preliminary molecular characterising of how cancer cells transfer aggressive phenotypic characteristics via exosomes"

September 2011-October 2011

Position: Co-supervisor of senior sophister pharmacy student (Sinéad Hyland B.Sc (Pharm.))
Title: "Investigating naturally occurring nano-sized vesicles in cancer"